Multivariate and multiple criteria optimisation of hydraulic fracturing; with particular application to tight gas reservoirs.

Author:
Rahman, Md Motiur

Publication Date:
2002

DOI:
https://doi.org/10.26190/unsworks/4969

CERTIFICATE OF ORIGINALITY

I hereby declare that this submission is my own work and to the best of my knowledge it contains no materials previously published or written by another person, nor material which to a substantial extent has been accepted for the award of any other degree or diploma at UNSW or any other educational institution, except where due acknowledgement is made in the thesis. Any contribution made to the research by others, with whom I have worked at UNSW or elsewhere, is explicitly acknowledged in the thesis.

I also declare that the intellectual content of this thesis is the product of my own work, except to the extent that assistance from others in the project's design and conception or in style, presentation and linguistic expression is acknowledged.

(Signed)

MULTIVARIATE AND MULTIPLE CRITERIA OPTIMISATION OF HYDRAULIC FRACTURING; WITH PARTICULAR APPLICATION TO TIGHT GAS RESERVOIRS

By

MD MOTIUR RAHMAN

A dissertation submitted to The University of New South Wales in partial fulfillment of the requirements for the Degree of Doctor of Philosophy

September, 2002

School of Petroleum Engineering
The University of New South Wales,
Sydney 2052, NSW,
AUSTRALIA

ACKNOWLEDGEMENTS

I would like to express my sincerest gratitude to A/Prof. Sheik Rahman and Dr. M.K. Rahman (Khalil) from the School of Petroleum Engineering, the University of New South Wales, for their careful supervision, constant guidance, constructive comments and enthusiastic encouragement.

I express my special gratitude to Dr. M.K. Rahman for providing the source code of the optimisation algorithm, which has been used for hydraulic fracturing optimisation in this thesis.

I would also like to thank Dr. M.M. Hossain and Dr. Z. Chen of School of Petroleum Engineering, UNSW, Mr. Simmon Chipperfield.of Santos Limited, Adelaide, A/Prof. Peter P Valko of Texas A&M University and Dr. Michael B Smith of NSI, USA, for their assistance at various stages of this work. Thanks are also due to Mr. Nino Zajaczkowski for his assistance with regard to computing resources.

I am indebted to the Cornell Fracture Group, Cornell University, NY, USA, for permission to use their FRANC 3D and HYFRANC 3D boundary element based fracture analysis software. I am also indebted to Resources Engineering Systems Inc., USA for their software FRACPRO for hydraulic fracture design and optimisation.

Thanks are also due to the Commonwealth of Australia for providing me with the Australian Postgraduate Award scholarship throughout this study.

Last but not the least, I thank my wife Moriom, and daughters Sylvia and Mridula for their continuous love and patience during this work.

ABSTRACT

Optimisation of hydraulic fracturing treatment has been identified as a technique to exploit tight gas formation economically and is currently being practiced in the industry using commercial software/operator-designed program. Full benefits of engineering optimisation, however, are not utilised due to lack of systematic formulation of optimisation criteria and various design related requirements. This study has been carried out to identify various aspects of hydraulic fracturing treatments and their complexities and to formulate them mathematically for incorporation in an optimisation tool, and hence to improve the efficiency of hydraulic fracturing treatment optimisation and the effectiveness of a designed treatment. The thesis has three main parts addressing hydraulic fracture model, production model and proposed optimisation model, encompassing all aspects of hydraulic fracturing.

In the first part, computer programs have been developed for the prediction of fracture geometry using two fracture models, 2D PKN-C and P-3D-C, the improved version of PKN and P-3D fracture models, respectively, by incorporating the Carter Equation II. Parametric comparisons of PKN-C and P-3D-C fracture models suggest that 2D PKN-C model is sufficient to design fracture treatments for three-layer problems.

In the second part, fluid flow from a fractured tight-gas reservoir has been modeled analytically for production estimation. For tight gas formations, transient and pseudo-steady state flow behaviours have been combined to form a hybrid model for production estimation and sensitivity of this model to various reservoir permeabilities is conducted. This study has demonstrated that appropriate production estimation for a fractured reservoir is required while modeling optimisation of hydraulic fracturing treatment design.

In the third part, a procedural optimisation model has been developed integrating fracture model, production model, in-situ reservoir properties, treatment parameters, treatment costs, design constraints, optimisation algorithm and design objective(s). The

model is formulated within the framework of a multivariate and multiobjective optimisation method, based on the combined features of Genetic Algorithm and Evolutionary Operation. Various design constraints are formulated mathematically to alleviate fracturing complexities. The model is applied to a typical tight gas reservoir and has demonstrated that optimisation is instrumental in improving treatment design and achieving a goal-oriented optimum design is possible in a conflicting environment. About 12-13% compromise with maximum possible production or net present value over 10 years can save up to 44-52% of initial hydraulic fracturing treatment cost. The other capabilities and benefits of this model are alleviation of fracturing complexities, which are not properly dealt with by commercial software. This has been demonstrated by applying the proposed model and other available tools to a fracturing program carried out in a field onshore Australia. Finally, it is recognised that the conventional fracturing may not be effective in highly naturally fractured reservoirs for which the potentiality of a proppant-free fracturing is assessed applying to the field case.

PUBLICATIONS

The following publications, based on work presented in this dissertation, appeared during the course of the work:

Rahman, M.M., Rahman, M.K., and Rahman, S.S., (2000), The recognition and alleviation of complexity with hydraulic fracturing onshore Australia, *J. of the Aust. Pet. Prod. and Expl. Association*, **40**, 469-480.

Rahman, M.K., Rahman, M.M. and Rahman, S.S., (2001), A decision support system for improving hydraulic fracture treatment for hydrocarbon reservoirs, *J. of the Aust. Pet. Prod. and Expl. Association*, **41**, 633-648.

Rahman, M.M., Rahman, M.K. and Rahman, S.S. (2001), An integrated model for multi-objective design optimization of hydraulic fracturing, *J. of Pet. Sci. and Eng.*, **31**, 41-62.

Rahman, M.M., Rahman, M.K. and Rahman, S.S., (2001), Optimizing treatment parameters for enhanced hydrocarbon production by hydraulic fracturing, *J. of Canadian Pet. Tech.* (submitted for review).

Rahman, M.M., Rahman, M.K. and Rahman, S.S. (2002), Control of Hydraulic-Fracturing-Induced Formation Damage by Optimizing Treatments With Constraints, SPE 73754, *SPE Int. Symp. and Exh. on Formation Damage Control*, Lafayette, Louisiana, USA, February 20-21.

Rahman, M.M., Rahman, M.K. and Rahman, S.S. (2002), Multivariate Fracture Treatment Optimization for Enhanced Gas Production From Tight Reservoirs, SPE 75702, *SPE Gas Technology Synposium*, Calgary, Alberta, Canada, April 30-May 2.

Rahman, M.M., Rahman, M.K. and Rahman, S.S. (2002), An Analytical Model for Production Estimation from Hydraulically Fractured Tight-Gas Reservoirs, SPE 77901, *SPE Asia Pacific Oil & Gas Conference & Exhibition*, Melbourne, Australia, October 08-10.

TABLE OF CONTENTS

CHAPTER SIX

INTERPRETATION AND ALLEVIATION OF COMPLEXITY WITH HYDRAULIC FRACTURING IN THE FIELD

CHAPTER SEVEN

CONCLUSIONS AND RECOMMENDATIONS

LIST OF FIGURES AND TABLES

CHAPTER ONE

CHAPTER TWO

CHAPTER THREE

CHAPTER FOUR

CHAPTER FIVE

CHAPTER SIX

APPENDIX D

APPENDIX E

LIST OF TABLES

CHAPTER ONE

INTRODUCTION

1.1. Hydraulic fracturing treatment

Hydraulic fracturing is a process whereby proppant-laden fluid is injected into wellbores under high pressures to initiate and propagate fractures deep into reservoirs. Once the pump pressure is withdrawn, these propped fractures subsequently become the principal conduits for the flow of hydrocarbons from the reservoir to the wellbore. Today, it has become a common stimulation technique that is widely used in the petroleum industry to enhance production from tight oil and gas reservoirs. Of the production wells drilled in North America since 1950s, about 70% of gas wells and 50% of oil wells have been hydraulically fractured (Valko and Economides, 1995). Designing of hydraulic fracturing treatments is, therefore, an important task in petroleum industry.

To design and plan a fracturing treatment, it is important to gather various reservoir and well data including mechanical completion configuration. These data are used to determine a desired fracture geometry to achieve a certain degree of treatment efficiency. The fracture geometry is usually coupled to a number of controllable treatment parameters such as fracturing fluid viscosity, injection rate of fracturing fluid and duration of injection. The fracturing fluid viscosity not only influences the fracture growth but also plays a key role to transport and place proppant efficiently in the fracture. Together with other treatment parameters, an appropriate concentration of a suitable proppant type is a most important parameter to influence the treatment efficiency. For a given reservoir, suitable values of these parameters are decided in the petroleum industry using commercial software, past experience and various analytical

methods. To execute a designed treatment, suitable surface and downhole equipment are assembled.

The design is usually performed using certain assumptions based on which various fracture models are developed. It is assumed that two wings of a planar fracture initiate and propagate along the maximum horizontal in-situ stress direction from a vertical well in a normal faulting stress regime. Similarly, the preferred direction for fracture growth can be predicted from the fundamental knowledge of fracture mechanics for any other stress conditions and well trajectory. To make the design task mathematically tractable and computationally feasible, this idealised fracture behaviour is modelled using uniform and linearly elastic rock properties. The behaviour of hydraulic fracture in the field, however, may be much more complex due to randomly oriented pre-existing natural fractures/flaws, multiple fractures created by inappropriate perforation orientation and bad treatment practice, and fracture re-orientation (turning and twisting) during propagation due to inappropriate perforation and well trajectory for prevailing stress condition. Any combination of these conditions induces near-wellbore fracture tortuosity which results in the requirement of higher treatment pressure than predicted during design, inefficient proppant transport causing proppant blocking and relatively low proppant concentration in the fracture front compared to its designed value (Davidson *et al.*, 1993; Cleary *et al.*, 1993; Aud *et al.*, 1994). These result in significantly low well productivity, or any other index for treatment efficiency. Many of these fracture complexities arise due to in-situ conditions and some of them can be minimised by adjusting well trajectory and perforation job. To avoid complexities arising from high-density natural fractures and flows, alternative stimulation strategy may be a better option.

Apart from complexities arising from pure in-situ conditions, an inappropriately designed treatment itself may induce many of the complexities. Inappropriate fracturing fluid viscosity and proppant type affect the effectiveness of proppant transportation and placement in the fracture, which ultimately affect the productivity of the reservoir. Inferior design may also create undesirable formation damage by uncontrolled fracture

growth, multiple secondary fracture initiation, induce excessive loss of fracturing fluid and sand production due to formation failure around the wellbore wall and perforation tunnels (particularly in weak formation). An inferior design may also require very high injection pressure to execute in the field (particularly in tight formations) and the designed treatment even may not be executable effectively and safely using the available surface and downhole equipment. Such complexities arising from design inadequacy ultimately incur a huge financial loss. While achieving the maximum efficiency in the design is the prime effort of a designer, even empirical adjustment of a design to avoid such complexities requires systematic guidelines and formulations of these complexities as functions of treatment parameters.

1.2. Current practice of treatment design

The petroleum industry has long been applying hydraulic fracturing treatment as a technique to stimulate oil and gas production and improve hydrocarbon recovery. Currently there are several approaches for hydraulic fracturing treatment design, incorporating two-dimensional (2D), or pseudo-three-dimensional (P-3D) fracture models. Some operators often rely on historical databases of stimulation jobs performed previously, personal/team experience, handbooks and industry-standard simulators. Some operators have developed their in-house methodologies based on past experiences and trial and error methods through continuous development and improvement process. Although such approaches are invaluable for finding a practical solution to the problem, it is largely either 'ad-hoc', or the fundamental physics are not well documented and widely published. Therefore, the author believes that the development of a systematic and unified procedure with theoretical details of every aspect of a complete design task will contribute to improve the chances of finding an efficient treatment. Also integration of a procedural optimisation technique in the design cycle will ensure to create a favourable hydraulic fracture geometry and meet various design objectives while the complexities discussed in the previous section can be minimised with relatively ease.

Most industrial design problems are usually modelled in terms of a number of free design variables (parameters that are adjusted), design constraints (mathematical requirements to ensure certain features in the design) and one or more design objectives (mathematical functions that reflect the efficiency of the design). Such models are solved using various optimisation methods to achieve the maximum efficiency in the final design. In the oil and gas engineering discipline, a limited number of such optimisation works have been reported in the area of production system design (Carroll and Horne, 1992; Fujii and Horne, 1995) and development planning and management of petroleum reservoirs (McFarland *et al.*, 1984). Surprisingly, the use of any formal mathematical optimisation method to investigate various issues in hydraulic fracture treatment design was very rare until recently. Meng and Brown (1987) first proposed a complete model for fracture treatment optimisation by coupling a 2D fracture geometry model with treatment parameters and reservoir productivity. However, the model was not coupled with any optimisation method. Rather, the net present value (NPV) was plotted based on parametric analysis by systematically varying various treatment parameters and fracture length. The maximum point on the NPV curve was taken as the optimum design. Although the work mentioned about various design constraints, they were not formulated and it was not demonstrated how an optimum design taken from the graph would satisfy these constraints. Hareland *et al.* (1993) and Hareland and Rampersad (1994) conducted a similar parametric study using P-3D fracture model. Later, Aggour and Economides (1998) studied the performance of high permeability fractured wells using a 2D fracture model. Rimmer *et al.* (2000) conducted fracture geometry optimisation in a similar way using a fracture simulator, and indicated that if the zone above the pay zone possesses lower stress than the pay zone, there is a possibility of uncontrolled height growth. They also suggested that such uncontrolled fracture growth could be prevented by appropriate selection of the fracturing fluid system and/or adjusting the injection rate and proppant concentration. However, no formal mathematical optimisation method was integrated in any of these studies, and therefore neither of them included mathematical formulations for any of the design requirements/constraints, nor was the procedure of finding the optimum design satisfying those constrains automated.

Yang *et al.* (1996) made an attempt for procedural optimisation of hydraulic fracturing integrating a 2D fracture model with Sequential Unconstrained Minimisation Technique (SUMT). Similar to many works, Yang's work also did not consider any design constraints. The three variables (injection rate, injection time and proppant concentration) were optimised within specified ranges to maximise incremental NPV systematically varying the fracture length with a fixed height. Thus, the work did not exploit the full benefit of optimisation procedure; rather it reduced to another effort to improve design by parametric analysis. The optimisation algorithm only helped to keep the three variables within their specified ranges and ensured that their optimum values satisfied their material balance coupling relationships with the fracture geometry for each fracture length considered.

Rietman (1998) conducted a productivity matching study for hydraulically fractured tight gas wells. The analytical model for predicting production performance included three flow regimes: pre-pseudoradial transient, transient radial and pseudo-steady state radial. The predicted productivity was matched with well test productivity to ascertain potential values for permeability-thickness, drainage area and the fracture length created by treatment. Using production derivative and cost derivative, Rietman showed how to ascertain some uncertain reservoir parameters like porosity, permeability, pay thickness, drainage area, initial pressure and water saturation, and what could be the optimum fracture length and treatment cost for the characterised reservoir conditions. The work thus falls more in line of reservoir characterisation rather than hydraulic fracturing treatment optimisation.

Mohaghegh *et al.* (1996, 1999) reported a hybrid system consisting of two neural networks and a genetic algorithm routine for design and optimisation of hydraulic fracture treatment processing historical data. Their methodology is useful where better design by conventional methods is somewhat uncertain due to lack of necessary data such as detail stress, thickness, porosity and permeability profiles. They replaced the mathematical formulations and computation of fracture geometry and well productivity

by the historical treatment data and well productivity. The neural networks established relationships between the reservoir conditions and treatment parameters by processing these data. Using these interrelationships, the genetic algorithm then established optimum treatment parameters with respect to well productivity for a given reservoir condition whose information is not in the current database. Therefore, they correctly acknowledged that their methodology is not a substitution for physics-based approaches, which leaves room for the kind of work presented in this thesis.

Langedijk *et al.* (2000) presented case studies of hydraulic fracture optimisation in deep, multilayered gas-condensate reservoirs. It is claimed that the significant challenges in fracturing deep, multi-layered gas-condensate reservoirs can be met by following their approach which used two types of state-of-the-art software to interpret mini-fracs and design the actual fracturing treatment. They claimed that their approach of optimisation considers from the beginning to capture all aspects of the project's learning and development cost. Unfortunately, physics and formulations of their design and optimisation models are not presented with any details.

Another recent hydraulic fracture optimisation work by Dempsey *et al.* (2001) is a case history evaluating the performance of stimulation by using a 3D simulator. They evaluated the effectiveness of the treatments by using several parameters including flow capacity, reservoir flow geometry, drained volume and productions of gas and water. With regard to fracture optimisation, procedural optimisation with design variables, design constraints and objective function are not well presented. This work reports that the fracture treatments often broke through to the water zones close to the gas producing zones and caused water production, which indicates the importance of fracture growth control requirements, probably not considered in their work. Aly *et al.* (2001) recently presented an optimisation technique to design fracture treatments by using both a compositional reservoir simulation model and a fracture propagation model to optimise gas production. They have also presented case studies using vertical and horizontal wells without much detail of their models. Further recent work is done by Aggour (2001) who conducted a procedural optimisation for hydraulic fractures in high

permeability reservoirs with NPV as design objective using the generalised gradient method for optimisation of nonlinear problem (Lasdon *et al.*, 1978). Unfortunately, Aggour like others did not consider any constraints to minimise the complexities that may arise due to uncontrolled optimisation.

The main drawbacks of the hydraulic fracturing treatment optimisation works reviewed can be summarised as follows:

(1) In most cases, the optimum design is identified by parametric sensitivity analysis, which is a tedious process, not automated and can not guarantee the globally optimum design.

(2) In most cases, the optimality of design is assessed in terms of NPV only. This author believes that there are other potential design objectives such as (a) maximise production, (b) maximise NPV and minimise treatment cost, (c) achieve target production with minimum treatment cost. Such flexibility in design optimisation with various objectives is likely to offer the operator a high degree of capability to obtain goal-oriented designs and make appropriate decisions on various grounds.

(3) Although emphasised the need for controlled treatments to avoid various undesired complexities, they have not been systematically identified, formulated and integrated as part of the design model in any of the works, such that the design process itself will ensure that an optimum design obtained will not suffer from these complexities. Even a post-design check for this purpose is not demonstrated in any of the works.

(4) None of the works has evaluated to check what sort of equipment capability will necessary to execute optimum designs and there is no systematic way to adjust a design without much deterioration in its optimality, so that it can be executed with the equipment available to the operators.

(5) Although a few works have used mathematical optimisation, none of the models is developed to consider essential features of design optimisation utilising the full capability of optimisation method used.

(6) In most cases, only a few parameters are varied to find the optimum design keeping most of the parameters fixed. Such an optimum design is most likely to suffer from non-optimum fracture geometry and reduced reservoir productivity.

(7) In most cases, physics and mathematics of design models are not comprehensively presented and in some cases they are ready-made software/simulator based with limited flexibility to incorporate some of the issues discussed so far.

As a result, there is a growing need for an improved design optimisation technique, which will enhance our abilities to design, execute and evaluate the fracturing treatment efficiently. Mahrer (1999), upon reviewing hydraulic fracturing design and execution practices, has correctly emphasised that optimising treatment parameters based on in-situ reservoir conditions is an area of technology that requires research and development.

1.3. Objectives and scope of the present work

The primary objectives of the present study can be summarized as follows:

1. To develop a general-purpose multivariate, multiobjective optimisation model for improved hydraulic fracturing treatment design, which will overcome the above-discussed shortcomings in the current design practices reviewed.

2. To demonstrate the benefits of the proposed model in terms of design improvement and decision-making under conflicting requirements.

3. To demonstrate that some of the current design practice/model/software may be one of the possible causes to induce undesirable complexities in the field, which the proposed model can minimise.

The above objectives are achieved by developing and integrating stand-alone computational modules for hydraulic fracture geometry, productivity from fractured wells, various design objectives and their multiobjective implementation and constraint functions to assess various design features. Free design variables are identified and modelled appropriately so that their optimum values remain within acceptable ranges and allow the development of optimum fracture geometry. A powerful optimisation method, which can handle discontinuity, nonlinearity, nondifferentiability in functions, is integrated to solve this multivariate, multiobjective and multiconstraints hydraulic fracturing design model.

By applying the model to a tight-gas formation, the importance of optimisation is demonstrated, and also demonstrated the importance of integrating equipment capability and fracture growth control requirements in the optimisation process. In addition, the criticality of integrating a strategy for sand production control in weak formations is demonstrated. The benefit of multiobjective analysis in decision making environment is demonstrated by investigating trade-offs between NPV and treatment cost, and production and treatment cost.

Finally, real-world complexities in fracture treatment of tight-gas wells onshore Australia are investigated using simulators. Among several recommendations to overcome the complexities, an optimum treatment redesigned by one of the simulators is assessed by the fracture growth control requirements and equipment capability requirements that are formulated in the proposed model. This assessment shows that the current option of treatment optimisation in the simulator is not adequate to adjust a design to satisfy these requirements, and therefore such an optimum design is highly likely to cause the sort of complexities, which were actually encountered in the field and

correctly identified by the proposed model. Finally, the treatment is redesigned by the proposed model satisfying all those requirements and therefore is highly likely to avoid these complexities without much sacrificing the design objective.

1.4. Overview of the proposed treatment optimisation model

System integration of the proposed hydraulic fracturing design optimisation model is presented in Figure 1.1. Each rectangular text box outside the bounding ellipse represents features, which are input to or output from the design process inside the bounding ellipse. Arrows explain inter-nodal interactions. The information is shown incoming to the design process from the three outside rectangular boxes, *in-situ reservoir properties*, *operational limitations* and *initial values and bounds of variables*; these are derived outside the fracturing design process. The *optimisation algorithm*, which is the solution tool, provides bi-directional interactions with the current *fracture geometry* at any stage of design process through *design constraints* and *design variables* to improve the *design objective* satisfying *fracture growth control* requirements and *operational limitations*. The final *optimum design* results from an iterative redesign process driven by the computational mechanism of the *optimisation algorithm*. Various elements of the proposed model are discussed briefly in following sections.

1.4.1. Design variables

The main task in a hydraulic fracturing design process is to decide on appropriate values for various stimulation parameters: fracturing fluid viscosity, injection rate, injection time and proppant concentration. These stimulation parameters are controllable at the surface and they control the final fracture geometry and hence production from the fractured reservoir; they are considered as four design variables for the model. The fracture half-length is considered as the fifth variable to allow the fracture geometry to develop as required for improvement in the objective function. The optimum values of these five design variables depend on in-situ reservoir properties, various operational limitations and the design objective (e.g. maximum production, maximum net present

value, etc.). The in-situ reservoir properties influence the optimum values of these variables through the fracture growth control strategy to make the designed treatment formation compatible. The effects of each of these variables in a hydraulic fracturing job are discussed briefly in the following sections.

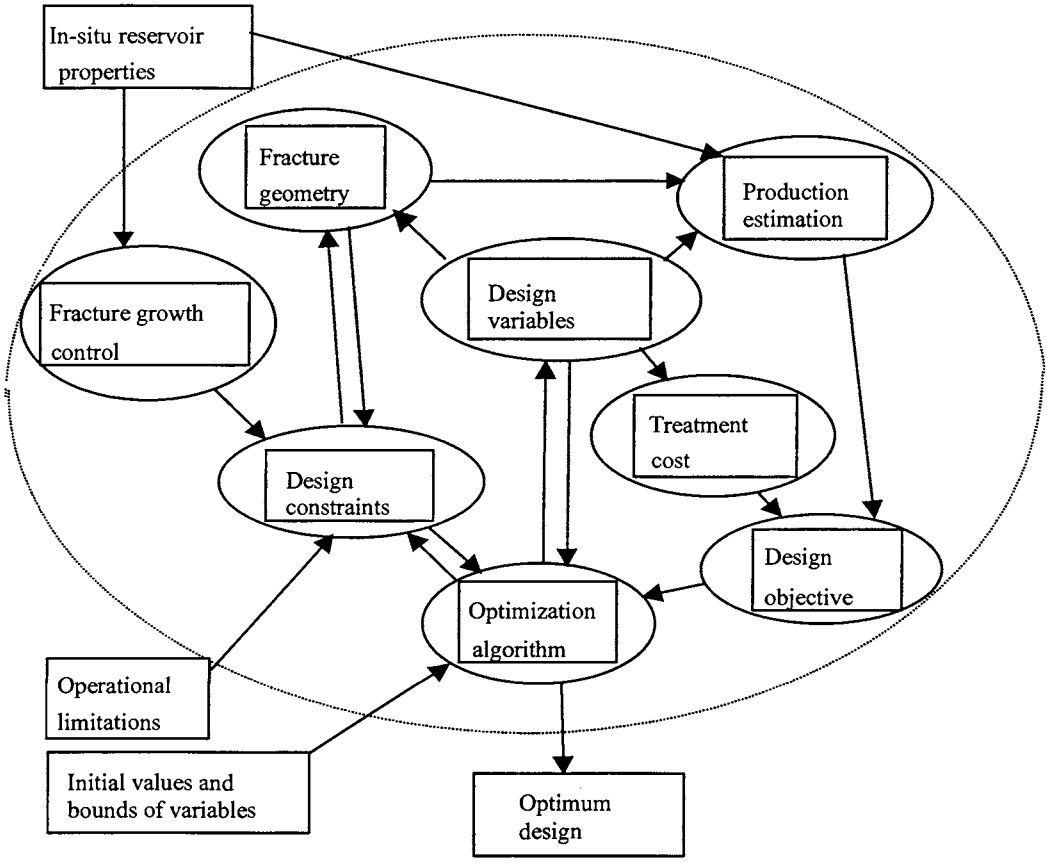

Figure 1.1. Integrated model of hydraulic fracturing design optimisation.

Fracturing fluid viscosity

The fracturing fluid viscosity is an important controllable parameter which influences the fracture growth, proppant transport, leakoff and proppant-pack permeability damage. Variation in viscosity over time is highly desirable for improved treatment efficiency. A highly viscous fluid creates a wider fracture and is better for transporting propping agents. However, it results in a higher treating pressure plus potentially undesired vertical height growth (Meng and Brown, 1987). Therefore, an ideal fluid has a low viscosity in the tubular to reduce the friction pressure and the required treating pressure.

After the fluid enters the fracture, the viscosity should have a high value to cause a larger fracture width and better proppant transport. However, after the treatment, the viscosity must be reduced considerably for efficient flow of produced hydrocarbon. These contradictory viscosity requirements are ensured by appropriate design of fracturing fluid (Brown and Economides, 1992). In this work, the viscosity of fracturing fluid refers to the viscosity in the fracture. While the fracturing fluid has strong influence on the dynamic fracture geometry and the propped geometry, it has also a weak relationship with the treatment cost through its price variation as a function of viscosity. Such a relationship has been developed based on regression analysis of industry data and is used in this study to obtain an optimum fluid viscosity. The fluid viscosity is selected for a fracturing job in the industry based on various considerations and it has never been optimised as a variable in previous research works. This work has taken a novel approach to optimise the fracturing fluid viscosity as a free design variable.

Proppant concentration

Proppant concentration determines the final propped fracture penetration and conductivity. Fracture permeability is a function of the proppant size/type, the proppant concentration and the residual damage to the fracture from the treatment fluids used. An optimum value of the end of the job (EOJ) proppant concentration is sought in this study for a given proppant type/size. The proppant concentration and its scheduling over the treatment period is related with pad volume and slurry volume, using the method proposed by Nolte (1986), detailed in chapter 3.

Injection rate

In general, a higher injection rate yields a larger fracture with greater width but may not yield the most efficient treatment. This is because the higher injection rate results in higher treating pressure and higher surface pressure. The high treating pressure may exceed the formation critical pressure and thus induce uneconomic fracture growth whereas the high surface pressure may damage the surface equipment. Moreover, the pipe friction and shear degradation of the fluid are critical to high injection rate. In

determining an optimum value of injection rate, these issues need to be taken into account.

Injection time

The injection of proppant-laden fracturing fluid over a period of time is essential to fracture the formation to an adequate size for desirable production. However, any prolonged injection would induce unnecessary fracture growth and thus incur additional treatment cost. Therefore, an optimum injection time is sought as a function of injection rate and other parameters.

Fracture half-length

Fracture length is an important dependent variable, which is mathematically related to fracture width and the fracture height. For a contained reservoir, the achieved half-length depends on the size of job pumped; the larger the job the greater the penetration (Rimmer *et al.*, 2000). For uncontrolled fracture height growth, fracture half-length becomes smaller meaning less penetration. The fracture penetration needed to achieve desired production depends on the reservoir permeability. Deeply penetrating fractures are usually recommended for low-permeability wells, but the incremental improvement on well production diminishes with length because the dimensionless fracture conductivity decreases with increasing length. Thus, a balance between fracture characteristics and reservoir properties must be achieved to optimise the reservoir deliverability (Meng and Brown, 1987). The fracture half-length is modelled as a free design variable in this study, and its dependency on other parameters is maintained through coupling relationships between fracture geometry and treatment parameters.

1.4.2. Bounds of design variables and initial values

Bounds of variables are also called bound constraints in optimisation terminology. Each variable has a lower bound and an upper bound. The designer should specify the bound values based on industry practices, practical considerations and other analytical means. The proposed model needs starting values of the variables within their respective bound

values to initiate the program. The optimum value of each variable is obtained within its bound values.

1.4.3. In-situ reservoir properties

In-situ reservoir properties strongly influence the hydraulic fracture growth and production from the fractured reservoir. The formation critical pressure and in-situ stresses influence the fracture growth and therefore a fracture growth control strategy is developed in terms of these properties to ensure formation compatible fracture growth, as discussed later. The initial permeability of the reservoir has a strong influence on the fluid flow behaviour and production from the reservoir.

1.4.4. Fracture geometry

The fracture geometry is defined by length, height and width of a fracture, and is assumed to develop as a function of stimulation parameters: fracturing fluid viscosity, injection rate and injection time. In the literature, various models are available to define the growth of fracture geometry as a function of stimulation parameters: two-dimensional (2D), pseudo-three-dimensional (P-3D) and fully three-dimensional (3D) models. A fully 3D model is computationally intensive (Hossain, 2001) and not suitable for incorporation in a design optimisation scheme, such as the proposed one, that involves a large number of repeating calculations. In order to idealize fracture growth in multi-layered formations, pseudo-three-dimensional (P-3D) models are proposed (Rahim and Holditch, 1995). If the pay zone does not include multi-layered formations, a 2D fracture model can be used for hydraulic fracturing optimisation. Both 2D and P-3D models have been used for hydraulic fracturing design optimisation in this thesis.

1.4.5. Design constraints

Fracture growth control requirements and operational limitations are two types of design constraints formulated in this work.

Fracture growth control requirements

Although the primary objective of a hydraulic fracturing program is to create a massive fracture for production enhancement, uncontrolled fracture growth may not only be uneconomic but also may decrease reservoir productivity. Therefore, an appropriate fracture growth control strategy should be an integral part of a fracturing design optimisation scheme. The fracture height growth is usually influenced by the stress contrast between the pay zone and the bounding layers. A fracture height migrating to the bounding layers (non-productive) with a large extent is not desirable from the production point of view. Similarly, initiation of multiple fractures and unnecessary loss of fracturing fluids are not desirable. To integrate these considerations into design optimisation, certain design constraints are formulated mathematically. Formation damage due to failure of near-wellbore perforation tunnels and resulting sand production is also formulated and constrained during design optimisation.

Operational limitations

An arbitrarily designed hydraulic fracturing program may not be possible to execute in the field due to the limitations of surface equipment and downhole tubing available. Hiring of new machineries with sufficient capacities incurs cost, which can easily be avoided if the fracturing program is designed satisfying the capacities of available machineries. Note that an optimum design compromised with equipment capacities is not necessarily inferior to an arbitrary design requiring higher equipment capacities. To achieve a design within the capacities of available surface equipment and downhole tubing, a computational scheme should be integrated to ensure that the required pump capacity and the developed pressures at the surface and in the downhole tube are less than of the pump capacity, the rated pressure of the surface equipment and the burst strength of the downhole tube, respectively. For this purpose, formulations have been developed to estimate the required pump capacity and developed pressures as functions of fracture geometry and treatment parameters appropriately accounting for hydrostatic and dynamic aspects of fracturing fluid. Design constraints are then formulated in the optimisation model to ensure that the optimum design is obtained by satisfying these

constraints, and thus the optimised treatment can certainly be executed using the specified equipment.

1.4.6. Production estimation

Production from a hydraulically fractured well can be predicted as a function of the propped fracture geometry and the in-situ reservoir properties. The final propped geometry depends on the closure stress and the values of stimulation parameters used during treatment. Thus the well production is, in turn, a function of stimulation parameters. The production performance from a fractured well also depends on the flow behaviour of hydrocarbon through a formation. The flow behaviour is, in turn, controlled by some of the in-situ properties, such as the initial reservoir permeability. Using such complex inter-relationships, a predictive model can be developed for production estimation. In order to develop a realistic predictive model, an appropriate fluid flow behaviour is defined by assessing the reservoir type, size, drainage area and other petrophysical properties. The formulations of production models are described in more detail in chapter 4.

1.4.7. Treatment cost

The cost associated with the execution of a hydraulic fracture treatment program is a direct function of the total volume of the fracturing fluid injected, the type of fracturing fluid and the total weight of proppant used. The total volume of fracturing fluid injected is the product of injection rate and injection time. A regressive relationship between fluid price and viscosity has been established in this study, based on industry data, to reflect the cost dependency of fracturing fluid in its viscosity optimisation. The total weight of proppant used can be calculated from proppant concentration and fluid volume. A fraction of fixed cost (not a function of treatment parameters) is also included to cover equipment hire and other expenses incurred during treatment. The formulation of total treatment cost is given in chapter 5.

1.4.8. Design objective

As mentioned earlier, it is necessary to consider a design objective to assess a design. The net present value, NPV, is usually used as a design objective for hydraulic fracturing treatment optimisation. NPV is calculated as discounted revenue from production during a number of years, minus the treatment cost. Although a maximum NPV design implicitly sets a target to minimise the treatment cost, it is observed that such a design heavily favours production maximisation to the limit of mathematically diminishing benefit in NPV, incurring a high treatment cost. From a practical point of view, improvement in NPV up to its absolute maximum may not be attractive if significant saving in the treatment cost can be achieved by marginal sacrifice of NPV. Therefore, depending on the company's current financial standing, it may be necessary to assign an explicit priority to minimise the treatment cost, compromising a certain percentage of production/NPV. The design for acceptable treatment cost can only be found by studying appropriate trade-offs between production/NPV and treatment cost. Also it may be necessary to design a treatment to meet a production target under certain circumstances. These issues require the overall design objective to be defined as a function of a number of individual design objectives (e.g. production, treatment cost, NPV) for assessing a design. The overall design objective is formulated by combining different individual functions in many design optimisation literatures. The multiobjective function for hydraulic fracturing optimisation has been formulated keeping an option to assign priorities and to achieve target values for individual design objectives.

1.4.9. Optimisation algorithm

It is evident from the foregoing sections that the hydraulic fracturing design optimisation problem involves finding the values of a number of stimulation parameters (at least the listed four) which would be able to create an appropriate fracture geometry (length, height, width). These parameters must satisfy the operational limitations and fracture growth control requirements, and improve the specified objective function as much as possible. These requirements are within the framework of various industrial design

optimisation problems, which are usually modeled in terms of a number of design variables, design constraints and design objectives. They are then solved using a procedural optimisation algorithm. The general structure to describe an optimisation problem is as follows:

$$\min_{\{x_1, x_2, \ldots, x_N\}} f(x_1, x_2, \ldots, x_N) \tag{1.1}$$

subject to

$$\left.\begin{array}{l} g_1(x_1, x_2, \ldots, x_N) \le b_1 \\ \quad \vdots \\ g_M(x_1, x_2, \ldots, x_N) \le b_M \end{array}\right\} \tag{1.2}$$

$$x_1 \ge 0, \ldots\ldots, x_N \ge 0 \tag{1.3}$$

This formulation also covers maximisation by replacing f by $-f$. Thus, the problem is determining the values of x_1, x_2, ..., x_N, known as decision or free variables, in the feasible region bounded by the constraints (Eqs 1.2 and 1.3) which minimizes the objective function $f(x_1, x_2, \ldots, x_N)$. Different variations of constraints (Eqs 1.2 and 1.3) can be written. However, various optimisation methods have various capabilities to handle certain features of optimisation problems. The method used in this thesis is developed based on the combined features of Genetic Algorithm and Evolutionary Operation. It can handle continuous, discrete and integer design variables; continuous, discontinuous, linear, nonlinear, differentiable, nondifferentiable, equality and inequality design constraints and single and multiple design objectives. These strengths has made the optimisation algorithm specially suitable for hydraulic fracturing design optimisation which involves highly nonlinear and nondifferentiable design constraints with certain degree of discontinuity due to frequent use of bi-section method and the

complementary error function to evaluate the constraints. All the design variables are considered as continuous and constraints are formulated as inequality constraints.

1.5. Outlines of the thesis

Since the hydraulic fracturing design model is formulated within the framework of an optimisation algorithm, various optimisation methods and multiobjective formulations are reviewed first in chapter 2, and also the details of an optimisation algorithm used in this thesis are presented. The algorithm is also validated in this chapter by applying it to several example problems and comparing results with their known solutions.

Chapter 3 provides a review of 2D and 3D fracture models for prediction of fracture geometry. A 2D PKN-C and a P-3D have been presented with their detailed formulations for the purpose of using them in the current work. The P-3D model has been improved by incorporating Carter solution of material balance. Fracture geometry and other parameters predicted by both models have been analysed and compared.

Chapter 4 describes the requirement of a suitable model for production estimation from hydraulically fractured reservoirs in the context of hydraulic fracture treatment optimisation. Different models with various flow conditions have been reviewed. A hybrid production model has been developed in this chapter, combining transient and pseudo-steady state flow conditions particularly for a tight gas formation. The computationally efficient analytical model is verified by comparing results with that from a reservoir simulator while the same fracture geometry is simulated.

Chapter 5 describes formulation of the problem of hydraulic fracture treatment design optimisation. This includes setting up the set of design variables, specifying their bound values, formulating various design constraints and multiple design objectives. By applying the model to a tight-gas reservoir, benefits of treatment optimisation and multiobjective analysis have been investigated and presented in this chapter using both 2D and P-3D fracture models. The model has also been applied to a relatively weak-gas

formation to demonstrate its capability to control sand production due to near-wellbore mechanical failure.

Chapter 6 describes treatment programs executed in actual tight-gas reservoirs onshore Australia and resulting treatment pressure anomalies and complexities encountered. The treatment programs have been analysed using a commonly used hydraulic fracturing simulator and a high capability nonplanar hydraulic fracture analysis program to establish a number of potential scenarios that might have caused the complexities. Redesigning the fracture treatment by the proposed model and comparing with simulator's results, the inadequacy of the current option in the simulator to design treatments, which could avoid those complexities, has been indicated. Among other recommendations, the potentiality of proppant-free water-farc treatment is assessed to avoid some of the complexities.

Chapter 7 summarizes and concludes the study and recommends directions for future studies.

CHAPTER TWO

MULTIVARIATE, MULTIOBJECTIVE OPTIMISATION METHODS: REVIEW AND A PROPOSED ALGORITHM

2.1. Introduction

Many alternative solutions of an engineering design problem can be produced even when only a single parameter is allowed to vary. The number of alternative solutions increases exponentially with increasing number of variable parameters. Various environmental conditions, capability requirements, regulatory restrictions, implementation infeasibilities and practical limitations, which collectively termed as design constraints, induce the designer to exclude some of these alternative solutions from potential acceptable designs. The space within a boundary by which all the potentially acceptable designs are separated is termed 'the feasible design space' or simply 'the design space'. With reduced number of variable parameters and design constraints, selection of a 'best possible design' from the design space may be possible by exhaustive search; however, it becomes virtually impossible when they increase to a few only. The main aim of optimising the design of an engineering problem is to pick up the best possible design from the design space by a mathematically systematic approach. The engineering design problem is described mathematically by identifying its free design variables (variable parameters) and formulating design constraints and a design objective as functions of free design variables. This mathematical model is then coupled with an optimisation method, within its framework, which solves the model efficiently to find the best possible design, often called 'optimum design'. The optimality in design is measured in terms of improvement in the design objective (also called design criterion) which virtually reflects the efficiency of a design.

Perhaps, mathematicians came up initially with the basic mathematics of function minimisation. Over the last few decades, mathematicians and engineers through their joint efforts have transformed the basic function minimisation techniques into various optimisation methods. Although further works are imperative in various optimisation methods, many of them are capable of handling satisfactorily many complexities in the models of real-world problems. Real-world design in many occasions calls for capabilities that are difficult to foresee when an optimisation system is devised. However, the formulation of the problem can often be modified to suit the capabilities at the hand. In parallel, fundamental investigations into the development of design optimisation systems with enhanced generality and flexibility to function in an engineering design environment are continual efforts. Extensive use of various optimisation methods is notable in land, offshore, marine and aero structural designs, transportation network design, electrical and communication applications and in manufacturing and production scheduling. Although any similar surge of applying procedural mathematical optimisation techniques is not so noticeable in the petroleum industry, efforts for optimising various aspects of petroleum production can be traced back to the 1950s and 1960s (Aronofsky and Lee, 1958; Aronofsky and Williams, 1962; Attra *et al.*, 1961; Rowan and Warren, 1967; Bohannon, 1970; O'Dell *et al.*, 1973; Rosenwald and Green, 1974). Practices for hydraulic fracturing treatment optimisation have been reviewed in chapter 1 and a recent trend of moving towards more procedural optimisation was noticed.

2.2. Optimisation methods: a brief review

The central problem of mathematical programming is usually stated as the optimisation (in the mathematical sense of maximisation or minimisation) of a function $f(x_1, x_2, ..., x_N)$ of several variables $x_1, x_2, ..., x_N$ subject to a set of constraints.

There are voluminous literatures on various optimisation methods and their applications to linear and nonlinear problems (Pierre, 1969; Wismer, 1971; Jacoby *et al.*, 1972; Wilson *et al.*, 1981; Bunday, 1984; Polyak, 1987 to name a few). To solve linear

optimisation problems, the simplex algorithm is a powerful tool and its primal and dual applications are widely documented (Ignizio, 1982; Lee, 1972). Most industrial design problems, however, involve nonlinear objective and constraint functions. The Sequential Linear Programming (SLP) has been a good tool for solving nonlinear problems (Mistree *et al.*, 1981). This method uses linear approximations of the original nonlinear problem and solves the transformed linear problem by the simplex algorithm. The linear approximations of nonlinear functions can be made by considering either first-order or second-order terms of the Taylor series expansion. The linear approximation depends on the current point around which the approximation is made. Therefore, the approximation and the solution procedures are repeated sequentially, until the optimisation process has converged to a minimum value of the objective function.

Quadratic Programming (QP) was also introduced to solve nonlinear problems. Several approaches and numerous algorithms were proposed for solving quadratic programming problems. These include the primal methods of Beale (1959), Dantzig (1963), Fletcher (1971), Goldfarb (1972), Bunch and Kaufman (1977), Gill and Murray (1978); the dual method of Lemke (1962), Van de Panne and Whinston (1964) and Goldfarb and Idnani (1983); the principal pivoting methods of Cottle and Dantzig (1968); the parametric methods of Grigoriadis and Ritter (1969); the primal-dual method of Goncalves (1972) and the subproblem optimisation method of Theil and Van de panne (1960). Like SLP, the sequential applications of QP to enhance its solution capability of higher-order nonlinear problems led to the development of Sequential Quadratic Programming (SQP) techniques (Powell, 1978; Gurwitz and Overton, 1989; Heinz and Spellucci, 1994; Murray and Prieto, 1995; Spellucci, 1998).

Other classical methods for continuous variable optimisation include mathematical programming, geometric programming, optimality criteria and augmented Lagrangian methods.

Mathematical programming methods are the classical techniques of optimisation, as applied to nonlinear programming. These methods are broadly classified by the way in which the mathematical functions are treated and by the choice of search techniques. The Steepest Descent algorithm (Gabay and Luenberger, 1976), in which the constraints of the problem are treated explicitly; and Sequential Unconstraint Minimisation Technique (SUMT) or Penalty Function method (Haftka and Starnes Jr., 1975), in which the constraints are combined with the objective function to form an unconstrained problem are well-known examples of classical nonlinear programming. Fox (1971) and Rao(1984) are notable early publications on classical nonlinear constrained optimisation techniques.

Peterson (1976) summarized the art of geometric programming. This method is suitable for problems having nonlinear inequality constraints. The problems are formulated using 'posynomial', i.e. polynomial which consists of groups of terms having a positive constant multiplied by a product of positive variables with each variable raised to an arbitrary power. Dembo (1976) demonstrated the solution capability of geometric programming applying it to a number of test problems. Morris (1972) developed a method of approximation to circumvent the difficulty with problems which are not directly amenable to the posynomial form.

The Optimality Criteria (OC) method is an indirect optimisation technique in which the optimum design is defined as a solution that satisfies a set of *a priori* conditions or criteria. There is no explicit design objective function; rather, the optimum design is taken as the combination of variable values which maximises the system efficiency. Berke and Venkayya (1974) and Khot *et al.* (1976) applied this method to weight minimisation in structural design. Convergence of the OC method is generally rapid and the number of redesign cycles is largely independent of the number of design variables.

Augmented Lagrangian methods (Pierre and Lowe, 1975), which are also called multiplier or dual methods, are also found promising for some applications. The numerical instability possessed by the conventional penalty function methods is

circumvented by the augmented Lagrangian methods using both penalty and Lagrangian functions to form a modified objective function. The interior-exterior penalty function is incorporated to handle problems with both equality and inequality constraints.

Most of the methods discussed above were invented by mathematicians based on classical differential calculus, and they inherit the assumptions of continuous differentiability, availability of gradient vectors and existence of second derivatives. For problems with differentiable smooth functions, these derivative based methods are reliable and computationally efficient. Many real-world engineering design problems, however, involve discontinuous and non-differentiable functions, design variables requiring a combination of continuous, integer and discrete values and conflicting multiple design objectives. The difficulty of non-differentiability in using the methods is attempted to overcome by various numerical differentiation techniques with various degrees of accuracy. In parallel, attentions have been focused to develop alternative algorithms, particularly direct search methods, by manipulating basic mathematics of optimisation methods. Some examples include normal-boundary intersection algorithm (NBI) (Das and Dennis, 1998), genetic algorithms (GA) (Goldberg, 1989; Wu and Chow, 1995; Ndiritu and Daniell, 1999), polytope algorithm (PA) (Nelder and Mead, 1965), entropy algorithms (Jaynes, 1957; Templeman, 1993; Kapur, 1989; Das *et al.* 1999) and evolutionary operation (EVOP) (Ghani, 1989; Marcelin, 1999). Direct search methods, such as GA, PA and EVOP are generally slow in convergence but are successful to find reliable optimum solutions of problems having high degree of various noises including discontinuity and non-differentiability in functions. Rasmussen and Lund (1997) addressed the issue of generality in design optimisation systems, and Lewis and Mistree (1998) reviewed various issues and applications of Multidisciplinary Design Optimisation (MDO).

2.3. The proposed optimisation algorithm, INTEMOB

The objective and constraint functions involved with hydraulic fracturing optimisation are highly non-linear and non-differentiable. These functions are also subjected to a

certain number of discontinuities. These include the production estimation function which is discontinuous at the transition of transient and pseudo-steady-state flow regimes and numerically unstable sub-functions, such as the complementary error function, bi-section solution, etc. Initial attempts were made to solve the problem using a number of derivative based algorithms including SLP (Rahman, 1998), SQP (Spellucci, 1998) and MATLAB routines with their in-built numerical differentiation features. With exhaustive efforts for noise reduction, it was possible to obtain optimum solutions for maximum NPV. When attempted with other design objectives, the success was very limited and unreliable. Finally, a direct search based algorithm was developed combining the major features of genetic algorithm and evolutionary operation. This new algorithm is called in this thesis an INTElligent Moving OBject (INTEMOB) algorithm, because it finds optimum solution by generating and moving an object (called 'compound') using 'intelligence' more than mathematics.

General formulations of INTEMOB can be expressed as:

Find

$$\underline{x}^{\mathrm{T}} = \{x_1, x_2, .., x_i, ..., x_N\} \tag{2.1}$$

subject to bound constraints

$$\left.\begin{array}{l} l_1 \le x_1 \le u_1 \\ . \quad . \quad . \\ . \quad . \quad . \\ l_N \le x_N \le u_N \end{array}\right\} \tag{2.2}$$

and design constraints

$$\left.\begin{array}{l} C_{l1} \le C_1(\underline{x}) \le C_{u1} \\ \cdot \quad \cdot \quad \cdot \\ \cdot \quad \cdot \quad \cdot \\ C_{lM} \le C_M(\underline{x}) \le C_{uM} \end{array}\right\} \tag{2.3}$$

to minimize

$$Z = f(\underline{x}) \tag{2.4}$$

where, $\underline{x}$ represents the vector of free design variables (the superscript 'T' for transpose); l_i's and u_i's are constants or functions of $\underline{x}$ (in the latter case the bound constraints constitute moving boundaries) representing the ranges of x_i's; C_{li}'s and C_{ui}'s are constants or functions of $\underline{x}$ representing the acceptable ranges of design constraints, $C_i(\underline{x})$'s; N is the total number of free design variables and M is the total number of design constraints.

2.3.1. INTEMOB solution procedure

The solution procedure of INTEMOB includes six major steps: (1) generation of 'vertices' and formation of a compound; (2) conditioning the worst vertex of a compound; (3) testing for collapse of a compound; (4) dealing with a collapsed compound; (5) moving a compound and (6) terminating the process by convergence tests.

2.3.1.1. Generating vertices and forming a compound

The optimisation procedure starts with an initial vertex (point, design) in the N-dimensional space bounded by the ranges of design variables, as shown in Figure 2.1 in a two-dimensional space for the convenience of description. Straight lines (l_1, u_1 and l_2, u_2) parallel to the co-ordinate axes represent the lower and upper bounds on variables, x_1 and x_2, respectively. Curved lines C_{l1} and C_{u1} represents the lower and upper bounds, respectively, on design constraint 1, $C_1(\underline{x})$, and C_{l2} and C_{u2} on design constraint 2, $C_2(\underline{x})$.

Certainly, there could be more than these two design constraints and their lower and upper bounds. The area along the hatched direction is the two-dimensional feasible search space. The initial vertex must be within the variable bounds, and may or may not satisfy the design constraints. If the initial vertex does not satisfy any of the design constraints (i.e. not within the hatched area), a random vertex is generated. If the random vertex is still in the infeasible region, the distance between theses two vertices is estimated and the generated vertex is moved stepwise halftimes the distance each time along the straight line with these two vertices until the vertex satisfies all the design constraints. If the positive step-length moves the vertex away from the unsatisfied design constraint bound(s), a negative step-length is used. The vertex 'a' is either an initial feasible vertex, or a vertex moved from its initial infeasible location. The coordinates of a random vertex are generated by:

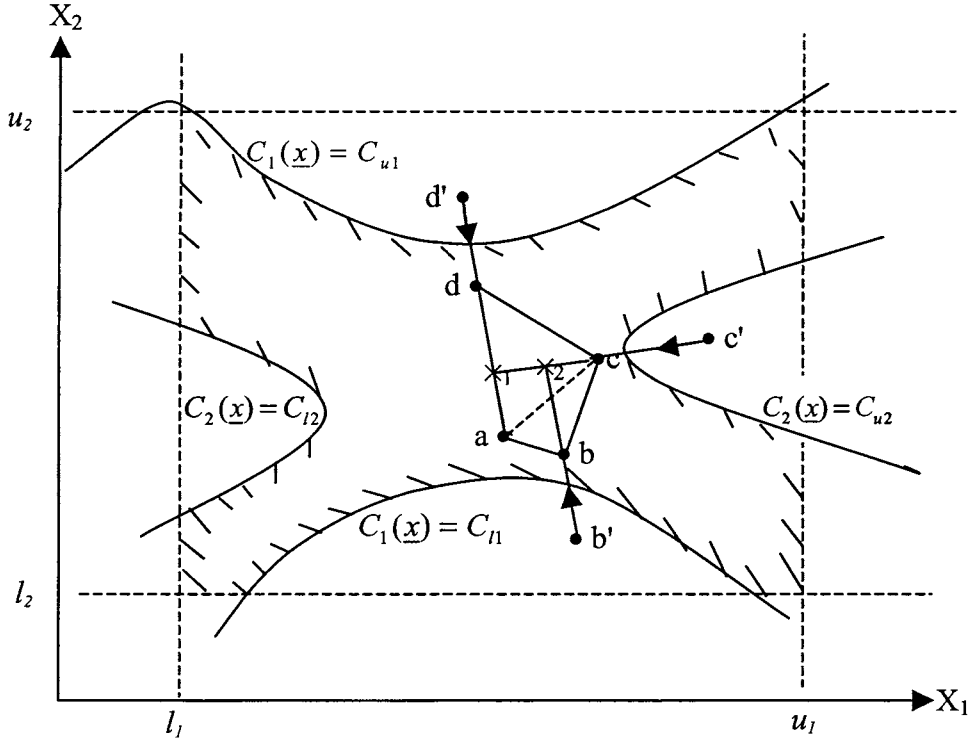

Figure 2.1. Generation of the initial compound with four vertices.

$$x_i = l_i + r_i(u_i - l_i); \qquad i = 1, \ldots\ldots, N \tag{2.5}$$

The pseudo-random deviate r_i rectangularly distributes over the interval (0, 1) and is controlled by the known value, x_{in} for the i-th coordinate of the initial vertex.

Executing Eq. 2.5 K-1 times, further K-1 different random points are generated, where $K = 2N$ for $N \leq 5$ and $K = N + 1$ for $N > 5$. Eq. 2.5 itself ensures that the randomly generated points remain in the space bounded by the ranges of variables defined by Eq. 2.2. However, any of the generated points may initially violate any of the design constraints defined by Eq. 2.3 and therefore a technique, better than described above, is required to move such points towards satisfying Eq. 2.3. The four vertices for two-dimensional space ($2N$) a, b', c' and d' are shown (Figure 2.1). Obviously, vertices b', c' and d' violate Eq. 2.3. These vertices are modified in the order of d', c' and b' by moving successively towards the centriod, $\underline{c}$ by:

$$\underline{x} = \frac{1}{2}(\underline{c} + \underline{x'}) \tag{2.6}$$

until the new point, $\underline{x}$ satisfies Eq. 2.3. The coordinates of the cenrtriod, $\underline{c}$ are calculated using vertices that have already satisfied Eq. 2.3 as follows:

$$c_i = \frac{1}{n}\sum_{i=1}^{n} x_i \tag{2.7}$$

where n is the number of vertices which have already satisfied Eq. 2.3.

The modified points are a, b, c and d which satisfy both Eqs. 2.2 and 2.3. These four feasible vertices comprise an object called 'compound' abcd, as shown in Figure 2.1. The values of the objective function, f(a), f(b), f(c) and f(d) at these four vertices are

calculated and assumed to be in the order of $f(a)<f(b)<f(c)<f(d)$. If the initial notations of vertices do not satisfy this order, vertices are re-denoted according to this order.

For a convex feasible parameter space the above method for moving an infeasible vertex to the feasible space would, without fail, succeed in generating a compound with K vertices. If the parameter space is nonconvex, and the centroid happens to lie in the infeasible area, there is every chance that a compound can not be generated. Figure 2.2 shows such a possibility. Three vertices a, b and c in the feasible parameter space have already been generated. In order to generate the fourth feasible vertex a trial point, T_1 satisfying the variable bounds is created. However, T_1 is infeasible as it violates a design constraint. In order to make T_1 feasible it is continually moved halfway towards the centroid, X. Since the centroid itself is infeasible no amount of such moves would make T_1 feasible, and a compound with four vertices can never be generated. Safeguard against such a possibility is never to allow an infeasible centroid. If a new feasible vertex results in the new centroid to lie in the infeasible area, that new vertex is discarded, and another generated until a feasible centroid is obtained.

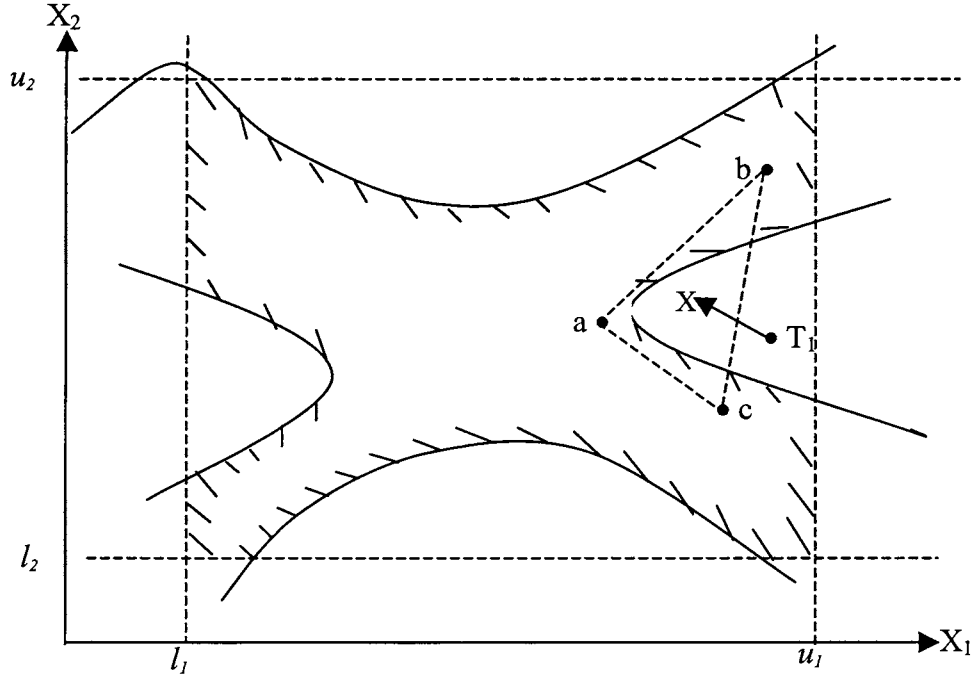

Figure 2.2. A compound with four vertices 'a, b, c, d' can not be generated.

2.3.1.2. Conditioning the worst vertex of a compound

In the context of minimising an objective function, the worst vertex in a compound is one that gives the highest value of the objective function. This vertex must be improved by over-reflecting on the centroid (reflection will be described later). If the search space is non-convex, there is a possibility that the compound would collapse during conditioning by over-reflection. For example, referring to Figure 2.3, the worst point, d is reflected over the centroid, X to create a trial point, T_1 which violates a design constraint. Since the centroid itself is in the infeasible region, repeated movement of point, T_1 halfway towards the centroid would result in collapse of the point on the centroid. The new compound has now three vertices a, b and c. One more such collapse would result in complete collapse of the compound, because an object with two vertices can not span a two dimensional space, because a space of N dimensions can only be spanned by $N+1$ vertices.

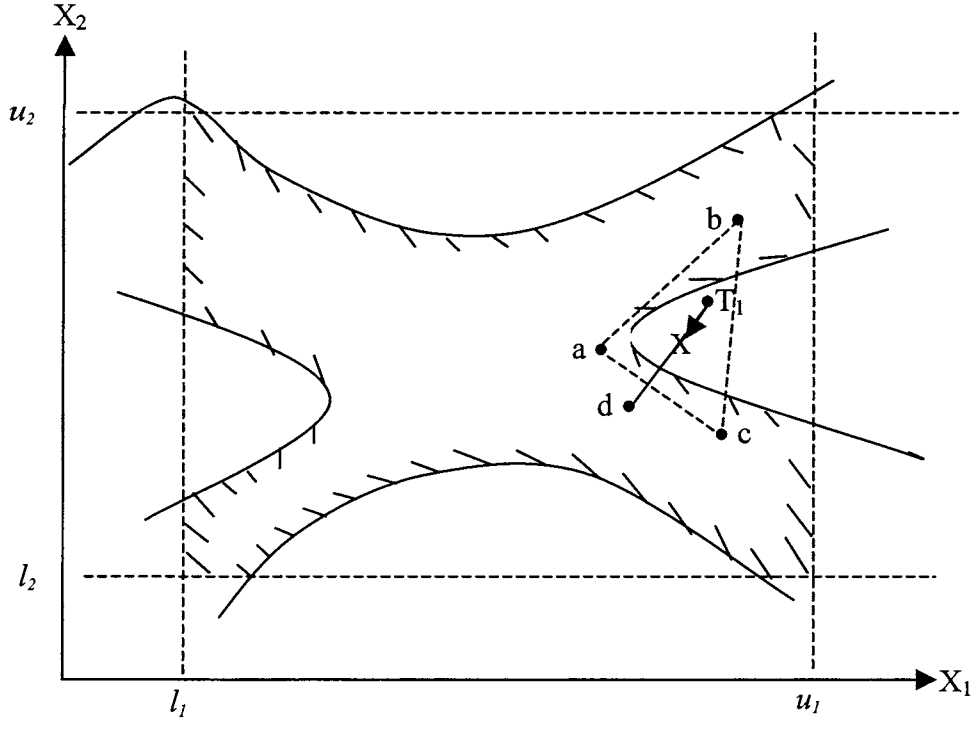

Figure 2.3. The possibility of collapse of a trial point onto the centriod.

Such a problem in an N-dimensional space can be overcome as follows:

1. The compound vertices having highest, second highest and lowest objective function values are identified, and numbered by integers 'nh', 'nm' and 'nl', respectively. Next the centroid of all vertices except 'nh' is calculated, and its feasibility is verified.

2. If the centroid is feasible, the steps below here are not necessary and the process then passes on to the next step which is testing for collapse of a compound. Otherwise, continue from (3) below.

3. Vertex 'nm' is excluded, and the centroid of all other vertices is calculated (i.e. excluding vertices 'nh' and 'nm').

4. If the centroid is the previous feasible centroid then continue from (5) below. Otherwise, if the centroid is infeasible a new compound of normal size is generated using vertex 'nl' as the starting point, and steps from (1) are repeated. A check is made to ascertain whether the compound is the initial one. If so, 'nl' is set to K to ensure a high probability that the starting point for the new compound is well inside the feasible space. However, if the new centroid is feasible then steps from (5) below are continued.

5. Vertex 'nm' is replaced by a randomly generated feasible point.

6. The new centroid of all vertices except 'nh' is once again calculated, and its feasibility is checked.

7. If the centroid is feasible the function value at the newly generated vertex 'nm' is calculated, and steps from (1) are repeated. Otherwise, steps from (3) are repeated.

2.3.1.3. Testing for collapse of a compound

A compound is said to have collapsed in a subspace if the absolute difference between the *i*-th coordinate of the compound centroid and that of all *K* vertices becomes less than a specified value. This is a sufficiency condition and detects collapse of a compound when it lies parallel along a coordinate axis. Once a compound has collapsed to a subspace it can never again be able to span the original space.

A resolution factor, φ_{cpx} is used to specify the value of the difference of a coordinate of the centroid and that of all vertices of the compound, below which value the compound is considered collapsed. For example, if the value of *i-th* coordinate of compound centroid is v_1 and the farthest value of that coordinate among the vertices of that compound is v_2, the compound will be considered to collapse if v_1 and $(v_1 + \varphi_{cpx} \times v_2)$ are identical within the resolution of φ_{cpx}. If φ_{cpx} is set to 10^{-1}, the compound is considered collapsed if v_1 and v_2 differ at the most by the least significant digit. If φ_{cpx} is set to 10^{-2}, the compound is considered collapsed if v_1 and v_2 differ by not more than the last two significant digits. Its value is, however, used much finer, typically 10^{-11} for double precision computation.

Figure 2.4 shows a compound with vertices a, *b*, *c* and *d* and centroid, *X*, which has collapsed to virtually a one-dimensional line. The x_2 coordinates of all vertices and the centroid are identical within the resolution of φ_{cpx}. As can be seen, the vertices of the compound can now move only along the x_1 coordinate direction.

2.3.1.4. Dealing with a collapsed compound

On detecting the collapse of a compound the following actions are taken:

1. If the compound has collapsed for the first time the coordinates of the centroid are stored.

2. Another compound is generated with vertex 'nl' as the starting point.

3. If the compound has collapsed consecutively more than once, the centroid of the currently collapsed compound is adjusted as $\underline{c} = \underline{c1} + 10\varphi_{cpx}(\underline{cc} - \underline{c1})$ in which $\underline{c1}$ is the centroid of the first collapsed compound and $\underline{cc}$ is the centroid of the currently collapsed compound. The distance between the centroid of the first collapsed compound and this adjusted centroid is calculated.

4. If this distance is zero, a compound of normal size is generated with vertex 'nl' as the starting point, and no further testing for collapse of compound is carried out.

5. Otherwise, whether the compound has collapsed consecutively for the second time is determined. If so, the objective function value f_o at the centroid of the first collapsed compound is calculated.

6. The function value f_c at the centroid of the currently collapsed compound is calculated.

7. If $f_c < f_o$, the centroid of the first collapsed compound is over-reflected on the centroid of the currently collapsed compound.

8. Otherwise, compounds are continuously regenerated on each consecutive collapse using 'nl' as the starting point, and steps from (6) above are repeated.

2.3.1.5. Moving a compound

As mentioned earlier, a compound is moved by shifting its worst vertex in this algorithm to lead the search process towards an optimum location in the feasible space. The movement process begins by over-reflecting the worst vertex 'nh' of a compound on the feasible centroid of the remaining vertices. This over-reflection generates a new trial point $\underline{x}_t$:

$$\underline{x}_t = (1.+\alpha)\underline{c} - \alpha \underline{x}_{nh} \tag{2.8}$$

where α is the reflection coefficient in the range of 1.0 to 2.0 and the vector $\underline{x}_{nh}$ contains the coordinate values of vertex 'nh'. If a coordinate value of the trial point violates its any of the bounds, that coordinate is just shifted inside the violated bound by a small distance, i.e. $x_a = x_b \pm \delta$, where x_a is the adjusted coordinate, x_b is the bound value violated by that coordinate, and δ is a very small value (added when the lower bound is violated and subtracted when the upper bound is violated), 10^{-12} is used for double precision computation. If any design constraint is violated, the trial point is repeatedly moved halfway towards the centroid of the rest of the vertices (i.e. excluding the vertex 'nh' and the trial point $\underline{x}_t$) in the compound until the constraint is satisfied. The new trial point that satisfies all the variable bounds and design constraints is called feasible trial point, $\underline{x}_{ft}$.

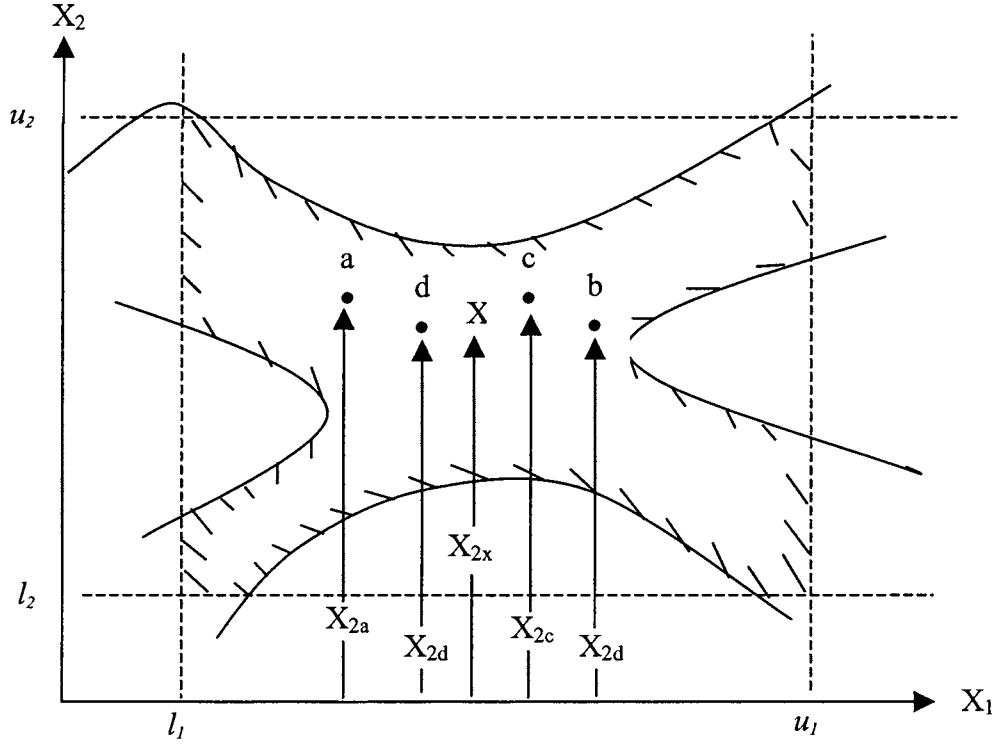

Figure 2.4. Collapse of a compound to a one-dimensional subspace.

The function value at the feasible trial point, $\underline{x}_{ft}$ is next evaluated. The reflection step is considered successful if the objective function value at this new trial point is lower than that at vertex 'nm'. The current vertex 'nh' is then deleted and the vertex 'nm' is redefined as vertex 'nh' and the successful trial point as vertex 'nm' to form a new and superior compound. If, however, the objective function value at the trial point is greater than that at vertex 'nm' of the current compound, the trial point would still be the worst vertex in the new compound. The reflection step is, therefore, considered unsuccessful and a contraction step is applied. Depending on the outcome of current over-reflection, any of the following three contraction schemes is applied.

If $f(\underline{x}_{nm}) \leq f(\underline{x}_{ft}) < f(\underline{x}_{nh})$, the trial point suffers from excessive over-reflection, and the coordinates of a new trial point $\underline{x}$ is generated as:

$$\underline{x} = (1.+\beta)\underline{c} - \beta\underline{x}_{nh} \tag{2.9}$$

If $f(\underline{x}_{ft}) \geq f(\underline{x}_{nh})$, the coordinates of the new trial point are estimated as:

$$\underline{x} = \beta\underline{x}_{nh} + (1.-\beta)\underline{c} \tag{2.10}$$

In Eqs. 2.9 and 2.10, the range of β is 0.0 to 1.0. The third type of contraction is generation of a small compound using vertex 'nl' as the starting point. This type of contraction is applied only after first and second types of contraction (Eq. 2.9 and 2.10, respectively) have been previously applied consecutively for more than $2K$ times.

Figure 2.5 explains the first type of contraction for the two-dimensional example. The worst vertex, d of the current compound 'abcd' is over-reflected on the feasible centroid, X of 'abc'. The trial point, T_1 so obtained is moved just inside the variable bound to T_2 as $x_2 = l_2 + \delta$, which still violates a design constraint. T_2 is moved towards the centroid, X according to half-step procedure in section 2.3.1.1 along the line joining the two resulting in a completely feasible trial point, T_3. Function value at T_3 is

calculated, and found to be intermediate between the second highest function value at vertex, c, and the highest function value at vertex, d. If the vertex, d is replaced by the feasible trial point, T_3 to form a new compound '$abcT_3$', then T_3 would be the worst vertex in the new compound, and thus no real improvement is achieved in the compound. The reflection step is, therefore, considered unsuccessful, point T_3 is rejected, and the first type of contraction (Eq. 2.9) is applied. Due to this contraction, the worst vertex, d is now under-reflected on the feasible centroid, X to T_4. Since the trial point, T_4 violates a design constraint it is moved halfway towards the centroid to T_5. The trial point, T_5 is feasible, and replaces the worst vertex, d to form a new complex '$abcT_5$'.

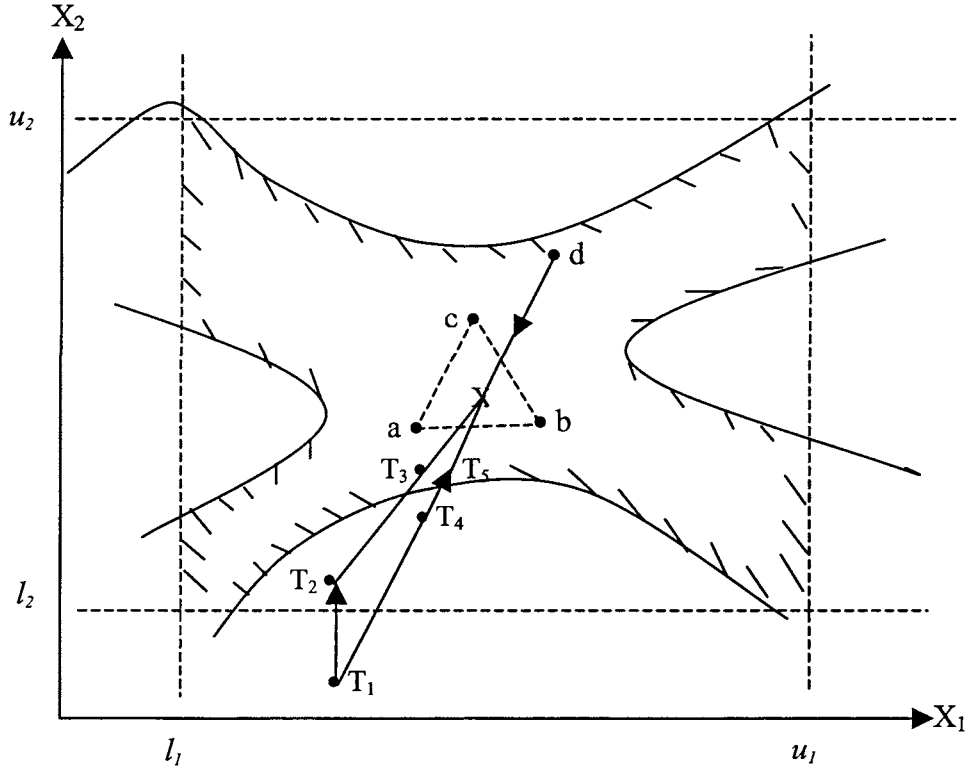

Figure 2.5. Unsuccessful over-reflection and application of first type of contraction.

If the second type of contraction was necessary to apply, the trial point, T_4 would be closer to vertex, d, then it has been for the first type of contraction. Then the movement of this point, if it were in the infeasible region, to the feasible space would be similar.

If on over-reflection the trial point has not violated any constraints (i.e. $\underline{x}_t$ and $\underline{x}_{ft}$ are identical without any movement), and has an objective function value lower than the lowest function value at vertex 'nl' of the current compound (i.e. $f(\underline{x}_t) < f(\underline{x}_{nl})$), and the previous action was not contraction by any of the three schemes, this over-reflection is considered over-successful. An expansion attempt is then taken to generate a new trial point further away from the feasible centroid along the same straight line used for over-reflection. The co-ordinates of this expanded trial point is given by:

$$\underline{x}_e = \gamma \underline{x}_t + (1.-\gamma)\underline{c} \tag{2.11}$$

The usual range of γ is 1.0-3.0. Feasibility of this expanded trial point, $\underline{x}_e$ is next checked. If any of variable bounds or design constraints is violated, the expansion attempt is considered unsuccessful, and a new compound is formed with the over-reflected feasible trial point $\underline{x}_t$ that replaces the worst vertex 'nh' of the current compound. Otherwise, the objective function value at $\underline{x}_e$ is evaluated. If $f(\underline{x}_e) < f(\underline{x}_t)$, the expansion attempt is considered successful. The expanded vertex, $\underline{x}_e$ then replaces the worst vertex 'nh' to form the new compound. If $f(\underline{x}_e) \geq f(\underline{x}_t)$, the expansion attempt is also considered unsuccessful. The expanded vertex, $\underline{x}_e$ is rejected and the trial point, $\underline{x}_t$ is used to form the new compound.

2.3.1.6. Terminating the process by convergence tests

While executing the process of compound movement, tests for convergence are carried out periodically after certain preset number of evaluations of the objective function. Three levels of convergence tests are conducted. The first convergence test is considered successful if a predefined number of consecutive values of the objective function are found identical within the resolution of a convergence parameter, φ. The second test for convergence verifies whether the objective function values at all vertices of the current compound are also identical within the resolution of the convergence parameter. The

second test is conducted only if the first test has succeeded. The typical value of φ for double precision computation is 10^{-10}. The value of φ_{cpx} for compound collapse detection is recommended to be a decade lower than φ (i.e. if $\varphi = 10^{-10}$ then $\varphi_{cpx} = 10^{-11}$) to avoid premature convergence.

When both the above convergence tests are successful, the current optimum point is preserved and the whole computation procedure is repeated, this time starting with the current optimum point, to verify if there are any better optimum points (e.g. multi minima). This repetition continues as long as the objective function value can be improved within the resolution of another convergence parameter. The nested three-looped convergence procedure continues as long as the objective function can be improved.

2.3.2. Dealing with equality constraints and integer/discrete variables

It is obvious that the procedure presented so far does not directly deal with equality constraints in the form of $h_j(\underline{x}) = 0$, j=1,2, ..., L in which L is the number of equality constraints. These equality constraints can, however, be satisfied by minimising an augmented objective function as:

$$f(\underline{x}, \underline{\lambda}) = f(\underline{x}) + \sum_{j=1}^{L} \lambda_j h_j(\underline{x}) \qquad (2.12)$$

where λ_j's are the weighting factors to equality constraints such that all $h_j(\underline{x})$ vanishes at the minimum of $f(\underline{x}, \underline{\lambda})$.

An integer variable is treated as continuous until a compound is formed with feasible vertices. The computation of centroid of a compound is performed using continuous (real) values of the integer variable. During over-reflection, contraction and expansion of the compound, the variable is integerised as follows:

$$\Delta x = x - x_{\text{int}}$$
$$\text{if } \Delta x < 0.5; \quad x_i = x_{\text{int}} \text{ for } x \geq 0$$
$$\text{if } \Delta x \geq 0.5; \quad x_i = x_{\text{int}} - 1 \text{ for } x < 0 \qquad (2.13)$$
$$x_i = x_{\text{int}} + 1 \text{ for } x > 0$$

where x is the continuous value of the variable to be integerised, x_{int} is integer portion of x and x_{i} is the integerised value. If x_{i} from Eq. 2.13 violates its bounds, the following adjustment is made:

If $x_{\text{i}} > x_{\text{max}}$, integerise x_{max} to x_{imax} with the same rule in Eq. 2.13 replacing all x's by x_{max}. Then,

$$\text{If } x_{\text{imax}} > x_{\text{max}};\ x_{\text{i}} = x_{\text{imax}} - 1;\ \text{else } x_{\text{i}} = x_{\text{imax}} \qquad (2.14)$$

Similarly, if $x_{\text{i}} < x_{\text{min}}$, integerise x_{min} to x_{imin} with same rule in Eq. 2.13 replacing all x's by x_{min}. Then,

$$\text{If } x_{\text{imin}} < x_{\text{min}};\ x_{\text{i}} = x_{\text{imin}} + 1;\ \text{else } x_{\text{i}} = x_{\text{imin}} \qquad (2.15)$$

It is noted that the test for compound collapse should be bypassed for optimisation problems with mixed integer and continuous variables.

A discrete variable is also initially treated as continuous, similar to an integer variable. During over-reflection, contraction and expansion of the compound, the variable is discretised as follows:

$$\text{If } f(\underline{x}_{ud}) < f(\underline{x}_{ld});\ x_d = x_{ud};\ \text{else } x_d = x_{ld} \qquad (2.16)$$

where x_{d} is the discrete value of the variable; x_{ud} is the upper discrete value closest to its continuous value, x; x_{ld} is the lower discrete value closest to x; $f(\underline{x}_{ud})$ is the objective function value with variable vector containing the upper discrete value, x_{ud} and $f(\underline{x}_{ld})$ is the objective function value with variable vector containing the lower discrete value, x_{ld}.

If x_d violates any of its bounds and/or design constraints, the closest upper or the lower discrete value will certainly satisfy such constraints and will replace the value of x_d obtained from Eq. 2.18, because they were previously satisfied by its continuous value, x. It is important to note here that, like integer variables, the compound centroid must be calculated using continuous value, x of the discrete variable and the compound collapse test must be bypassed. Also, the integerisation and/or discretisation process is performed in every movement or change of the compound.

2.3.3. Verification of the algorithm

The algorithm has been so far applied to numerous algebraic equations and complex design problems, and provided very satisfactory solutions. To minimise discussions, solutions of only two algebraic equations and two small engineering design problems will be presented here.

Algebraic problem 1

The problem is stated as (Klingman and Himmelblau, 1964):

$$\text{Minimise } f(\underline{x}) = -\exp\left\{-(x_1-1)^2 - \frac{(x_2^2-0.5)^2}{0.132}\right\} \tag{2.17}$$

subject to

$$\begin{aligned} 0.2 \le x_1 \le 2.0 \\ 0.2 \le x_2 \le 2.0 \end{aligned} \tag{2.18}$$

and

$$-10000 \le (x_1^2 + x_2^2) \le 4.0\,. \tag{2.19}$$

The algorithm correctly found its solution at the minimum, x_1 =1.0 and x_2 = 0.707.

Algebraic problem 2

This problem is stated as (Goldstein and Price, 1971):

$$\text{Minimise} f(x) = \exp\left\{\tfrac{1}{2}(x_1^2 + x_2^2 - 25)\right\}^2 + \sin^4(4x_1 - 3x_2) + \tfrac{1}{2}(2x_1 + x_2 - 10)^2 \quad (2.20)$$

The original problem was unconstrained. The following bound and design constraints were used for compatibility with the algorithm:

$$\begin{aligned} -5.0 \le x_1 \le 5.0 \\ -5.0 \le x_2 \le 5.0 \end{aligned} \quad (2.21)$$

and

$$-180.2182 \le \left\{\tfrac{1}{2}(x_1^2 + x_2^2 - 25)\right\}^2 \quad (2.22)$$

The algorithm correctly found coordinates of minimum as $x_1 = 3.0$ and $x_2 = 4.0$.

Pressure vessel design problem

The design objective is to minimize the combined cost of materials, forming and welding and also satisfy the ASME design code requirements (Ndiritu and Daniell, 1999). The four design variables are the cylindrical shell thickness x_1, the spherical head thickness x_2, the radius of the cylindrical shell x_3 and the length of the shell x_4. The shell thickness and the spherical head thickness are required to be discrete multiples of 0.0625 inches according to the available sizes of rolled steel plates while the radius of the cylindrical shell and the length of the shell are continuous variables. Mathematically, the problem can be described as:

Find

$$\underline{x} = \{x_1, x_2, x_3, x_4\}^T \tag{2.23}$$

to minimise

$$f(\underline{x}) = 0.6224x_1x_3x_4 + 1.7781x_2x_3^2 + 3.1611x_1^2x_4 + 19.84x_1^2x_3 \tag{2.24}$$

subject to bound constraints

$$\begin{aligned} &1.125 \le x_1 \le 65.0625 \\ &0.625 \le x_2 \le 64.5625 \\ &40 \le x_3 \le 80 \\ &20 \le x_4 \le 60 \end{aligned} \tag{2.25}$$

and design constraints

$$\begin{aligned} &g_1(\underline{x}) = 0.0193x_3 - x_1 \le 0 \\ &g_2(\underline{x}) = 0.00954x_3 - x_2 \le 0 \\ &g_3(\underline{x}) = 750\times1728 - \pi x_3^2 x_4 - {}^4\!/_3\,\pi x_3^3 \le 0 \end{aligned} \tag{2.26}$$

The problem was reformulated within the framework of INTEMOB and solved. The INTEMOB design is compared with published designs in Table 2.1.

Table 2.1: Optimum designs of pressure vessel by INTEMOB and other studies

Case	x_1	x_2	x_3	x_4	$f(\underline{x})$
Ndiritu and Daniell (1999)	1.125	0.625	58.2209	44.086	7202.517
Wu and Chow (1995)	1.125	0.625	58.1978	44.2930	7207.497
Sandgren (1990)	1.125	0.625	48.97	106.72	7982.5
Fu *et al.* (1991)	1.125	0.625	48.3807	111.7449	8048.619
INTEMOB	1.125	0.625	58.2367	44.0247	7204.32

Spring coil design problem

The objective of this problem is to minimise the volume of wire used to manufacture a coil compression spring. The three design variables include the number of spring coils N which is an integer variable, the winding (coil) diameter D which is a continuous variable, and the wire diameter d which is a discrete variable and has to be chosen from the discrete values listed in Table 2.2.

Table 2.2. Allowable wire diameters for spring coil

0.0090	0.0150	0.0280	0.0720	0.1620	0.2830
0.0095	0.0162	0.0320	0.0800	0.1770	0.3070
0.104	0.0173	0.0350	0.920	0.1920	0.3310
0.0118	0.0180	0.0410	0.1050	0.2070	0.3620
0.0128	0.0200	0.0470	0.1200	0.2250	0.3940
0.0132	0.0230	0.0540	0.1350	0.2440	0.4375
0.140	0.0250	0.0630	0.1480	0.2630	0.5000

The mathematical formulations of this problem are as follows (Siddall, 1982):

$$\text{Find } \underline{x} = \{x_1, x_2, x_3\}^T = \{N, D, d\}^T \tag{2.27}$$

$$\text{To minimise } f(\underline{x}) = \pi^2 x_2 x_3^2 (x_1 + 2.0)/4.0 \tag{2.28}$$

Subject to bound constraints

$$\begin{aligned} 1 &\le x_1 \le 32 \\ 0.01 &\le x_2 \le 2.00 \\ 0.0090 &\le x_3 \le 0.50 \end{aligned} \tag{2.29}$$

and design constraints

$$
\begin{aligned}
g_1(\underline{x}) &= \frac{8C_f F_{\max} x_2}{\pi x_3^3} - S \le 0 \\
g_2(\underline{x}) &= l_f - l_{\max} \le 0 \\
g_3(\underline{x}) &= d_{\min} - x_3 \le 0 \\
g_4(\underline{x}) &= x_2 + x_3 - D_{\max} \le 0 \\
g_5(\underline{x}) &= 3.0 - \frac{x_2}{x_3} \le 0 \\
g_6(\underline{x}) &= \delta_p - \delta_{pm} \le 0 \\
g_7(\underline{x}) &= \delta_p + \frac{F_{\max} - F_p}{K} + 1.05(x_1 + 2)x_3 - l_f \le 0 \\
g_8(\underline{x}) &= \delta_w - \frac{F_{\max} - F_p}{K} \le 0
\end{aligned}
\tag{2.30}
$$

where

$$
\begin{aligned}
C_f &= \frac{4(x_2/x_3) - 1}{4(x_2/x_3) - 4} - \frac{0.165 x_3}{x_2} \\
K &= \frac{G x_3^4}{8 x_1 x_2^3} \\
l_f &= \frac{F_{\max}}{K} + 1.05(x_1 + 2)x_3 \\
\delta_p &= \frac{F_p}{K}
\end{aligned}
$$

Various parameters used in the design constraints are specified as follows:

(a) the maximum working load, F_{max} = 1000.0 lb

(b) the allowable maximum shear stress, S = 189000.0 psi

(c) the maximum free length, l_{max} = 14.0 inch

(d) the minimum wire diameter, d_{min} = 0.2 inch

(e) the maximum outside diameter of spring, D_{max} = 3.0 inch

(f) the preload compression force, F_p = 300.0 lb

(g) the allowable maximum deflection under preload, δ_{pm} = 6.0 inch

(h) the deflection from preload position to maximum load position, δ_w = 1.25 inch

(i) the shear modulus of the material, G = 11.5×10^6 psi.

The problem was formulated within the framework of INTEMOB and solved. The INTEMOB design is compared with other published designs in Table 2.3.

Table 2.3. Optimum designs of coil spring

Items	**Source of optimum design**				**Type of variable**
	Sandgren (1990)	Chen and Tsao (1993)	Wu & Chow (1995)	INTEMOB	
x_1	10	9	9	9	integer
x_2	1.180701	1.2287	1.227411	1.16	continuous
x_3	0.283	0.283	0.283	0.265	discrete
$f(\underline{x})$	2.7995	2.6709	2.6681	2.205	

2.4. Multi-objective optimisation

Multi-objective optimisation is different from single objective optimisation in the definition of optimality. In most of the industrial design problems, the designer desires to optimise several conflicting objectives, such as to minimise treatment cost and to maximise production from a hydraulically fractured well. For such conflicting objective optimisation problems, one can not speak of an optimum solution point, but of a satisfying solution which is called a Pareto-optimum, or non-inferior or non-dominated solution. Therefore, any acceptable solution of such a conflicting multi-objective design problem is a Pareto-optimum design.

The general form of a multi-objective formulation is given by Duckstein (1984) for a minimisation problem having total I different objectives as

Find $\underline{x} \in X$ which minimises $f_i(\underline{x}), i = 1,2,\ldots\ldots\ldots\ldots, I$ (2.31)

where X is the subject of a finite-dimensional Euclidean space, called the feasible set and is determined by a set of constraints of the form:

$$X = \{\underline{x} \setminus \underline{x} \in R^m,\ g(\underline{x}) \leq 0,\ h(\underline{x}) = 0\} \tag{2.32}$$

R^m is a m dimensional domain, $g(\underline{x})$ and $h(\underline{x})$ are the inequality and equality constraints, respectively, defined in slightly different forms for INTEMOB.

The Pareto-optimal of the above formulation is defined by different authors (Evans, 1984; Balachandran and Gero, 1984; Koski, 1984 and Duckstein, 1984) in the following way:

"A feasible solution to a multi-objective optimisation problem is Pareto-optimal if there exists no other feasible solution that will yield an improvement in one objective without causing deterioration in at least one other objective".

Mathematically two types of Pareto-optimal solutions are defined. They are weak Pareto-optimal and strong Pareto-optimal solutions.

Weak Pareto-optimal: A point $\bar{x} \in X$ is called a weak Pareto-optimal solution if there is no $\underline{x} \in X$ such that $f_i(\underline{x}) < f_i(\bar{x})$, for $i = 1, 2, \ldots\ldots\ldots\ldots I$.

Strong Pareto-optimal: A point $\bar{x} \in X$ is called a strong Pareto-optimal solution if there is no $\underline{x} \in X$ such that $f_i(\underline{x}) \leq f_i(\bar{x})$, for $i = 1, 2, \ldots\ldots\ldots\ldots I$ and for at least one value of i, $f_i(\underline{x}) < f_i(\bar{x})$.

Thus, if $\bar{x}$ is a strong Pareto-optimal, it is also a weak Pareto-optimal but the converse is not necessarily true.

2.5. Multi-objective formulation techniques

The mathematics of vector optimisation, or the solution of mathematical programming models having more than a single objective function, is not new. A review by Cohon and Marks (1975) and the later review by Evans (1984) and the recent review by Coello and Christiansen (1999), Lewis and Mistree (1998) and Cheng and Li (1999) have summarised the continuing development in this area, since the first formulation and presentation of sufficient conditions for Pareto-optimal solutions by Kuhn and Tucker (1951), and Koopmans (1951). Further works by Keeny and Raiffa (1976) and Ignizio (1982) and many others should also be referred to regarding this development. Such voluminous works have contributed a variety of methods to generating Pareto-optimal solutions of the mathematical model of a design problem. Only three of them, namely Weighting, Constraint and Goal programming methods will be described here very briefly.

2.5.1. Weighting method

Weighting the objectives to obtain Pareto-optimal solutions is perhaps the oldest and the simplest technique to solve a multi-objective decision problem. This method converts a multi-objective problem to a scalar optimisation problem, in which the objective function becomes a weighted sum of the objective functions of the multi-objective model. That is

$$\text{minimise} \sum_{i=1}^{I} c_i f_i(\underline{x}) \tag{2.33}$$

subject to $\underline{x} \in X$

where $i \geq 0$ for all I, and strictly positive for at least one.

The above problem is an equivalent single-objective optimisation problem, which can be solved by any traditional optimisation method including INTEMOB. By altering the weighting factors c_i, which reflect the relative importance of various objective functions, a set of Pareto-optimal solutions can be generated. The optimum solution for a certain objective can be found by putting the weight for that objective equal to 1 where the weights for other objectives are zero. Such solutions obtained from individual optimisation of objectives are the end points of the Pareto set. Then a systematic variation of the weights may be followed to produce a sufficient number of Pareto-optimal solutions. Without any mathematical and numerical proof, Balachandran and Gero (1984) mentioned that the success of this method is strictly restricted to the convex criteria space only.

2.5.2. Constraint method

This method involves selecting the most important objective f_l and setting up upper bounds ε_k for the objectives f_k for $k \neq l$ such that the designer does not accept any solution with value higher than ε_k. These convert the multi-objective programming problem into a single-objective minimisation problem having the form:

$$\text{minimise } f_l(\underline{x}) \tag{2.34}$$

subject to $\underline{x} \in X$

$$f_k(\underline{x}) \leq \varepsilon_k \qquad (k \neq l)$$

The choice of l and the upper bounds ε_k ($k \neq$ l), which represent the subjective preferences of the designer, determines the optimal solution of the problem, which is to be accepted as the optimal solution of the original multi-objective problem. A problem possesses no feasible solution if bounds ε_k are too low. In such a case, at least one of these bounds must be relaxed.

2.5.3. Goal programming method

Charnes and Cooper (1961) are generally credited for the development of the goal programming method, and applying the same to industrial problems. Very extensive texts on goal programming for linear functions are available, such as Lee (1972) and Ignizio (1982). There are very successful uses of this technique for different decision-making problems, such as advertising (de Kluyver, 1979), fleet replacement (Sen and Bari, 1985) and optimisation of marine structures (Shi, 1988). The general goal programming method in association with the linear programming technique has been proved to be a very successful and efficient tool for solving large, nonlinear optimisation problems through successively linearised approximations (Mistree *et al.*, 1981).

For a problem with conflicting objectives having some target values, where all target values may not be achievable within the constraints, goal programming finds a solution that approaches the objectives as close to the target values as possible within the given feasible region. The simplest goal programming method may be stated as (Duckstein, 1984):

$$\text{minimise} \sum_{i=1}^{I} \left(f_i(\underline{x}) - T_i \right) \tag{2.35}$$

subject to $\underline{x} \in X$

where T_i denotes the target or goal set by the designer for the i-th objective function $f_i(\underline{x})$, and X represents the feasible region. The criterion, then, is to minimise the sum of the absolute values of the differences between target values and actually achieved values. The more general formulation of the goal programming objective function is a weighted sum of the deviation $\left(f_i(\underline{x}) - T_i \right)$ (Haims *et al.*, 1975).

The simplex method has been the most widely used algorithm for solving goal-programming problems. It needs linear approximations of objective and constraint functions, if they are nonlinear, which converts the original problem to a linear programming. The resulting linearised general goal programming method can be written as

$$\text{minimise } Z = \sum_{i=1}^{I} P_i\left(w_i^+ d_i^+ + w_i^- d_i^-\right) \tag{2.36}$$

subject to $\underline{x} \in X$

$f_i(\underline{x}) - d_i^+ + d_i^- = T_i$

$d_i^+, d_i^- \geq 0, i = 1,2,\ldots\ldots\ldots\ldots\ldots, I$ and other design constraints

in which d_i^+ and d_i^- are deviational variables for over and under–achievements and defined as

$$d_i^+ = \frac{1}{2}\{(f_i(\underline{x}) - T_i) + [f_i(\underline{x}) - T_i]\}$$

$$d_i^- = \frac{1}{2}\{(f_i(\underline{x}) - T_i) + [f_i(\underline{x}) - T_i]\}$$

P_i is the priority assigned to the deviational variables associated with the goals; w_i^+ and w_i^- are relative weights given to positive and negative deviations, respectively, for each target T_i. If a minimisation problem is considered, choosing the w_i^+ to be larger than w_i^- would be expressing preference for under-achievement of a goal.

It is not possible to have both under and over-achievements of a goal simultaneously. Therefore, one or both of the deviational variables must have zero values; that is

$$d_i^+ . d_i^- = 0$$

This constraint is automatically fulfilled by the simplex method, because the objective function will derive either d_i^+ or d_i^- or both quantities simultaneously to zero for all i.

The choice of priorities and weights dictates the solution, and it is important to experiment with them to obtain the solution that adequately reflects the designer's expectation. According to the importance hierarchy of goals to the designer, these priorities may be given to the individual goals either in an Archimedean or in pre-emptive approach. In the Archimedean approach, the numerical values of priorities reflect the desire to achieve certain goals more than some others. In the pre-emptive approach, goals are ranked according to the designer's preferences but those preferences are not expressed by any numerical value. If this rank is denoted by P_1, P_2, ..., P_I where P_1 is preferred to P_2 which in turn is preferred to P_3 and so on, then deviational variables of rank P_1 are minimised before those of rank P_2 and so on. Further details are given in Mistree *et al.* (1985). The conceptual difference between P_i and w_i in Eq. 2.36 is explained in Goicoechea *et al.* (1982). Lewis and Mistree (1998) and Coello and Christiansen (1999) have recently reviewed other methods for multi-objective optimisation. Cheng and Li (1999) proposed a generalised centre method for multi-objective engineering optimisation.

2.5.4. Proposed Technique

As explained in the goal programming method, in the solution of an equivalent linear problem by the simplex algorithm, all deviational variables are effectively variables in the simplex table and an additional equality constraint is formed by the actual achievement, a deviational variable and the target value for each goal. These certainly slow down the solution procedure. On the other hand, being the oldest and simplest method for solving multiple objective decision problems, the weighting method has been the basis for many practical designs. For example, the design model proposed by

Caldwell (1972) provided a useful non-dimensional objective function combining weight and initial cost together, for ship structural design, as

$$Z = K\frac{W}{W_0} + (1-K)\frac{C}{C_0} \tag{2.37}$$

in which K is a factor controlling the relative importance of weight W and cost C, and W_0 and C_0 are the weight and initial cost of some basis or standard design, respectively.

There were some practical difficulties in using Eq. 2.37 (Rahman, 1991). To resolve the difficulties, and to make it applicable to any engineering multi-objective optimisation problem, Rahman (1991) proposed a more general equation:

$$\text{minimise } Z = \sum_{i=1}^{I} \frac{(f_i(\underline{x}) - T_i)}{D_i} P_i \tag{2.38}$$

where $f_i(\underline{x})$ is the objective function for i-th objective; T_i is the target value for the i-th objective; D_i is the dividing factor for i-th objective equation and P_i is the priority to achieve the i-th objective.

The target value, which is desired to achieve for the corresponding objective either may refer to a specified numerical value or can be calculated as a function of design variables. If a particular objective has no target value, that objective requires minimisation only. This can be achieved by simply equating the corresponding T_i to zero. If necessary, any of the objectives can be excluded by equating the corresponding priority factor to zero. The maximisation of a particular objective can be achieved by using either a very high target value for that objective, or minimising the negative function for that objective. It is better to formulate an inequality constraint if only over-achievement or under-achievement (with respect to a target value) for an objective is needed.

Normalization by dividing by D_i is required to ensure contributions of equal magnitude (at least within some reasonable range) by the individual objectives to the overall combined objective function. This normalization factor eliminates the necessity of information on the basis design, and the wide and trial variation of priority factors to obtain proper trade-off among objectives. The problem of wide and trial variation of priority factors in using the conventional goal programming equation was reported by Balachandran and Gero (1984). However, the selection of proper values for normalization factors in using the proposed equation (Eq. 2.38) provided very sensitive trade-offs among various objectives for very small changes of priority factors (Rahman and Caldwell, 1992; Rahman, 1996). Therefore, this technique has been used to investigate the multi-objective optimisation issues associated with hydraulic fracturing design.

CHAPTER THREE

HYDRAULIC FRACTURE MODELS: REVIEW, SELECTION AND DEVELOPMENT OF AN IMPROVED PSEUDO-3D MODEL

3.1. Introduction

To design hydraulic fracturing treatment, it is first necessary to predict the growth of fracture geometry as a function of treatment parameters. Length, height and width of a fracture define the fracture geometry, which eventually influences the production from the fractured reservoir. Actual growth of fracture geometry in heterogeneous formation is a complex phenomena and very difficult to predict with certainty. Over the years, however, various models are used to approximately define the development of fracture geometry. Among the models used in the petroleum industry, the KGD and the PKN models are most popular.

All the fracture models can be broadly classified into 2D and 3D categories. Early attempts were devoted to describing the fracture geometry using simplified 2D models. When the pay zone does not include multi-layered formations, there is little interest in extending a fracture into bounding layers. With an appropriate design tool, it is possible to adjust stimulation parameters such that the fracture is to some extent contained in the pay zone. In such a case, a 2D-fracture model can be used for hydraulic fracturing optimisation. However, if the fracture height is strictly contained in the pay zone at the wellbore, the productive height of the fracture definitely excludes a portion of the pay zone. This is mainly because towards its lateral end the fracture height most likely becomes less than the fracture height at the wellbore (i.e. pay zone height) in reality, although theoretically it is assumed to remain constant. Also the fracture has less productive width adjacent to its edges. However, such a loss of productive zone can

partly be recovered, while the fracture is designed using a 2D fracture model, by allowing the fracture height in the bounding layers to some extent. Rahim and Holditch (1995) suggested that the use of 2D models is accurate enough for reservoirs containing even a number of various formation layers. A 2D fracture model is, therefore, considered first for the development of the proposed hydraulic fracturing optimisation model.

A 2D PKN-C fracture model is developed by incorporating the Carter Equation II (Howard and Fast, 1957) in the original PKN model (Perkins and Kern, 1961; Nordgren, 1972) for material balance at a constant injection rate with the fluid leakoff. Another 2D fracture model, KGD (Khristianovitch and Zheltov, 1955; Geertsma and deKlerk, 1969) has also its KGD-C version. However, the PKN-C model is selected for the current work, because its vertical plane strain assumption is physically more acceptable for the proposed height-contained fractures where the fracture length becomes considerably greater than the fracture height (Valko and Economides, 1995). Rahim and Holditch (1995) have also reported that, for most problems, the PKN-C model predicts fracture lengths closer to those computed by 3D models for correct fracture heights than does the KGD-C model. This finding also supports the acceptance of PKN-C model. Both the original PKN and KGD models have been converted to other various versions by introducing various material (fracturing fluid) balance techniques, including PKN-N and KGD-N for material balance proposed by Nolte (1979, 1989), PKN-α and KGD-α for power law length growth material balance, PKN-NMB for numerical material balance and so on. Descriptions of these models together with mathematical formulations are presented by Valko and Economides (1995).

The development of fully 3D models stems from two major requirements: firstly, the need to understand the nature of fracture growth when the fracture initiates in a non-preferred direction or plane and secondly, the need to idealize fracture growth in adjacent multi-layered formations with different properties and in-situ stresses. Usually, a fully fluid flow coupled 3D model is required to meet the first requirement. Such a model is not suitable for hydraulic fracturing design optimisation involving a large

number of repetitive computations. In order to meet the second requirement, pseudo-three-dimensional (P-3D) models are proposed (Simonson *et al.*, 1978; Settari and Cleary, 1986; Warpinski and Smith, 1989). This P-3D model is also selected for current work because of its simplification of height growth at the wellbore in multi-layered formations. The model is then improved by incorporating the Carter Equation II and is denoted as P-3D-C fracture model.

The remaining of this chapter briefly presents the basic mathematical formulations of PKN and P-3D fracture models and their improvements with Carter Equation II. The PKN-C and P-3D-C models are applied to a typical tight-gas formation to compare their predictive differences for a number of parameters. The model equations (particularly 2D models) are presented in SI units and the results were converted into oil field units using appropriate conversion factors.

3.2. Two dimensional fracture models

Two two-dimensional fracture models, both assuming constant height and radial propagation mode, have long been used for hydraulic fracture propagation. Khristianovitch and Zheltov (1955), based upon the assumptions of plane strain condition in horizontal planes developed the first model. This horizontal plan strain geometry approximately represents a fracture with a horizontal penetration much smaller than the vertical one. The fracture shape should not depend on the vertical position. This condition was further developed by Geertsma and deKlerk (1969) and is often referred to as the KGD fracture model. This model is shown in Figure 3.1; it has a constant and uniform height and a rectangular cross-section.

Perkins and Kern (1961), based upon assumptions of plane strain condition in vertical planes developed the second model. This condition exists when there is a large confinement, hence the fracture is limited to a given zone. In this model, vertical plane strain, along a fracture with considerably larger length than height, allows vertical parallel planes to slide against each other and each vertical cross section deforms

independently of the others. Nordgren (1972) further developed this condition and the model is referred to as the PKN fracture model. The fracture widths in vertical planes are coupled through the fluid-flow and continuity equations. Since there is no vertical extension (or fluid flow) in each vertical section, the pressure is uniform; hence, the shape of the fracture is elliptical (Economides and Nolte, 1989). The model is shown in Figure 3.2.

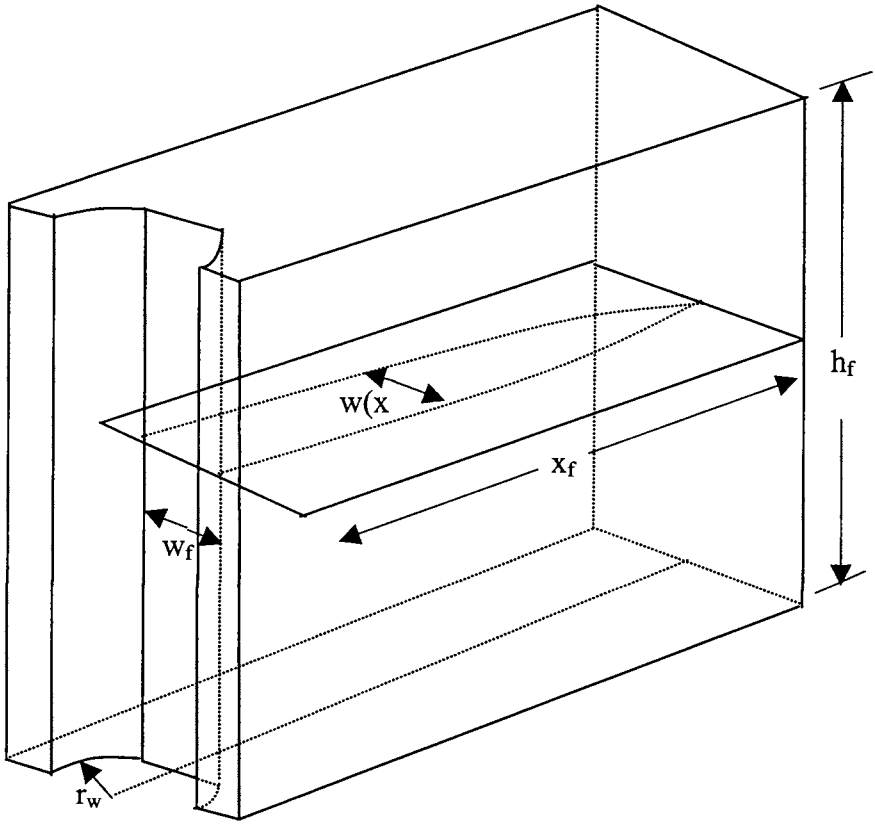

Figure 3.1. The KGD fracture model.

The development of PKN-C model will be described herein, because its formulations are used for the optimisation model. The KGD model and its various version can be found in any standard literature of hydraulic fracture mechanics.

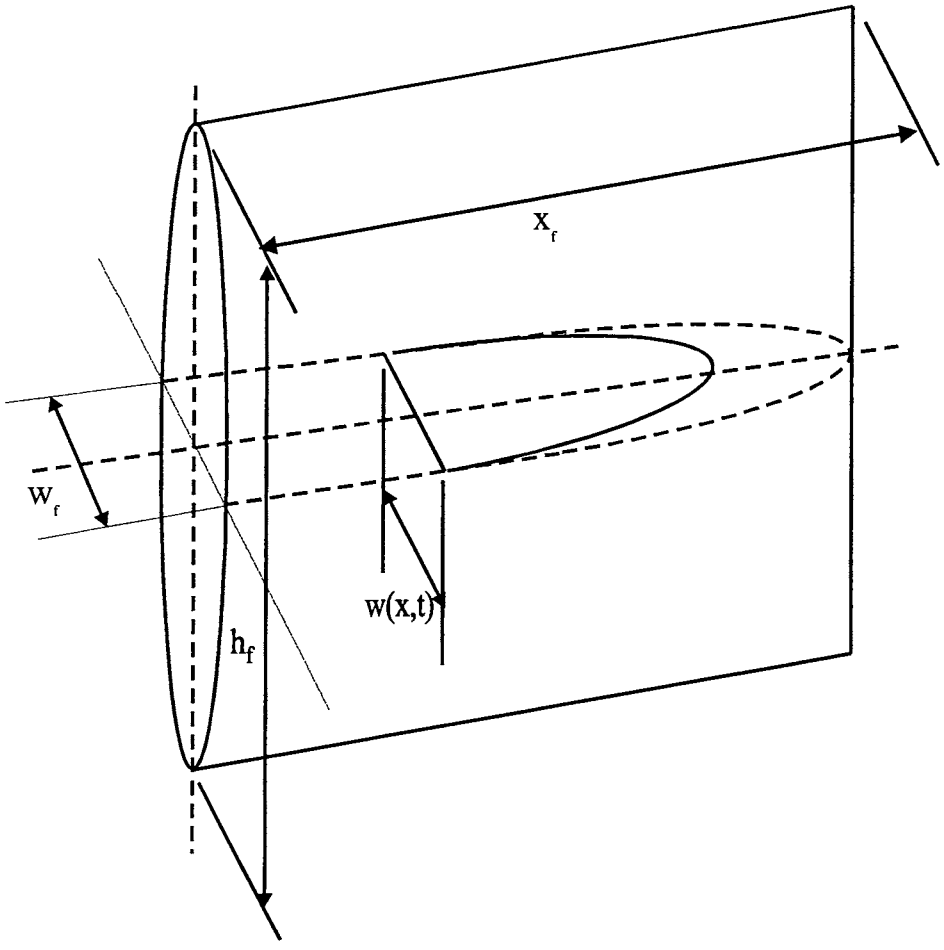

Figure 3.2. The PKN fracture model.

3.2.1. Perkins-Kern model with no-leakoff

The main assumptions for this model are: the fracture height is constant, the fracture length is greater than the fracture height, there is no flow in vertical direction, the pressure in a vertical cross section of the fracture is constant, the fracture has an elliptical shape; also there is no elastic coupling between the planes. The fracture width can be expressed as a function of the local pressure. The only coupling between the different vertical cross sections is due to the fluid flow in the fracture. Reservoir rock stiffness prevails in the vertical plane. So, the model applies a quasi-plane strain assumption (Valko and Economides, 1995). The fracturing fluid pressure in vertical cross-sections perpendicular to the direction of propagation is considered the net

fracture pressure, p_{net}, which is a function of the lateral coordinate. This net fracture pressure creates an elliptical cross-section with maximum width at the wellbore, which is given by

$$w_0 = \frac{2h_f p_{net}}{E'} \tag{3.1}$$

where

$$E' = \frac{E}{(1-\nu^2)} \tag{3.2}$$

Here, h_f is the fracture height, E' is the plane strain modulus, E is the elastic modulus and ν is the poisson's ratio. The maximum width, w_o, is a function of the lateral coordinate. At the wellbore it is denoted by w_f.

The fluid pressure gradient during propagating in x_f direction is given by the flow resistance in a narrow, elliptical flow channel. For Newtonian flow behavior with constant viscosity, pressure drop is given by

$$\frac{\Delta P}{x_f} = \frac{64\mu}{\pi w_0^3 h_f} \times \frac{q_i}{2} \tag{3.3}$$

where μ is the viscosity of the fracturing fluid and q_i is the injection rate. Thus, half of q_i is the flow rate in one wing of the fracture. The injection rate is assumed to be constant and the fluid flow in the fracture is laminar.

Perkins and Kern (1961) postulated that the net pressure is zero at the fracture tip. The elliptical cross-section has maximum width at the center, which gives maximum fracture width at the wellbore. Thus, integrating the above equation between the

wellbore and the tip, and further simplifying, maximum width at the wellbore, which is the Perkins-Kern width equation, is given by

$$w_f = 3.57\left(\frac{\mu q_i x_f}{2E'}\right)^{\frac{1}{4}} \tag{3.4}$$

The average width is calculated by multiplying it by a constant shape factor, γ, because of elliptic shape of the fracture. The average width is given by

$$\overline{w} = \gamma w_f \tag{3.5}$$

Considering the elliptical shape along the vertical direction and the lateral variation of the width, γ is found to be $\pi/5$. Thus, the average fracture width, $\overline{w}$ is given by

$$\overline{w} = 2.24\left(\frac{\mu q_i x_f}{2E'}\right)^{\frac{1}{4}} \tag{3.6}$$

For the constant-injection-rate and no-leakoff case, coupling of the average width equation with simple material balance gives the following expressions for injected fluid volume (for two wings), fracture half length, fracture width at the wellbore and net fracture pressure at the wellbore in terms of injection time (Valko and Economides, 1995).

$$V_i = q_i t_i = 2\overline{w} x_f h_f = 2\times 2.24\left(\frac{\mu q_i x_f^5 h_f^4}{2E'}\right)^{1/4} \tag{3.7}$$

$$x_f = 0.524\left(\frac{q_i^3 E'}{8\mu h_f^4}\right)^{1/5} t_i^{4/5} \tag{3.8}$$

$$w_f = 3.04\left(\frac{q_i^2 \mu}{4E' h_f}\right)^{1/5} t_i^{1/5} \tag{3.9}$$

$$p_{net} = 1.52\left(\frac{E'^4 \mu q_i^2}{4h_f^6}\right)^{1/5} t_i^{1/5} \tag{3.10}$$

Here, t_i is the injection time. Thus, in the no-leakoff Perkins-Kern model, fracture length and width grow with the injection time and the net pressure is also increasing with injection time.

3.3. PKN model with leak-off

The Carter Equation II for material balance to account for fluid-leak-off during propagation of PKN fracture and the resulting 2D PKN-C fracture model, as presented by Valko and Economides (1995), are described in the following sections.

3.3.1. The Carter Equation II

The basic solution for estimating the extent of the fracture area taking into account the effect of fluid leaking into the formation and fracture propagation is derived from Carter Equation (Howard and Fast, 1957). Fracture width and height are assumed to be constant and fracture length is a variable. Injection rate is also assumed to be constant. The leak-off flow rate, normal to the fracture faces, corresponding to the given surface element is given by

$$\frac{\partial V_L}{\partial t} = \frac{C_L}{\sqrt{t-\tau}} \partial A \tag{3.11}$$

where, τ is the opening time at which filtration starts and every surface element has its own τ. The actual time is denoted by t, C_L is the overall fluid leak-off coefficient, V_L is the volume being leaked and A is the surface area of fracture faces.

If the growth rate of fracture surface area, $dA/d\tau$ is known, then the leak-off flow rate through the two fracture faces of one wing is the summation of the different flow rates along the surface elements of different age. The leak-off flow rate in one wing (for two fracture faces) is given by

$$2\int_0^t \frac{C_L}{\sqrt{t-\tau}}\left(\frac{dA}{d\tau}\right)dA \tag{3.12}$$

The fluids are partly leaking into the formation and partly engaged in fracture growth. The volumetric fracture growth rate and the spurt loss rate at the new fracture surface are given by

$$w\frac{dA}{dt} + A\frac{dw}{dt} + 2S_p\frac{dA}{dt} \tag{3.13}$$

where S_p is the spurt loss and w is the constant fracture width.

Carter (Howard and Fast, 1957) formulated the material balance in terms of flow rates. At any injection time t, the injection rate entering one wing of the fracture is equal to the sum of the different leak-off rates plus the growth rate of the fracture volume. Hence, the injection rate can be balanced as

$$\frac{q_i}{2} = 2\int_0^t \frac{C_L}{\sqrt{t-\tau}}\left(\frac{dA}{dt}\right)d\tau + \left(w+2S_p\right)\frac{dA}{dt} + A\frac{dw}{dt}. \tag{3.14}$$

Note that q_i is the total rate of injection.

Carter solved a simplified version of the material balance and obtained an analytical solution for the constant injection rate, neglecting the fact that the width increases during the fracture growth. The solution is given by

$$A(t) = \frac{(w+2S_p)}{4C_L^2\pi}\frac{q_i}{2}\left[\exp(\beta^2)erfc(\beta)+\frac{2\beta}{\sqrt{\pi}}-1\right] \tag{3.15}$$

where

$$\beta = \frac{2C_L\sqrt{\pi t}}{w+2S_p} \tag{3.16}$$

This solution gives fracture surface area, A for any given injection time, t and fracture width, w. Since the width w is assumed constant in the above equation, it can be replaced by the average fracture width, $\overline{w}$ developed at the end of injection.

3.3.2. The PKN-C fracture model

The relationship between treatment parameters, rock properties and fracture width at the wellbore for no-leakoff situation was given by Eq. 3.4. Valko and Economides (1995) argued that a considerable part of the petroleum engineering literature considers that Eq. 3.4 is somewhat inaccurate and they recommended the following improved expression for the fracture width at the wellbore, w_f.

$$w_f = 3.27\left(\frac{\mu q_i x_f}{2E'}\right)^{\frac{1}{4}} \tag{3.17}$$

where the constant 3.27 is derived from a limiting result of Nordgren (1972).

When a non-Newtonian fracturing fluid is used, the maximum width at the wellbore in terms of power law parameters can be expressed as:

$$w_f = 9.15^{\left(\frac{1}{2n+2}\right)}3.98^{\left(\frac{n}{2n+2}\right)}\left[\frac{1+2.14n}{n}\right]^{\left(\frac{n}{2n+2}\right)}K^{\left(\frac{1}{2n+2}\right)}\left(\left(\frac{q_i}{2}\right)^n\frac{h_f^{1-n}x_f}{E'}\right)^{\left(\frac{1}{2n+2}\right)} \tag{3.18}$$

where n is the power law exponent (dimensionless) and K is the consistency index (Pa-sec^n).

Based on a large amount of test data provided by an industry (Chipperfield, 2000), the power law parameters are correlated with viscosity of fracturing fluid in this study as follows:

$$n = 0.1756(1000\mu)^{-0.1233} \tag{3.19}$$

$$K = (500\mu - 0.0159)47.880 \tag{3.20}$$

Note that general validity of Eqs. 3.19 and 3.20 is not emphasised here.

Using the shape factor ($\pi/5$) for the PKN model, the average width along the fracture length is given by

$$\overline{w} = \frac{\pi}{5} w_f \tag{3.21}$$

Using the Carter Equation II (Eq. 3.15) with average fracture width, the expression for the fracture half-length/fracture height can be given as:

$$x_f = \frac{(\overline{w} + 2S_p)}{4C_L^2 \pi h_f} \frac{q_i}{2} \left[\exp(\beta^2) erfc(\beta) + \frac{2\beta}{\sqrt{\pi}} - 1 \right] \tag{3.22}$$

where

$$\beta = \frac{2C_L \sqrt{\pi t_i}}{\overline{w} + 2S_p} \tag{3.23}$$

Here, t_i is the injection time. Eqs. 3.21-3.23 constitute the solutions of the fracture propagation problem. From this closed system of equations, either fracture length or injection time can be easily determined using a numerical root-finding method. If values of x_f and q_i are known, the fracture height, h_f can also be calculated solving Eqs. 3.18-3.23 using an iterative procedure when non-Newtonian fluid is used.

The net fracture pressure, p_{net}, is then calculated as:

$$p_{net} = \frac{E'}{2h_f} w_f \tag{3.24}$$

Here p_{net} is inversely proportional to the fracture height and directly proportional to fracture width at the wellbore.

The fracture treatment pressure at the wellbore is then given by

$$p_{treat} = \sigma_1 + p_{net} \tag{3.25}$$

where σ_1 is the minimum horizontal in-situ stress in the pay zone.

3.4. Propped fracture behaviour and proppant scheduling

While the 2D fracture model presented so far provides equation for dynamic behaviours of various fracture parameters, the improvement of well productivity depends on final propped fracture geometry and fracture conductivity. This depends on transport of proppant in the fracture and its placement, which is an important issue in hydraulic fracture treatment design. The total injection during treatment is performed in two stages. At the early stage, the fracturing fluid is pumped without proppant to initiate the fracture and to develop it up to a certain size. This period is called pad time and the volume injected during this period is called pad volume. The proppant is then gradually

added to the fracturing fluid over time intervals to achieve a target end of the job (EOJ) proppant concentration. Nolte (1986) presented a method of approximating the optimum pad volume and proppant scheduling based on the fracturing fluid efficiency.

During fracture growth at any time, the general material balance relationship is:

$$V_i = V_f + V_L \tag{3.26}$$

where V_i is the total fluid volume injected ($q_i \times t_i$) including proppant volume, V_f is the fracture volume and V_L is the fluid volume leaked.

The fracture volume, V_f, and fracture surface area, A_f, at any time for the linear propagating PKN-type fracture are defined, respectively, as follows for a two-sided symmetric fracture (Economides and Nolte, 1989):

$$V_f = \frac{\pi}{2} h_f x_f w_f \tag{3.27}$$

and

$$A_f = 4 x_f h_f \tag{3.28}$$

The final propped width after the closure of fracture (Economides *et al.*, 1994) is

$$w_p = \frac{W_{pr}}{2 x_f h_f (1-\phi_p)\rho_p} \tag{3.29}$$

where W_{pr} is the weight of proppant, ϕ_p is the proppant porosity (dimensionless) and ρ_p is the proppant density. Here, $2x_f h_f$ is the propped fracture area for both wings. It is assumed that a weight of proppant, W_{pr}, has been injected in the fracture (both wing)

and proppant is uniformly distributed. The formulation of W_{pr} is given in the later section.

The fracturing fluid efficiency is:

$$\eta = \frac{V_f}{V_i} \tag{3.30}$$

The pad volume, V_{pad}, can be obtained from the relationship between the total fluid volume injected, V_i and the fracturing fluid efficiency, η and is given as (Nolte, 1986; Meng and Brown, 1987):

$$V_{pad} = V_i\left(\frac{1-\eta}{1+\eta}\right) \tag{3.31}$$

The injection time for pad volume, called pad time, t_{pad} is given by

$$t_{pad} = \frac{V_{pad}}{q_i} \tag{3.32}$$

3.4.1. Proppant weight and proppant scheduling

The start of proppant addition and proppant concentrations over time depend on the fluid efficiency. In the previous section the onset of proppant addition was determined after the pad volume and pad time were determined.

The total weight of proppant to be pumped can be calculated from the following equation, derivation of which is given in Appendix A.

$$W_{pr} = \left(\frac{V_{pl}}{\frac{1}{\overline{P}_c} + \frac{1}{\rho_p}} \right) \tag{3.33}$$

where $\overline{P}_c$ is the average proppant concentration and is given as follows:

$$\overline{P}_c = \eta P_c \tag{3.34}$$

Here P_c is the EOJ proppant concentraiton.

The volume of proppant-laden fluid (slurry), V_{pl}, which is the summation of proppant volume (V_{pr}) and fracturing fluid volume (V_{fl}), is:

$$V_{pl} = V_i - V_{pad} \tag{3.35}$$

Therefore, the total volume of fluid injected, V_i can be expressed as:

$$V_i = V_{pad} + V_{fl} + V_{pr} \tag{3.36}$$

Total fracturing fluid volume (without proppant), V_{tfl} is:

$$V_{tfl} = V_{pad} + V_{fl} \tag{3.37}$$

The fracturing fluid volume, V_{fl} (the amount only mixed with the proppant), is given by

$$V_{fl} = \frac{W_{pr}}{\overline{P}_c} \tag{3.38}$$

Based on a material balance, the continuous proppant addition (ramped proppant schedule versus time) is given by the following expression (Nolte, 1986; Meng and Brown, 1987):

$$P_c(t) = P_c\left(\frac{t - t_{pad}}{t_i - t_{pad}}\right)^{\varepsilon} \tag{3.39}$$

where $P_c(t)$ is the slurry concentration at time t. The Pad time, t_{pad} is given by the Eq. 3.32.

The exponent ε depends on the fluid efficiency and is given by:

$$\varepsilon = \frac{1-\eta}{1+\eta} \tag{3.40}$$

Eqs. 3.39-3.40 simply denote the appropriate proppant addition mode so that the entire hydraulic length coincides with the propped length. This is not entirely realistic, since the fracture length, beyond the point where the hydraulic width is smaller than three times the proppant diameters, can not accept proppant due to proppant bridging problem (Economides *et al.*, 1994). This is true at anywhere in the fracture and, therefore, the fracture width has to be sufficient enough not to cause this problem. Hence, in hydraulic fracture treatment design optimisation (chapter 5) a design constraint has been formulated not to allow the average dynamic fracture width to be less than 4 times the proppant diameters (Schechter, 1992).

3.5. Three-dimensional and pseudo-three-dimensional models

This section reviews the current understanding of 3D models in brief and presents the improvement of P-3D model.

3.5.1. The 3D model

A fully 3D model coupled with full two-dimensional fluid flow is required to predict the fracture growth in a 3D space. These models are developed based on the fundamental theories of linear elastic fracture mechanics coupling with the effects of complex fluid flow patterns inside fractures (Hossain, 2001). Fracture growth is simulated sequentially using a mixed-mode fracture propagation criterion (in terms of the local stress-dispalcement field around the crack tip) by highly capable finite/boundary element methods. The fracture is allowed to propagate laterally and vertically, and change plane of original direction, depending on the presence of natural fractures/flaws, induced perforation, deviation of well, local stress distribution and rock properties (Economides *et al.*, 1994; Hossain, 2001). To the best of author's knowledge, only Hydraulic Fracture Analysis Code (HYFRANC3D), developed by the Cornell Fracture Group at Cornell University (www.cfg.cornell.edu), possesses the above discussed features. Such fully 3D models require significant amounts of data to justify their use and are extremely computationally intensive. It has been experienced that the simulation of 3D hydraulic fracture propagation, in some cases, took over a month (Hossain, 2001; Rahman *et al.*, 2002) to propagate up to 6 cm using a fully devoted high power computer. These are not suitable for incorporation in a design optimisation scheme that involves a large number of repeating calculations. However, these fully 3D models are very valuable in academic research in which it enables us to understand various fundamental aspects of hydraulic fracture growth and to diagnose the causes of some difficulties with actual hydraulic fracturing in the field.

3.5.2. The P-3D Model

In order to idealize fracture growth in multi-layered formations, P-3D models are proposed. These 3D models are called 'pseudo', because they do not consider the variation of fracture geometry in a three-dimensional space, rather it modifies the 2D (PKN) model by adding height variation along the fracture length and its effect on the fracture width. The height variation along the fracture length can be considered linear or parabolic. Settari and Cleary (1986) first introduced the concept of modeling hydraulic

fracturing by P-3D model. In their work, the equations of lateral fluid flow were solved by a finite difference technique, and the vertical propagation problem was solved by numerical implementation of a singular integral equation on a suitable set of Chebyshev points. Due to lack of simplified closed-form equations, the method is not quite suitable for the optimisation model proposed herein, although the work has been incorporated in many hydraulic fracturing simulators (Bouteca, 1988; Morales and Abu-sayed, 1989).

Simonson *et al.* (1978) first showed that the fracture growth in a layered medium can be modelled if each stressed layer is assumed to have homogeneous material properties and the vertical pressure distribution in the fracture is assumed to be constant. This was a relatively simplified approach for a symmetric geometry, using the concept of equilibrium condition in multi-layered formation in terms of stress intensity factors (Rice, 1968), but can easily be generalised to more complex situations. The method later related the stress contrast between layers, net fracturing pressure and fracture height migration at the wellbore. Neglecting the hydrostatic effect of fluid inside the fracture, Warpinski and Smith (1989) expressed in SPE monograph the condition of fracture growth in multi-layered formations by means of a very elegant and concise system of equations. This work has aided research in the area of investigating optimum hydraulic fracture dimensions (Hareland *et al.*, 1993; Hareland and Rampersad, 1994; Rahim and Holditch, 1995). While such a model is not as accurate as numerical simulator, it requires less computing time, is less expensive to develop and easier to use.

3.5.3. Fracture height growth in P-3D model

The equilibrium height of a hydraulic fracture for a given internal pressure in a layered-stress environment can be calculated if material property variations in each stress layer are neglected and vertical pressure distribution in the fracture is assumed constant. The stress-intensity factors are calculated at the top and bottom tips of the fracture and set equal to the fracture toughnesses of the materials, resulting in a unique height and position, or centering of the crack with respect to the stress field (Warpinski and Smith, 1989).

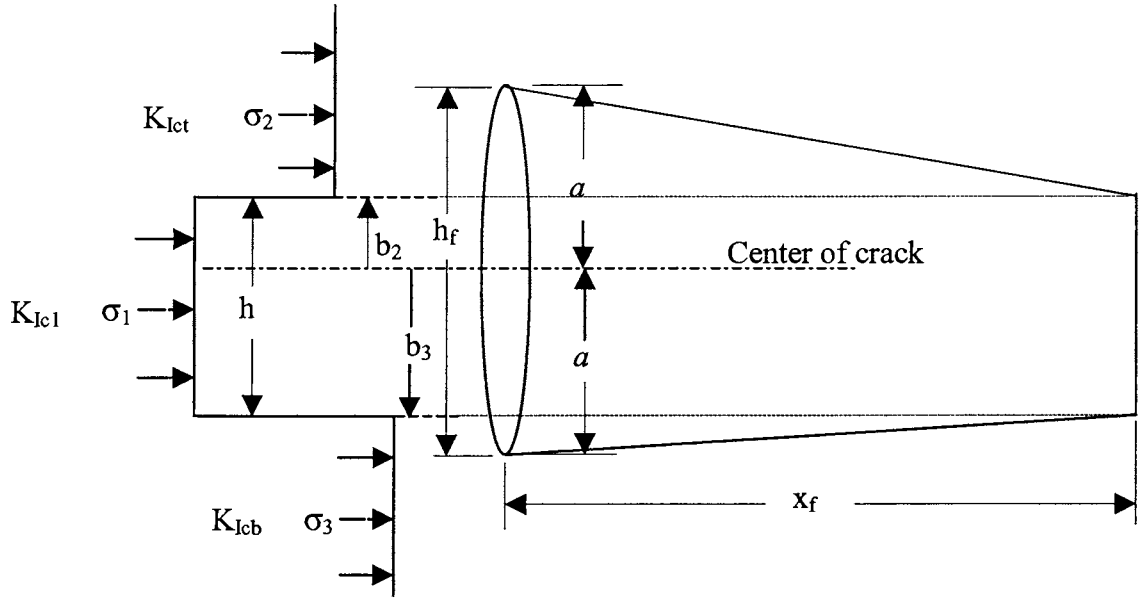

Figure 3.3. The P-3D fracture model: fracture in a layered stress medium.

For geometry shown in Figure 3.3, the stress-intensity factor at the top of the fracture (K_{Itop}) can be determined by (Rice, 1968)

$$K_{Itop} = \frac{1}{\sqrt{\pi a}} \int_{-a}^{a} p(y) \sqrt{\frac{a+y}{a-y}} dy \tag{3.41}$$

Here, a is the fracture half-height and $p(y)$ is the net fracture pressure distribution opening the fracture. The net fracture pressure distribution is given by

$$p(y) = p_w - \sigma_3 \quad \text{for} \quad -a \le y \le -b_3 \tag{3.42}$$

$$p(y) = p_w - \sigma_1 \quad \text{for} \quad -b_3 \le y \le b_2 \tag{3.43}$$

and

$$p(y) = p_w - \sigma_2 \quad \text{for} \quad b_2 \le y \le a \tag{3.44}$$

with an additional geometry constraint of

$$b_3 = h - b_2 \tag{3.45}$$

The integration of Eq. 3.41 and a similar equation for the bottom layer yields two equations, which can be solved for the fracture height. After the two equations are added and subtracted the final forms are given as follows (Warpinski and Smith, 1989):

$$\frac{\sqrt{\pi}}{2\sqrt{a}}(K_{Icb} + K_{Ict}) = (\sigma_2 - \sigma_1)\sin^{-1}\left(\frac{b_2}{a}\right) + (\sigma_3 - \sigma_1) \times \sin^{-1}\left(\frac{b_3}{a}\right) - (\sigma_2 + \sigma_3 - 2p_w)\frac{\pi}{2} \tag{3.46}$$

and

$$\frac{\sqrt{\pi}}{2}(K_{Icb} - K_{Ict}) = (\sigma_2 - \sigma_1)\sqrt{a^2 - b_2^2} - (\sigma_3 - \sigma_1)\sqrt{a^2 - b_3^2} \tag{3.47}$$

Here, K_{Icb} and K_{Ict} are critical intensity factors (fracture toughnesses) at the bottom and top layers, respectively. σ_1, σ_2, σ_3 are stresses of the layers as shown in Figure 3.3 and p_w represent the treatment pressure at the wellbore. A simultaneous solution of Eqs. 3.45-3.47, which will make the estimated treatment pressure from Eq. 3.46 equal to the actual treatment pressure, will give height growth of the fracture in the multi-layered formation. An iterative algorithm will be described in the following section to estimate the fracture height and other parameters.

3.5.4. Coupling of P-3D model with the Carter Equation II

In order to determine the fracture width, an equilibrium condition for pressure in the wellbore and the fracture is required with some closed-form equations. Rahim and Holditch (1995) recommended the 2D PKN-C equations for this purpose. The actual

treatment pressure required to solve the P-3D model (Eqs. 3.41-3.47) in the iterative process of calculating fracture height is thus estimated using Eqs. 3.18 and 3.24 of PKN-C model. For a given injection rate of a fracturing fluid, the fracture propagation length can be coupled with the injection time using Cater's material balance equations (Eqs. 3.22-3.23) iteratively.

An initial estimate of fracture height at the wellbore, a is made ($a = \frac{h_f}{2} = \frac{h}{2}$ is a good start). Then b_2 is calculated numerically from Eq. 3.47 and p_w is calculated from Eq. 3.46. The maximum fracture width at the wellbore, w_f is calculated from Eq. 3.18 for a target fracture half-length using the above fracture height. The net fracture pressure and the treatment pressure at the wellbore are calculated from Eqs. 3.24 and 3.25, respectively. This fracture treatment pressure is then compared to p_w estimated from Eq. 3.46. The fracture height is then increased or decreased by an adaptive step value until these pressures converge with a specified tolerance. The flow chart of this iterative procedure is shown in Figure 3.4. Initially, the fracture height is changed with a large value of Δh_f (say $\Delta h_f = 0.1 h_f$) and an increase or decrease in fracture height is decided based on the change of pressure values in two successive iterations. When the pressure values reverse their magnitude in two successive iterations, the step value is halved ($\Delta h_f = \Delta h_f / 2$) and the change in fracture height is reversed in the next iteration. The converged solution gives the fracture height, maximum fracture width and the treatment pressure at the wellbore.

The average fracture width at the wellbore, $\overline{w}$ is calculated from Eq. 3.21. For linear height variation along the fracture half-length, x_f, fracture area, A_p (for one wing) can be calculated as

$$A_p = x_f \frac{h_f + h}{2} \tag{3.48}$$

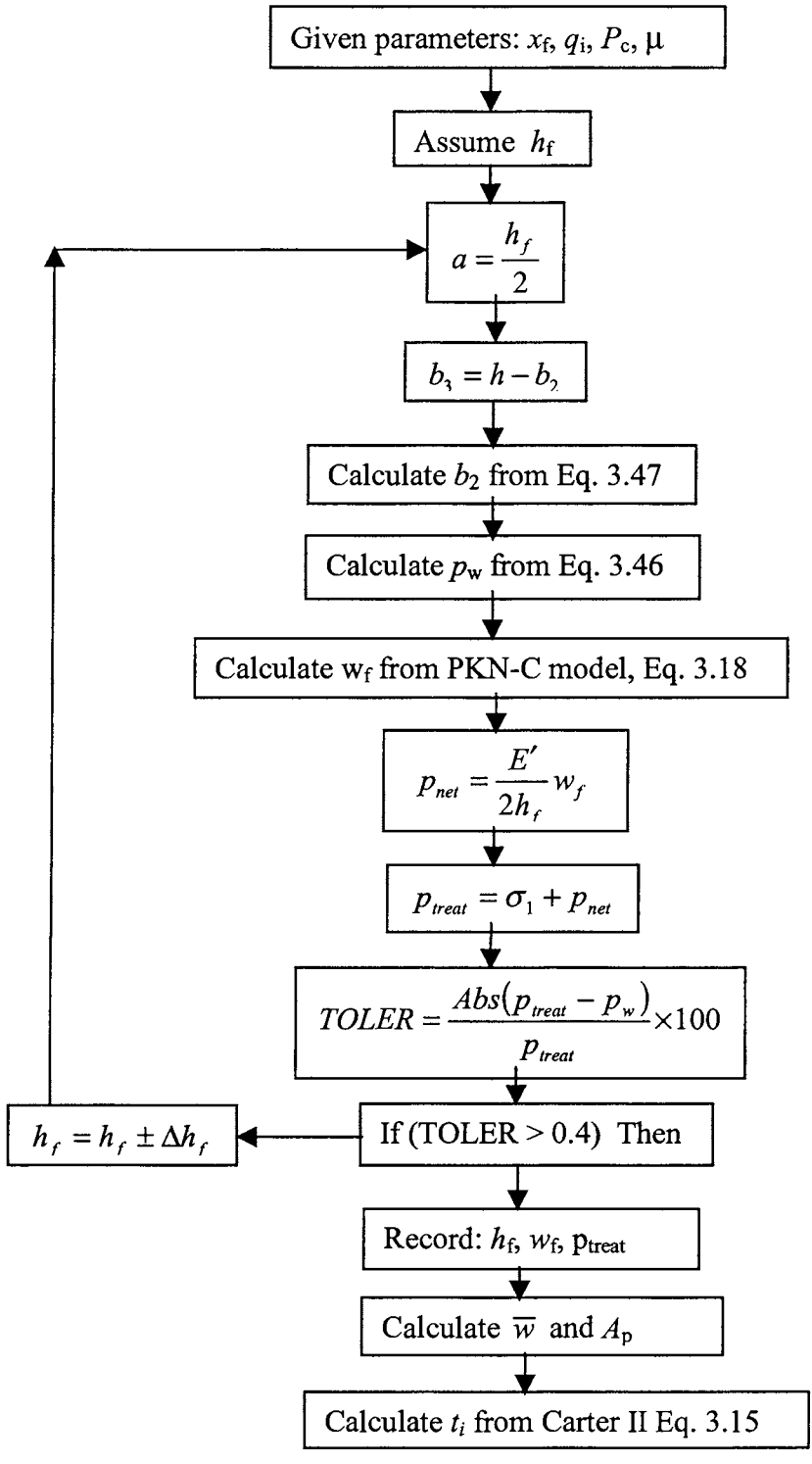

Figure 3.4. Flow chart of computer program for P-3D fracture model to calculate fracture height at the wellbore and injection time.

Using Carter Equation II, the relationship between fracture half-length, height, width and injection time for a given injection rate can be expressed as:

$$x_f = \frac{\left(\overline{w} + 2S_p\right)}{4C_L^2\pi} \frac{q_i}{\left(h_f + h\right)} \left[\exp\left(\beta^2\right) erfc(\beta) + \frac{2\beta}{\sqrt{\pi}} - 1 \right] \tag{3.49}$$

where β is given by Eq. 3.23. The injection time, t_i can then be calculated solving Eqs. 3.49 and 3.23 numerically.

The fracture volume, V_f for both fracture wings can be obtained as follows (similar to Eq. 3.27):

$$V_f = \frac{\pi}{2} \gamma \left(\frac{h_f + h}{2} \right) x_f w_f \tag{3.50}$$

For both wings, the total fracture surface area, A_f is given by $4A_p$ and the propped fracture area is given by $x_f(h_f + h)$. The fracturing fluid efficiency, pad volume and proppant scheduling can be obtained from equations presented in section 3.4.

3.6. Fracture conductivity and non-dimensional fracture conductivity

The primary goal of fracturing a well is to create a highly conductive, propped fracture which will improve the connection from the formation to the wellbore. Fracture conductivity and non-dimensional fracture conductivity are two important parameters to indicate the capacity of the fracture to transmit fluids down the fracture and into the wellbore with the ability of the formation to deliver fluid into the fracture. Their use in hydraulic fracture treatment design dates back to the earliest days of hydraulic fracturing in the 1950's (Pearson, 2001) and are still equally important in design considerations.

3.6.1. Fracture conductivity

Fracture conductivity is the product of fracture permeability and propped fracture width left after the fracture has closed. The permeability typically is measured in the laboratory for the particular proppant being used, while the fracture width are calculated numerically by use of an approximate fracture model. The American Petroleum Institute (API) published a series of standard testing procedures that involve laboratory measurement of fracture conductivity/permeability using various proppant (Pearson, 2001). Significant improvements in fracture conductivity, and thus well productivity, could be realised simply through better proppant selection. Various proppants and proppant selection procedures are presented by Smith (1992) where typical fracture conductivity data (laboratory measured) for various types of proppants are presented. The procedural selection of proppant has not been discussed here, rather how to estimate the effective fracture conductivity for incorporation in the production model as well as in the optimisation program is presented here in brief.

The values for fracture conductivity are generally taken from laboratory data (API standard) based on proppant type and closure stress. The API standard test for such data is to measure linear flow through a proppant pack between steel plates under a certain pressure. The proppant pack is tested at a concentration of 2 lb/ft^2. Most published data are measured according to this API test (Smith, 1992), which are only for the laboratory fracture capacity. The laboratory data is then corrected from the laboratory concentration (2 lb/ft^2) to the expected in-situ concentration in the following way:

$$k_{wf\,(in-situ)} = \frac{P_{c(in-situ)}}{2.0} k_{wf\,(lab)} \tag{3.51}$$

where $k_{wf(in\text{-}situ)}$ is the fracture conductivity after correction for in-situ concentration, $k_{wf(lab)}$ is the laboratory measured conductivity for a particular proppant at some closure stress and $P_{c(in\text{-}situ)}$ is the in-situ proppant concentration in the fracture after closure.

Experience shows that the in-situ proppant concentration greater than 1 lb/ft^2 is difficult to achieve under most conditions (Smith, 1992) and is given by

$$P_{c(in-situ)} = \frac{W_{pr}}{A_f} \tag{3.52}$$

If the permeability at closure stress is known for the proppant type used, the in-situ fracture conductivity can be estimated as

$$k_{wf\,(in-situ)} = k_{cs} \times w_p \tag{3.53}$$

where k_{cs} is the permeability at closure stresss and w_p is the final propped fracture width after the closure of fracture (Eq. 3.29).

Even after correcting for in-situ concentration, it has been found that laboratory data for fracture capacity give unrealistically high values. A realistic estimation of effective fracture conductivity is, therefore, a critical to the overall process and can only be achieved once the effects of long-term strength degradation, gel damage, temperature, embedment, formation fines, non-Darcy turbulent flow and non-Darcy multiphase flow have been considered. These effects are discussed in more detail by Smith (1992) and Richardson (2000). The summation of these effects can dramatically reduce the effective fracture conductivity. In some cases, the reduction is 10 to 20 fold, but the impairment can be so severe as to reduce the effective fracture conductivity to near zero (Richardson, 2000). Therefore, a conductivity damage factor, which approximately incorporates the above effects, is necessary to be considered. Smith (1992) reported that the best method for determining the proper conductivity damage factor for a particular field or formation is to compare fracture design values with in-situ values determined from pressure transient tests. However, a common rule of thumb is to arbitrarily reduce laboratory data by a large factor. A common practice is to reduce the conductivity values by 50-60%. This reduction is applied after correcting for in-situ concentrations (Eq. 3.51) and the effective fracture conductivity, k_{wf}, can be given by

$$k_{wf} = k_{wf(in-situ)} \times C_{ef} \tag{3.54}$$

where C_{ef} is the effective conductivity factor and is given by

$$C_{ef} = 1 - C_{df} \tag{3.55}$$

Here C_{df} is the conductivity damage factor.

3.6.2. Non-dimensional fracture conductivity

The non-dimensional fracture conductivity, F_{CD} can be defined as (Cinco-Ley *et al.*, 1978):

$$F_{CD} = \frac{k_{wf}}{k \times x_f} \tag{3.56}$$

where k is the permeability of the reservoir.

The optimum value of non-dimensional fracture conductivity, F_{CD} is important not only for the productivity of well, but also for fracturing fluid recovery after the fracture treatment. Poor fracturing fluid recovery increases the effect of gel damage on fracture conductivity, particularly in gas reservoirs with low mobile water saturation (Montgomery *et al.*, 1990; Sherman and Holditch, 1991). Therefore, the optimum F_{CD} to clean up the created fracture may be much higher than that necessary to produce from the reservoir and high conductivity fractures will clean up more quickly of this invaded zone than low conductivity fractures will (Soliman and Hunt, 1985; Montgomery *et al.*, 1990). Prats (1961) first recognized that there exists only one optimal non-dimensional fracture conductivity for a given volume of fracture and also determined that for a fracture of any volume and a production well of zero radius, the maximum production

rate is obtained when F_{CD} is about 1.3. Elbel (1985) later confirmed that for a given volume of proppant, the optimum F_{CD} is equal to 1.3, but for permeability less than 0.1 md, it should be much more than 1.3. Valko *et al.* (1997) determined that for any reservoir, well and proppant, the optimum F_{CD} is a constant equal to 1.6. Therefore, the optimum F_{CD} in the range of 1.3 to 1.6 represents the best compromise between the capacity of the fracture to conduct and the capacity of the reservoir to deliver hydrocarbon (Ricahrdson, 2000).

Richardson (2000) also reported that the values of F_{CD} may be more than this range and has kept it constant in his optimisation program to cleanup the fracture and to increase deliverability of the well. Then the program finds the optimum fracture half-length and other values by conducting a number of sensitivity runs. In this thesis, F_{CD} is not fixed or constant, rather laboratory-measured fracture conductivity is constant as discussed in the previous section, and then the effective fracture conductivity and F_{CD} are derived. Therefore, the value of F_{CD} depends on the amount of proppant in the fracture, fracture half-length and conductivity damage factor considered.

3.7. Parametric comparison of 2D and P-3D fracture models

A gas well located in a tight formation has been considered to illustrate the application of both PKN-C and P-3D-C fracture models. The reservoir is assumed to be a square one with a drainage area of 640-acre and a well at the centre. It has a pay zone of 100 *ft* thickness bounded above and below by shale subjected to higher stresses. Petrophysical and mechanical properties and other well data of the reservoir are presented in Table 3.1. A hydraulic fracture treatment was assumed for both fracture models: injection rate, 20 bbl/min; EOJ proppant concentration, 14 ppg; fracturing fluid viscosity, 100 cp; for which the injection time and fracture half-length or fracture height were calculated.

A 20/40 Westprop is selected as the propping agent, which has a prescribed laboratory measured fracture conductivity data at 2 lb/ft^2 proppant concentration. The laboratory data is modified from the laboratory concentration to the expected in-situ concentration.

A conductivity damage factor also has been applied after correcting for in-situ concentration to get reasonable fracture conductivity. Proppant selection data are presented in Table 3.2.

Table 3.1. Reservoir and formation properties and well data.

Drainage area	640 acres
Average depth	7,500 ft
Thickness	100 ft
Shape (square)	$5{,}280 \times 5{,}280$ ft^2
Equivalent drainage radius	2980 ft
Porosity	10 %
Permeability	0.20 mD
Initial reservoir pressure	4,400 psi
Reservoir temperature	200° F
Gas saturation	0.8
Gas gravity	0.85
Initial Z-factor	0.890
Initial gas viscosity, cp	0.02831
Water compressibility	3.0E-6
Pore compressibility	8.6E-6
Skin factor	0.0
Max. horizontal stress, σ_H	7,000 psi
Min. horizontal stress, σ_1	6,000 psi
Min. horizontal stress (shale), σ_2	6,700 psi
Min. horizontal stress (shale), σ_3	7,200 psi
Fracture toughness (bottom), K_{Icb}	1,700 psi-in$^{0.5}$
Fracture toughness (top), K_{Ict}	1,500 psi-in$^{0.5}$
Young's modulus	5.075E6 psi
Poisson's ratio	0.20
Leakoff coefficient	0.00025 ft/min$^{0.5}$
Spurt loss coefficient	0.0
Wellbore radius	0.35 ft
Flowing bottomhole pressure	1,700 psi
Tubing inside diameter	2.992 inch

Table 3.2. Proppant selection data.

Proppant type	20/40 Westprop
Specific gravity	3.1
Diameter	0.0248 inch
Porosity	0.35
Lab-measured fracture-conductivity at 2 lb/ft^2 proppant conc. and 6000 psi closure stress	6700 md-ft
Conductivity damage factor	0.60

3.7.1. Presentation of results

Two separate computer programs were developed using two fracture models. The P-3D-C model as defined in section 3.5 was run for different fracture half-lengths (from 400 – 2750 ft), and injection time and fracture height at the wellbore were calculated. The program also produced the values of other parameters: fracture width at the wellbore, fracture volume, fracturing fluid efficiency, fracture width after closure, in-situ proppant concentration, fracture conductivity, non-dimensional fracture conductivity and net fracture pressure. It could also produce pad volume and treatment schedules, which are not presented here. For the convenience of comparison, the values of fracture height and injection time as obtained from P-3D-C model are entered in PKN-C model and then fracture half-length is calculated.

Fracture dimensions as obtained from both models are compared in Figures 3.5-3.8. Figure 3.5 shows how the fracture height at the wellbore in both models grows with increasing injection time. Figure 3.6 presents the variation of average fracture height $\left(\frac{h+h_f}{2}\right)$ of P-3D-C model with respect to injection time; which shows the extent of difference between this average fracture height and the fracture height at wellbore in both models. Figure 3.7 shows that the fracture half-length is predicted slightly higher by P-3D-C model for any injection time. This is because the fracture half-length and the average fracture height in Eq. 3.49 are inversely proportional to each other. As average fracture height from P-3D-C is always lower than the fracture height in the PKN-C

model, the fracture half-length from P-3D-C is found always higher than that in PKN-C model. As per width equation (Eq. 3.18), a higher fracture half-length in P-3D-C model produces a higher fracture width at the wellbore, which is evident in Figure 3.8. Fracture net pressure is directly function of fracture width and, therefore, it is higher from P-3D-C model. A profile of net fracture pressure with respect to injection time, like width profile in Figure 3.8 is observed in Figure 3.9.

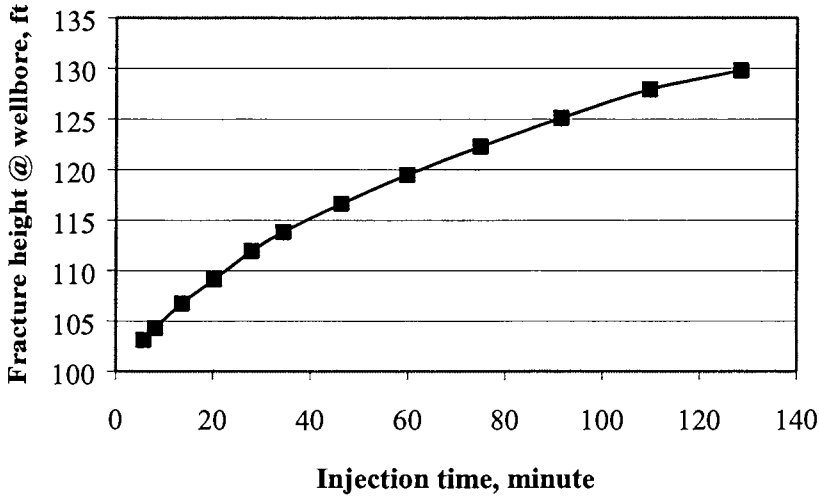

Figure 3.5. Fracture height growth at the wellbore with injection time for both fracture models.

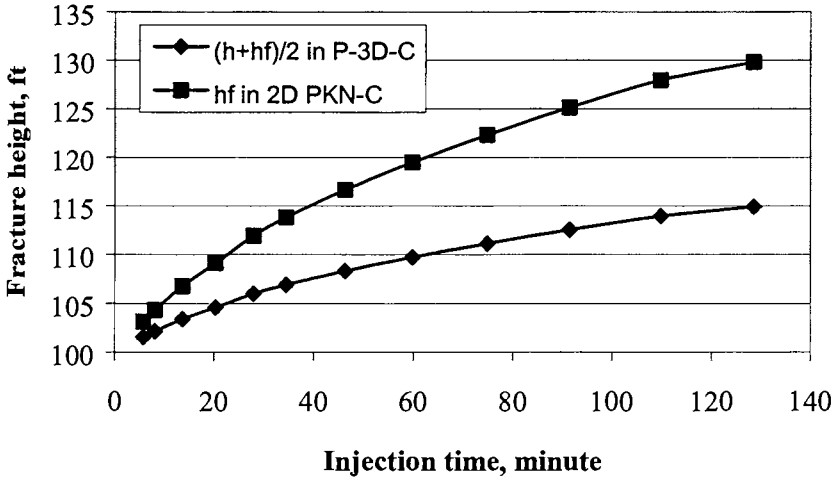

Figure 3.6. Variation of fracture height with injection time.

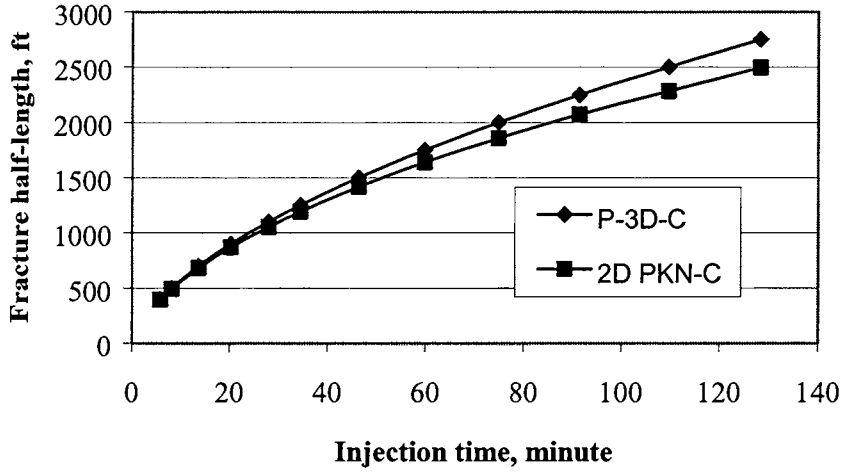

Figure 3.7. Variation of fracture half-length with injection time.

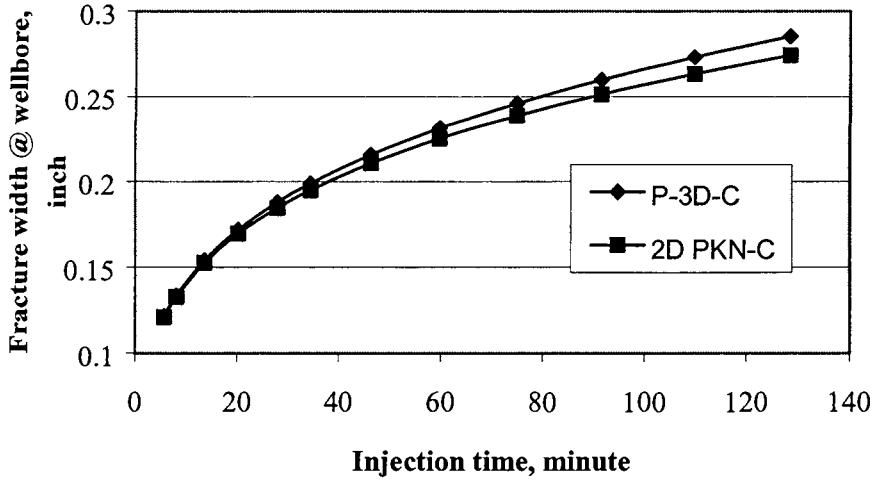

Figure 3.8. Variation of fracture width at the wellbore with injection time.

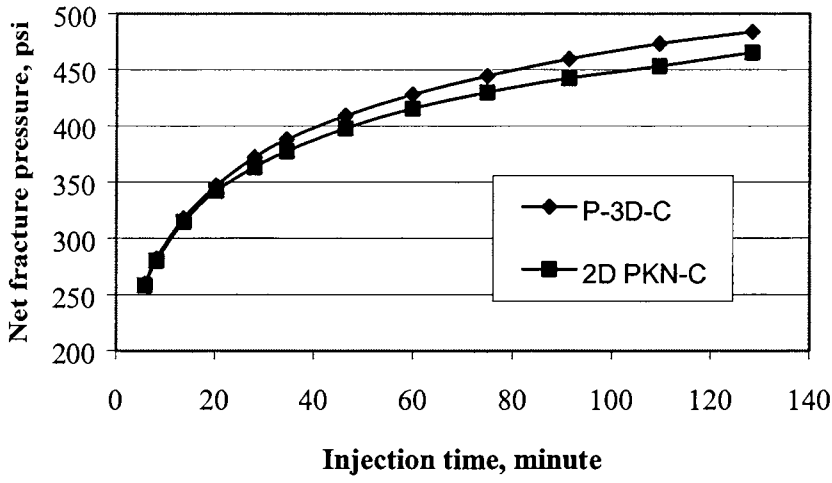

Figure 3.9. Effect of injection time on net fracture pressure.

The fracturing fluid efficiency with injection time is presented in Figure 3.10. The figure shows that the efficiency is decreasing with injection time. This is because the fracture surface area increases with time and the fracture fluid leaks-off more with both increasing time and surface area. As the same fracture height at the wellbore is used in both models and this fracture height remains constant along the fracture length in PKN-C model, the fracture area by the 2D model is higher and hence the fluid efficiency is lower.

Figures 3.11-3.13 show the variation of propped fracture width (fracture width after closure), in-situ proppant concentration and fracture conductivity with injection time, respectively. It is interesting to note that the trends of profiles in these figures are similar. This is because that these parameters are mainly function of total amount of proppant placed in the fracture. The productivity of a reservoir contributed by the fracture directly depends on these parameters. In the first part of injection time (till injection time of about 40 minutes as shown in figures), the values of these parameters in PKN-C model is slightly higher than those in P-3D-C model. But in the later part it is just opposite with higher differences as the injection time increases. This is because the differences in fracture half-length and the fracture width between the models increase with increasing injection time. Also the fluid efficiency influences the pad volume, the

proppant-laden fluid volume and the average proppant concentration. With increasing fluid efficiency, the proppant-laden fluid volume and the average proppant concentration increase, which ultimately increases the total amount of proppant in the fracture. Therefore, there is difference in the amount of proppant in two models although the same treatment is used. This difference in proppant amount influences the profiles of two fracture models in Figures 3.11-3.13. However, the difference in the amount of proppant between the models is small (as shown in Figure 3.14) as compared to the amount of proppant injected.

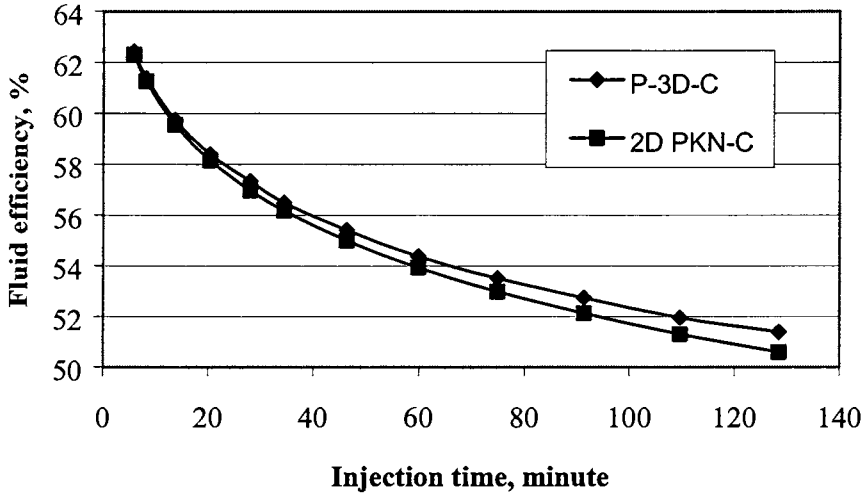

Figure 3.10. Effect of injection time on fluid efficiency.

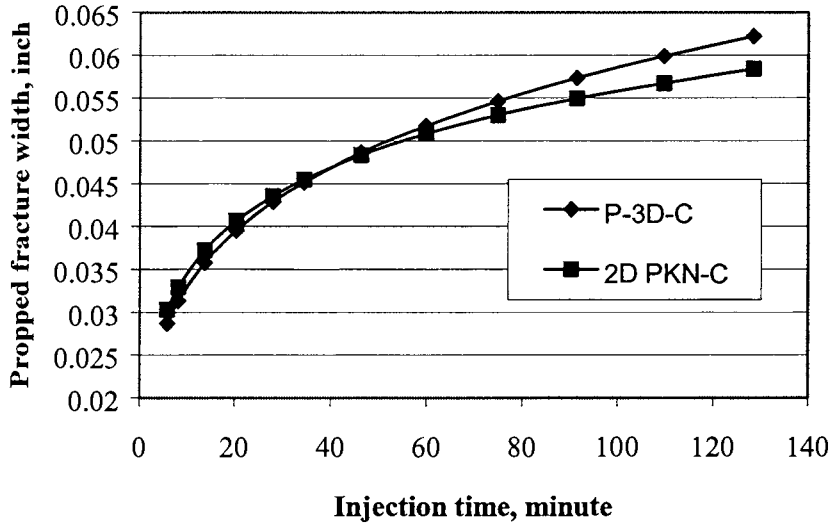

Figure 3.11. Variation of propped fracture width with injection time.

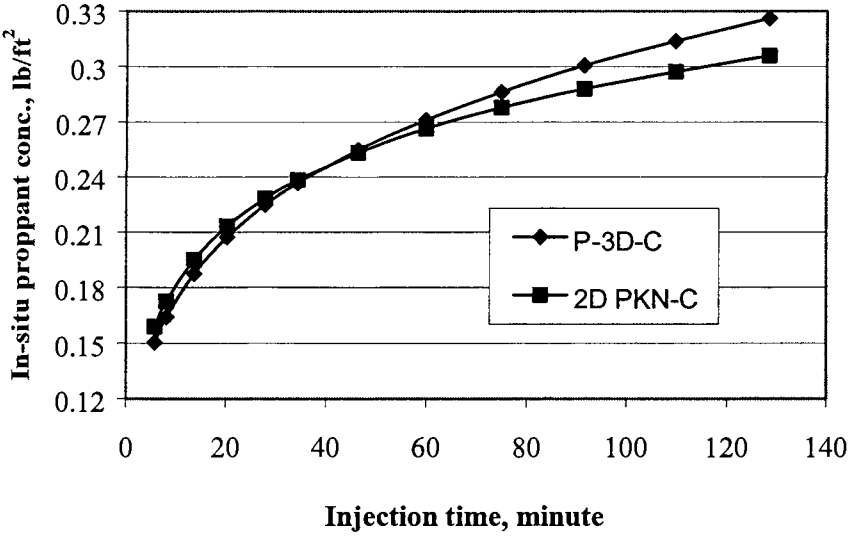

Figure 3.12. Variation of in-situ proppant concentration with injection time.

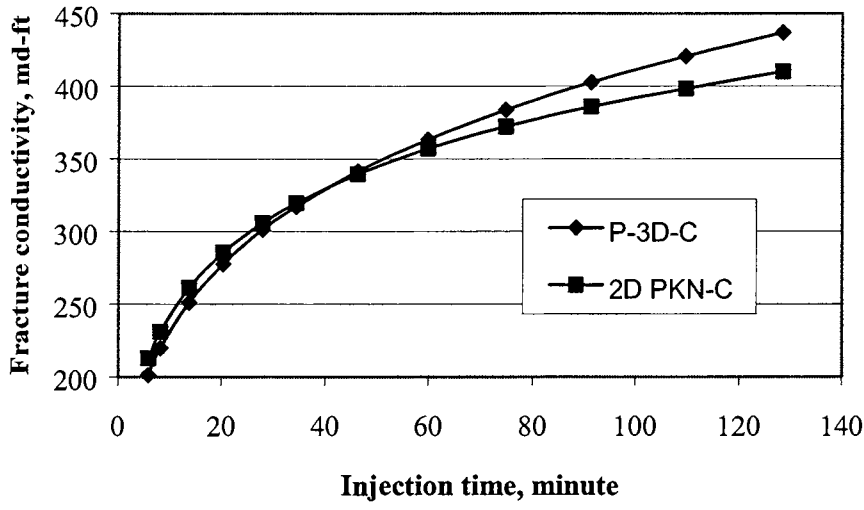

Figure 3.13. Variation of fracture conductivity with injection time.

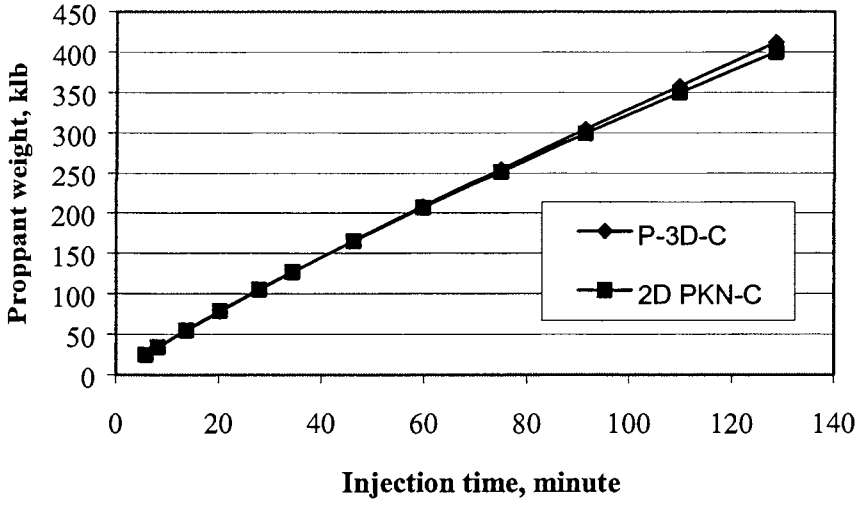

Figure 3.14. Amount of proppant injected with injection time.

The non-dimensional fracture conductivity, F_{CD} is directly function of effective fracture conductivity and is inversely proportional to the fracture half-length (Eq. 3.56). Figures 3.15 and 3.16 (with conductivity damage factor, C_{df} of 0.6 and 0.0, respectively) show that F_{CD} is decreasing with injection time. This is because the fracture half-length is increasing (F_{CD} decreasing) with increasing injection time, which exceeds the increment in F_{CD} through increased effective fracture conductivity, and ultimately F_{CD} is

decreasing. It is interesting to note that there is little difference in the values of F_{CD} between the models with slightly higher in PKN-C model, which means that with the same treatment both models will create fractures that will produce almost the same from the reservoir. Figures show that the value of F_{CD} also depends on the value of C_{df} considered by the designer and is higher with lower value of C_{df}. Within the range of C_{df} of 0.6-0.0, the value of F_{CD} varies from 2.5 to 6.7 (at the beginning of injection) and from 0.8 to 2.0 (at the end of injection). The optimum value of F_{CD} (as mentioned in section 3.6.2) falls reasonably within this range (0.8 to 2.0, which is the final F_{CD}).

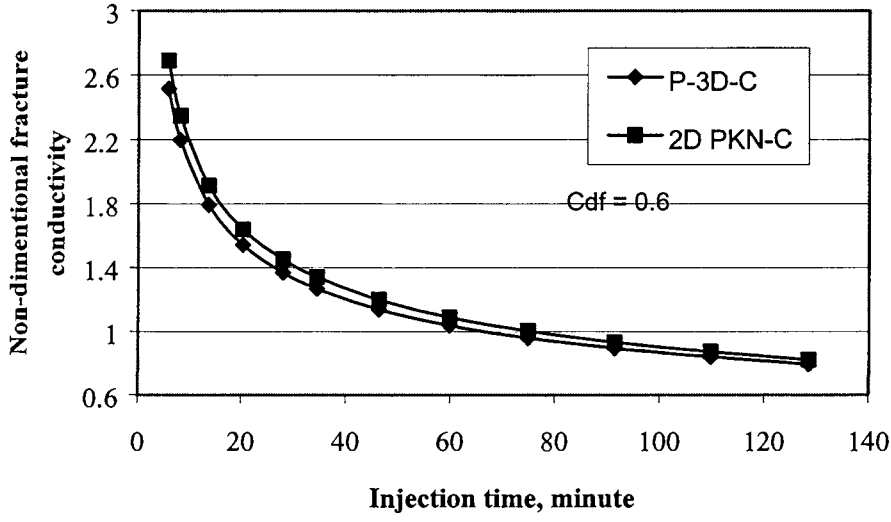

Figure 3.15. Non-dimensional fracture conductivity with injection time (conductivity damage factor is 0.6).

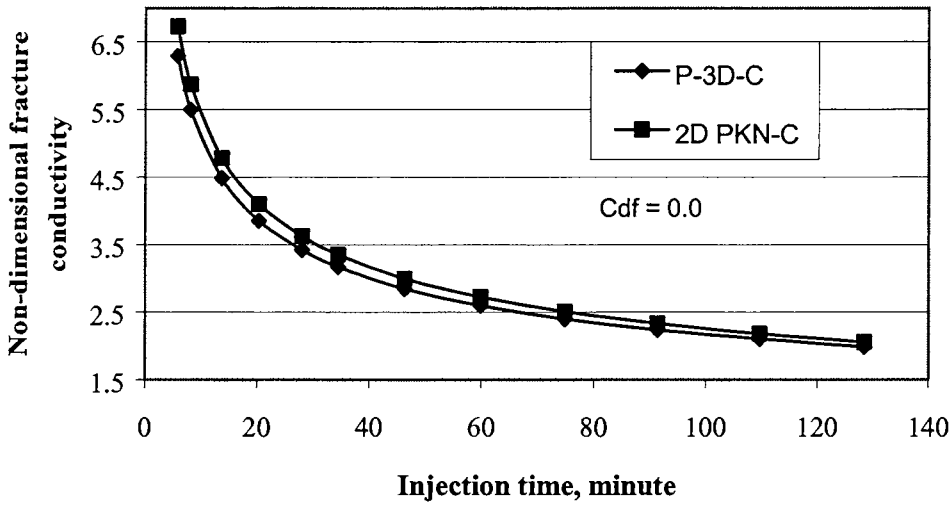

Figure 3.16. Non-dimensional fracture conductivity with injection time (conductivity damage factor is 0.0).

3.8. Conclusions

Comparison of parametric results obtained from both models leads to the following conclusions:

1. For a given injection time and a given fracture height at the wellbore, the fracture half-length, width, net pressure and fluid efficiency obtained from P-3D-C model are slightly higher than that from PKN-C model.

2. For a given injection time and a given fracture height at the wellbore, the propped fracture width, in-situ proppant concentration and fracture conductivity are slightly higher according to PKN-C model up to a certain injection period beyond which the reverse is true.

3. The non-dimensional fracture conductivity is found slightly lower by P-3D-C model, and is significantly reduced with increasing conductivity damage factor. Therefore, the use of an appropriate damage factor is crucial in hydraulic fracturing so that the design and predicted productivity come closer to the reality.

4. In terms of variation in various fracture parameters, very little difference is found between PKN-C and P-3D-C models. Therefore, the 2D PKN-C model is sufficient to design fracture treatments certainly for three-layer problems and may be multi-layer problems as well (Rahim and Holditch, 1995). Although both models will be integrated with the proposed model for treatment optimisation, very little difference in optimised treatment parameters is expected.

CHAPTER FOUR

DEVELOPMENT OF AN ANALYTICAL MODEL FOR PRODUCTION ESTIMATION FROM A FRACTURED RESERVOIR

4.1. Introduction

Formulation of objective function for hydraulic fracturing design optimisation requires a cumulative production over a period of time from hydraulically fractured reservoirs. The cumulative production during the period can be estimated if a constant production rate can be maintained by regulating the bottom hole flowing pressure with changing reservoir pressure due to production. The bottom hole flowing pressure requires to be adjusted at a regular time interval. Alternatively, the reservoir can be produced with a constant bottom hole flowing pressure (Agarwal *et al.*, 1979). In this case, the production rate will vary with time due to declining reservoir pressure proportionately with production. The varying production rates over the period can be estimated at a regular time interval to obtain the cumulative production by rate-time integration. Both cases can be simulated by a numerical reservoir simulator to obtain the desired parameter (i.e., either bottom hole flowing pressures, or production rates, at a time interval). Such numerical simulation is computationally intensive and not feasible to couple with any optimisation program and to repeat many times, as required during optimisation. An approximate analytical method is, therefore, given emphasis in this study. It is, however, sensible to conduct a post-design production evaluation by using a numerical simulator for the fracture that will be optimised using the analytical method developed in this chapter.

The basis of the approximate method is the familiar radial diffusivity equation for fluid flow to a well through the porous formation. This basic equation can be solved using

appropriate boundary conditions for various flow conditions in the reservoir. Many modifications are incorporated in the solutions, based on analytical, numerical and experimental investigations over time, to consider various flow conditions, fluid properties, formation damage effects and hydraulic fracture effects. It is important to note that more than one flow condition may occur in the same reservoir during its production life. This poses a complexity to appropriately divide the total production life into different flow regimes and then use the appropriate flow solution for each regime. Moreover, smooth coupling between two different regimes is also a considerable problem.

In order to incorporate the features discussed above in the development of the approximate analytical model for production estimation, various flow conditions and their corresponding pressure and boundary conditions are summarised. It is pointed out that the type of reservoir considered in this study may be subjected to both transient and pseudo-steady-state flow conditions. Various analytical formulations for these flow conditions are reviewed and selected for this study. It is assumed that the bottom hole flowing pressure will be kept constant over the production life and therefore adjusted production rates will be estimated with a regular time interval. During each time interval, the production rate is estimated based on constant rate flow analysis. There are considerable debates about how many flow regimes (e.g. transient, late-transient, pseudo-steady-state) are involved in the production life and what the duration are for individual regimes. Based on productivity index matching, an approximate technique for defining flow regimes and hybridisation between these regimes is then presented. Results from the proposed production model are compared with numerical simulation results for assumed hydraulic fractures.

4.2. Reservoir flow conditions

The reservoir productivity is estimated by solving a basic partial differential equation, usually called diffusivity equation, for fluid flow in porous media. The equation is solved using initial and boundary conditions imposed during production. Three most

common conditions for which reservoir engineers seek constant terminal rate solutions are transient, pseudo-steady-state and steady-state. These conditions are applicable at different times after the start of production and for different, imposed (or assumed) boundary conditions.

4.2.1. Transient condition

Once a pressure disturbance is created in the reservoir, such as by starting production, or by changing the rate of production, the transient flow condition occurs in the reservoir. During this condition, the pressure redistribution occurs around the well and does not reach the reservoir boundary. Thus, the reservoir appears infinite in extent, and both the pressure and the pressure derivative in this region become functions of time and radial distance from the well. This condition is mainly applied to well tests to measure and analyse the pressure response for a brief period of few hours after the production rate is changed deliberately. The transient period is usually assumed very short and ignored in estimating reservoir production. The total duration of transient period, however, depends mainly on the permeability and size of the reservoir. For a relatively large reservoir in low-permeability formations, the transient period becomes considerably long and therefore the well production during this period should be estimated by solving the diffusivity equation using the transient boundary condition.

4.2.2. Pseudo-steady-state condition

This condition (called semi-steady-state condition in some literatures) is applicable to a reservoir, which has been producing for a sufficient period of time so that the transient response has been over and the effect of the outer boundary has been felt. The condition persists, after the transient period, in a depletion type reservoir, which is assumed to be surrounded by a solid brick wall that prevents the flow of fluids into the radial cell. Because of no flow (or very insignificant flow) from surrounding formations, the pressure in the reservoir region declines proportionately with production. For a constant rate production well, the pressure decline rate with respect to time remains constant throughout the reservoir and during the production period.

4.2.3. Steady-state condition

This condition exists, after the transient period, in a producing reservoir that has outer boundaries completely open to aquifer or artificial water injection. It is assumed that production from the reservoir is exactly balanced by fluid entry across the open boundary. Therefore, the reservoir pressure at the boundary remains constant and the pressure distribution within the reservoir does not change with time.

4.3. Transient production model

When a well is allowed to produce first time after perforation / fracturing, the pressure in the wellbore normally continues to decrease as the flow time increases. Simultaneously, the area from which the gas is drained increases and the pressure transience moves further out into the reservoir until it reaches the boundary.

As discussed earlier, the transient effect in a fractured reservoir with moderate to high permeablity is of no importance. In low permeability sand, transient flow is important as it may continue for a significantly long period depending also on reservoir pressure and bottom hole flowing pressure. Hydraulically fractured gas wells in low permeability formations are normally produced at constant bottom hole flowing pressure, rather than a constant-rate (Agarwal *et al.*, 1979). Therefore, the production rate versus time curve appears more appropriate for analysing production performance. This requires a constant production rate to be estimated over a time interval. Therefore, approximate equations will be developed first to estimate production with a constant rate (for transient condition in this section and for pseudo-steady state condition in the following section). The way the equations will be used as functions of production time will be discussed later.

4.3.1. Diffusivity equation for gas flow in porous media

During the transient period, the gas flow rate in a reservoir is approximated based on Darcy's law and the continuity principle. Using the mass conservation law, the equation for gas flow rate in the transient condition is derived from the following general expression (Dake, 1978; Economides *et al.*, 1994):

$$\phi \frac{\partial \rho}{\partial t} = \nabla \left(\rho \frac{k}{\mu_g} \nabla p \right) \tag{4.1}$$

where ϕ is the porosity, ρ is the density of gas, t is the flow time, μ_g is the viscosity of gas, k is the formation permeability and p is the pressure.

The basic assumptions for radial flow of a fluid in the vicinity of a well include homogeneous and isotropic reservoir, well producing across the entire formation thickness and the formation saturated with a single-phase fluid. Considering radial co-ordinates and real gas law, the above equation can be converted to:

$$\frac{\phi}{k} \frac{\partial}{\partial t} \left(\frac{p}{Z_g} \right) = \frac{1}{r} \frac{\partial}{\partial r} \left(\frac{p}{\mu_g Z_g} r \frac{\partial p}{\partial r} \right) \tag{4.2}$$

where Z_g is the gas deviation factor (Z-factor) and r is an arbitrary radial distance from the well centre.

Performing differentiation and further re-arranging, the above equation can be written as:

$$\frac{\partial^2 p^2}{\partial r^2} + \frac{1}{r} \frac{\partial p^2}{\partial r} = \frac{\phi \mu_g}{kp} \frac{\partial p^2}{\partial t} \tag{4.3}$$

Considering ideal gas for which gas compressibility, c_g, is approximately equal to $1/p$, the above equation can be expressed as follows:

$$\frac{\partial^2 p^2}{\partial r^2} + \frac{1}{r}\frac{\partial p^2}{\partial r} = \frac{\phi \mu_g c_g}{k}\frac{\partial p^2}{\partial t} \tag{4.4}$$

Al-Hussainy and Ramey (1966) developed a pressure drawdown solution of the above diffusivity equation using a real gas pseudo-pressure function in order to consider the effect of changing gas properties as functions of pressure. The real gas pseudo-pressure, $m(p)$ is defined as:

$$m(p) = 2\int_{p_0}^{p} \frac{p}{\mu_g Z_g} dp \tag{4.5}$$

where p_o is a low base pressure, the value of which is very low (may be zero). The differential pseudo-pressure $\Delta m(p)$, defined as $m(p_i) - m(p_{wf})$, is then the driving force in the reservoir in which p_i is the initial pressure and p_{wf} is the bottom hole flowing pressure. At a low pressure, the product of initial gas properties, $\mu_g Z_g$ and the product of average gas properties, $\overline{\mu}_g \overline{Z}_g$ remain constant, which is an adequate approximation for some gases, and $\Delta m(p)$ is then given as:

$$2\int_{P_{wf}}^{P_i} \frac{p}{\mu_g Z_g} dp \approx \frac{p_i^2 - p_{wf}^2}{\overline{\mu}_g \overline{Z}_g} \tag{4.6}$$

where the average properties $\overline{\mu}_g$ and $\overline{Z}_g$ are evaluated at an average pressure (discussed later) within the drainage area of the well.

At high pressures (both p_i and p_{wf} higher than 3000 psi), $\Delta m(p)$ is approximated as follows (Dake, 1978):

$$2\int_{P_{wf}}^{P_i}\frac{p}{\mu_g Z_g}dp \approx 2\frac{\overline{p}}{\overline{\mu}_g \overline{Z}_g}\left(p_i - p_{wf}\right) \tag{4.7}$$

Note that $\overline{p}$ in the above equation represents the average reservoir pressure.

The diffusivity equation for natural gases was then derived by replacing p^2 in Eq. 4.4 by the pseudo-pressure *m(p)* as follows:

$$\frac{\partial^2 m(p)}{\partial r^2}+\frac{1}{r}\frac{\partial m(p)}{\partial r}=\frac{\phi\mu_g c_g}{k}\frac{\partial m(p)}{\partial t} \tag{4.8}$$

The real gas pseudo-pressure drawdown at a constant flow rate in the transient phase is then expressed as (Economides *et al.*, 1994; Lee and Wattenbarger, 1996):

$$m(p_i)-m(p_{wf})=\frac{57{,}910 q_g p_{sc} T}{khT_{sc}}\left(\log t+\log\frac{k}{\phi\overline{\mu}_g\overline{c}_t r_w^2}-3.23+0.869s'\right) \tag{4.9}$$

where, q_g is the gas flow rate in Mscf/D, T is the reservoir temperature, p_{sc} and T_{sc} are pressure and temperature at standard conditions, h is the pay zone thickness, $\overline{c}_t$ is the total system compressibility at the average pressure in the drainage area, and s' is the total skin factor that includes the skin resulting from true formation damage or stimulation, s, and a non-Darcy flow effect, Dq_g. The calculations of s' and $\overline{c}_t$ are discussed later.

For $p_{sc} = 14.7 psia$ and $T_{sc} = 520^o R$, the above equation becomes:

$$m(p_i)-m(p_{wf})=\frac{1637 q_g T}{kh}\left(\log t+\log\frac{k}{\phi\overline{\mu}_g\overline{c}_t r_w^2}-3.23+0.869s'\right) \tag{4.10}$$

Russell *et al.* (1966) adopted a different approach and developed the pressure-squared (or sometimes known as p^2) formula to relate the pressure drawdown with the flow rate of gases. Lee and Wattenbarger (1996) argued that for some gases at low pressures (e.g. below 2000 psia), the product $\mu_g Z_g$ and $\overline{\mu}_g \overline{Z}_g$ are approximately equal and constant. In such cases, the pseudo-pressure difference can be conveniently defined by Eq. 4.6 the substitution of which in Eq. 4.10 also gives the pressure-squared formula presented by Lee and Wattenbarger (1996) as follows:

$$p_i^2 - p_{wf}^2 = \frac{1637 q_g T \overline{Z}_g \overline{\mu}_g}{kh}\left(\log t + \log\frac{k}{\phi \overline{\mu}_g \overline{c}_t r_w^2} - 3.23 + 0.869 s'\right) \tag{4.11}$$

It is important to note that the last term in Eq. 4.11 is added later to the original pressure-squared formula in order to account for skin resulting from formation damage, stimulation and non-Darcy flow effect. A slightly different equation can also be obtained using the pseudo-pressure defined by Eq. 4.7 for some gases at higher pressure (both p_i and p_{wf} higher than 3000 psi). Further variations in the relationship of pressure drawdown and flow rate in some particular cases are reviewed and presented by Lee and Wattenbarger (1996).

Review presented so far in this chapter and those by Lee and Wattenbarger (1996) reveal that there are considerable variations in this relationship and consequently, uncertainties in using an appropriate relationship for a given case. In brief, the pseudo-pressure relationship is more general and correct to cover the whole range of reservoir pressure and the pressure drawdown. The main disadvantage is the calculation of the pseudo-pressure, which can be performed by using some sort of numerical integration technique if basic PVT data for the reservoir gas are available. In the absence of such data, the pressure-squared relationship is more convenient to use and therefore it is widely used in the industry. In many cases, the pressure-squared and the pseudo-pressure solutions give identical results (AL-Hussainy and Ramey, 1966; Ramey and Wattenbarger, 1968; Aziz *et al.*, 1976). A degree of inaccuracy is generally involved in the pressure-squared relationship when both the reservoir pressure and the pressure

drawdown are high (Dake, 1978). The percentage of error is, however, not numerically established. Also at the preliminary stage of reservoir development by hydraulic fracturing, the modelling involves many other uncertainties associated with formation characteristics, fracturing fluids and fracture geometry, and PVT data may not be available at all. These are enough reasons for engineers to accept the pressure-squared relationship widely without much emphasis on numerical accuracy. The relationship also facilitates computationally efficient repeated approximations involved either in the preliminary design stage, or in the optimisation process.

Based on the above arguments, the pressure-squared relationship is adopted for this study as well and to calculate the production rate during the transient flow period the relationship is converted into the following form:

$$q_g = \frac{kh\left[p_i^2 - p_{wf}^2\right]}{1637\bar{\mu}_g \bar{Z}_g T}\left[\log t + \log\frac{k}{\phi\bar{\mu}_g \bar{c}_t r_w^2} - 3.23 + 0.869s'\right]^{-1} \tag{4.12}$$

This equation can also be used for transient inflow performance curves for a gas well at different values of t and p_{wf}.

4.3.2. Production rate equation for fractured wells

Eq. 4.12 is adjusted for estimation of transient production rates from a fractured well by replacing the wellbore radius, r_w by an effective wellbore radius (r_w') to account for the effect of fracture. Lee and Wattenbarger (1996), based on the works of Van Everdingen (1953) and Mathews and Russell (1967) present the following expression for effective wellbore radius:

$$r_w' = r_w e^{-s_f} \tag{4.13}$$

Cinco-Ley and Samaniego (1981) proposed a graphical method for determining the pseudo-skin, s_f in Eq. 4.13, considering a bilinear flow characteristic in a finite-

conductivity fracture, which represents a hydraulically fractured well more reasonably than an infinite-conductivity fracture described by Gringarten and Ramey (1974). The pseudo-skin is obtained from the following relationship:

$$F = s_f + \ln\frac{x_f}{r_w}. \tag{4.14}$$

From the estimated value of non-dimensional fracture conductivity, F_{CD}, for proppant used, the value of F is read from the graph and then s_f is calculated from the known value of wellbore radius, r_w and fracture half-length, x_f. Recently, Valko *et al.* (1997) have converted the graphical data of Cinco-Ley and Samaniego (1981) into a programmable equation, which provides a simple but accurate curve fit of the graphical representation to calculate F as follows:

$$F = \frac{1.65 - 0.328u + 0.116u^2}{1 + 0.18u + 0.064u^2 + 0.005u^3} \tag{4.15}$$

where

$$u = \ln(F_{CD}) \tag{4.16}$$

and

$$F_{CD} = \frac{k_{wf}}{kx_f} \tag{4.17}$$

Here, k_{wf} is the fracture conductivity in md-ft, F_{CD} is the non-dimensional fracture conductivity, and x_f is the fracture half-length.

4.3.3. Non-Darcy effects during transient flow period

The basic assumption for Darcy's law to describe fluid flow through a porous media is that the flow is at low to moderate rates for which the pressure drop in the direction of flow is proportional to the fluid velocity. At the starting of gas production from a fractured well, the flow rate is very high and consequently the pressure drop in the fracture is very high and the flux distribution along the fracture becomes irregular due to viscous and inertial force components. These effects are called non-Darcy effects, because they make the flow deviate from the Darcy's law. These non-Darcy effects significantly influence gas production performance in a fractured well (Fligelman *et al.*, 1989; Rangel-German and Samaniego-V, 2000; Umnuayponwiwat *et al.*, 2000). These effects can be taken into account by adding a non-Darcy component to the usual Darcy's equation, which leads to the Forchheimer's equation. In the pressure drawdown solution of the flow equation, this non-Darcy component is included in the skin factor – an approach that is widely used by reservoir engineers and also adopted in this study (Eqs. 4.9-4.12). The total skin factor, s' that incorporates a non-Darcy component is expressed as follows (Dake, 1978):

$$s' = s + Dq_g \tag{4.18}$$

in which s is the usual formation damage and stimulation skin factor and D is a constant known as the non-Darcy flow co-efficient (in D/Mscf). The term Dq_g thus accounts for the turbulence skin effect or rate-dependent pseudoskin in high production rate wells. An empirical relationship for non-Darcy flow coefficient is given as (Economides *et al.*, 1994):

$$D = \frac{6\times10^{-5}\gamma k_s^{-0.1} h}{\mu_{g,wf} r_w h_{perf}^2}, \tag{4.19}$$

where γ is the gas gravity, k_s is the near-wellbore permeability in md, h and h_{perf} the net and perforated thickness, both in ft, and μ_g is the gas viscosity in cp, evaluated at the bottom hole flowing pressure.

Another equation for non-Darcy co-efficient is presented by Lee and Wattenbarger (1996) as follows:

$$D = \frac{2.715\times10^{-15}\beta kMp_{sc}}{hr_w T_{sc}\mu_{g,wf}} \tag{4.20}$$

where M is molecular weight, $\mu_{g,wf}$ is pressure-dependent gas viscosity evaluated at P_{wf} and β is a turbulence parameter inversely proportional to permeability, which can be determined from the following equation (Jones, 1987).

$$\beta = 1.88\times10^{10}k^{-1.47}\phi^{-0.53} \tag{4.21}$$

Substituting the value of total skin factor, s' and the effective wellbore radius, r_w' in Eq. 4.12, the transient flow rate equation for a fractured well becomes:

$$q_g = \frac{kh\left[p_i^2 - p_{wf}^2\right]}{1637\overline{\mu}_g\overline{Z}_g T}\left[\log t + \log\frac{k}{\phi\overline{\mu}_g\overline{c}_t r_w'^2} - 3.23 + 0.869\left(s + Dq_g\right)\right]^{-1} \tag{4.22}$$

It is important to note that Eq. 4.22 becomes quadratic, which is solved for production rate in this study by a numerical technique.

4.4. Pseudo-steady state production model

As mentioned earlier, when the reservoir is surrounded by no-flow boundaries either by natural limits, such as faults, pinchouts, etc., or artificially induced limits by production

from adjoining wells, the pressure at the outer boundary declines at a constant rate with time. This condition is described as pseudo-steady-state which prevails after the transient period.

The basic radial diffusivity equation (Eq. 4.4) can be solved for this condition. Following the approach taken by Russell *et al.* (1966), the final inflow equation for gases can be expressed as (Dake, 1978):

$$\bar{p}^2 - p_{wf}^2 = \frac{1422 q_g \bar{\mu}_g \bar{Z}_g T}{kh}\left(\ln\frac{r_e}{r_w} - \frac{3}{4} + s\right) \tag{4.23}$$

in which $\bar{\mu}_g$ and $\bar{Z}_g$ are evaluated at the average of $\bar{p}$ and p_{wf} and $\bar{p}$ is the average reservoir pressure. Evaluations of $\bar{p}$, $\bar{\mu}_g$ and $\bar{Z}_g$ are discussed later. Taking the term ¾ into logarithm, Economides *et al.* (1994) rearranged the above equation as follows:

$$\bar{p}^2 - p_{wf}^2 = \frac{1424 q_g \bar{\mu}_g \bar{Z}_g T}{kh}\left(\ln\frac{0.472 r_e}{r_w} + s\right) \tag{4.24}$$

Valko *et al.* (1997) modified Eq. 4.24 taking the fracture effect into account from which the gas flow can be estimated as follows:

$$q_g = \frac{kh\left(\bar{p}^2 - p_{wf}^2\right)}{1424 \mu_g Z_g T} \times \frac{1}{\ln\left(\frac{0.472 r_e}{x_f}\right) + \left(s_f + \ln\frac{x_f}{r_w}\right)} \tag{4.25}$$

Note that the pseudo-skin, s_f created by the fracture is defined in the previous section (Eq. 4.14).

4.5. Time-interval implementation of constant production rate equations

As mentioned earlier, the well is assumed to produce at a constant bottom hole flowing pressure. The production rate under this condition will decline with the declining reservoir pressure as a function of cumulative production. In order to adjust the constant rate flow equations (Eqs. 4.22 and 4.25) for this production condition, the total production life is defined as cumulative of a small time interval. After each cumulative period, the average reservoir pressure and gas properties ($\overline{\mu}_g$ and $\overline{Z}_g$) are evaluated as functions of cumulative production up to that period and used them to estimate the constant production rate during the small time interval which then cumulate the production up to the next production period.

Let us define the small time interval as Δt. Successive time steps are indexed as i = 0, 1, 2, 3,....., n. At i = 0, all parameters correspond to the initial reservoir condition and they are used for production with constant rate estimated by Eq. 4.22 during Δt period. Assuming Δt in hour, the cumulative production during this period will be q_g x ($\Delta t/24$). The average reservoir pressure, which will be less than the initial pressure due to gas production, will be calculated. The calculated average reservoir pressure will be used to calculate the average gas properties ($\overline{\mu}_g$ and $\overline{Z}_g$). At the next time step, i = 1, the average pressure and gas properties will be used to calculate production rate that is constant over next Δt, after which the total cumulative production, G_p will be calculated and the procedure will be repeated. Obviously, the transient production rate equation will be used in this procedure until the pseudo-steady state condition becomes active after which the equation for pseudo-steady state condition will be used. Transition between these conditions will be detailed later. Mathematical relationships for deriving average gas properties in every time step are presented in the following section for depletion type reservoirs.

4.5.1 Average gas properties in depletion type reservoirs

As this type of reservoir is confined by impermeable strata and there is no or insignificant water influx from the adjoining aquifer, the reservoir pressure declines with production. The reservoir volume occupied by hydrocarbon, however, does not decrease significantly, except for a slight reduction, due to connate water expansion and pore volume compaction with the declined reservoir pressure. The sate of a real gas in the reservoir can be expressed as follows:

$$E_i = 35.37\frac{p_i}{Z_i T} \tag{4.26}$$

where E_i is the initial gas expansion factor (scf/rcf), p_i is the initial reservoir pressure (psia), Z_i is the initial Z-factor, T is the reservoir temperature (^{o}R).

The initial gas in place, G in the reservoir can be calculated from the following equation:

$$G = V\phi(1 - S_{wc})E_i \tag{4.27}$$

V is the net bulk volume of the reservoir; S_{wc} is the connate water saturation.

From material balance in the depletion reservoir at an isothermal condition, the state of the reservoir at any stage of gas production can be as follows (Dake, 1978):

$$\frac{G_p}{G} = 1 - \left[1 - \frac{(C_w S_w + C_f)\Delta p}{1 - S_{wc}}\right]\frac{E}{E_i} \tag{4.28}$$

where, E is the gas expansion factor, G_p is the cumulative gas production, C_w is the compressibility of water (psi^{-1}), S_w is the water saturation, C_f is the pore compressibility (psi^{-1}), and $\Delta p = p_i - \overline{p}$, where $\overline{p}$ is the average reservoir pressure (psia).

Generally, the gas expansion factor can be obtained from standard PVT analysis as a linear function of reservoir pressure as follows:

$$E = E_i + a_e(\overline{p} - p_i) \tag{4.29}$$

where a_e is the slope of experimental E vs. p data. Substituting Eq. 4.29 into Eq. 4.28, one can obtain the following pressure equation in quadratic form (Guo and Evans, 1993):

$$A(\overline{p} - p_i)^2 + B(\overline{p} - p_i) + C = 0 \tag{4.30}$$

The solution of Eq. 4.30 for time step production condition described above can be expressed as:

$$(\overline{p})^i = p_i + \frac{-(B)^i \pm \sqrt{[(B)^i]^2 - 4(A)^i(C)^i}}{2(A)^i} \qquad \text{(for A} \neq 0\text{)} \tag{4.31}$$

$$(\overline{p})^i = p_i - \frac{(C)^i}{(B)^i} \qquad \text{(for A} = 0\text{, B} \neq 0\text{)} \tag{4.32}$$

where

$$(A)^i = a_e\left(\frac{C_w(S_w)^{i-1} - C_f}{1 - S_{wc}}\right) \tag{4.33}$$

$$(B)^i = a_e + E_i\left(\frac{C_w(S_w)^{i-1} - C_f}{1 - S_{wc}}\right) \tag{4.34}$$

$$(C)^i = E_i\left(\frac{(G_p)^{i-1}}{G}\right) \tag{4.35}$$

Note that '*i*' superscripts represent time steps, 1, 2, 3, ..., not power. Values of $\overline{Z}_g, \overline{\mu}_g$ and $\overline{c}_t$ are adjusted at the *i*-th time step as follows:

$$(\overline{Z}_g)^i = 35.37\frac{\left((\overline{p})^i + p_{wf}\right)}{2(E)^i T} \tag{4.36}$$

$$(\overline{\mu}_g)^i = 4.0\times10^{-6}\left(\frac{(\overline{p})^i + p_{wf}}{2}\right) + 0.0107 \tag{4.37}$$

$$(\overline{c}_t)^i = (S_g)^i (c_g)^i \tag{4.38}$$

in which

$$(E)^i = E_i + a_e\left\{\left[\frac{(\overline{p})^i + p_{wf}}{2}\right] - p_i\right\} \tag{4.39}$$

$$(S_g)^i = 1 - (S_w)^i \tag{4.40}$$

$$(S_w)^i = \frac{S_{wc}\left[1 + C_w\left(p_{in} - (\overline{p})^i\right)\right]}{1 - \left(\frac{C_w(S_w)^{i-1} - C_f}{1 - S_w}\right)\left[P_i - (\overline{p})^i\right]} \tag{4.41}$$

$$(c_g)^i = \frac{1}{(\bar{p})^i} \tag{4.42}$$

Eq. 4.37 is developed based on a set of pressure-viscosity data of a particular reservoir gas of gravity 0.85 at temperature 200^oF (as per an example application discussed later). The pressure-viscosity relationship was developed as: $\mu = 4.0\times10^{-6}\, p + 0.0107$. To calculate the average viscosity in the i-th production time-step $(\bar{\mu}_g)^i$, the pressure p is replaced by the average pressure $(\bar{p} + p_{wf})/2$, which gives Eq. 4.37.

The cumulative gas production, G_p and the recovery factor, RF at the end of i-th time step are:

$$(G_p)^i = (G_p)^{i-1} + (q_g)^i \Delta t \tag{4.43}$$

$$(RF)^i = \frac{(G_p)^i}{G} \tag{4.44}$$

In computational implementation of time-step production estimation, one day (24 hours) is used as the time interval, Δt in this study. In the first day, i.e. $i = 0$, the rate equation is used with the reservoir pressure and gas properties, and then average values are calculated according to above formulations after each 24 hour period. To use Eq. 4.12, the cumulative value of t has been adjusted daily basis, i.e. at $i = 1$, $t = 24$ hours, at $i = 2$, $t = 48$ hours, at $i = 3$, $t = 72$ hours, etc. Note that Δt in Eq. 4.43 is required to be used in days, because the production rate q_g is in Mscf/D.

4.6. Hybridisation of transient and pseudo-steady-state production regimes

As discussed in the previous section, for a tight reservoir (relatively low permeability) involving volumetric gas depletion, production of gas from a hydraulically fractured well starts with a transient flow, leading eventually to a pseudo-steady state flow. A short transition period between these two flow regimes is also mentioned in some literatures.

There is no guide in the literature about the duration of the transient flow regime. Earlougher (1977), however, suggested the following equation to estimate the time when the pseudo-steady state regime starts:

$$t_{pss} = \frac{\phi \mu c_t A t_{DA}}{0.000264k} \tag{4.45}$$

where t_{pss} is the time in hour at which the pseudo-steady state regime begins, A is the drainage area (ft^2) and c_t is the system compressibility at the initial reservoir condition. The non-dimensional pseudo-steady state time, t_{DA} has a characteristic value that depends on the drainage shape and well location, and several discrete values are suggested for various drainage shapes. For a regular shape such as a circle or a square with a well in the centre, it is about 0.1.

Hybridisation of two regimes involves establishing a smooth production rate versus time curve between these two regimes coupling their effects with the reservoir pressure. The author first assumed that the transient flow regime would continue until t_{pss}, which yielded a notable mismatch in the production rate versus time curve at t_{pss} as schematically shown in Figure 4.1. While simulated by a numerical reservoir simulator over 10 years, the production rate curve was found smooth which is also more realistic in the field under a constant bottom hole flowing pressure.

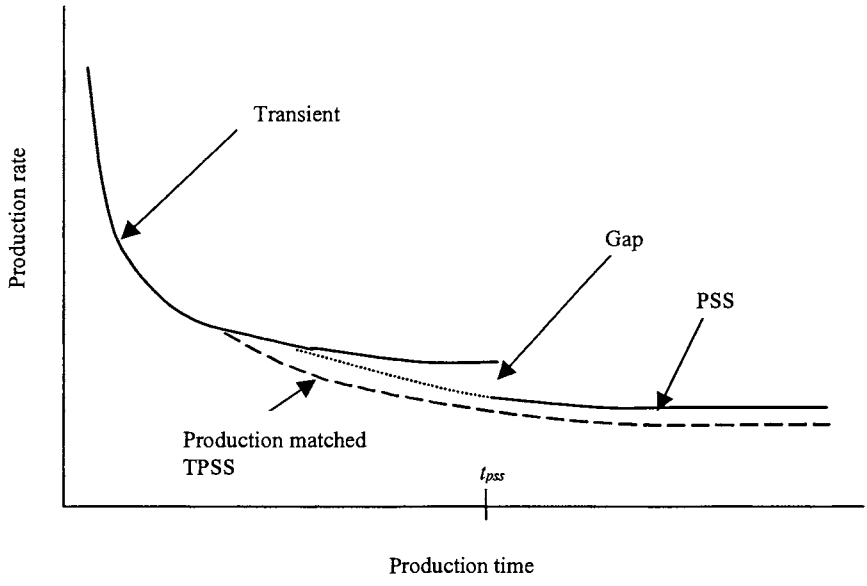

Figure 4.1. Schematic of hybridisation of transient and pseudo-steady state production regimes.

The second technique was shortening the transient flow regime and extending back the pseudo-steady state flow regime (i.e. reducing the value of t_{DA} from its idealised value) until the production rates between these two regimes matched with a tolerance. A simple numerical iteration procedure was used for this purpose. This technique is justified based on the argument that a real drainage shape seldom matches with an idealised shape, such as a circle or a square. A degree of deviation in the non-dimensional time t_{DA} is, therefore, acceptable – a view that is also supported by Valko (2000). It is important to note here that this technique is not just tracing back the pseudo-steady state curve until it intersects the transient curve in Figure 4.1 produced by the first attempt. This is because the pseudo-steady state production rates in the period, which was initially assumed to be in the transient regime, are different from the rates initially estimated based on the transient condition. Consequently, the average reservoir pressure will be different through revised cumulative production. When the production rates are calculated based on this reservoir pressure, the production rate at t_{pss}, and beyond, becomes different from that when the transient regime is continued until t_{pss}. As will be evident from results presented in the next section, the second technique yields production rate curves very close to that produced by numerical reservoir simulation for

very low-permeability reservoirs. For relatively high permeability reservoirs, the technique, however, produce a kink in the curve at the point of rate matching between the two regimes, and the trends of two different curves became very noticeable.

4.7. Applications of production models to a reservoir

A gas well located in a reservoir of tight permeability has been considered for application of the pseudo-steady state model (PSS) and the transient-pseudo-steady state hybrid model (TPSS) discussed so far. The well is assumed to be hydraulically fractured, whose fracture geometry is designed according to 2D PKN-C fracture model (presented in chapter 3). The same fracture geometry is modeled in the *IMEX Blackoil Simulator* and is run to obtain production profile and reservoir pressure profile for ten years. Production profiles and pressure profiles obtained from both analytical models are compared with those from *IMEX*.

The reservoir is assumed to be a square one with a drainage area of 640-acre and a well at the centre. It has a pay zone of 100 *ft* thickness bounded above and below by shale subjected to higher stresses. Petrophysical and mechanical properties and other well data of the reservoir are presented in Table 3.1 (chapter 3). A hydraulic treatment was assumed as: injection rate, 20 bbl/min; injection time, 55 minutes; end of the job proppant concentration, 14 ppg; fracturing fluid viscosity, 100 cp; for which the fracture half-length, x_f, was calculated to be 1220 ft. Non-dimensional fracture conductivity, F_{CD}, was calculated using proppant data in Table 3.2 (chapter 3). Procedures to calculate fracture conductivity and non-dimensional fracture conductivity are presented in chapter 3.

4.7.1. Modelling by IMEX Blackoil Simulator

The reservoir described above was simulated by using *IMEX Blackoil Simulator* as shown in Figure 4.2. The simulation procedure involves discretization of the pay zone into cells, preparation of input data sheet, initialization of the model and simulation of time-dependent gas production. A wellbore at the centre of the reservoir and the fracture geometry discussed above were simulated. The square reservoir was discritized as: 41 blocks in the *i*-direction, 41 blocks in the *j*-direction and 2 layers in the *k*-direction. The fracture is along the *j*-direction at the centre and the fracture plane is perpendicular to the *i*-direction. The block dimension in the *j*-direction is constant (128.78 ft), whereas the block dimension in the *i*-direction is adjusted to have fine grids along the fracture length. Two layers in the k-direction are of each 50ft thickness. The production simulation was run for ten years.

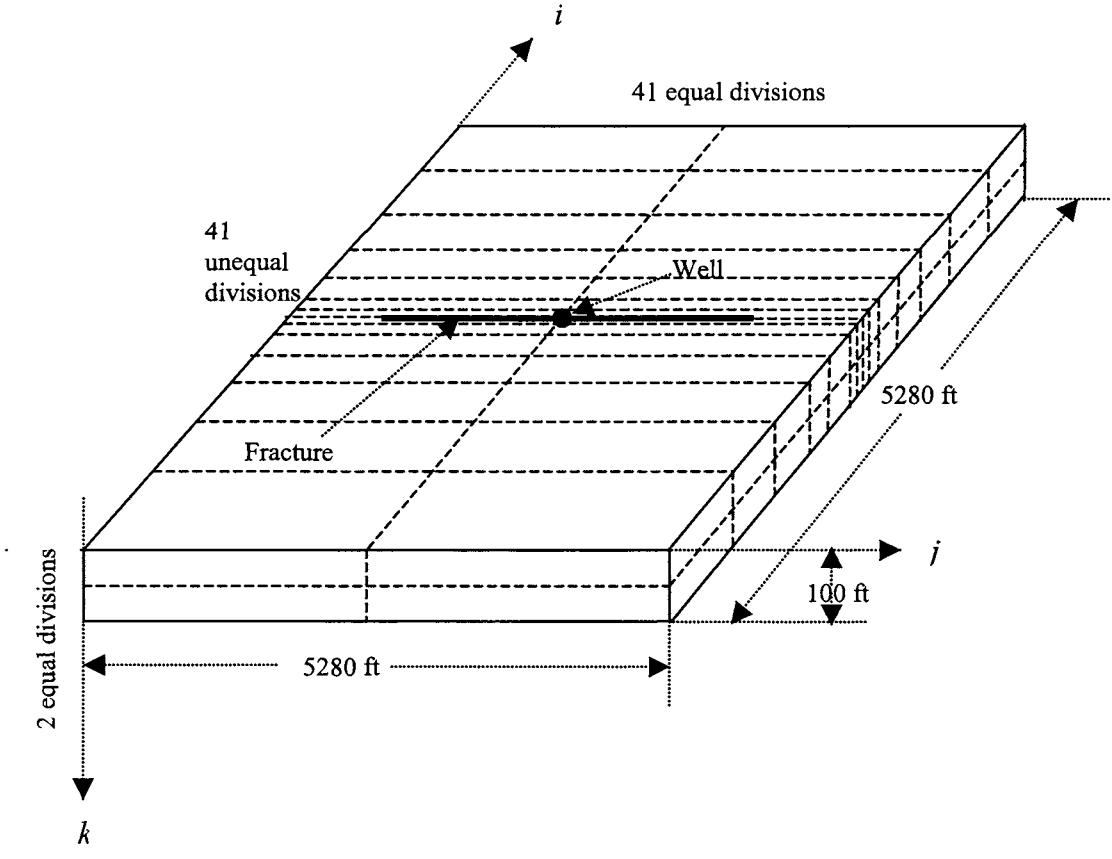

Figure 4.2. Reservoir model simulated in IMEX

4.7.2. Presentation of results

A computer programme was developed to implement the analytical production models discussed in the previous sections. Analytical studies were performed to investigate the behaviour of different production models and to compare their behaviour with that from IMEX for the same fracture geometry and reservoir properties.

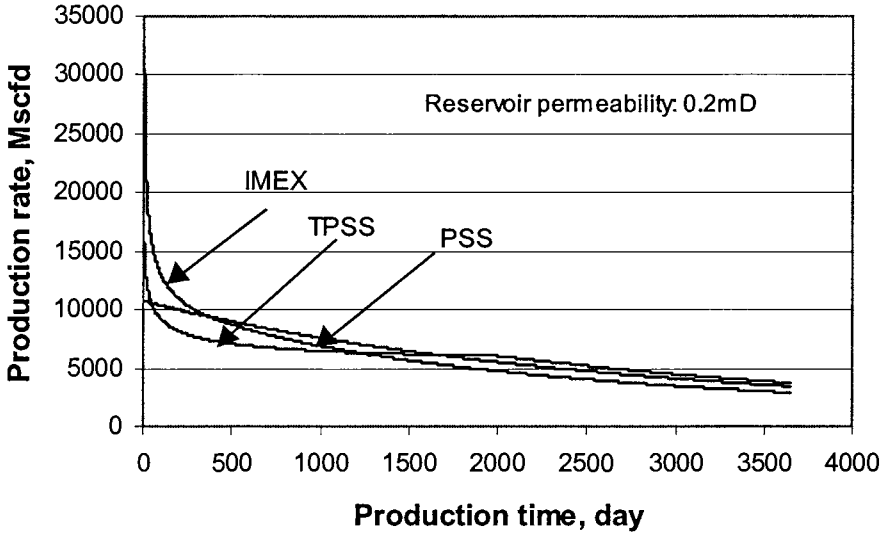

Figure 4.3. Production profiles of analytical models and IMEX from a reservoir of permeability 0.2 mD.

Results of analytical studies in terms of production profile and pressure profile obtained from analytical production models are presented in Figures 4.3 and 4.4 respectively, which also present the results from IMEX. Figure 4.3 shows that PSS production profile is different from that of TPSS and IMEX, particularly in the transient regime; whereas the TPSS production profile is very close to that of the IMEX. Cumulative productions for ten years of these production models and from IMEX run are presented in Table 4.1, which shows that at permeability of 0.2 mD, PSS cumulative production is 5.8% higher than that of IMEX, whereas TPSS cumulative production is only 0.8% higher. Figure 4.4 presents the reservoir pressure profiles as a result of production profiles in Figure 4.3. Figure 4.4 shows that the pressure decline due to PSS production is greater than that

due to TPSS production. This is justifiable, because the higher PSS cumulative production causes greater pressure decline compared to TPSS production. The pressure profile from IMEX simulator, which is based on different theories, is lower than other pressure profiles, but the trend is reasonably consistent with them.

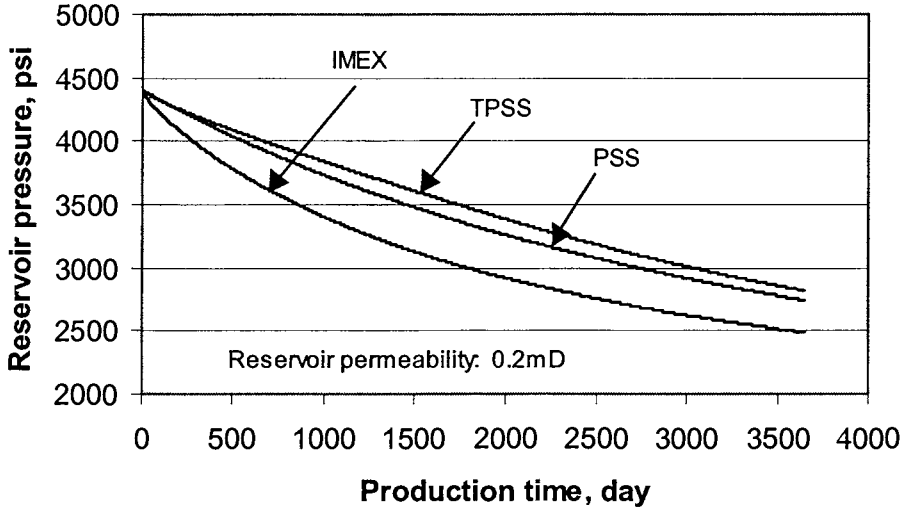

Figure 4.4. Reservoir pressure profile predicted by all models and IMEX for a reservoir of 0.2 mD.

Table 4.1. Cumulative production by different production model at different reservoir permeability.

Reservoir permeability, mD	TPSS (bscf)	PSS (bscf)	IMEX (bscf)
0.05	12.04468	11.50023	11.79797
0.1	16.30748	16.94984	16.45412
0.2	21.68661	22.75651	21.50820
0.5	29.16496	29.70417	27.86236
1.0	33.72574	34.00075	31.74587
2.0	36.43516	36.55480	34.07251
3.0	37.12109	37.16328	34.62918

4.7.3. Sensitivity of production models to varying reservoir permeability

To investigate the production behaviour predicted by these analytical models with varying reservoir permeability, a sensitivity analysis was carried out and results from IMEX were used to verify their reliability. Figures 4.5 and 4.6, representing very low reservoir permeability of 0.05 and 0.1 mD respectively, show that PSS production profile is further different from that of TPSS particularly in the transient regime and is also different from the IMEX profile, whereas TPSS production profile is more close to the IMEX profile. Corresponding pressure profiles, presented in Figures 4.7 and 4.8, also show that higher production causes greater pressure decline with time, which is noticeable among the TPSS and PSS models (see corresponding data in Table 4.1). Pressure profile obtained from IMEX is different, but consistent with others as explained earlier.

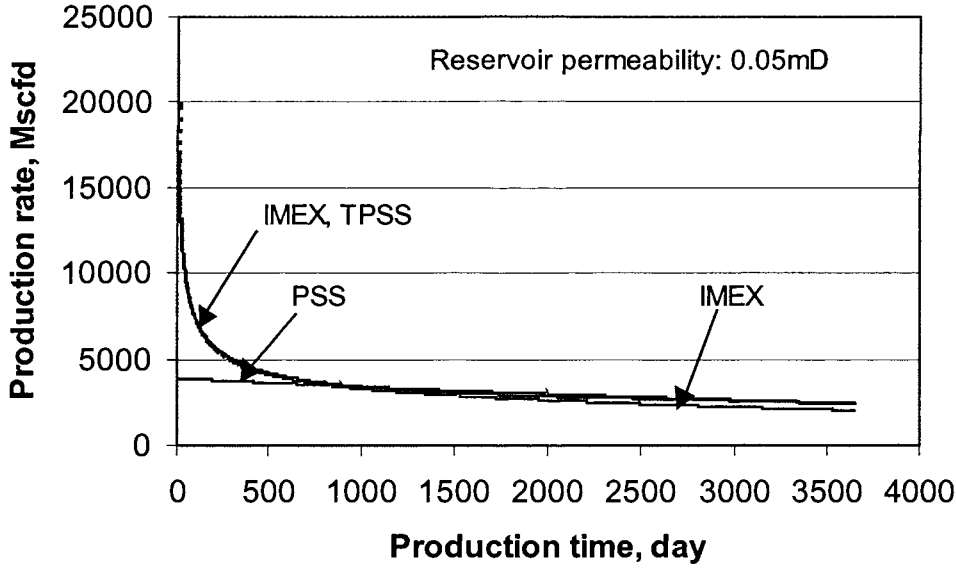

Figure 4.5. Production profiles predicted by models and IMEX for reservoir permeability of 0.05 mD.

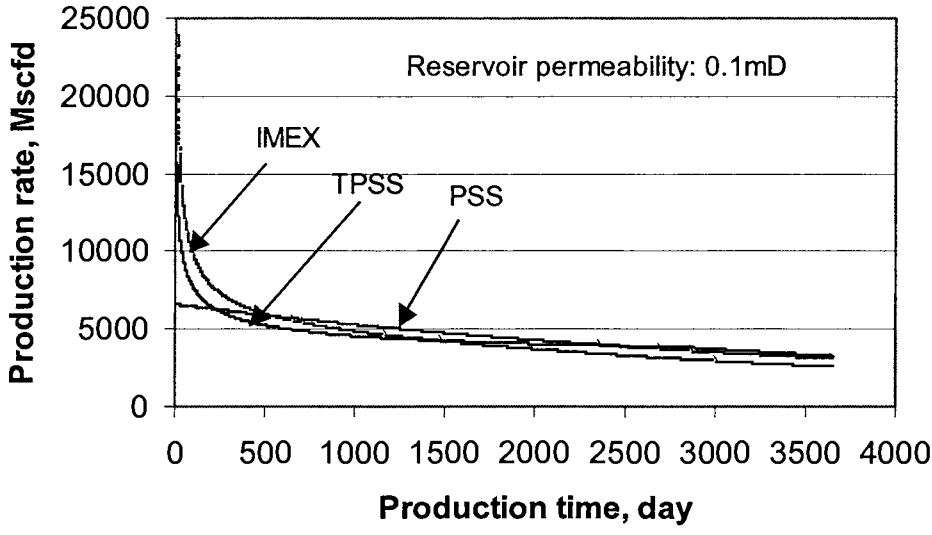

Figure 4.6. Production profiles predicted by models and IMEX for reservoir permeability of 0.1 mD.

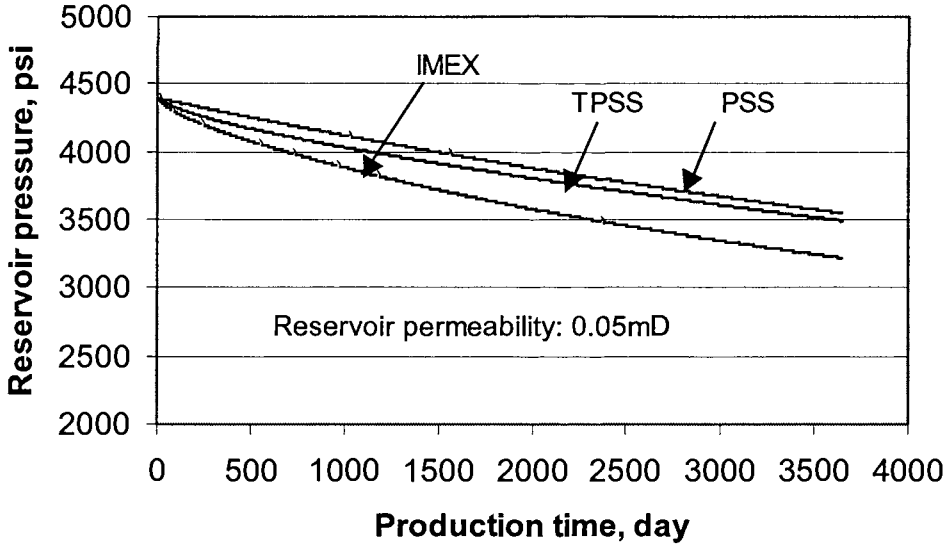

Figure 4.7. Reservoir pressure profiles predicted by models and IMEX for reservoir permeability of 0.05 mD.

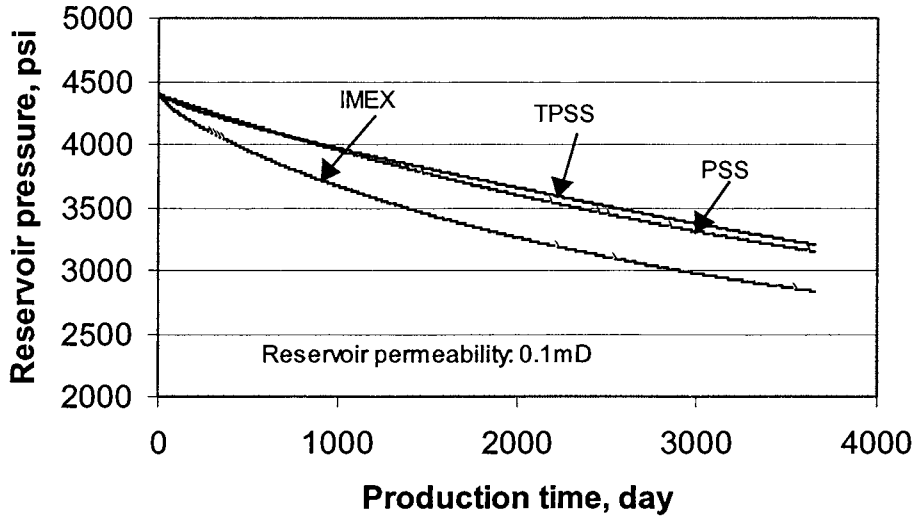

Figure 4.8. Reservoir pressure profiles predicted by models and IMEX for reservoir permeability of 0.1 mD.

Production and pressure profiles for reservoir permeability of 0.2 mD are already discussed as presented in Figures 4.3 and 4.4. Production profiles for reservoir permeability of 0.5, 1.0, 2.0 and 3.0 mD in Figures 4.9, 4.10, 4.11 and 4.12, respectively, show that PSS production profiles become closer to IMEX with increasing reservoir permeability. As the permeability increases, the transient regime becomes shorter and a kink in the TPSS production profile becomes prominent. These kinks represent the production matching of two different production trends in the transient and the pseudo-steady state regimes. Cumulative productions for different reservoir permeabilities are summarised in Table 4.1, which shows very close predictions by PSS and TPSS models, both being slightly higher than IMEX results particularly in the permeability range of 1.0-2.0 mD. Corresponding reservoir pressure profiles are plotted in Figures 4.13, 4.14, 4.15 and 4.16, whose trends are consistent with their cumulative production, as described earlier. It is evident from these figures that as permeability increases, reservoir pressures predicted by two models and IMEX at the end of production life become closer and closer. For permeability of 3.0 mD, they almost meet

at the same point (about 1717 psi), which is just above the fixed bottomhole flowing pressure (1700 psi) (see Figure 4.16).

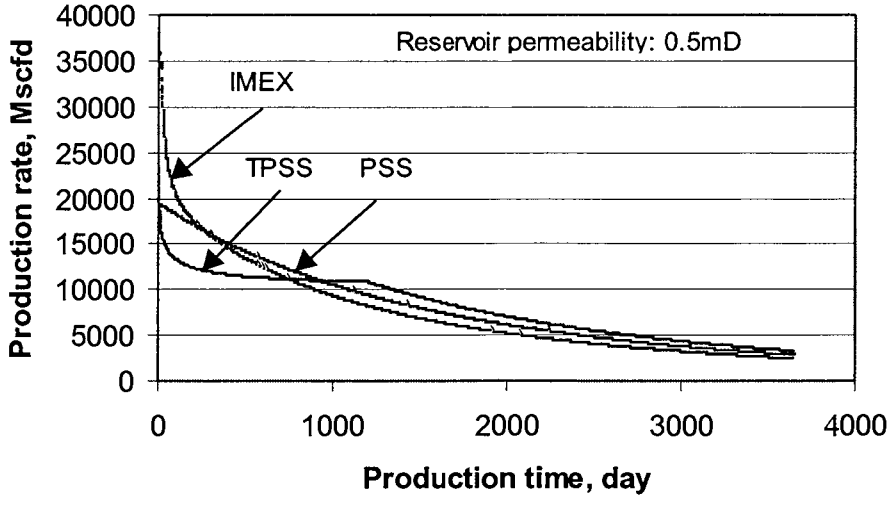

Figure 4.9. Production profiles predicted by models and IMEX for reservoir permeability of 0.5 mD.

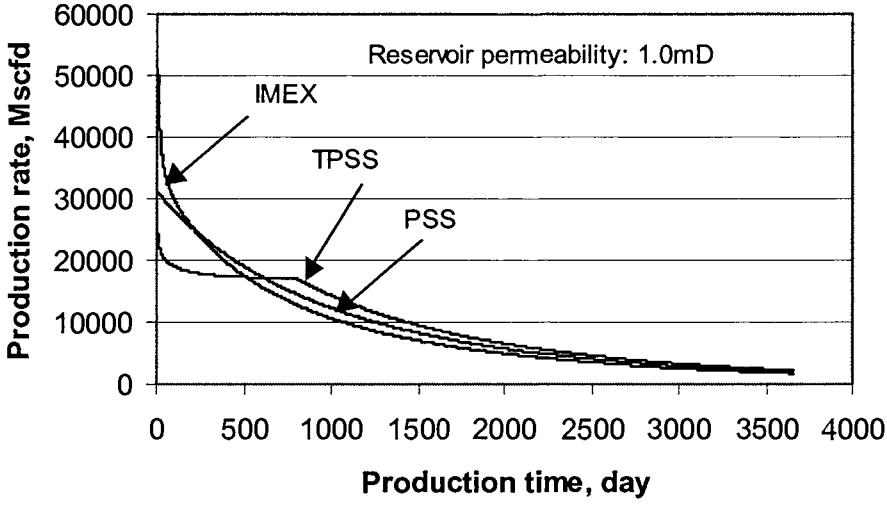

Figure 4.10. Production profiles predicted by models and IMEX for reservoir permeability of 1.0 mD.

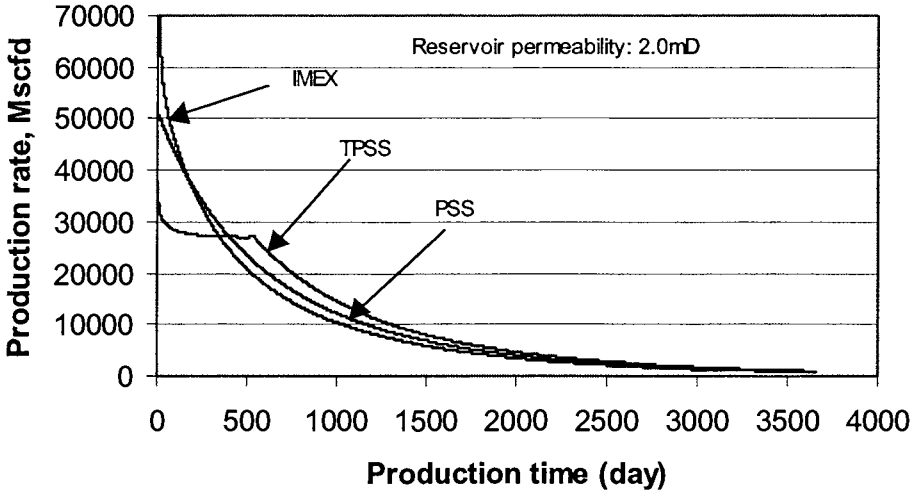

Figure 4.11. Production profiles predicted by models and IMEX for reservoir permeability of 2.0 mD.

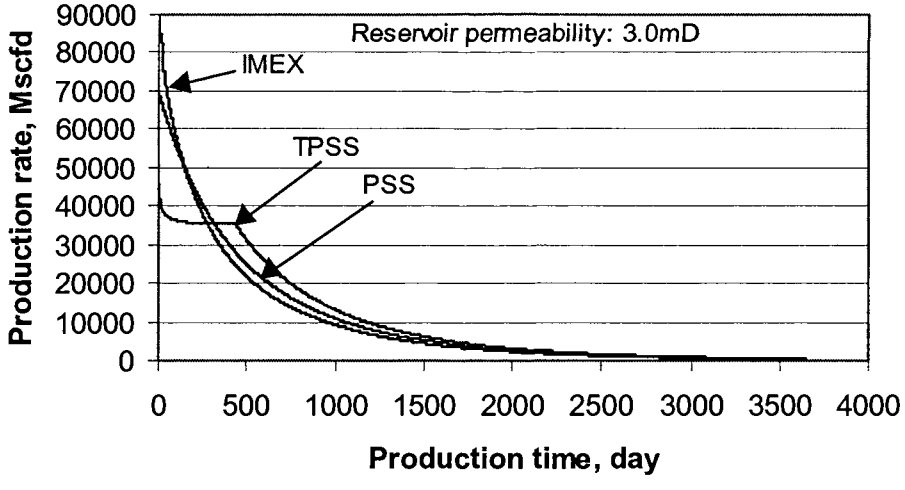

Figure 4.12. Production profiles predicted by models and IMEX for reservoir permeability of 3.0 mD.

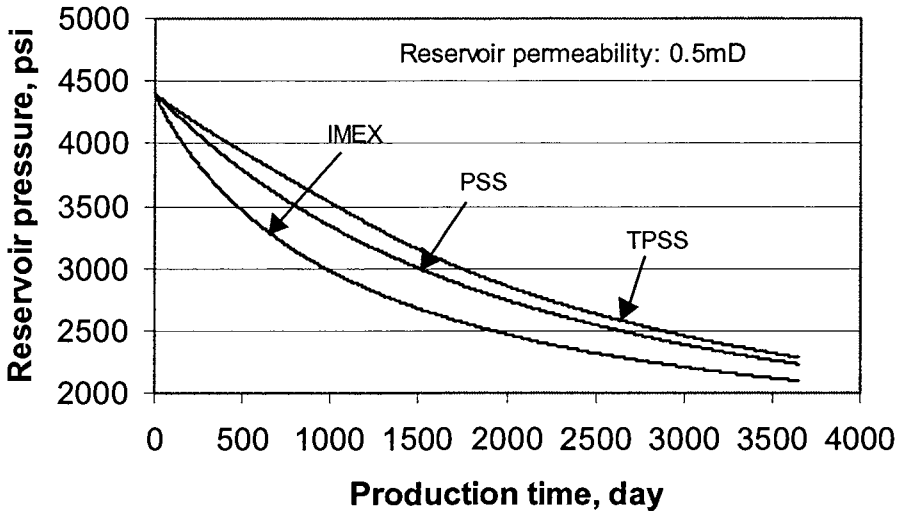

Figure 4.13. Reservoir pressure profiles predicted by models and IMEX for reservoir permeability of 0.5 mD.

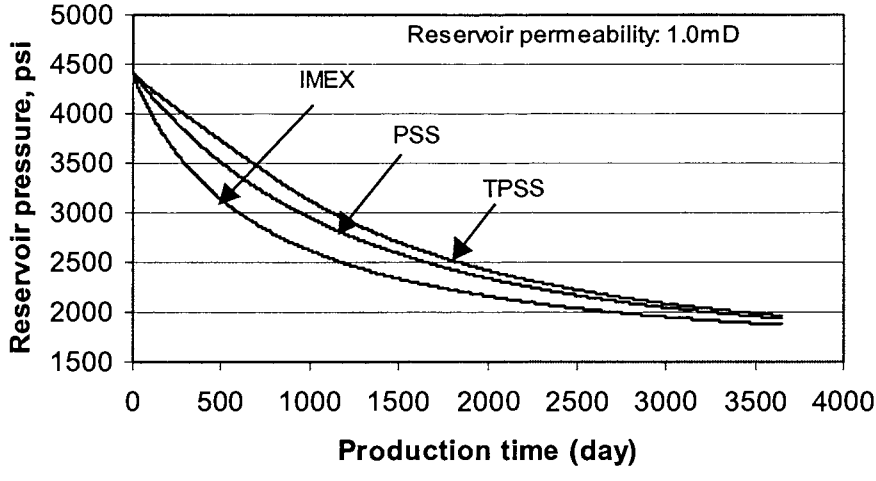

Figure 4.14. Reservoir pressure profiles predicted by models and IMEX for reservoir permeability of 1.0 mD.

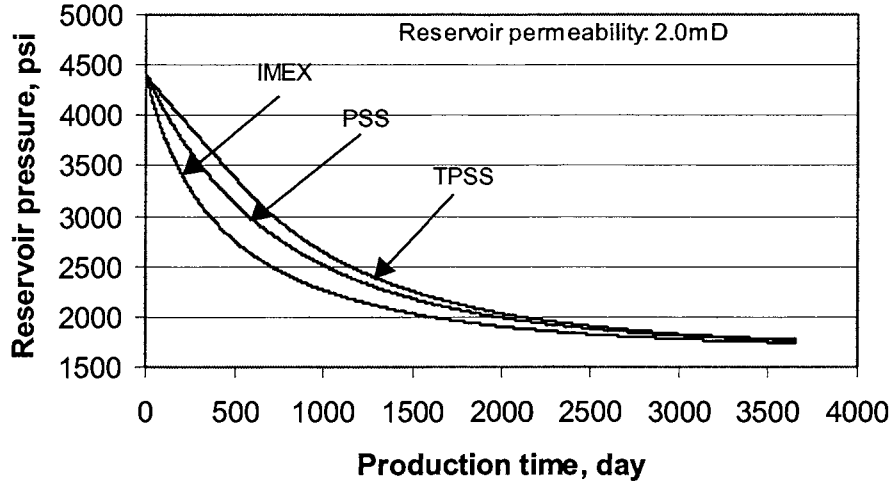

Figure 4.15. Reservoir pressure profiles predicted by models and IMEX for reservoir permeability of 2.0 mD.

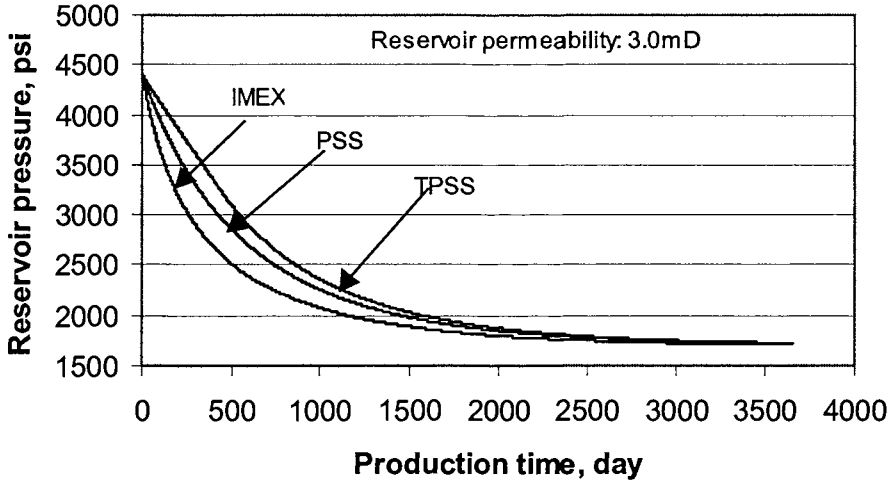

Figure 4.16. Reservoir pressure profiles predicted by models and IMEX for reservoir permeability of 3.0 mD.

4.8. Conclusions

Analytical production models for depletion type fractured reservoir (dry gas) under constant bottomhole flowing pressure have been investigated and compared with *IMEX Balckoil Simulator* as discussed in the above sections. The following conclusions can be drawn from this study:

1. For very low-permeability gas reservoirs, the transient flow regime is significantly long as it is seen from the kinks in Figures 4.3, 4.5, 4.6 and 4.9. In order to consider this long transient regime, a hybridized transient-pseudo-steady state (TPSS) production model is proposed in which the transient and pseudo-steady state flow regimes are coupled based on productivity matching. The production profile predicted by this proposed model is found very close to that simulated by a numerical simulator for reservoir permeability less than 0.5 mD.

2. For reservoir permeability equal to and above 0.5 mD, the pseudo-steady state production model has predicted production profiles, which are close to simulation results.

3. In spite of different behaviours in time-dependent production profiles with varying reservoir permeability, the cumulative production from both TPSS and PSS models over 10 years are found very close, both being slightly higher than simulation results. It indicates that if the interest simply lies in the total production from a reservoir, the PSS model is sufficient to predict with acceptable accuracy.

4. Reservoir pressure declines as a result of production are consistently proportional to cumulative productions from TPSS and PSS models.

CHAPTER FIVE

MULTIVARIATE HYDRAULIC FRACTURING OPTIMISATION WITH MULTIPLE DESIGN OBJECTIVES

5.1. Introduction

Deciding a set of values for treatment parameters is the most important task in hydraulic fracture treatment design. For a given reservoir, one must decide values of injection rate of the fluid, injection time, EOJ proppant concentration, fracturing fluid viscosity etc., such that a favourable hydraulic fracture geometry is created to improve a design objective. As reviewed in chapter 1, the net present value (NPV) has been usually used as an objective function for hydraulic fracturing treatment design, where the improvement in NPV is attempted by parametric sensitivity analysis. The height of the fracture is assumed to be a known value (often equal to the pay zone height) and a set of discrete values is taken for each of the treatment parameters. For each combination of these treatment parameters, the NPV is calculated for a given fracture length. The procedure is repeated for a number of fracture lengths and NPV versus length curves are plotted. From these curves, values of stimulation parameters and the resulting fracture length are ascertained as optimum based on a maximum value of NPV. This type of design optimisation procedure by parametric sensitivity analysis is tedious. Although the procedure can find a design better than an arbitrary design, it is almost impossible to explore all potential design scenarios and to satisfy various operational limitations (pump capacity, tubular strength, pressure rating of surface equipment, etc.) and fracture growth control requirements based on formation characteristics. Furthermore, the industry may benefit by considering other design objectives, such as maximise production, minimise treatment cost, achieve a production target, etc. Thus, the overall hydraulic fracturing design optimisation task is redefined in this work to find a 'best

possible' set of values for treatment and other parameters while the revenue/production from a well is maximised with minimum treatment cost, and operational limitations and fracture growth control requirements are satisfied.

This chapter presents detailed formulations of the optimisation model for hydraulic fracturing within the framework of the optimisation algorithm presented in chapter 2. Various design constraints to satisfy operational requirements, fracture growth control requirements and desirable geometric configurations are formulated using fracture models presented in chapter 3. The design objective function is formulated as a function of cumulative production from the fractured well, as described in chapter 4. Time and place dependent reservoir properties and price data can be entered into the model in order to obtain an automated optimum design using selected fracturing fluid and proppant type.

The main objectives of this chapter are:

- to present the proposed model with detailed formulations,
- to demonstrate the benefits and capabilities of the model to investigate various design issues for improved decision-making,
- to perform sensitivity analysis of treatment parameters on NPV by a series of applications to a tight-gas reservoir,
- to compare treatments designed using 2D PKN-C and P-3D-C fracture models,
- and to demonstrate its capability to control formation damage and resulting sand production due to near-wellbore mechanical failure by application to a relatively weak-gas formation.

5.2. Model formulation for hydraulic fracturing design optimisation

The overall problem of hydraulic fracturing optimisation is formulated within the framework of the optimisation algorithm in the following sections.

5.2.1. Free design variables

As mentioned earlier, four stimulation parameters, injection rate, injection time, EOJ proppant concentration and fracturing fluid viscosity and the fracture half-length are modelled as free design variables. These five free design variables with their units and symbols are presented in Table 5.1.

Table 5.1. Free design variables.

Variable name (unit)	**Variable symbol**	**INTEMOB variable**
Injection rate (bbl/min)	q_i	x_1
Injection time (min)	t_i	x_2
EOJ Proppant concentration (ppg)	P_c	x_3
Fracturing fluid viscosity (cp)	μ	x_4
Fracture half-length (ft)	x_f	x_5

The fracture height and width are calculated as functions of these five variables by solving the material balance relationship (detailed in chapter 3).

5.2.2. Bound constraints

The following bound constraints are formulated with their upper and lower bounds based on industry practice and other considerations:

1. $10 \leq q_i \leq 45$: from field experience (Chipperfield, 2000).

2. $10 \leq t_i \leq 500$: the upper bound 500 minutes was chosen so that the optimum value of t_i is never constrained by its upper bound.

3. $5 \leq P_c \leq 15$: based on industry practice (Meng and Brown, 1987; Chipperfield, 2000).

4. $70 \leq \mu \leq 800$: based on industry data and recommendations for minimum viscosity for effective proppant transport (Economides *et al.*, 1994; Smith, 1992; Chipperfield, 2000).

5. $100 \leq x_f \leq 2600$: the upper bound was chosen such that the fracture does not exceed the reservoir boundary.

5.2.3. Design constraints

Design constraints are formulated based on operational limitations and fracture growth control requirements as follows:

Operational limitations

1. $1.0 \leq C_1(\underline{x}) \leq 10.0$: where $C_1(\underline{x}) = (HP_{av} \times P_{eff})/HP_{reqd}$; HP_{av} is the horsepower available from the pump to be used and P_{eff} is the pump efficiency factor. The lower bound on this constraint ensures that the horsepower required, HP_{reqd} (Appendix B) to deliver net fracture pressure, p_{net}, is within the capacity of the pump and the upper bound is set arbitrarily. The fracture net pressure is estimated as a function of design variables and formation properties. The upper bound is defined arbitrarily to meet the standard requirement of optimisation algorithm. This is also true for other constraints formulated below, unless mentioned otherwise.

2. $1.0 \leq C_2(\underline{x}) \leq 15$: where $C_2(\underline{x}) = P_{burst}/(P_{surf} \times SF)$; P_{burst} is the burst strength of the tube in use, P_{surf} is the pressure developed at the surface and SF is a safety factor. The lower bound on this constraint ensures that the pressure developed inside the tube at the surface level is below the burst strength of the tube during injection. P_{surf}

is calculated based on the required net fracture pressure accounting for static head and dynamic frictional loss (Appendix B). For estimation of dynamic frictional loss, fluid consistency indexes are calculated based on industry data (chapter 3).

3. $1.0 \leq C_3(\underline{x}) \leq 15$: where $C_3(\underline{x}) = P_{seqp}/P_{surf}$; P_{seqp} is the minimum pressure among the rated pressures of various surface equipment in the injection line. The lower bound on this constraint ensures that the pressure developed at the surface does not exceed the pressure capacity of the critical equipment.

Fracture growth control requirements (geometric considerations)

4. $1.0 \leq C_4(\underline{x}) \leq 10.0$: where $C_4(\underline{x}) = (1.25 \text{ x } h)/h_f$. The lower bound on this constraint ensures that the fracture height, h_f does not migrate to the bounding layers by more than 25% (Smith, 1992) of the pay zone thickness, h. The fracture height, h_f is calculated as a function of design variables by solving fracture geometry model (Eqs. 3.18-3.23 of chapter 3).

5. $1.0 \leq C_5(\underline{x}) \leq 50.0$: where $C_5(\underline{x}) = x_f/h_f$. The lower bound on this constraint ensures that the fracture half-length is always greater than the fracture height, which is a basic assumption in the PKN-C fracture geometry model.

6. $1.0 \leq C_6(\underline{x}) \leq 5.0$: where $C_6(\underline{x}) = \overline{w}/(4P_d)$; $\overline{w}$ is the average dynamic fracture width calculated according to fracture geometry model and P_d is the proppant diameter. The lower bound on this constraint ensures that the average dynamic fracture width is at least four times the proppant diameter for effective proppant transport (Schechter, 1992).

7. $0.5 \leq C_7(\underline{x}) \leq 1.0$: where $C_7(\underline{x}) = V_f/V_i$; V_f is the total fracture volume calculated from fracture dimensions and lateral and vertical shape factors, and V_i is the total injected volume. The lower bound on this constraint ensures that the fluid efficiency, V_f/V_i, is greater than 0.5 and the upper bound ensure that the fracture volume is less than the

injected volume. In typical fracturing treatments, the fluid efficiency varies between 0.7 and 0.4 (Smith, 1992).

Fracture growth control requirements (formation considerations)

8. $1.0 \leq C_8(\underline{x}) \leq 10.0$: where $C_8(\underline{x}) = P_{fcr}/P_{treat}$; P_{fcr} is the formation critical pressure and P_{treat} is the fracture treatment pressure, calculated as a function of design variables and formation in-situ stress. The formation critical pressure can be available from special in-situ stress tests and previous massive hydraulic fracturing tests in the region and fracture mechanics studies (Nolte, 1979; Nolte and Smith, 1981; Nolte, 1982; Ahmed *et al.*, 1985; Nolte, 1988). The lower bound on this constraint ensures that the treatment pressure is kept below the formation critical pressure to prevent uncontrolled fracture growth (Meng and Brown, 1987; Nolte and Smith, 1981).

9. $1.0 \leq C_9(\underline{x}) \leq 10.0$: where $C_9(\underline{x}) = \Delta\sigma_h/p_{net}$; $\Delta\sigma_h$ is the difference between the minimum horizontal stresses in the pay zone and the bounding layers. The lower bound ensures that the fracture net pressure does not induce excessive fracture height growth into the bounding layers (Nolte and Smith, 1981).

10. $1.0 \leq C_{10}(\underline{x}) \leq 10.0$: where $C_{10}(\underline{x}) = \Delta\sigma/(0.7 \times p_{net})$; $\Delta\sigma$ is the difference between the maximum and the minimum horizontal in-situ stresses in the pay zone. The lower bound ensures that the fracture net pressure does not cause the initiation of auxiliary (secondary) fractures, which result in large fluid loss (Nolte and Smith, 1981).

Near wellbore failure and sand control requirements

Sand production due to near-wellbore failure of perforation tunnel is a common problem in weak formation. The following constraint is formulated to prevent this problem.

11. $1.0 \leq C_{11}(\underline{x}) \leq 10.0$: where $C_{11}(\underline{x}) = CDP/ODP$; the lower bound ensures that the created fracture geometry is controlled so that the induced critical drawdown pressure, *CDP* to cause mechanical failure of perforation tunnels and hence sand production does not fall below the operator's used drawdown pressure, *ODP* at the

later production stage, because wells that do not initially produce sands may produce later (Weingarten and Perkins, 1995), as *CDP* decreases with time due to decreasing reservoir pressure during production. The critical drawdown pressure *CDP* is estimated as function of depleting reservoir pressure, cohesive strength of formation and fracture geometry using Mohr-Coulomb shear failure theory (Weingarten and Perkins, 1995; Fletcher *et al.*, 1996). The formulation of *CDP* is detailed in Appendix-C. Recently, Casares and Talavera (2001) observed the successful results of sand control by hydraulic fracturing, though they did not present either the theory that acted behind their success or any fracture treatment optimisation procedure.

5.2.4. Design objective functions

As mentioned earlier, a prioritized goal-set combined objective function (Eq. 2.38, chapter 2) is used to formulate various design objective functions for hydraulic fracturing optimisation.

1. Maximise total production, G_p, over a number of years.

   There is only one objective to maximise without any target value. Therefore, $I = 1$, $T_1 = 0$, $P_1 = 1$ and $D_1 = 1$ can be used in Eq. 2.38, giving $Z = f_1(\underline{x}) = G_p$. To maximise this, the optimisation statement is:

   $$\text{minimise } Z = \text{minimise}(-G_p) \tag{5.1}$$

2. Maximize net present value, NPV, over a number of years.

   Similar to production maximisation statement, the NPV maximisation statement is:

   $$\text{minimise } Z = \text{minimise}(-NPV) \tag{5.2}$$

3. Maximize NPV and minimize treatment cost, C_{tr}.

   There are two explicit design objectives in this case; maximse NPV and minimise treatment cost. Thus, $I = 2$ which gives the optimisation statement as

$$\text{minimise } Z = \text{minimise}\left[\frac{-NPV}{D_1}P_1 + \frac{C_{tr}}{D_2}P_2\right] \tag{5.3}$$

Note that negative NPV is minimised in Eq. 5.3 to actually maximise NPV.

Values of D_1 and D_2 are adjusted such that the value of both terms at the right hand side of Eq. 5.3 approaches to 0.5. P_1 and P_2 are set to 1 to assign equal priorities to maximise NPV and minimise treatment cost.

4. Achieve a production target, T_1, and minimise treatment cost, C_{tr}.
   Similar to formulation in 3, with a target of production T_1 for G_p the combined objective for this case can be formulated as:

$$\text{minimise } Z = \text{minimise}\left[\frac{|G_p - T_1|}{D_1}P_1 + \frac{C_{tr}}{D_2}P_2\right] \tag{5.4}$$

   Values of D_1, D_2, P_1 and P_2 are set, similar to the above design, to reflect equal priorities for achieving the production target and minimising the treatment cost.

The cumulative production, G_p from hydraulically fractured wells in tight-gas reservoirs is estimated combining transient and pseudo-steady-state flow regimes (chapter 4). The NPV is formulated as follows:

$$NPV = \sum_{n=1}^{NY}\frac{R_n}{(1+i)^n} - C_{tr} \tag{5.5}$$

where, R_n is the revenue generated (A$) at year n, NY is the total number of years during which revenue to be generated, i is the discount rate and C_{tr} is the treatment cost (A$). The revenue, R_n in the year n is calculated as the product of the total production, G_{pn} (Mscf) at the n-th year and an average gas price ($/Mscf).

The treatment cost is a direct function of the total volume of the fracturing fluid injected, the type of fracturing fluid and the total weight of proppant used. A fraction of fixed cost is also included to cover equipment hire and other expenses incurred during treatment. The formulation of total treatment cost is as follows:

$$C_{tr} = P_{fl} \times V_{tfl} + P_{pr} \times W_{pr} + P_{pump} \times HP_{av} + FC \tag{5.6}$$

Here, C_{tr} is the treatment cost (A$), P_{fl} is the price of fracturing fluid ($/gal), V_{tfl} is the total volume of proppant-free fracturing fluid (gal), P_{pr} is the price of proppant ($/lb), W_{pr} is the weight of proppant (lb), P_{pump} is the pumping price ($/hp), and FC is the fixed and miscellaneous costs (section 3.4.1 of chapter 3 for V_{tfl} and W_{pr}). The fracturing fluid price is related to viscosity, which is developed based on industry data to reflect the cost dependency on the fluid type used as follows:

$$P_{fl} = 0.001\mu + 0.6721 \tag{5.7}$$

where μ is the viscosity of fracturing fluid.

The flow-chart of the optimisation process is shown in Figure 5.1.

5.2.5. Optimisation formulation using P-3D-C model

Model formulation for treatment optimisation using P-3D-C fracture model is similar to that using PKN-C fracture model, as described in the foregoing sections, with a few exceptions. Optimisation with P-3D-C fracture model consider four free design variables: injection rate, EOJ proppant concentration, fracturing fluid viscosity and fracture half-length. The injection time is calculated by solving the material balance equations (Eqs. 3.49 & 3.23) for this model. The fracture height, width and treatment pressure are calculated according to the theory and algorithm presented in chapter 3 for this model. Therefore, any direct design constraint on height growth (like constraint 4) is

not imposed. The other design constraints are similar to that for PKN-C model, and formulated using required parameters from P-3D-C fracture model.

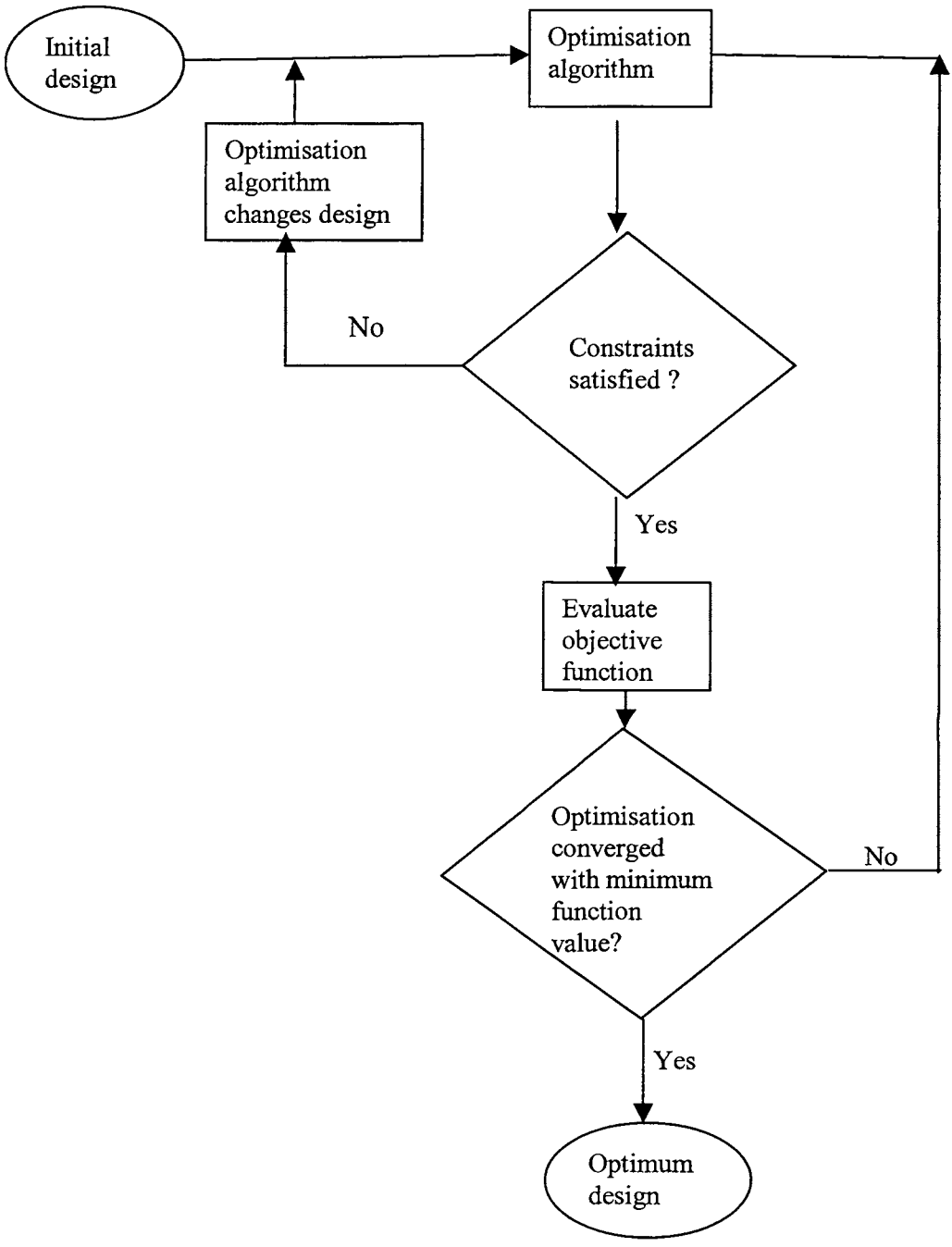

Figure 5.1. Flow-chart for design optimisation

5.3. Optimum treatment design with 2D PKN-C and P-3D-C fracture models

An example of a gas well located in a tight formation is used to illustrate the application of the multi-objective optimisation model. Reservoir and formation properties and well data of this example application are already described in chapter 3 (Table 3.1). Fracture mechanics data required for analyses are presented in Table 5.2, which also contains information on various operational limitations.

Proppant selection data are presented in chapter 3 (Table 3.2). The laboratory-measured fracture conductivity data is corrected to the expected in-situ concentration in a way detailed in chapter 3. A conductivity damage factor (0.6) has also been applied after correcting for in-situ concentration to get realistic fracture conductivity. Economics data are presented in Table 5.3. NPV and production have been calculated for ten years.

Table 5.2. Fracture mechanics and operational limitation data.

Fracture geometry model	PKN-C / P-3D-C
Closure stress	6,000 psi
Young's modulus	5.075E6
Poisson's ratio	0.20
Leakoff coefficient	0.00025 ft/min$^{0.5}$
Spurt loss coefficient	0.0
Burst strength of the tube	13000 psi
Horse power of the pump	14000 hp
Pump efficiency	85%
Rated pressure of surface equipment	14000 psi

Table 5.3. Economics data.

Proppant cost	$1.0 /lb
Fracturing fluid cost	Varying with viscosity
Pumping cost for 14000 hhp	$20 /hhp
Fixed cost	$10,000
Gas price	$1.0/Mscf
Discount rate	0.10
Number of years	10

5.3.1. Improvement of objective function by redesign iterations

In order to demonstrate the benefit of using the optimisation scheme in hydraulic fracturing design, three different designs are prepared arbitrarily (i.e. without using any optimisation procedure according to PKN-C fracture model). These designs are named as Initial Design 1, Initial Design 2 and Initial Design 3, presented in Table 5.4. Using these three initial designs as starting points, the optimisation scheme was run to achieve maximum NPV. The optimisation scheme achieved the final optimum design by executing a number of redesign iterations for each initial design. Three optimum designs, starting with the three initial designs, were slightly different within the convergence tolerance. One of the optimum designs is presented in the last column of Table 5.4. Iterative redesigns performed by the optimisation scheme, are plotted in Figure 5.2 for the three initial designs. The first three points on the graph at 0 iteration represent NPVs of the three arbitrarily obtained initial designs. It is evident from the graph that these three designs have been improved significantly by the optimisation scheme: specifically, Initial Design 1 improved by 16%, Initial Design 2 improved by 23% and Initial Design 3 improved by 50%, with corresponding NPV increments of $2.15m, $2.93m and $5.24m, respectively.

Table 5.4. Three initial designs to initiate optimisation process with PKN-C model.

Variable symbol	Initial Design 1	Initial Design 2	Initial Design 3	Optimum Design
q_i (bbl/min)	19	20	30	27.58
t_i (minute)	96.67	83.33	66.67	113.60
P_c (ppg)	14	8	7	15.00
μ (cp)	122	120	210	212.40
x_f (ft)	1678	2000	550	2499.9
NPV, m$	13.51650	12.72597	10.41850	15.66389
G_p, bscf	21.73059	20.37621	16.96039	25.51099
C_{tr}, m$	0.63984	0.52296	0.541264	1.013669

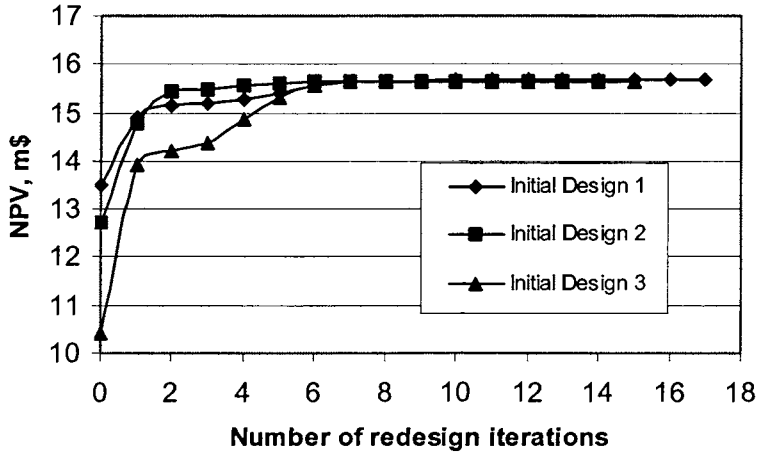

Figure 5.2. Convergence to optimum design from different initial designs with PKN-C fracture model.

Table 5.5. Three initial designs to initiate optimisation process with P-3D-C model.

Parameters symbol	Initial Design 1	Initial Design 2	Initial Design 3	Optimum Design
q_i (bbl/min)	18	22	40	26
t_i (minute)	137.5	38.8	6.3	187.5
P_c (ppg)	14	14	6	14.7
μ (cp)	220	90	230	367.86
x_f (ft)	2000	1500	500	2500
NPV, m$	14.98208	12.99973	10.51501	16.445022
G_p, bscf	24.18771	20.70079	16.78647	27.367199
C_{tr}, m$	0.815695	0.466748	0.328343	1.4606686

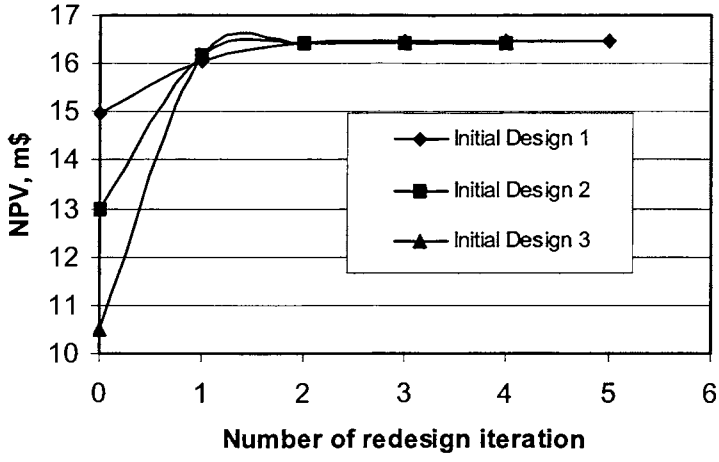

Figure 5.3. Convergence to optimum design from different initial designs with P-3D-C fracture model.

Similar investigations were conducted with P-3D-C fracture model. Three initial designs and the optimum design are presented in Table 5.5 and iterative redesigns are plotted in Figure 5.3. It is evident from the figure that these designs also have been improved significantly by the optimisation scheme similar to that with PKN-C model. Initial Design 1 is improved by 10%, Initial Design 2 by 26%, and Initial Design 3 by 56%, with corresponding NPV increments of $1.46m, $3.44m and $5.92m, respectively.

Comparison of optimum designs using the two fracture models shows that the optimum design using P-3D-C model predicts about 5% higher NPV and 7.3% higher production, but involves about 44% higher treatment cost. This is because the unconstrained height growth by P-3D-C model allowed higher productive width of the fracture.

From Figures 5.2 and 5.3, it can be seen that the optimisation with P-3D-C model requires significantly less redesign iterations compared to that with PKN-C model. This is primarily due to the reduced number of design variables and constraints. The iterative computation of injection time, however, required a significant time. Therefore, the overall optimisation time with P-3D-C model was almost 3 folds of that with PKN-C model.

Finally, these results indicate that an optimisation tool, such as the one used herein, will greatly enhance the capability of a designer to achieve the best possible design satisfying highly complex constraints. Without such a tool, a design can be obtained by tedious trial and error in order to satisfy the constraints but it rarely provides an improved design.

5.3.2. Active constraints

It was found that design constraints 8 and 9 became severely active in determining the optimum design with both fracture models. The design satisfied their lower bounds very tightly. Other active constraints can be ordered 2, 10 and then 3, based on the severity of satisfying their lower bounds. The order of active constraints indicates that a higher treatment pressure would develop from the treatment designed for the reservoir. If constraints 8 and 9 were not formulated, the design could be improved apparently in terms of cumulative production but the treatment pressure would damage the formation resulting in uncontrolled fracture growth. Similarly, if constraints 2, 10 and 3 were also excluded from the optimisation scheme, a higher production design could be apparently achievable. But when that design were executed in the field, in addition to further formation damage by initiation of auxiliary multiple fractures the operator would have to use higher strength tube and equipment. Because of these complexities, the actual fracture conductivity would have been severely inadequate compared to its designed value, and consequently, the production would have been significantly lower compared to its predicted value. These predicted complexities were in fact observed in the field in many instances when fracturing treatments designed without such constraints (using a commercial software) were executed (more details in chapter 6).

5.3.3. Optimum design with different objective functions

The way the optimum design changes with the change in design objective is demonstrated by achieving four optimum designs for the four design objective functions discussed in the previous section. Results for both fracture models are presented in Table 5.6.

Table 5.6. Optimum designs for four different objectives using both fracture models.

Parameters symbol	Fracture model	Design 1	Design 2	Design 3	Design 4
q_i (bbl/min)	2D PKN-C	26.60	27.58	14.21	15.06
	P-3D-C	26.2	26.0	32.6	27.51
t_i (minute)	2D PKN-C	118.53	113.60	75.50	29.27
	P-3D-C	187.5	187.5	19.1	18.8
P_c (ppg)	2D PKN-C	15.00	15.00	13.96	13.51
	P-3D-C	15.0	14.7	14.75	9.88
μ (cp)	2D PKN-C	213.96	212.40	180.08	181.26
	P-3D-C	379.41	367.86	129.34	504.56
x_f (ft)	2D PKN-C	2500.0	2499.9	1455.0	822.1
	P-3D-C	2500.0	2500.0	1066.6	617.3
h_f (ft)	2D PKN-C	125.0	125.0	100.4	98.0
	P-3D-C	180.6	180.6	120.4	135.4
NPV (m$)	2D PKN-C	15.65653	15.66389	13.75216	11.05378
	P-3D-C	16.51851	16.44502	12.94533	12.027306
G_p (bscf)	2D PKN-C	25.5110	25.51099	21.89491	17.79512
	P-3D-C	27.53007	27.36720	20.58428	19.15583
C_{tr} (m$)	2D PKN-C	1.013205	1.013669	0.514185	0.387652
	P-3D-C	1.49453	1.460669	0.443065	0.4034704

It has been observed that for both fracture models, the maximum NPV design (Design 2) is very close to the maximum production design (Design 1), whereas other designs are significantly different. With PKN-C fracture model, a significant percentage (49%) of treatment cost saving has been achieved over the maximum NPV design by setting the design objective to maximise NPV and minimise treatment cost (Design 3 by Eq. 5.3). This saving, however, has resulted in 12% NPV reduction over 10 years. This shows the conflict between the design objectives, NPV and treatment cost. It is however possible to achieve a compromised design, which may also be biased to a certain degree to a particular objective, by adjusting priority factors to individual objectives. For design 4 (Table 5.6), 70% of the maximum production (25.511 bscf), was set to achieve (i.e. T_1

= 0.7 x 25.511) with minimum treatment cost. The optimum design (Design 4) has achieved the full target.

Similarly with P-3D-C fracture model, Design 3 enables a designer to achieve a significant percentage (69%) of treatment cost saving, resulting in 21% of NPV reduction over 10 years. For design 4, 70% of the maximum production (27.3672 bscf) was the target to achieve (i.e. T1 = 0.7 x 27.3672) with minimum treatment cost. The optimum design (Design 4) has achieved the full target (19.15583 bscf). P-3D-C model shows higher production because the fracture height is much higher allowing higher productive width in the pay zone. Effect of fracture height on production/NPV will be discussed in a later section.

In both Designs 3 & 4, there is an objective of treatment cost minimisation, but one is with NPV maximisation and the other is with target production (70%). Design 3 has achieved design objectives of treatment cost minimisation and NPV maximisation, resulting in 75% production of the maximum possible production, whereas Design 4 has achieved the target of 70% production. The optimisation scheme very sensibly has reduced a 9% treatment cost in its treatment design for 70% production compared to 75% production.

The time-dependent production rate and resulting decline in average reservoir pressures, if the reservoir were treated by the four optimum treatments mentioned above with PKN-C model, are plotted in Figures 5.4 and 5.5. Similar plots for P-3D-C fracture model are presented in Figures 5.6 and 5.7. The figures show that curves for Designs 1 and 2 (i.e. maximum production and maximum NPV) are identical, because there is not much difference between these designs. The decline of reservoir pressure would be more if the well were produced by higher production rate treatments, such as by maximum production or NPV design. The slight kinks in the production rate curves show the transition between the transient state and the pseudo-steady state in production estimation. The curves indicate that the transient production period in tight reservoirs is significantly long, which has been discussed in chapter 4.

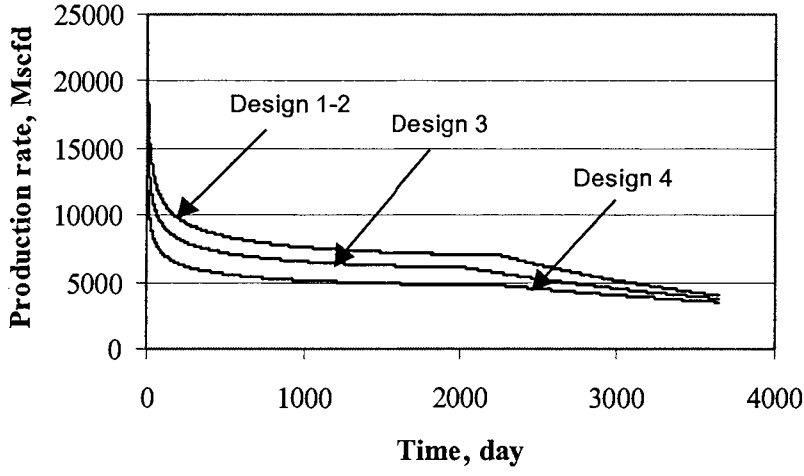

Figure 5.4. Time-dependent production rates for optimum designs with PKN-C fracture model

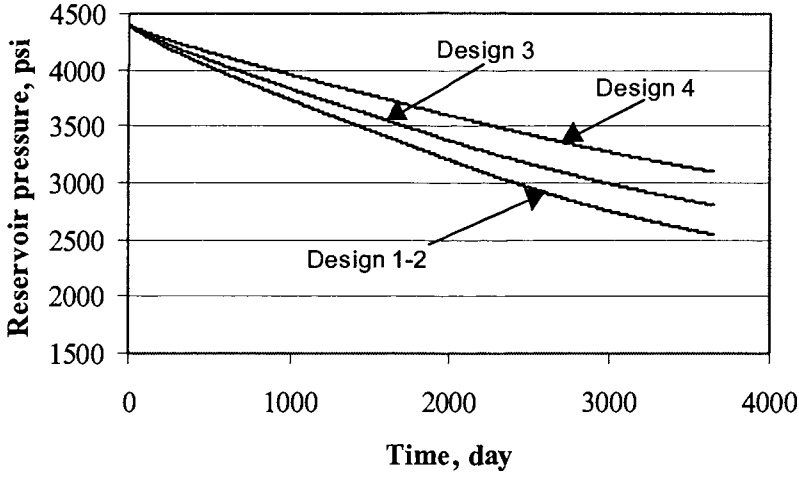

Figure 5.5. Time-dependent decline in reservoir pressure for optimum designs with PKN-C fracture model.

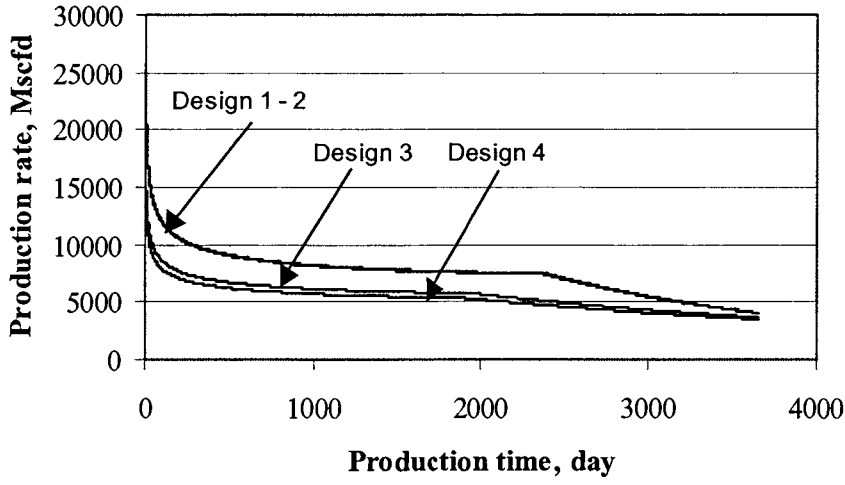

Figure 5.6. Time-dependent production rates for optimum designs with P-3D-C fracture model

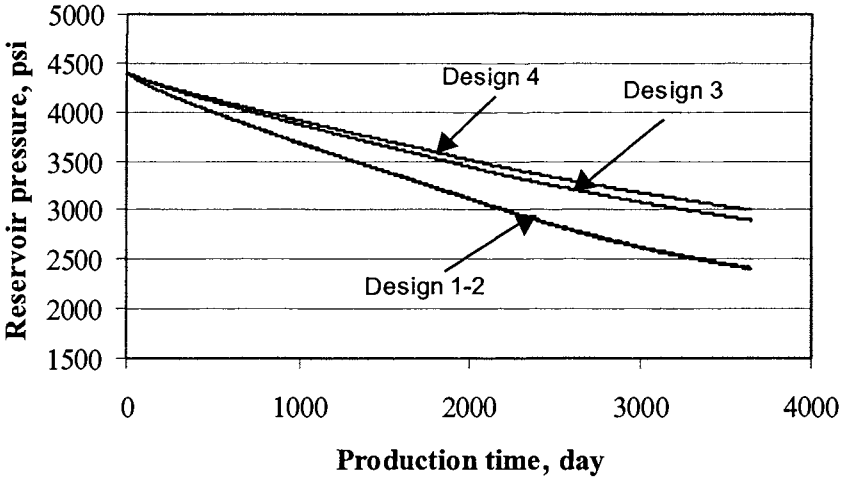

Figure 5.7. Time-dependent decline in reservoir pressure for optimum designs with P-3D-C fracture model.

The proppant scheduling designed for the four designs with PKN-C fracture model is presented in Figure 5.8, which clearly shows that the treatment for higher production requires higher proppant concentration over a longer period but delayed proppant loading. Similar plot is presented in Figure 5.9 for P-3D-C fracture model. In Designs 1 and 2, proppant scheduling is almost the same. In Design 3, proppant scheduling is totally different, as the optimum design is significantly different from Design 1 and 2. Proppant scheduling of Design 4 is also different from those of Designs 1 & 2, but a bit close to that of Design 3.

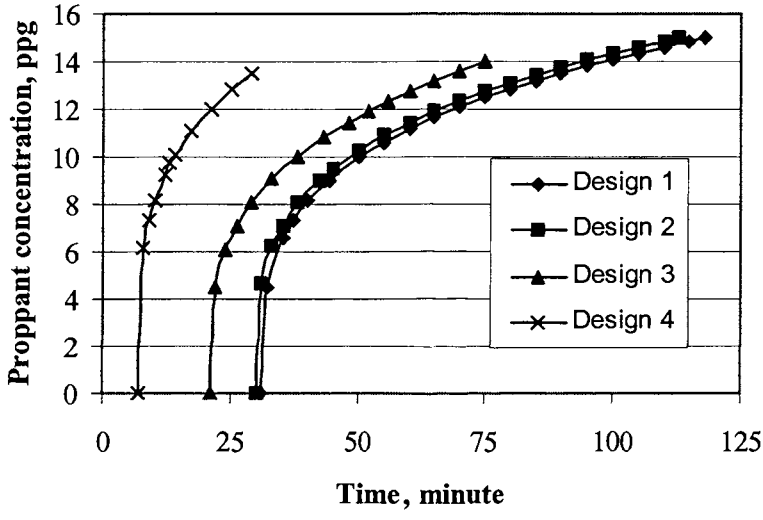

Figure 5.8. Designed proppant scheduling for optimum designs with PKN-C fracture model.

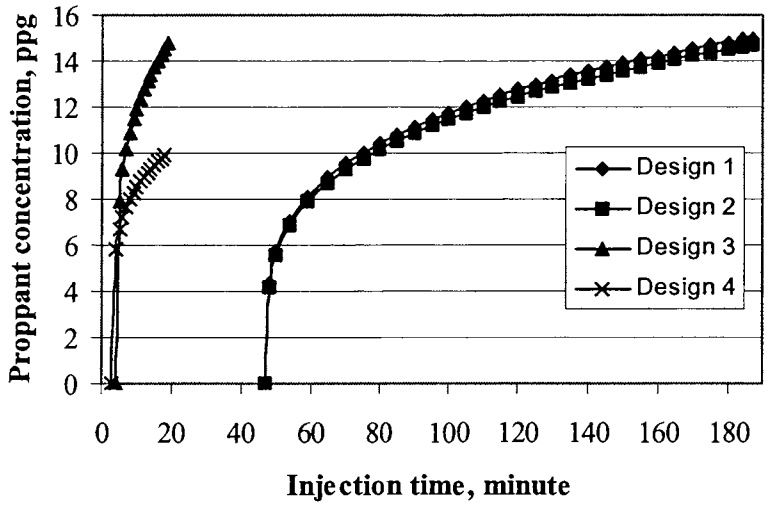

Figure 5.9. Designed proppant scheduling for optimum designs with P-3D-C fracture model.

5.3.4. Simulation by IMEX Blackoil Simulator

The main component in formulating objective functions (Eqs. 5.1-5.4) for optimisation is cumulative production over a number of years. The reliability of an optimum design is thus primarily dependent on realistic production estimation from the fractured reservoir. As presented in chapter 4, the total production from the hydraulically fractured well is estimated by summing up the productions in the transient and the pseudo-steady state periods. The powerful reservoir simulator, IMEX, was used to verify the overall production behaviour predicted by this analytical model in maximising NPV. For this purpose, the optimum fracture geometry for maximum NPV design was simulated in IMEX. Simulation procedure is detailed in chapter 4. The production simulation was then run over 10 years using the same reservoir properties and PVT parameters as used in the optimisation scheme. The production behaviors as estimated by the analytical method and the reservoir simulator are compared in Figure 5.10. It is evident from this figure that the production decline rate estimated by the analytical method is close to that obtained by the simulator, both in transient and pseudo-steady state flow regimes. The

Cumulative production in ten years time is 24.544 bscf by IMEX and 25.511 bscf by the analytical model. The analytical estimation has been only about 4% higher than that obtained from reservoir simulation. The computational effort required by the simulator was about 100 times of that required by the analytical method. This is for one cycle of computation of cumulative production for the final optimum design. To derive this design, the optimisation algorithm performed hundreds of designs internally, each requiring the estimation of cumulative production. Therefore, even if the simulator could be made interacted with optimisation scheme by some special interface design, the computation time would have been prohibitive.

Similar plot is presented in Figure 5.11 for P-3D-C fracture model. With P-3D-C fracture model, the cumulative production in ten years is 27.3672 bscf by the model and 25.995 bscf by IMEX and model's estimation has been only 5.3% higher than that obtained from IMEX. The average reservoir pressure profiles (Figures 5.12 and 5.13) are also found to be reasonably consistent.

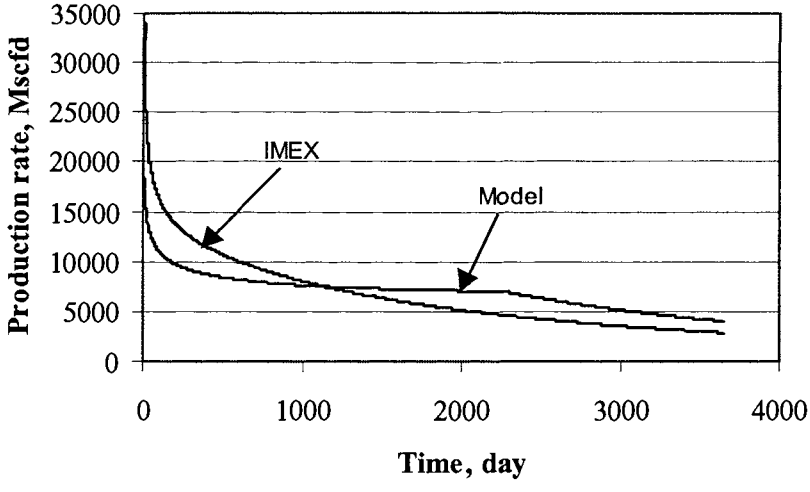

Figure 5.10. Comparison of production rates estimated by the analytical model and IMEX for the design with PKN-C fracture model.

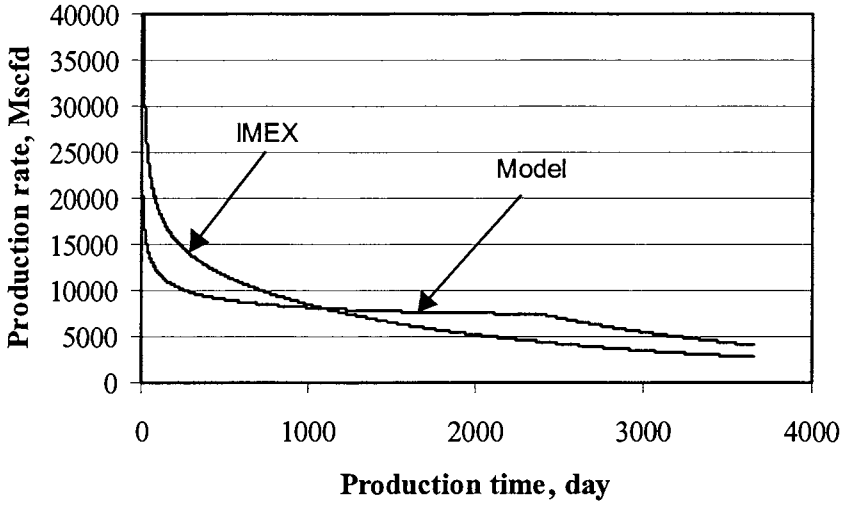

Figure 5.11. Comparison of production rates estimated by the analytical model and IMEX for the design with P-3D-C fracture model.

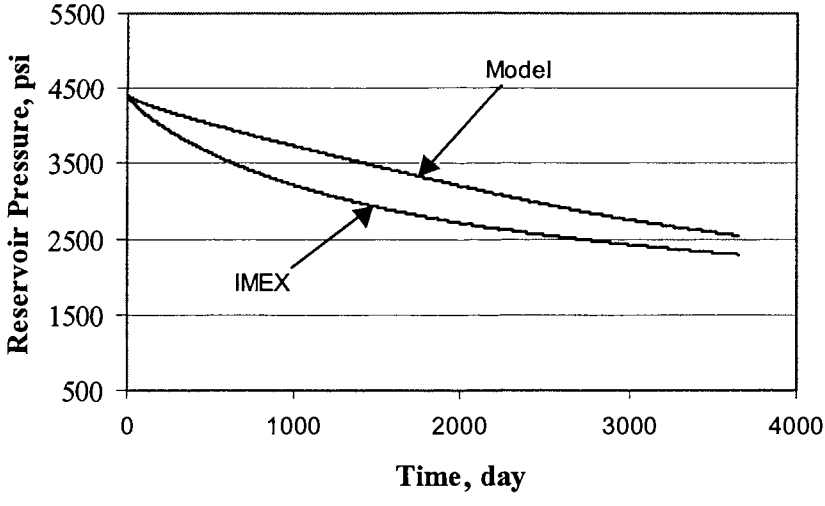

Figure 5.12. Average reservoir pressure profiles estimated by the analytical model and the IMEX for the design with PKN-C fracture model.

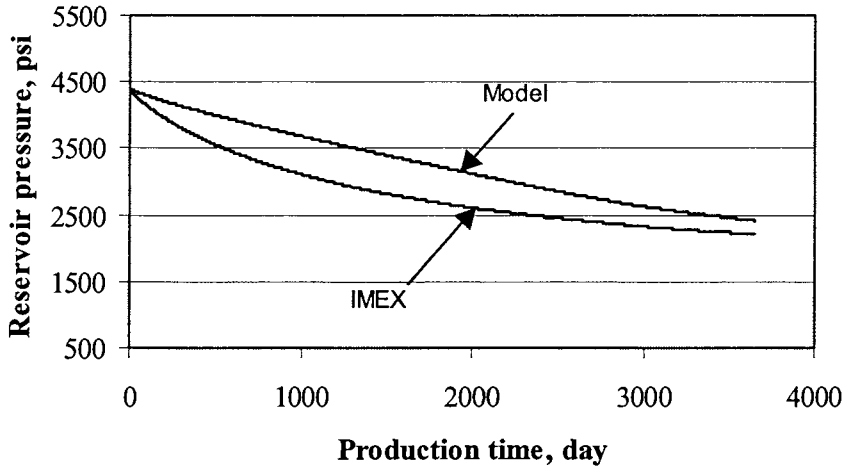

Figure 5.13. Average reservoir pressure profiles estimated by the analytical model and the IMEX for the design with P-3D-C fracture model.

5.3.5. Trade-offs between treatment cost and production/NPV

Figure 5.14 presents a trade-off analysis between treatment cost and production while optimising with PKN-C fracture model. For the upper curve, the maximum production design was achieved first using the objective function defined by Eq. 5.1 (the point at production factor, PF = 1). Values of target production, T_1, were then set to achieve production factors (PF is defined as the ratio of actual production to the maximum production) of 0.95, 0.9, 0.85, 0.8, 0.75, 0.7 and corresponding optimum designs were obtained. Note that no effort was made to minimise the treatment cost for these designs, as the objective function was formulated as minimise (G_p - T_1), and full production targets were always possible to achieve. Treatment costs associated with these designs are plotted against production factors (upper curve). For the lower curve, optimum designs were obtained by setting production target, T_1 to achieve production factors of 0.7, 0.75, 0.8, 0.85, 0.9, 0.95 and 1.0 in the objective function defined by Eq. 5.4. Note that the minimisation of treatment cost is attempted in these designs while the production is achieved as close to the target value as possible. The full production

targets were met up to the production factors of 0.80 beyond which a compromise is necessary with the production target in order to minimise the treatment cost. Thus, the actual production factor on the lower curve falls behind compared to the upper curve and it was not possible to achieve more than 0.88 production factor while T_1 was set by production factors between 0.9 - 1.0. It is quite sensible that the treatment cost is always lower (in the lower curve) when an attempt is made to minimize it. It is particularly interesting that only a 12% compromise with the production (i.e. production factor of 0.88) saves about 44% of the treatment cost. Similar trade-off between treatment cost and NPV are shown in Figure 5.15, which gives an immediate treatment cost saving of \$0.455m compromising \$1.4606m NPV over 10 years.

Similar plots are presented in Figures 5.16 and 5.17 for P-3D-C fracture model. It is evident, similarly as observed with PKN-C fracture model, that only a 13% compromise with the production saves about 52% of the treatment cost. The implication of this type of trade-off analyses is that a company may prefer to compromise with a small percentage of production/NPV over an uncertain period to save immediate cash in treatment cost. To make such a decision, the design tool must have the capability, as the proposed tool has, to adjust design with optimality for any target production/NPV.

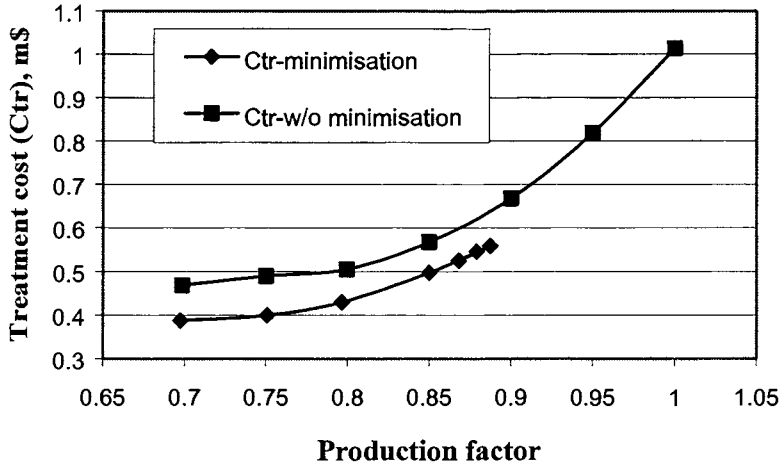

Figure 5.14. Trade-offs between treatment cost and production for the design with PKN-C fracture model.

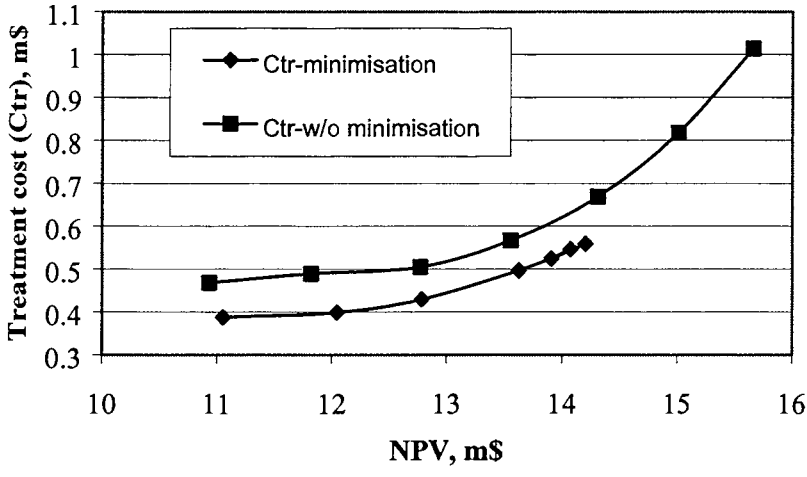

Figure 5.15. Trade-offs between treatment cost and NPV for the design with PKN-C fracture model.

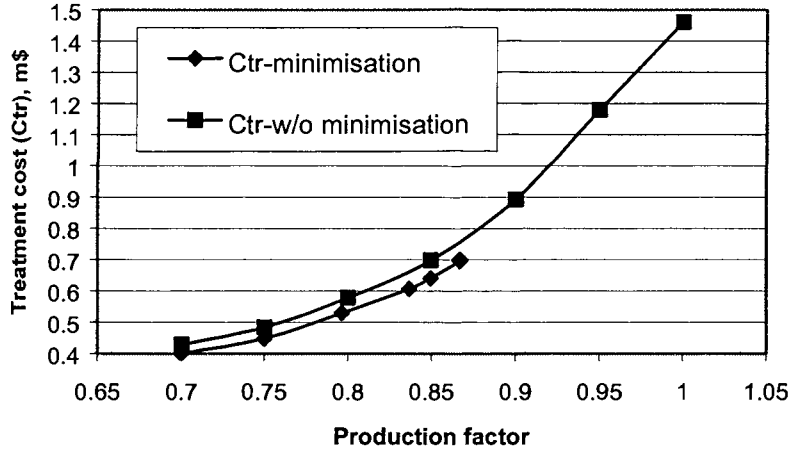

Figure 5.16. Trade-offs between treatment cost and production for the design with P-3D-C fracture model.

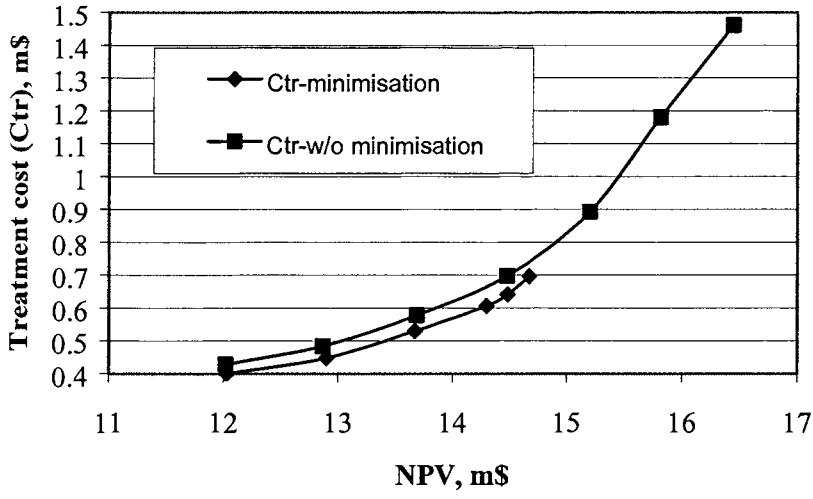

Figure 5.17. Trade-offs between treatment cost and NPV for the design with P-3D-C fracture model.

5.3.6. Sensitivity of design variables on NPV

Optimum values of the free design variables modeled in this study are already presented in Table 5.6 for various design objectives. It may, however, be necessary or convenient to use slightly different values of certain parameters while the treatment is executed in the field. Fixing a certain parameter to a value other than its optimum value deteriorates the objective function, which can however be improved to some extent if remaining parameters are re-optimised. This is studied by fixing each variable to a value around its optimum value for maximum NPV and optimising remaining four variables to improve NPV. The sensitivity results presented herein, therefore, might look different from other works (Meng and Brown, 1987; Hareland *et al.*, 1993; Hareland and Rampersad, 1994; Yang *et al.*, 1996; Aggour and Economides, 1998; Rietman, 1998; Aggour, 2001) in which remaining parameters were not adjusted to yield a maximum NPV, which has been done in this study, for a certain value of the varying parameter.

Fracture half-length

Figures 5.18 and 5.19 show the variation in the maximum NPV with fracture half-length, x_f while optimising with PKN-C and P-3D-C fracture models, respectively. The remaining four variables were optimised for each value of x_f. The free optimum value for this variable is 2500 ft (Table 5.6, Designs 1 & 2). The maximum NPV increases as the fracture half-length increases up to this value beyond which the improvement in NPV diminishes. This is because the non-dimensional fracture conductivity decreases and the treatment cost exceeds the return with increasing fracture length beyond 2500 ft. However, even this 2500 ft half-length represents a massive fracture. The optimum fracture length shortened significantly for high permeability reservoirs (presented in later section). This indicates that a deeply penetrating massive fracture is usually required for very low-permeability reservoirs such as the one studied.

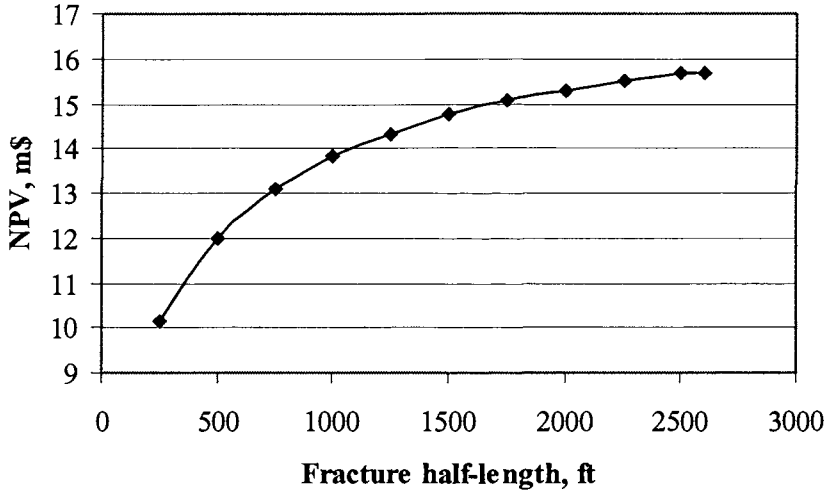

Figure 5.18. Effect of fracture half-length on NPV for the design with PKN-C fracture model.

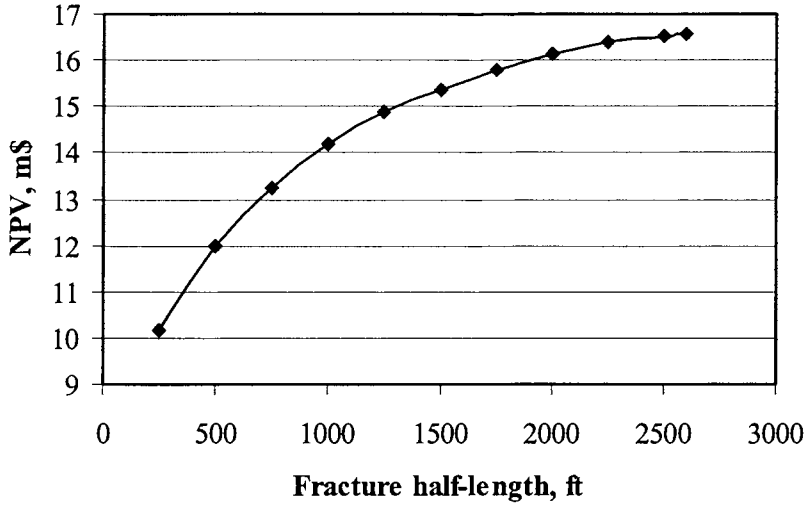

Figure 5.19. Effect of fracture half-length on NPV for the design with P-3D-C fracture model.

Fracturing fluid viscosity

Figure 5.20 shows that for PKN-C fracture model the maximum NPV increases with increasing viscosity up to its free optimum value, 212 cp (Table 5.6, Design 2) beyond which the NPV decreases. Initially, the increase in viscosity increases fracture width and height, which increases the fracture conductivity, in turn the production return. It has been observed (Figure 5.21) that with the increase in viscosity, optimum injection rate decreases slowly, but beyond 212 cp of viscosity, the optimum injection rate drops significantly, keeping the fracture height and width almost unchanged to their values at 212 cp of viscosity. To satisfy the material balance relationships, a shorter fracture half-length is required for viscosity higher than 212 cp. With shorter fracture half-lengths, the fracturing fluid efficiency decreases, which decreases the fracture conductivity and ultimately the production (see the cumulative production curve in Figure 5.21) and the NPV. It has been observed that treatment cost decreases with increasing viscosity in this range despite the fracturing fluid price increases with increasing viscosity. This is because the fracturing fluid volume and the amount of proppant required decrease with the decrease of fluid efficiency. This is favourable to increase NPV; however, the improvement in NPV due to reduced treatment cost is subsided by the decrease in NPV due to reduced fracture conductivity.

Similar plots are presented in Figures 5.22 and 5.23 while optimising with P-3D-C fracture model. Here, maximum NPV is obtained at fracturing fluid of 368 cp, beyond which NPV is dropping because of similar reasons discussed for PKN-C model. It is noticed that the optimum value of viscosity is much higher than that with PKN-C model. Because there is no imposed height growth constraint (e.g. constraint 4) in P-3D-C model, which has allowed a higher fracture height determined by the equilibrium condition based on stress intensity factors, as described in chapter 3. This higher fracture height allows a higher fracture width and requires a higher viscosity to satisfy material balance relationships. Figures 5.24 and 5.25 show the average dynamic fracture width and fracture height versus fluid viscosity, respectively. Fracture width and height increase with the increase of viscosity up to a certain limit of viscosity (368 cp), then remain steady, which is possibly because of other fracture growth control constraints based on formation considerations (e.g. constraints 8-10).

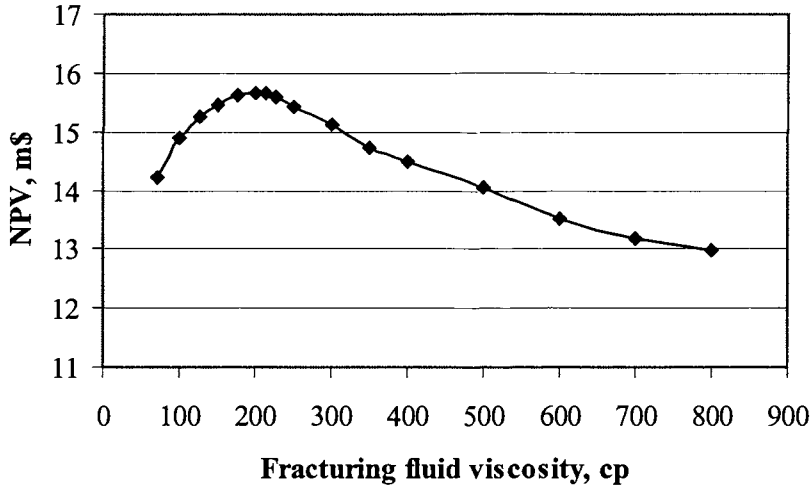

Figure 5.20. Effect of fracturing fluid viscosity on NPV for the design with PKN-C fracture model.

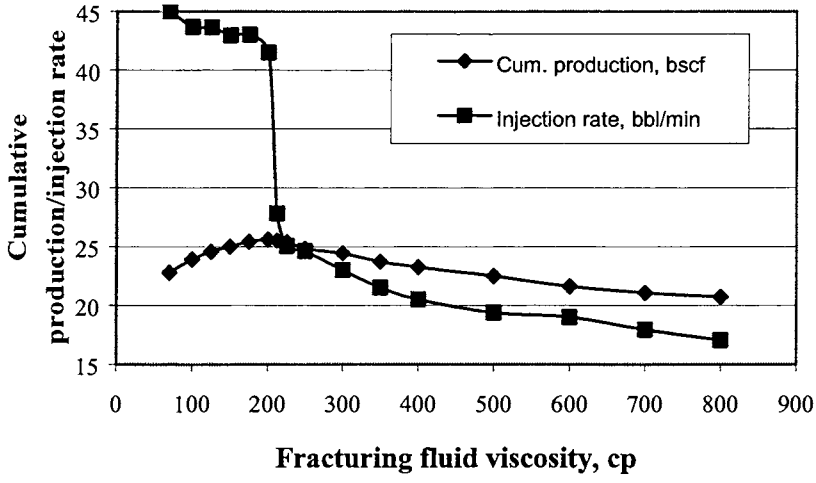

Figure 5.21. Variation of cumulative production and injection rate with change of fracturing fluid viscosity for the design with PKN-C fracture model.

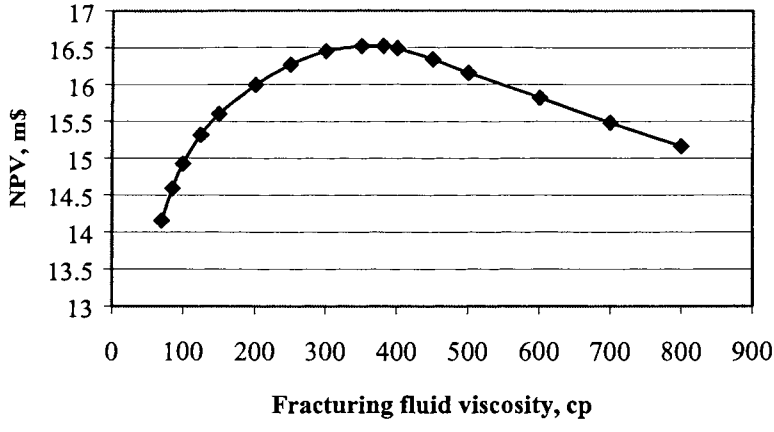

Figure 5.22. Effect of fracturing fluid viscosity on NPV for the design with P-3D-C fracture model.

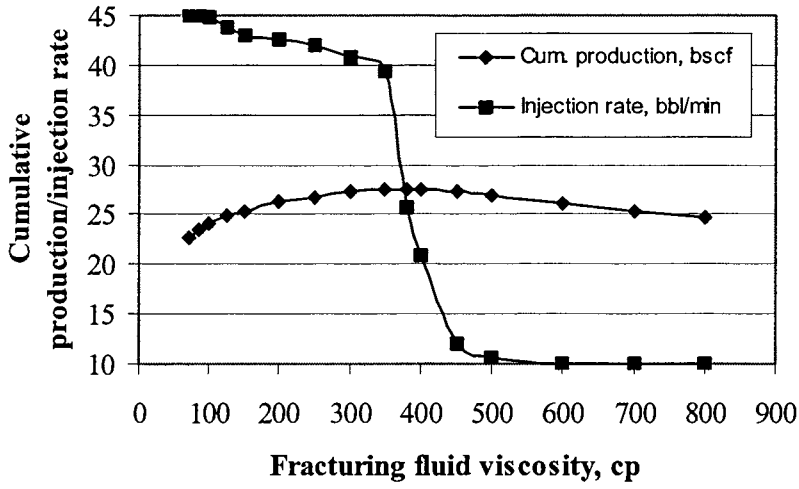

Figure 5.23. Variation of cumulative production and injection rate with change of fracturing fluid viscosity for the design with P-3D-C fracture model.

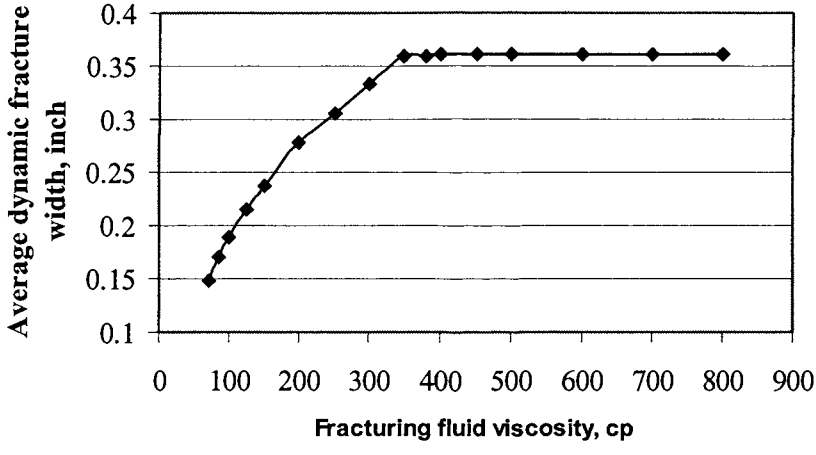

Figure 5.24. Effect of fracturing fluid viscosity on average dynamic fracture width for the design with P-3D-C fracture model.

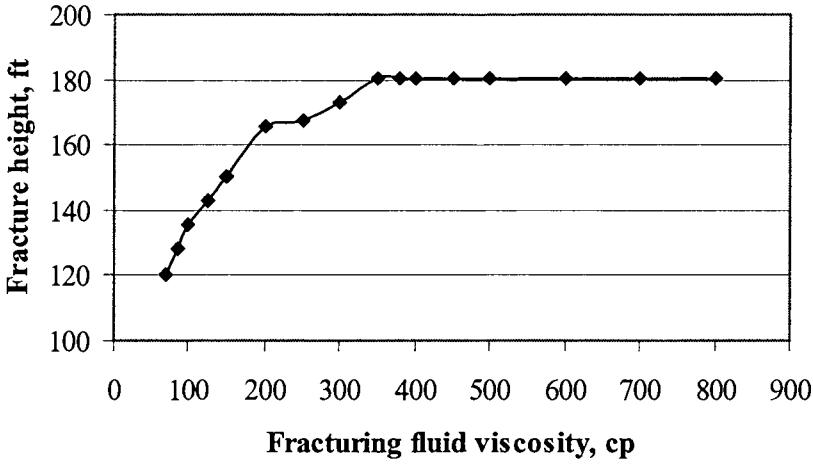

Figure 5.25. Effect of fracturing fluid viscosity on fracture height for the design with P-3D-C fracture model.

Proppant concentration

Figures 5.26 and 5.27 show that the maximum NPV increases smoothly as the proppant concentration increases, while the treatments are optimised with fracture models PKN-C and P-3D-C, respectively. This is because the proppant concentration directly increases the fracture conductivity, and in turn the production return, which exceeds the increase in proppant cost. Because of this nature, the upper bound on this parameter has been optimum when it is freely optimised for maximum NPV and maximum production designs.

Injection rate and time

Figure 5.28 shows the maximum NPV versus injection rate while optimising with PKN-C fracture model. It is interesting to note that NPV rapidly increases up to 20 bbl/min injection rate beyond which NPV remains almost flat with slight increase up to 40 bbl/min from where it decreases sharply. This justifies the free optimum injection rate of 27.6 bbl/min for maximum NPV design (Table 5.6, Design 2) falls on this plateau. Figure 5.29 shows the maximum NPV versus injection time while optimising with PKN-C fracture model. It exhibits very similar nature to that of NPV versus injection rate. Figure 5.30 shows that the optimum injection time sensibly decreased when the injection rate was fixed at higher values. However, the fluid volume injected remained

unchanged over the NPV plateau. Since the treatment cost is a function of fracturing fluid volume, and not a direct function of injection time and rate, the treatment cost also remained almost unchanged over this plateau. This follows that the fracture conductivity, in turn the production returns, is not very sensitive to the injection rate within this range.

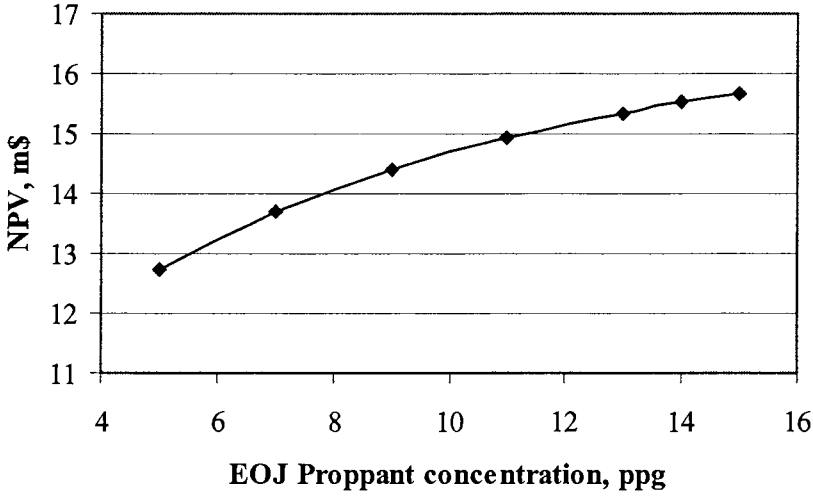

Figure 5.26. Effect of EOJ proppant concentration on NPV for the design with PKN-C fracture model.

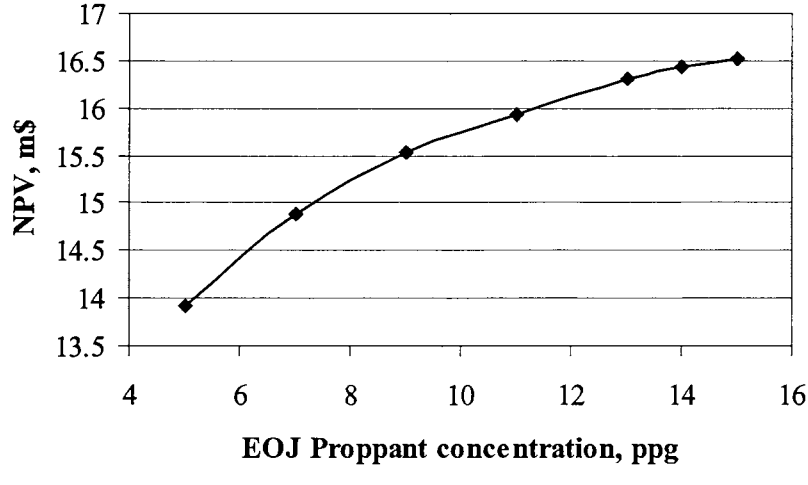

Figure 5.27. Effect of EOJ proppant concentration on NPV for the design with P-3D-C fracture model.

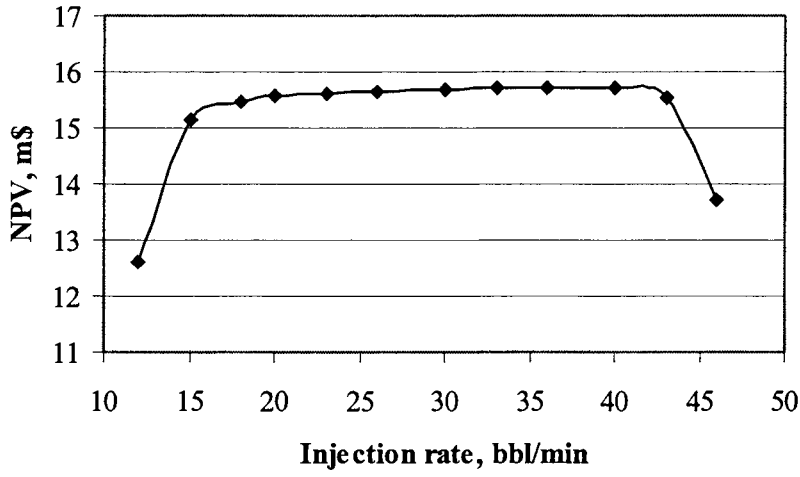

Figure 5.28. Effect of injection rate on NPV for the design with PKN-C fracture model.

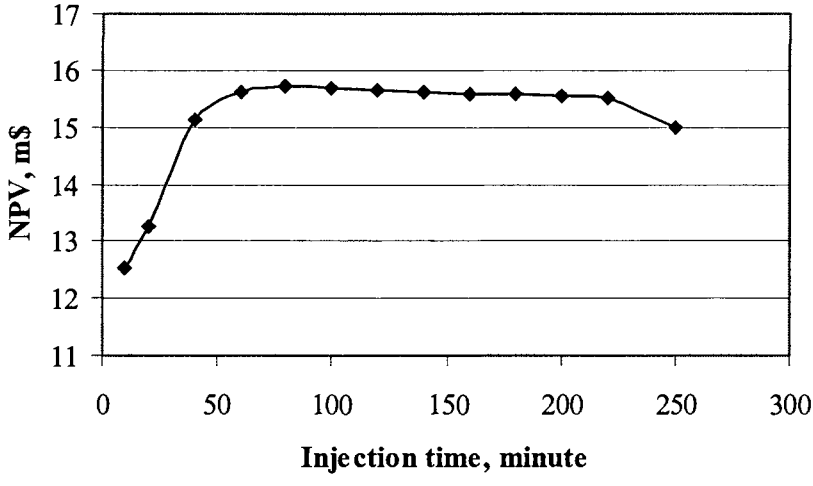

Figure 5.29. Effect of Injection time on NPV for the design with PKN-C fracture model.

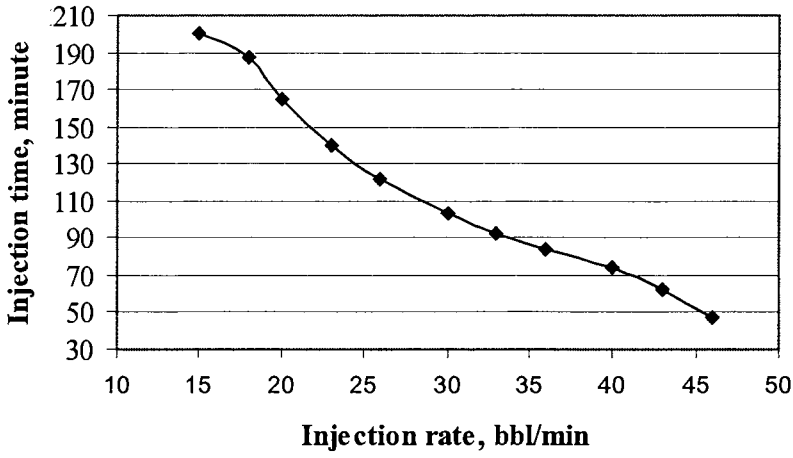

Figure 5.30. Injection time versus injection rate for the design with PKN-C fracture model.

Similar plots are presented in Figures 5.31 and 5.32 while optimising with P-3D-C fracture model for the effect of injection rate on NPV. Similar observations are noticed for the plateau developed between 20-40 bbl/min. The free optimum injection rate of 26 bbl/min (Table 5.6, Design 2) falls on this plateau. It is also noticed that the optimum injection time at each injection rate decreases with the increase of injection rate (Figure 5.32).

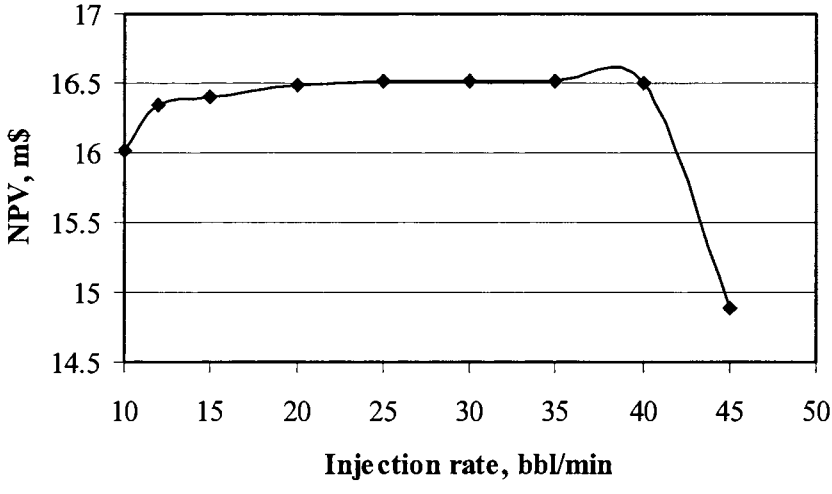

Figure 5.31. Effect of injection rate on NPV for the design with P-3D-C fracture model.

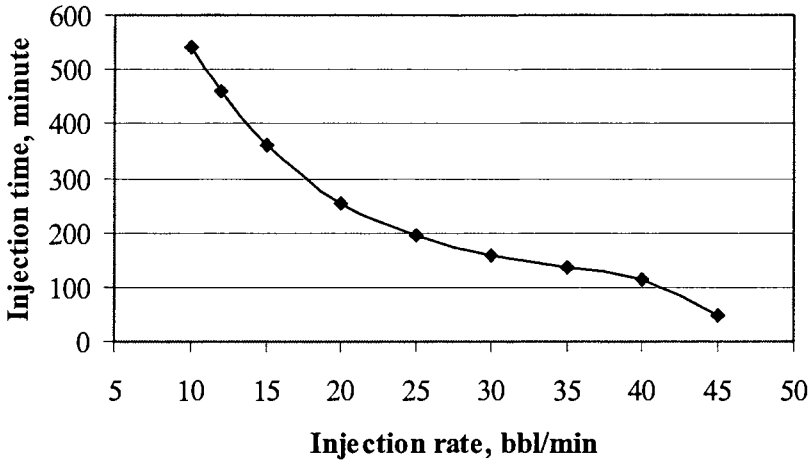

Figure 5.32. Injection time versus injection rate for the design with P-3D-C fracture model.

5.3.7. Effect of fracture height migration on NPV

In many field design and research works, fracture migration to boundary layers is perceived uneconomic, as these layers do not contribute to production. For design optimization results presented so far in this paper, the fracture height is constraint such that it does not migrate to the bounding layers by more than 25% of the pay zone height, based on the NSI fracture handbook (Smith, 1992). To quantify the effect of fracture migration into bounding layers on NPV maximisation, the height migration constraint was later adjusted such that the ratio of pay zone height to fracture height (h/h_f) varied from 1.0 to 2.0. Figure 5.33 shows the variation in the maximum NPV with increasing fracture height migration into bounding layers. Slight fracture migration into bounding layers has drastically improved the maximum NPV design. The improvement in NPV is almost linear up to a value of 1.5 for the ratio beyond which very little improvement is noticed. This indicates that allowing fracture migration into bounding layers by 50% of the pay zone height (100 ft) would have been more economic for the reservoir considered in this study. Figure shows that the NPV is maximum at about fracture height migration of 80% of the pay zone height. Although bounding layers do not

directly produce, fracture migration into bounding layers contributes to production enhancement in two ways. First, the increased fracture height increases fracture width which in turn increases production. Second, the non-producible width around the edges of the fracture falls completely in the bounding layers and thus the height proportion of the fracture that stays inside the pay zone becomes fully producible. However, excessive migration does not result in any net benefit because of increased treatment cost. Therefore, deciding an appropriate amount of fracture migration into bounding layers is a critical issue in designing an economic hydraulic fracturing treatment. This was not studied for optimisation with P-3D-C fracture model because the fracture height growth was not restricted by any direct constraint based on the pay zone height. Therefore, an optimum height was automatically achieved in a design with P-3D-C model.

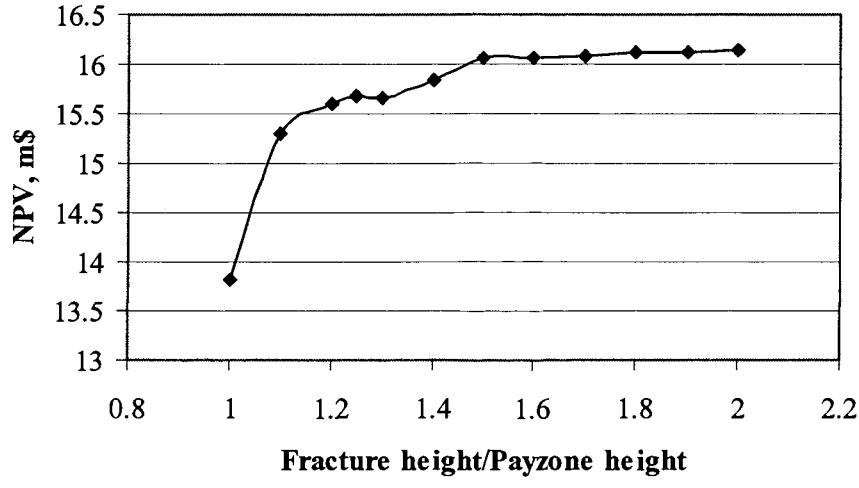

Figure 5.33. Effect of fracture height migration on NPV for the design with PKN-C fracture model.

5.3.8. Effect of reservoir permeability on maximum NPV design

Tables 5.7 and 5.8 present maximum NPV designs with PKN-C and P-3D-C fracture models, respectively, for a range of initial reservoir permeability. With increasing permeability, a short fracture and a high viscous fluid are optimum and consequently the optimum volume of injection ($q_i \times t_i$) is low. The optimum proppant concentration,

however, remains almost unchanged. Productions and resulting NPVs are significantly high for high permeable reservoirs even with shorter fractures. This implies that larger fractures will be optimum in low permeable reservoirs to enhance production and NPV.

Table 5.7. Effect of reservoir permeability on optimum design with PKN-C model.

k (md)	x_f (ft)	q_i (bbl/m)	EOJ P_c (ppg)	μ_f (cp)	t_i (min)	NPV (m$)	G_p (bscf)
0.06	2500.00	24.069	14.95	170.775	108.512	11.37682	18.44477
0.1	2499.86	29.315	15.00	209.767	105.875	12.85956	21.33594
0.2	2499.87	27.577	15.00	212.390	113.604	15.66389	25.51099
0.35	1808.66	23.128	15.00	302.144	95.861	18.27886	28.50819
0.5	2004.54	23.584	15.00	271.721	105.476	20.39765	31.00426
0.75	1701.77	23.840	15.00	319.263	86.399	22.72425	33.23808
1.0	1619.94	24.462	15.00	333.807	79.348	24.33400	34.61662
2.0	1226.54	24.666	15.00	443.431	57.530	27.76161	36.71626
3.0	724.86	20.656	15.00	799.765	39.156	29.37658	37.20516

Table 5.8. Effect of reservoir permeability on optimum design with P-3D-C model.

k (md)	x_f (ft)	q_i (bbl/m)	EOJ P_c (ppg)	μ_f (cp)	t_i (min)	NPV (m$)	G_p (bscf)
0.06	2500.00	35.424	15.00	351.886	132.50	11.95254	20.23381
0.1	2500.00	33.339	15.00	342.139	140.00	13.41789	22.86483
0.2	2500.00	25.991	14.70	367.862	187.50	16.44502	27.36720
0.35	2499.10	34.510	15.00	330.843	132.50	19.29646	30.76054
0.5	2414.46	38.151	15.00	362.392	117.50	21.20809	32.72814
0.75	1781.10	31.697	15.00	516.884	103.75	23.34497	34.31279
1.0	1559.62	37.458	15.00	544.933	72.50	24.83080	35.34235
2.0	1083.64	37.653	14.50	732.383	45.63	27.97998	36.89166
3.0	880.01	26.556	14.20	755.115	46.25	29.41463	37.24769

5.4. Comparison between optimum designs using two fracture models

Although various results have already been discussed, maximum NPV designs with PKN-C and P-3D-C fracture models are directly compared in Table 5.9. In this table, the column two under PKN-C shows the optimum results when the fracture height was not allowed to grow into the bounding layers by more than 25% of pay zone height. These results may not be comparable to those obtained from the scheme with P-3D-C model, where there is no imposed constraint on fracture height growth. The column four shows the results of the scheme with P-3D-C model, where the fracture height at the wellbore is found to be 180.6 ft. It was evident from the effect of fracture height migration on NPV (section 5.3.7) while optimising with PKN-C model that the absolute maximum NPV was found with fracture height migration of 80% and remains almost unchanged till migration of 100% of the pay zone height. Thus, the optimisation scheme with PKN-C model is run again allowing fracture height migration into the bounding layers up to 200% of the pay zone height to make this constraint effectively inactive, so that the results can be compared with that obtained from P-3D-C model. These results are presented under PKN-C* column in Table 5.9.

It can be seen that optimum treatment parameters obtained from both optimisation schemes (PKN-C* and P-3D-C) are fairly close (except the injection rate). Also the optimum fracture height from the PKN-C model has been 183.7 ft, which is very close to 180.6 ft from P-3D-C model. The optimum fluid viscosity has also increased to 358.4 cp, very close to 368 cp from P-3D-C model. Due to the difference of height variations in two models, PKN-C fracture volume will be higher than P-3D-C fracture volume, because the optimum fracture dimensions from both models are very close. Therefore, the PKN-C fracture has consumed more fracturing fluid and proppant, incurring a higher treatment cost. Therefore, the NPV obtained from P-3D-C is slightly higher although the production is slightly higher from PKN-C model.

Table 5.9. A comparison between the optimum parameters from two optimisation schemes (* allowing fracture height migration into the bounding layers by 200% of pay zone height).

Parameters	PKN-C	PKN-C*	P-3D-C
Treatment parameters			
Injection rate, bbl/min	27.58	34.47	25.99
Injection time, min.	113.6	185.3	187.5
Frac. fluid viscosity, cp	212.4	358.37	367.86
Proppant conc., ppg	15.0	14.7	14.7
Total weight of proppant, klb	628.829	1322.547	998.004
Total volume of fracturing fluid, bbl	2554.05	5171.10	3954.79
Total volume injected, bbl	3132.78	6388.27	4873.28
Fracture parameters			
Fracture half-length, ft	2500.0	2454.3	2500.0
Fracture height @ wellbore, ft	125.0	183.74	180.6
Dynamic fracture width, inch (average)	0.2496	0.3651	0.3548
Propped fracture width, inch	0.0960	0.1399	0.1357
Propped fracture area, ft^2	625000.0	901892.2	701500.0
Fracture volume, ft^3	10204.2	21537.96	16288.05
Fracture conductivity, md-ft	505.61	736.87	714.89
In-situ proppant conc., lb/ft^2	0.5031	0.7332	0.7113
Dimensionless fracture conductivity	1.011	1.501	1.430
Fracturing fluid efficiency, %	58.01	60.05	59.53
Production and cost			
Treatment cost, m$	1.01367	1.83625	1.46067
Cumulative production in 10 years, bscf (Cum. production by IMEX simulation)	25.51099 (24.544)	27.43904 (26.093)	27.36720 (25.995)
Net Present Value (NPV), m$	15.66389	16.11680	16.44502

The implication of this comparative analysis is not that when the treatment optimised using a certain fracture model will be executed in the field, the actual fracture will closely follow the model behaviour and thus, the study will indicate the superiority of one model to the other in terms of field benefits. Rather, the study is intended to show the predictive difference of the two models. From this point of view, not much

difference is found between the two models for the type of reservoir considered in this study. This finding is consistent with the indication of Rahim and Holditch (1995) that the incorporation of PKN-C fracture model is sufficient in the design scheme of hydraulic fracture treatment unless the number of formation layers is sufficiently high and the stress contrast between them is also high.

5.5. Hydraulic fracture optimisation for a weak-gas formation

As mentioned earlier, uncontrolled growth of hydraulic fractures and initiation of secondary multiple fractures may occur due to execution of a fracture treatment with inappropriate values for various treatment parameters. Such uncontrolled fracturing may damage the formation irreversibly, resulting in productivity lower than even unfractured wells. Also excessive pressure drawdown during production from hydraulically fractured wells may result in sand production due to mechanical failure of perforation tunnels. A weak formation is more susceptible to this type of formation failure. This section presents optimisation of treatment parameters for fracturing a weak-gas formation, to show how an additional constraint is necessary to prevent this failure and resulting sand production.

5.5.1. Application to a gas reservoir and results

Reservoir properties, formation properties and well data of a weak-gas formation are presented in Table 5.10. Proppant selection data are presented in Table 5.11. The prescribed laboratory measured permeability/conductivity of the proppant was corrected to the expected in-situ concentration with the application of conductivity damage factor to obtain realistic fracture conductivity (chapter 3). Economics data used for NPV calculation over 10 years production life are same as presented in Table 5.3, except the pumping cost is estimated for 12000 hhp. Burst strength of the tube and the rated pressures of surface equipment are same as presented in Table 5.2.

The NPV was maximised over 10 years using PKN-C fracture model. Because of the relatively high permeability in this reservoir, only the pseudo-steady state flow condition was used for production estimation. The optimum design is presented in Table 5.12 under 'Model' column. The production profile for the optimum design was again simulated by IMEX and compared in Figure 5.34. The figure shows an excellent agreement between the two production profiles, as expected for this relatively high-permeability reservoir.

Table 5.10. Reservoir and formation properties and well data of a weak-gas formation.

Drainage area	640 acres
Average depth	4000 ft
Thickness	30 ft
Shape (square)	5,280 x 5,280 ft^2
Equivalent drainage radius	2980 ft
Porosity	17 %
Permeability	9 mD
Initial reservoir pressure	3000 psi
Reservoir temperature	180° F
Gas gravity	0.687
Gas saturation	0.80
Initial gas compressibility factor (Z-factor)	0.85
Initial gas viscosity	0.02 cp
Water compressibility	3.0E-6 psi^{-1}
Pore compressibility	8.6E-6 psi^{-1}
Skin factor	0.0
Max. horizontal stress	4400 psi
Min. horizontal /closure stress	3600 psi
Min. horizontal stress (shale)	4000 psi
Cohesive strength	340 psi
Poisson's Ratio	0.20
Leakoff Coefficient	8.0E-4 $ft/min^{0.5}$
Wellbore radius	0.35 ft
Flowing bottomhole pressure	800 psi
Tubing inside diameter	3.0 inch
Measured depth to mid-perforation	4000 ft

Table 5.11. Proppant selection data

Proppant Type	Ottawa 20/40
Specific Gravity	2.65
Bulk density	96 lbm/ft^3
Diameter	0.024 inch
Packed Porosity	0.40
Conductivity @ closure stress	2800 md-ft
Conductivity Damage Factor	0.50

Table 5.12. Optimum treatment parameters and other optimum values

Design parameters/other optimum values	**Software**	**Model**
EOJ proppant conc., ppg	10.0	15.0
Fracturing fluid viscosity, cp	471.4	314.5
Injection rate, bbl/min	12.5	21.32
Injection time, minute	82.2	19.2
Fracture half-length, ft	1077	667.52
Fracture height, ft	38	37.5
Fracture width, inch	0.916	0.43
Fracture conductivity, md-ft	439.3	477.2
Fracture efficiency, %	86.0	61.8
Total injections, bbl	859.3	410
Total proppant injected, klb	105.7	85.323
Fixed cost, $	250,000	250,000
Variable cost, $	136,800	98,406.6
Treatment cost, $	386,800	348,406.6
Cum. gas production, bcf	15.807	16.46544
NPV, m$	12.11	13.176605

In order to show the comparative benefit of the proposed treatment optimisation model, an optimum treatment was also achieved by a commercial software (FRACPRO, 1996), and is presented in Table 5.12 under 'Software' column. Procedures of fracture optimisation by FRACPRO will be described in chapter 6. A comparison between the two designs shows that the treatment optimised by the model has created a shorter

fracture with narrower width, but yielded a higher conductivity due to higher proppant concentration. The optimisation by the software is of unconstrained nature. The optimum design by the software was therefore assessed to verify which constraints of the proposed model were violated. The design was found to violate constraints 8, 9 and 11 (section 5.2.3). The designed treatment pressure, 4148 psi exceeds the formation critical pressure, 4050 psi violating constraint 8, and the designed net pressure, 548 psi exceeds the difference between the minimum horizontal stresses in the pay zone and the bounding layers, 400 psi (4000-3600 psi) violating constraint 9 of section 5.2.3. Violation of these two constraints warns a high probability of uncontrolled fracture growth, should the treatment were executed in the field.

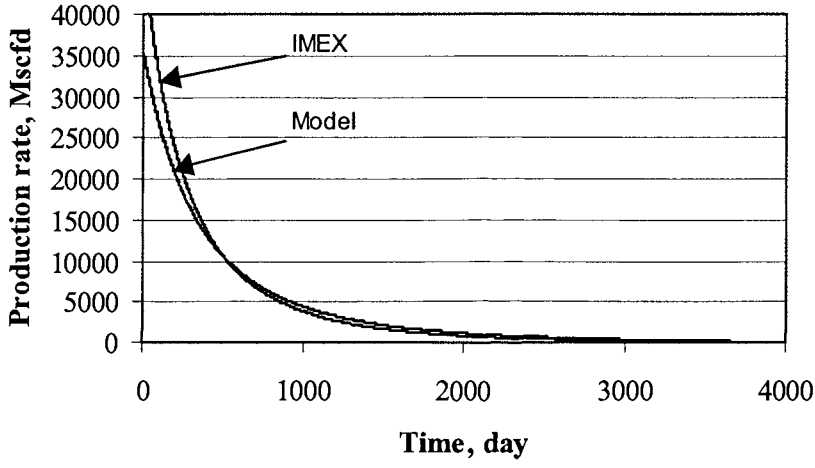

Figure 5.34. Comparison of production profiles from simulator and analytical method.

In order to verify the violation of critical drawdown pressure for sand production (constraint 11 of section 5.2.3), *CDP* was estimated as a function of time over 10 years, and is plotted in Figure 5.35 in which *CDP* of the optimum design by the proposed model is also presented. The figure shows the decreasing trend of *CDP* for both designs. *CDP* for the treatment designed by the commercial software crosses the *ODP* (operator's desired drawdown pressure) line at around the sixth year, suggesting that sand production would occur after that unless the drawdown pressure is decreased

(reducing the production rate). *CDP* for the treatment optimised by the proposed model meets the *ODP* line just at the end of 10th year, suggesting that it has been one of the active constraints for this design. In fact, these three constraints were active for the optimum design obtained by the model, emphasizing the need to constrain treatment design for such reservoirs in order to avoid hydraulic-fracturing-induced formation damage.

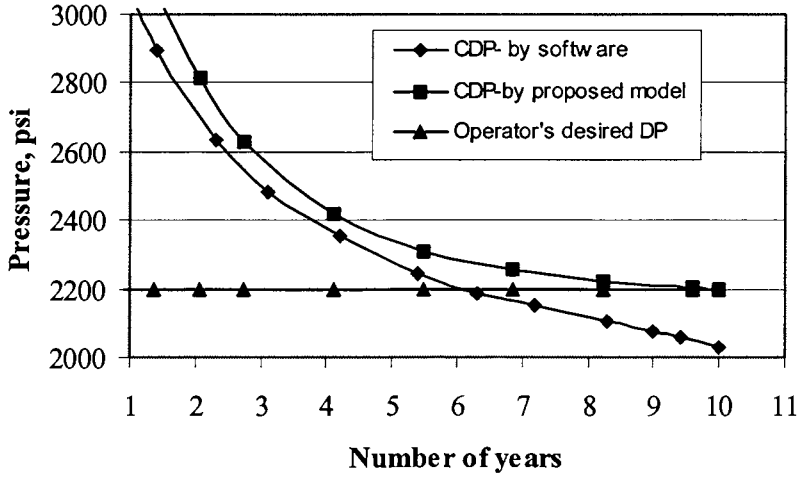

Figure 5.35. Critical drawdown pressures (CDP) during well production.

5.6. Conclusions

The integrated optimisation model for hydraulic fracture treatment design presented in this chapter has accounted for complex interactions among fracture geometry, treatment parameters, material balance, operational limitations, formation characteristics, production behaviours and various potential design objectives. The optimisation model is integrated with 2D PKN-C and P-3D-C fracture models separately. Applications of the optimisation model to a tight-gas reservoir and a soft-gas reservoir have resulted in the following conclusions:

1. The model is capable of finding a true optimum design starting with any initial design, which may or may not satisfy all the design constraints, and the optimum design is significantly better than any arbitrary design. This has been achieved using both fracture models.

2. An optimum design depends on the specified design objective. A maximum NPV design is almost identical to a maximum production design and both designs involve high treatment cost. By using the multi-objective optimisation technique, it is possible to resolve the conflict between production/NPV maximisation and treatment cost minimisation. It is also possible to obtain an optimum hydraulic fracturing design in order to achieve a production target as long as the target is below the maximum possible production. This has been analysed and discussed using both fracture models.

3. The well treated by maximum production/NPV design produces at higher rates and consequently the reservoir pressure decline is higher with time compared to other designs.

4. The model gives the proppant scheduling for the optimum fracture design. Proppant loading is delayed in maximum production/NPV design and the proppant scheduling is continued longer. The model shows higher EOJ proppant concentration with higher production targets.

5. A shorter fracture with higher fracturing fluid viscosity is optimum in a relatively high permeability reservoir.

6. The model is capable to produce an optimum treatment for a target production. Utilizing this capability of the model, trade-off analyses between production/NPV and associated treatment cost have been performed for a wide range of target productions. A balanced solution in terms of production/NPV and treatment cost can be identified from such analysis. For the set of reservoir, economic and other

data used for such analysis of the problem with PKN-C model, it is found that 44% of treatment cost-saving is possible with only 12% reduction in production/NPV over 10 years. Similarly, analysis of the problem with P-3D model shows that 52% of treatment cost-saving is possible with only 13% reduction in production/NPV over 10 years. This capability of the proposed model can enable an operator to achieve a treatment that would save a considerable amount of immediate treatment cost by sacrificing a marginal amount of production/NPV over an uncertain period of time.

7. Using this optimisation model, sensitivities of various treatment parameters have been studied in NPV maximisation. Results demonstrate that fixing a parameter to a value other than its free optimum value always deteriorates a design. The percentage of reduction in NPV can be estimated using the sensitivity results if a treatment parameter is necessary to fix to a non-optimum value for any practical convenience.

8. Although currently many designers design treatments fixing the fracture height to the pay zone height, the fracture migration by an appropriate extent into non-paying bounding layers increases reservoir production and NPV due to increased fracture width in the pay zone. Excessive fracture migration, however, diminishes the NPV increase due to increased treatment cost. The optimum fracture height migration may be reservoir dependent. Using the optimisation model, the optimum fracture height migration can be automatically determined for a specified design objective. The fracture height migration into bounding layers by about 80% of the pay zone height is found to yield an absolute maximum NPV design for the reservoir studied herein with PKN-C fracture model. Interestingly, optimum design with P-3D-C fracture model also shows migration into bounding layers by 80% of the pay zone height.

9. Most optimum fracture parameters and cumulative productions over 10 years obtained from the optimisation scheme using both PKN-C and P-3D-C fracture

models are close. Therefore, PKN-C fracture model can be successfully used to design a hydraulic fracture treatment for three-layered formations, unless there are multi-layered formations with high stress contrast in between them, for which case P-3D-C model is more appropriate.

10. Hydraulic-fracturing-induced formation damage due to uncontrolled fracture growth, multiple fracture initiation and perforation failure resulting in sand production is very likely in high permeability weak formation. The model with constrained treatment optimisation scheme is highly capable to offer a treatment that would avoid/minimise formation damage, can be executed with specified operational facilities and would ensure efficient treatments.

11. Critical drawdown pressure (*CDP*) for sand production decreases with production time as a function of depleting reservoir pressure among other factors. Thus, sand production at the latter production stage is highly likely. The proposed model would optimise treatment parameters to adjust fracture geometry so that a target producing drawdown pressure does not exceed *CDP*, and hence sand production is avoided. However, the operator can adjust the producing drawdown pressure to avoid sand production by an unconstrained treatment design if *CDP* is plotted against the resulting fracture geometry.

12. Fracture treatments designed/optimised by many available software may be likely to cause formation damage because of the unconstrained nature incorporated in their design/optimisation algorithms.

CHAPTER SIX

INTERPRETATION AND ALLEVIATION OF COMPLEXITY WITH HYDRAULIC FRACTURING IN THE FIELD

6.1. Introduction

Conventional hydraulic fracture treatment has been used to produce gas from low permeability reservoirs onshore Australia. The success rate of these treatments, however, was found significantly low. In general, treatments in these tight formations often experienced abnormally high treating pressures, premature screen-outs, and low in-place proppant concentrations, which led to inadequate fracture conductivities. Lengths of hydraulic fractures were found commonly shorter than anticipated as a result of premature screen-out. The wells invariably displayed poor post-frac productivity, often not commensurate with the added expense of fracturing the well.

The initial minifrac injection test also showed high net pressures and frictional pressure drops. In order to investigate the causes of high net pressures and frictional pressure drops, a number of tests were carried out: (1) Thermagel minifrac, (2) Slick water step-rate test, (3) Viscous gel slug, (4) Step-down test, and (5) Hybor minifrac test. The consistent features of these tests were: higher than expected closure stresses (~ 9100 psi; > 1.0 psi/ft); high net fracture pressures (~ 1500 psi); and high shut in pressure drop, which are indicative of high near wellbore frictional pressure losses.

Considering the background knowledge of complexities associated with hydraulic fracturing, as reviewed briefly in Introduction Chapter, it can be speculated that some complex near-wellbore fracture geometry may be the cause for injection pressure anomalies in the wells. The complex near-wellbore fracture geometry may be caused by

in-situ conditions such as prevailing stresses and presence of natural fractures as well as inappropriate perforation practice, any of which may lead to multiple fracturing. While these possibilities will be investigated in this studies to be more definitive about the causes of complexity associated with hydraulic fracturing, a special emphasis will be given to demonstrate how a poorly designed hydraulic fracturing treatment may also cause some of the complexities observed in the field. The potentiality of avoiding/minimizing the complexities by better design of fracturing treatments using the model developed in this study will also be demonstrated. However, it is recognized that the conventional fracturing technique may not be suitable at all if the reservoir is highly naturally fractured for which the waterfrac technique by shear dilation mechanism is solicited to be a promising alternative (Hossain, 2001). The possibility of this technique to enhance reservoir permeability with relatively low stimulation pressure is also investigated. Therefore, the main objectives of this chapter are:

- to analyse injection test pressure records to establish in-situ stress regime in the field,

- to conduct history-matching exercise with various fracture scenarios to shed light upon the causes of fracture complexities and resulting treatment pressure anomalies,

- to perform a 3D numerical study of hydraulic fracture propagation under the stress conditions prevailing in the field in order to explain the potential complexity in the fracture geometry,

- to analyse, in the light of the model developed in this thesis, the design of a treatment by a commercial software widely used in the industry to investigate if such a design itself may become the cause of the complexities encountered,

- to design a treatment by the model developed in this thesis to assess its potential benefits in mitigating the complexities, and

- to analyse the potential of water-frac stimulation in the field.

6.2. Analysis of injection tests for in-situ stress regime

In order to establish potential causes of complexity associated with hydraulic fracturing in the field, it was planned to carry out systematic analysis of injection tests by using FRACPRO (FRACPRO, 1996), a hydraulic fracture design and simulation software widely used in the industry, and HYFRANC-3D (Sousa *et al.*, 1993; Hossain, 2001, www.cfg.cornell.edu), a highly sophisticated software for analysing 3D complex development of hydraulic fractures, widely used in academic research.

Studies of different logs (including density and FMS) and injection tests as well as minifrac test data revealed that there could coexist three different stress regimes in the region. The subject of investigation of this thesis was in the zone under predominantly reverse faulting stress regime.

Minifrac tests indicated two closure pressures: a pressure much higher than the vertical stress, and a pressure roughly equivalent to the vertical stress. The observation can be explained as these closure pressures correspond roughly with different principal stresses acting to close the fracture. The near wellbore fracture closes first (at a higher pressure), under the influence of the wellbore stress concentration and the minimum horizontal stress, as the fracture initiated parallel to the wellbore axis. The fracture then twisted to be normal to the minimum principal stress, which is in this case, vertical stress that is less than the minimum horizontal stress in the reverse faulting regime. Therefore, the secondary fracture closure pressure corresponds to the vertical principal stress, as opposed to the minimum horizontal stress one observes in conventional (normal faulting) stress regimes. Studies of these logs and fracture tests also revealed that the principal stresses under reverse faulting stress regime could be as follows: moderate reverse faulting stress regime (σ_H = 9810 psi, σ_h = 9110 psi, and σ_v = 9090 psi) and

extreme reverse faulting stress regime (σ_H = 12 820 psi, σ_h = 10100 psi and σ_v = 9090 psi).

6.3. History matching exercise with FRACPRO

The problems experienced during stimulation of the wells onshore Australia are most likely due to poor hydraulic communication between the primary fracture and the wellbore. This section describes the results of a hindsight analysis study in which a fracture simulator was used to generate simulated treatment pressure records for a number of assumed fracture configurations. These simulated treating pressure records were then compared with those from field injection tests. As with all hindsight analyses, a number of 'feasible' scenarios for fracture configurations were derived, any one of which may represent the true state of the fracture. The feasibility of each fracture configuration is discussed, and suggestions are offered as to which is the most likely fracture configuration.

FRACPRO can, through modification of lumped coefficients, model multiple, parallel hydraulic fracture propagation, but cannot model complex three-dimensional fracture twisting and turning. For this purpose, numerical models with HYFRANC-3D will be discussed later.

A typical minifrac test with three injection rate changes and good bottom-hole treating pressure record was considered for hindsight analysis. The treatment schedule is described in Figure 6.1 and Table 6.1. This test employed 65 ppt Hybor cross-linked gel due to its superior ability to regain viscosity after shearing, presumably through a tortuous near wellbore region. In an attempt to build up injection rates without exceeding surface pressure limitations, slick water was initially injected at a rate of 23 bbl/min. This was followed by the 50000 gal Hybor stage. The minifrac was tailed in by a 1000 gal of 1 ppg 20/40 Carbo-Lite proppant stage. Upon shut-in the fracture experienced 1300 psi friction pressure drop, a large value, which was attributed to near-

wellbore tortuosity, as opposed to perforation friction. The closure stress was estimated to be 9086 psi, which suggests that the net fracture propagation pressure was approximately 2360 psi. As mentioned earlier, the characteristic features of this minifrac are: (1) high near wellbore friction; and (2) high net fracture propagation pressures.

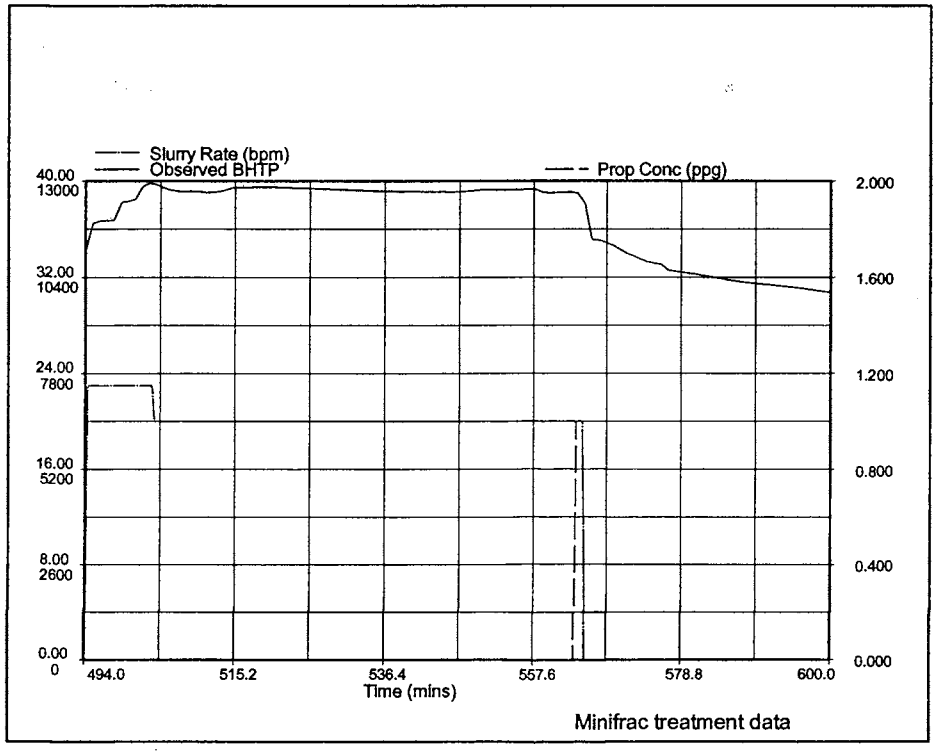

Figure 6.1. Typical treatment data for the mini-frac test in a well onshore Australia.

Table 6.1. Typical treatment schedule for a mini-frac test in a well onshore Australia.

Stage No.	Fluid	Injection Rate (bbl/min)	Proppant Conc. (ppg)	Stage Length (minute)
1	Slick Water	23	-	2
2	65 ppt Hybor	20	-	65.0
3	65 ppt Hybor	20	1.0	1.2
4	Shut-in			

For modelling, a simplified formation description was adopted, which consisted of a target sandstone layer bounded by only two shale layers, as illustrated in Figure 6.2. It is assumed that the entire sand was perforated. Figure 6.2 illustrates the geomechanical properties for these layers used for FRACPRO modelling.

The fracture simulator was run for a large number of assumed fracture configurations and reservoir conditions. Only three successful hindsight treatment pressure matches considered 'realistic' are described here.

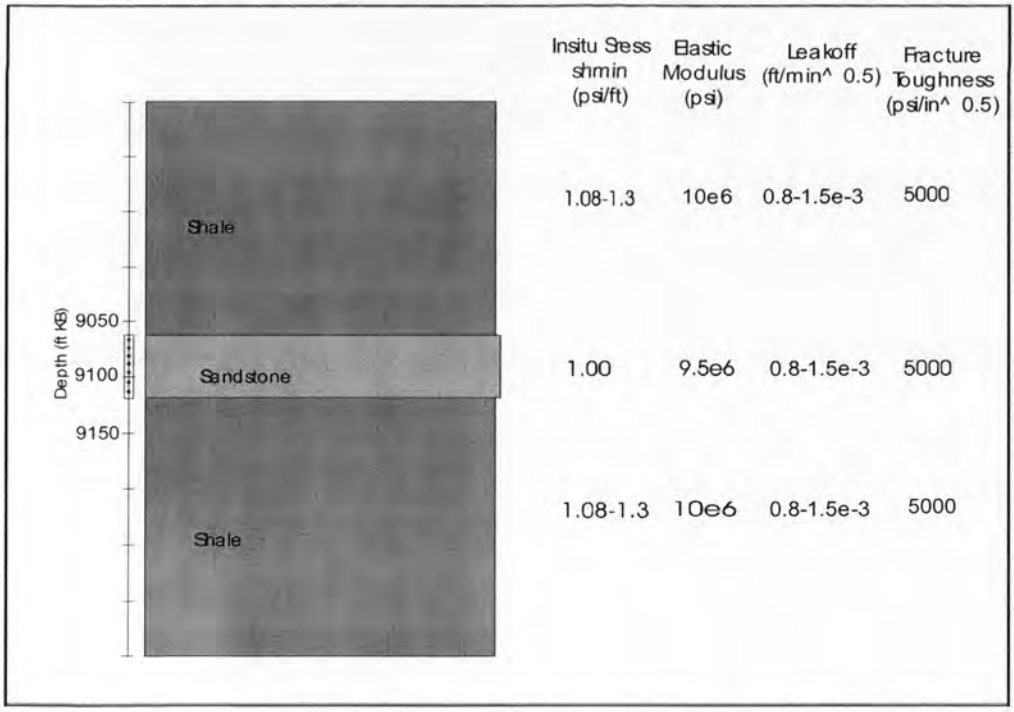

Figure 6.2. Simplified layer model adopted by the fracture hindsight analysis.

6.3.1. Highly confined vertical fracture

Studies on typical temperature log suggested that the hydraulic fracture formed was vertical, which is a likely orientation in normal or strike-slip stress regime. The study of fracture initiation and propagation (Hossain *et al.*, 2000) indicates that the initiation of a vertical fracture from a vertical well under a reverse faulting stress regime is also more likely, although the fracture may then turn to be horizontal at a distance from the well. A single vertical fracture is therefore a potential scenario if it matches with the observed treatment pressure response.

Good agreement between typically observed and model-predicted bottom-hole treating pressure was achieved by assuming that the sands and bounding shales possessed the minimum horizontal stress gradients of 1.0 psi/ft and 1.3 psi/ft respectively. Figure 6.3 compares the simulated and measured treatment pressures. The simulated bottom-hole treating pressures are comparable with those observed in the field. However, the simulated treating pressures display an increasing bottom-hole treating pressure with fracture propagation which is characteristic of highly confined hydraulic fractures. This contrasts with the relatively flat, even slightly declining observed treating pressure.

Such high stress conditions in the layers bounding the target sand are not expected. Previous studies in the region showed no evidence of significant fracture confinement and interpretation of logs suggested that interbedded coals, sandstones and siltstones overlie the target sand by approximately 100 ft (30.5 m). Such lithologies are not expected to attract significantly higher in-situ horizontal stresses than the target sand. The single highly confined fracture case also offers no explanations for the high near-wellbore friction pressure drops observed during all the injection tests performed. Therefore, the results displayed in Figure 6.3 do not necessarily support the existence of highly confined vertical fractures.

6.3.2. Vertical multiple fractures

Acknowledgement of the potential for the generation of multiple hydraulic fractures in the target sand was apparent in the use of a minimum number of perforations during completion of the well. Multiple fracturing may explain the higher than expected observed net pressures. Analysis of treatment strongly suggested that the target sand was susceptible to the initiation of multiple fractures.

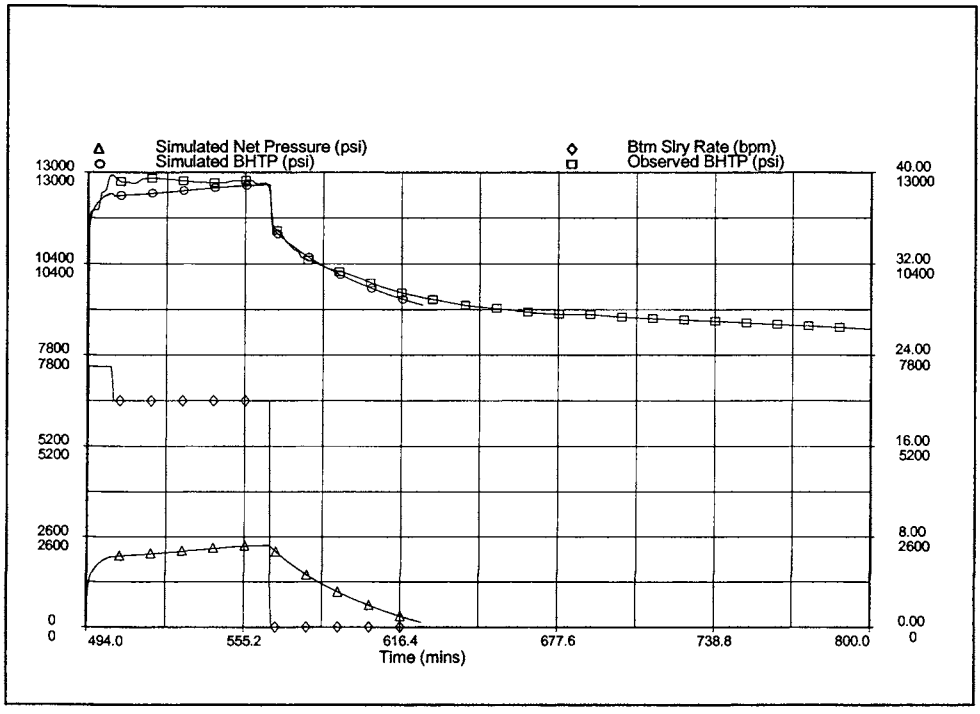

Figure 6.3. Comparison between modeled and typical bottom-hole treating and net pressures. Modeled results assume the presence of single vertical fracture.

Figure 6.4 compares the typically observed bottom-hole treating pressure with a FRACPRO model simulation which assumed the presence of four closely-spaced and identically shaped multiple hydraulic fractures. In order to match the observed shut-in pressure decline data, a leak-off coefficient of 5e-4 ft/min$^{0.5}$ was assigned to all layers. Other reservoir parameters are as described in Figure 6.2. This leak-off is lower than that estimated by the history match, and corresponds to a formation permeability of

approximately 0.002 mD. The permeability of the target sand was estimated to be 0.06 mD. Figure 6.4 displays a reasonable match between the observed and modeled bottom-hole treating pressures. The slight declining modeled fracture treatment pressure, in contrast with the flatter pressure observed in the field, suggests that slightly more fracture confinement is present in the field than is acknowledged in the model.

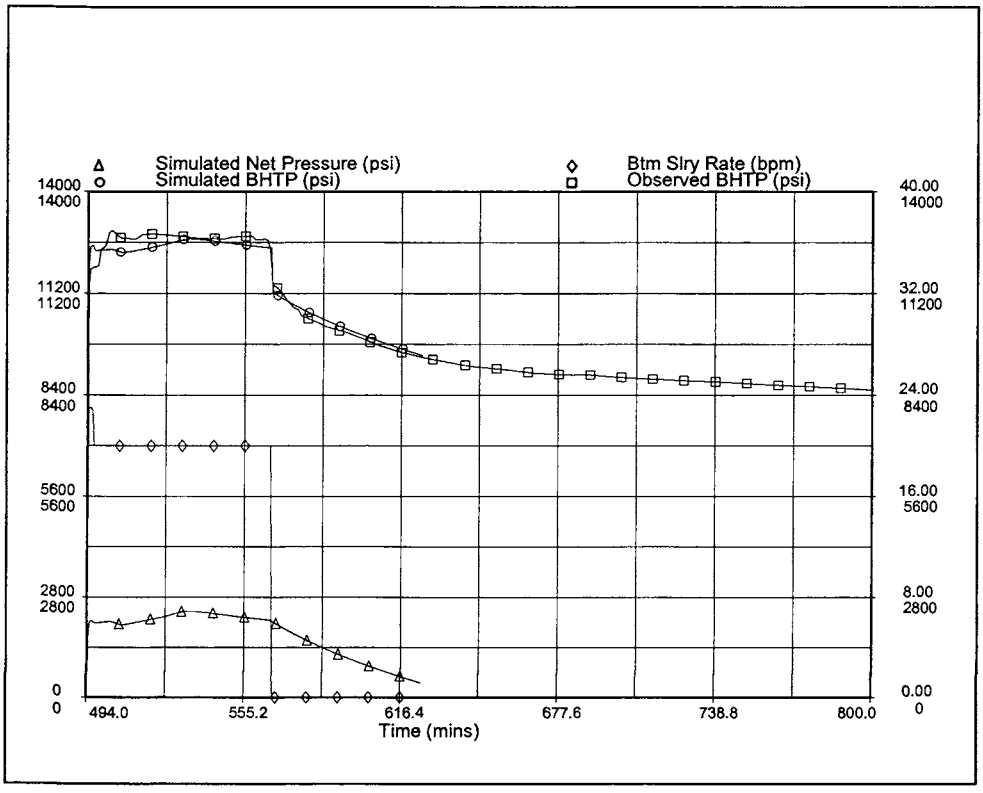

Figure 6.4. Comparison between modeled and typical bottom-hole treating and net pressures. Modeled results assume the presence of four vertical multiple fractures.

6.3.3. Multiple horizontal fractures

Due to the prevailing stress regime in which the minimum in-situ stress acts in the vertical direction, it is logical to explore the possibility of direct horizontal fracturing as well. As mentioned earlier, temperature log data suggests vertical fracture, though this does not provide reliable information regarding the geometry of the far field fracture

(Cleary *et al.*, 1991). It is generally accepted that due to the nature of near-wellbore stress concentrations, hydraulic fractures initiate and propagate initially along the wellbore, regardless of the in-situ stresses or wellbore orientation (McLennon *et al*, 1989). Therefore, where the far-field preferred fracture plane intersects the wellbore at a large angle, as is the case here due to reverse faulting stress regime, convoluted flow paths are expected to connect the far-field horizontal fracture with the vertical fracture at the wellbore.

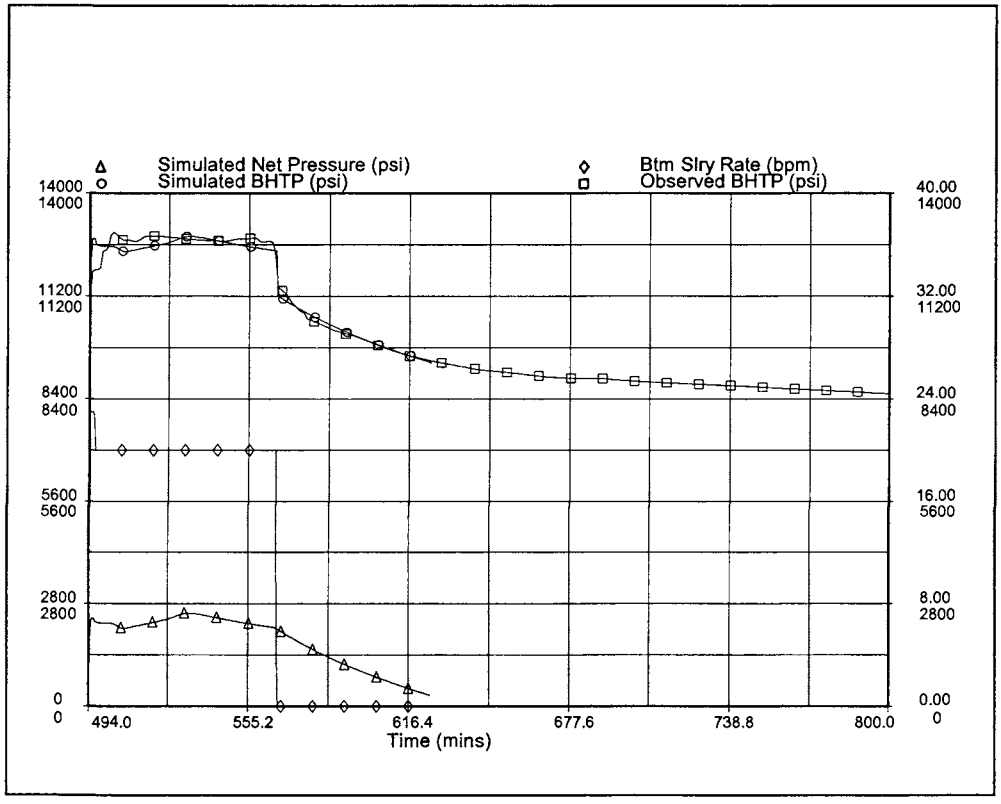

Figure 6.5. Comparison between modeled and typical bottom-hole treating and net pressures. Modeled results assume the presence of five horizontal multiple fractures.

Figure 6.5 compares the typically observed bottom-hole treating pressures with those derived through the simulation of the propagation of five closely spaced horizontal hydraulic fractures of identical shape. The simulation of these five hydraulic fractures

achieves the required high net pressures observed in the field, and displays a decreasing pressure trend which is characteristic of radially propagating fractures. To achieve the good match with field-measured shut-in pressure decline data, a much lower leak-off coefficient (1.5e-4 ft/min$^{0.5}$) was required. This translates to a reservoir permeability of 0.0002 mD, which is unacceptably low. This lower than anticipated leak-off rate may be a result of the highly idealised nature of the simulated horizontal fractures. As mentioned above, it is highly unlikely that horizontal fractures intersect the wellbore in an orthogonal fashion as is assumed in FRACPRO simulation. Rather, the convoluted geometry may take the form of 'twisting' or 'H-shaped' fractures and may explain the high near-wellbore friction (~1300 psi) consistently observed during the injection tests. The simplistic FRACPRO model exaggerates the 'collective' leak-off from the closely-spaced multiple fractures, which leads to the requirement of excessively low leak-off coefficients for history matching as illustrated in Figure 6.5. This exaggerated leak-off was also present in the multiple vertical fracture history match (Figure 6.4) though to a lesser degree.

6.4. Three-D numerical modeling of fracture development

As mentioned earlier, FRACPRO is not capable of simulating convoluted fractures which initiate vertically at the wellbore wall and then turn to be horizontal at the far-field under the influence of reverse faulting stress regime. A boundary element code, HYFRANC-3D (main features are briefly described in Appendix D) was therefore used to simulate 3D fracture and to study the influence of the in-situ stress regime prevailing in the target sand on fracture development. This study aimed to establish whether the existence of far-field horizontal fractures was physically possible (if so, to establish their consequences) while the fractures initiate vertically at the wellbore wall. This analysis was performed for the extreme reverse faulting and moderate reverse faulting stress regimes described earlier.

6.4.1. Model description and results

A half wellbore of diameter 8.5" was modeled within a block measuring 200"x200"x100" as shown in Figure 6.6. A penny-shaped 3D vertical crack of radius 2" was initiated. This fracture was centred at the midpoint of wellbore wall. The fracture surface was initially oriented normal to the minimum horizontal stress direction. The hydraulic fractures of both in-situ stress scenarios were propagated a distance of 22" from the wellbore using a constant injection rate of 10 in^3/sec. This is the fraction of the total injection rate (23 bbl/min) accepted by each perforation during the minifrac test, assuming that the flow is equally divided between perforations.

It was evident that the fracture propagated in the *moderate reverse faulting* stress regime did not undergo any noticeable re-orientation (Figure 6.7). For the *extreme reverse faulting* stress regime, a noticeable fracture deviation was observed during the propagation (Figure 6.8). The fracture re-orientation in case of extreme reverse faulting stress clearly suggests that the fracture will eventually turn to be horizontal at far from the wellbore wall under the influence of far field reverse faulting stress condition. However, even the sophisticated modeling capabilities of HYFRANC-3D is unable to describe the final complex geometry of twisting hydraulic fractures due to extremely long computational time required by the software.

Injection pressure profiles for both in-situ stress scenarios are illustrated in Figure 6.9. Although fracture pressures were compared for a very short injection period, they clearly show that the extreme reverse faulting stress regime develops higher fracture pressures for the same injection period compared to the moderate reverse faulting. Further, the crack opening in the extreme reverse faulting stress condition is lower than that in the moderate reverse faulting stress condition as shown in Figure 6.10. This suggests that higher injection periods as well as higher fluid pressures are required to produce the same fracture volume and fracture width for the extreme reverse faulting stress condition than that for the moderate reverse faulting stress condition.

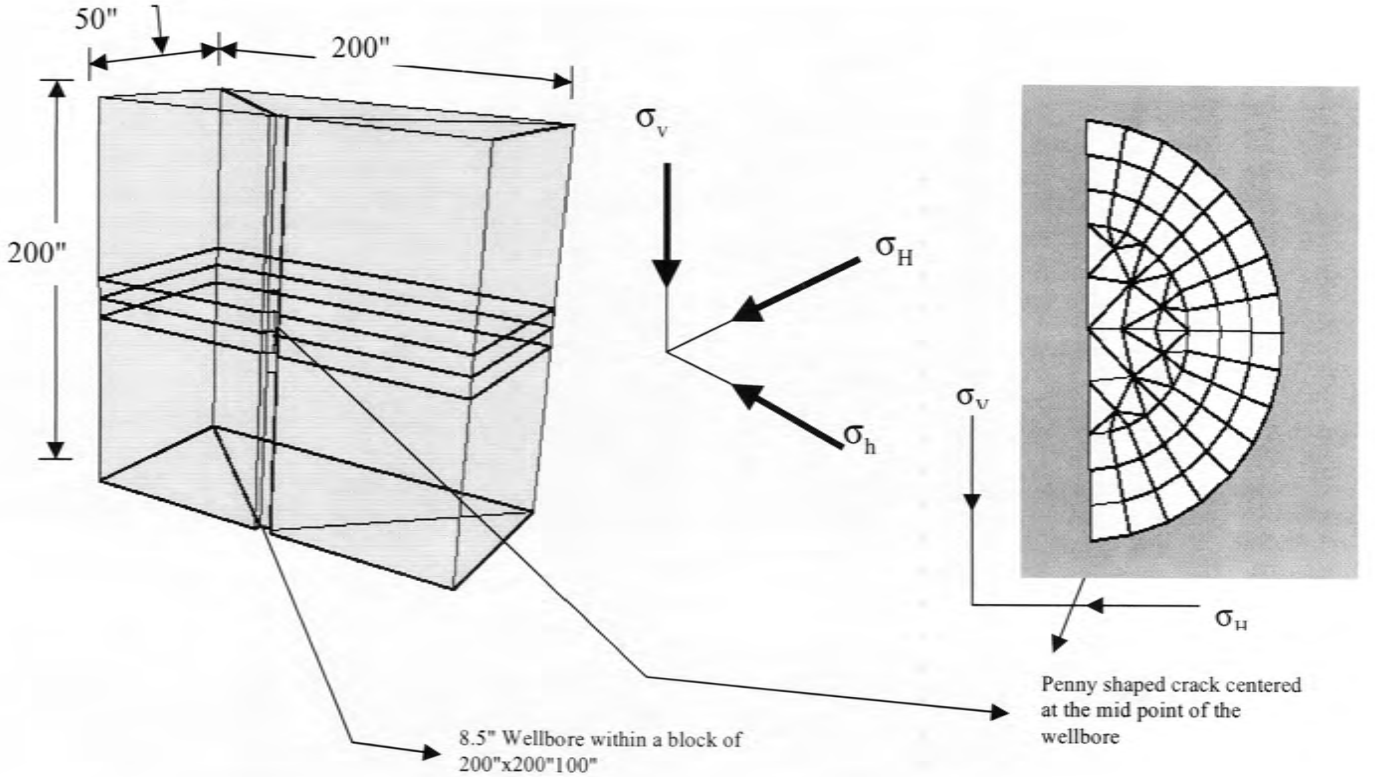

Figure 6.6. Details of half wellbore model

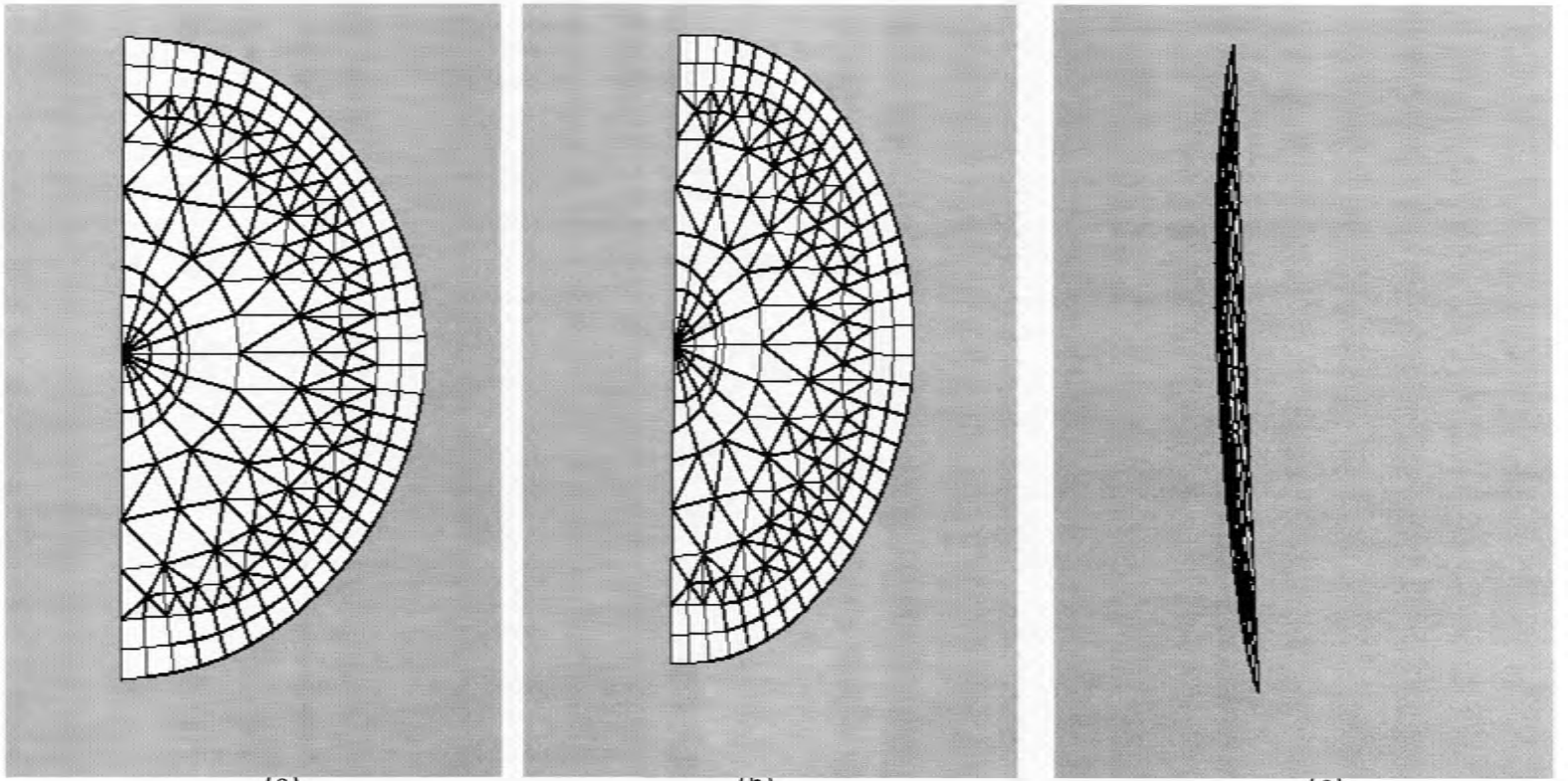

Figure 6.7. For the moderate reverse fault regime (σ_H = 9810 psi, σ_h = 9110 psi and σ_v = 9090 psi), (a) view normal to minimum horizontal stress direction (i.e, normal to crack surface), (b) view 30° to the maximum horizontal stress direction, and (c) view along the maximum horizontal stress direction (normal to crack tip).

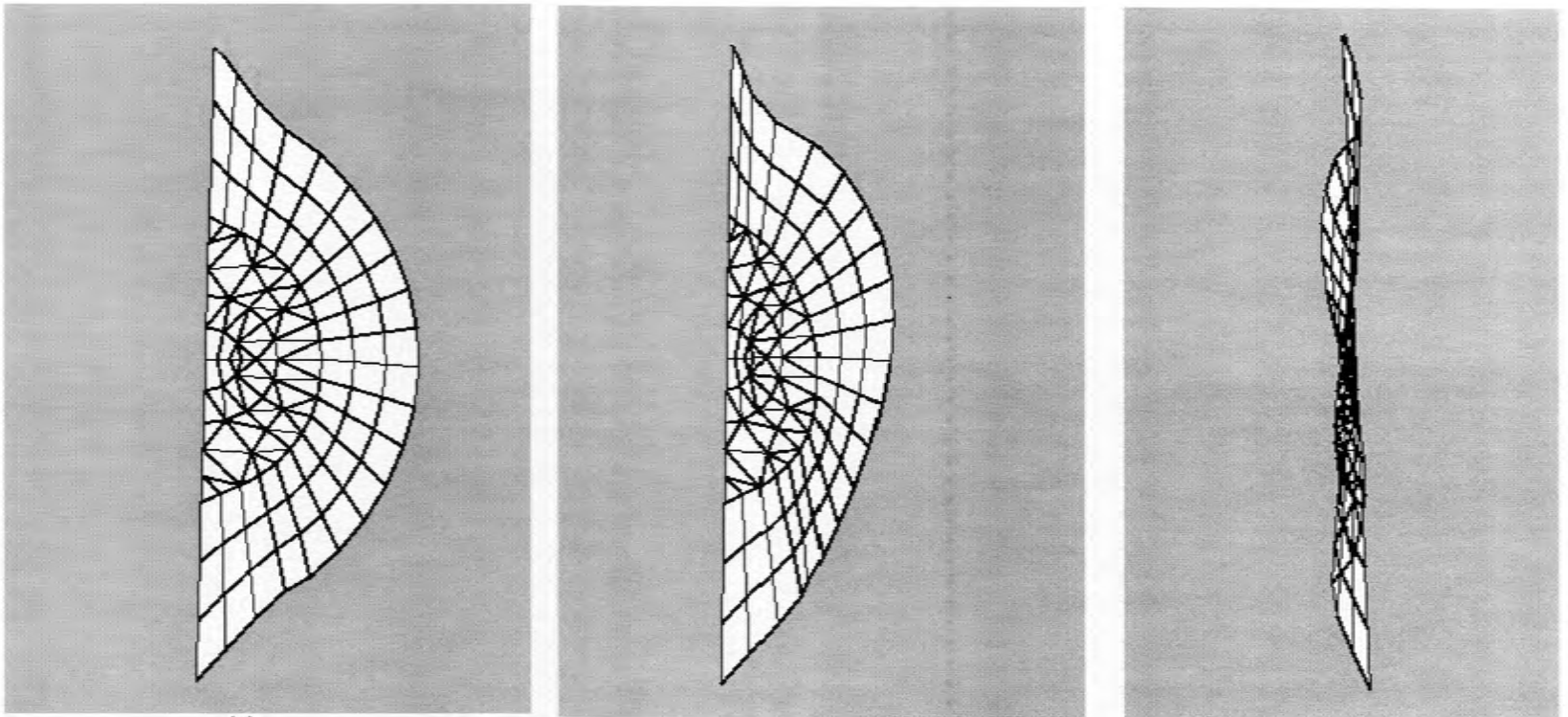

(a) (b) (c)

Figure 6.8. For the extreme reverse fault regime (σ_H = 12820 psi, σ_h = 10100 psi and σ_v = 9090 psi), (a) view normal to minimum horizontal stress direction (i.e, normal to crack surface), (b) view 30^o to the maximum horizontal stress direction, and (c) view along the maximum horizontal stress direction (normal to crack tip).

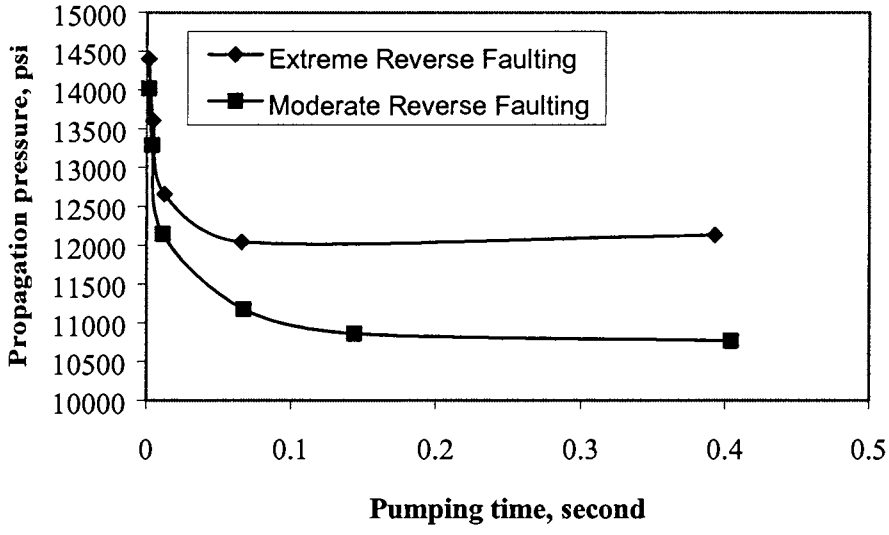

Figure 6.9. Comparison of fracture propagation pressures for the two in-situ stress scenarios.

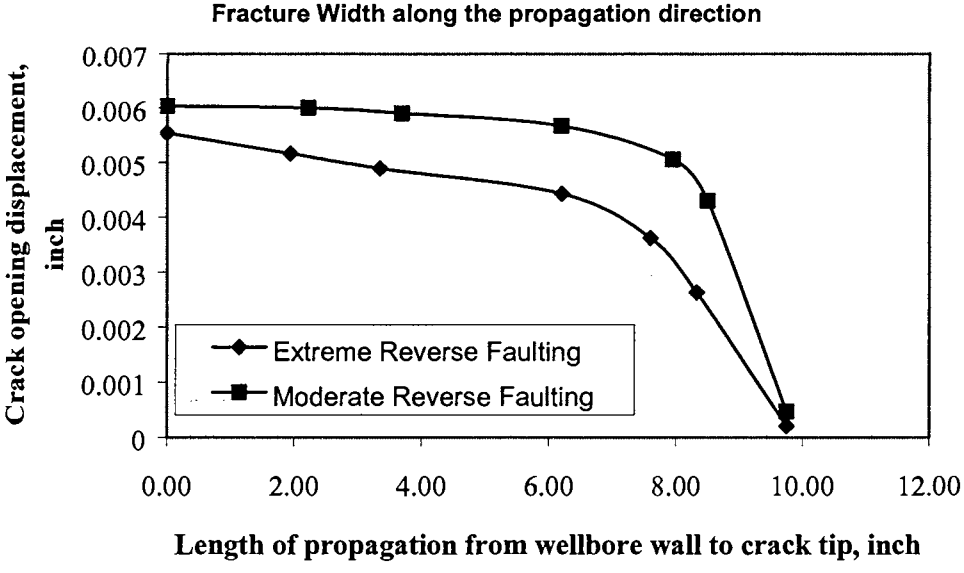

Figure 6.10. Comparison of crack opening displacement (crack width) for the two in-situ stress scenarios.

Hossain *et al.* (2001) recently studied the consequences of convoluting propagation of hydraulic fractures, which initiate in the non-preferred direction due to off-phase perforation and/or the presence of natural fractures, and multiple parallel fractures. It was found that these fractures turn, twist and diverge from each other during propagation and result in high treatment pressures and reduced fracture volume, which may eventually lead to treatment failure by premature screen-out.

6.5. Assessment of a fracturing treatment designed by FRACPRO

As it is mentioned, during the development of the author's proposed model for hydraulic fracturing design, that a proposed treatment must satisfy some constraints to theoretically ensure that secondary multiple fractures are not initiated and the formation is not damaged. In most commercial tools like FRACPRO, such requirements are not formulated explicitly and thus a design from such a tool becomes unconstrained. Onus is then on the designer to ensure that any design, which does not satisfy such requirements is not taken for execution in the field. Because such a design itself may be the primary source of hydraulic fracturing complexities studied in this chapter. It will be demonstrated first that it is often possible to end up with such a design and that how such a design can be modified to satisfy those requirements. Finally, the proposed model for the purpose of comparison will achieve an alternative design.

6.5.1. Hydraulic fracture treatment optimisation by FRACPRO

FRACPRO, developed and marketed by Resources Engineering Systems Inc., USA, is a commercial package for hydraulic treatment design, simulation and optimisation. It's fracture design mode allows engineers to generate an approximate treatment schedule, called "unit treatment schedule", required to achieve a reference propped length and average proppant concentration (lb/ft^2) for given fracture fluids, reservoir properties and pumping rates. In the fracture optimisation mode, the unit treatment schedule is scaled

over a range of treatment sizes (factors) of interest defined by a minimum, a maximum and a number of intermediate factors, each representing a treatment size. All stage volumes (injection rate, volume injected and proppant concentration) of the unit treatment schedule are multiplied by the numerical factor to obtain the corresponding treatment size. The adjusted stage volumes are then used to simulate the fracture treatment to obtain various treatment parameters, such as proppant scheduling, fracture geometry parameters, cumulative production, treatment cost, etc. The objective function value, NPV is then plotted against the treatment factors (see Figure 6.12) to find out the treatment that gives a maximum value of NPV. There is no option to use any design constraint in this process. Together with reservoir and economic data, two production constraints are entered: (1) the maximum production rate during the production life and (2) the minimum bottomhole flowing pressure. For more understanding of fracture treatment design, simulation and optimisation by FRACPRO, the readers are referred to FRACPRO user's Manuals.

6.5.2. FRACPRO optimised treatment for the reservoir

The reservoir was assumed to be square with 640 acres of drainage and 60 ft of net pay zone height, bounded above and below by shale stressed with about 1.3 psi/ft. From stress analysis of pay zone and bounding layer, the maximum net fracture pressure was estimated to be 1680 psi (for extreme reverse faulting). Fracturing fluid HL_HYB_H50_2 and proppant Carbo-Lt 20/40 were chosen, and their built-in properties in the package were used. Other reservoir properties and well data are presented in Table 6.2. Fracture mechanics data required for analyses are presented in Table 6.3, which also contains some operational data. Proppant selection data are presented in Table 6.4 and economics data are presented in Table 6.5.

Table 6.2. Reservoir and well data for a well onshore Australia

Drainage area	640 acres
Average depth	9091 ft
Thickness	60 ft
Shape (square)	5,280 x 5,280 ft^2
Equivalent drainage radius	2980 ft
Porosity	8%
Permeability	0.06 md
Initial reservoir pressure	4,478 psi
Reservoir temperature	321° F
Gas gravity	0.687
Gas saturation	0.82
Initial gas compressibility factor (Z-factor)	0.99
Initial gas viscosity	0.024 cp
Water compressibility	3.0E-6 psi^{-1}
Pore compressibility	8.6E-6 psi^{-1}
Skin factor	0.0
Max. horizontal stress	See section 6.2
Min. horizontal stress	See section 6.2
Min. horizontal stress (shale)	11,779 psi
Wellbore radius	0.21 ft
Flowing bottomhole pressure	1,000 psi
Tubing inside diameter	3.0 inch
Measured depth to mid-perf	9091 ft

Table 6.3. Fracture mechanics and operational limitation data

Fracture Geometry Model	2D PKN / PKN-C
Closure stress, psi	Min. horizontal stress
Formation critical pressure	11,500 psi
Young's Modulus	9.5E6 psi
Poisson's Ratio	0.20
Leakoff Coefficient	8.0E-4 $ft/min^{0.5}$
Fracture toughness	5,000 $psi/inch^{0.5}$
Spurt Loss Coefficient	0.0
Burst strength of the tube	13000 psi
Horse power of the pump	12000 hp
Pump efficiency	85%
Rated pressure of surface equipment	14000 psi

Table 6.4. Proppant selection data

Proppant type	Carbo-Lt2040
Specific gravity	2.71
Bulk density	100 lbm/ft^3
Diameter	0.029 inch
Packed porosity	0.409
Permeability @ closure stress	160910 mD
Conductivity damage factor	0.50

Table 6.5. Economics data

Proppant cost	$1.0 /lb
Fracturing fluid cost (for proposed optimisation model)	varying with viscosity
Fracturing fluid cost (for FRACPRO optimisation)	$1.0 /gallon
Pumping cost for 12000 hhp	$20 /hhp
Fixed cost	$10,000
Gas price	$1.0 /Mscf
Discount rate	0.10
Number of years	10

In order to find a unit treatment schedule, the Fracture Design mode was run for a target fracture length of 700 ft and an average proppant concentration of 1.0 lb/ft^2. Options selected in this mode included 2D PKN fracture model, no convection or settling of proppant, ignoring backstress effects, lithology based reservoir, FRACPRO calculated pad volume percentage and vertical fracture. A convergence criterion for prop length is considered 10%.

There is no in-built option in FRACPRO for fracture height optimisation. Initially, the Fracture Optimisation mode was therefore run for each of fracture heights 60, 75, 85, 90, 95, 100, 105 and 120 ft. From optimisation results, a curve of fracture height versus NPV is plotted in Figure 6.11, which shows an optimum height of 90 ft. The NPV was predicted over 10 years using cost/price data presented in Table 6.5. For fracture height of 90 ft, a reference fracture length of 700 ft and a reference average proppant concentration of 1.0 lb/ft^2, the Fracture Design mode was run to obtain the treatment

summary and the unit treatment schedule presented in Tables 6.6 and 6.7, respectively. The Fracture Optimisation mode was then run from a minimum factor of 1.0 to a maximum factor of 10.0. The NPV values are plotted against treatment factors in Figure 6.12, which shows that the treatment factor 7.0 defines the optimum fracture treatment. Details of the optimum treatment were not directly obtainable at the end of FRACPRO optimisation run, because the package gives the treatment details for the final point only, i.e. for factor 10.0. It was thus necessary to rerun the optimisation mode defining the maximum treatment factor to be 7.0. Design details and the treatment schedule for the optimum treatment (for factor 7.0) are presented in Tables 6.8 and 6.9.

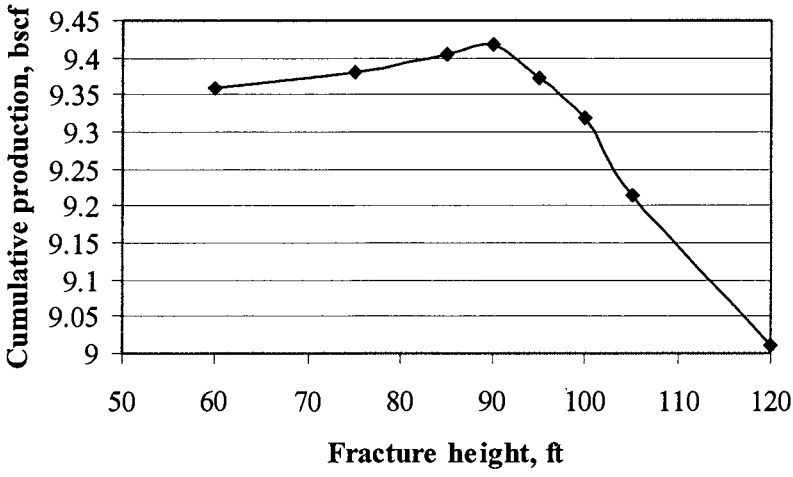

Figure 6.11. Cumulative production at different fracture height while optimising with FRACPRO.

Table 6.6. Results summary from fracture design mode with FRACPRO

Injection time, min	124.2
Fracture efficiency	0.51
Fracture half-length, ft	767.86
Propped half-length, ft	710.66
Fracture height, ft	90
Propped height, ft	90
Max. width at well, in	0.55
Avg. proppant conc. , lb/ft^2	1.14
Dimensionless cond. ratio	773.77
Total fluid, bbls	1090.9
Total sand, klbs	149.36

Table 6.7. Unit treatment schedules from fracture design mode with FRACPRO

Stage #	Time Elapsed (min.)	Pumping Rate (bpm)	Clean Volume (kgal)	Prop. Conc. (ppg)	Pumping (Fluid or Slurry)
1	33.92	10.0	14.247	0.0	Fluid
2	36.03	10.0	0.851	1.0	Slurry
3	41.08	10.0	1.949	2.0	Slurry
4	50.70	10.0	3.566	3.0	Slurry
5	66.02	10.0	5.468	4.0	Slurry
6	88.05	10.0	7.582	5.0	Slurry
7	117.77	10.0	9.861	6.0	Slurry
8	124.20	10.0	2.064	7.0	Slurry

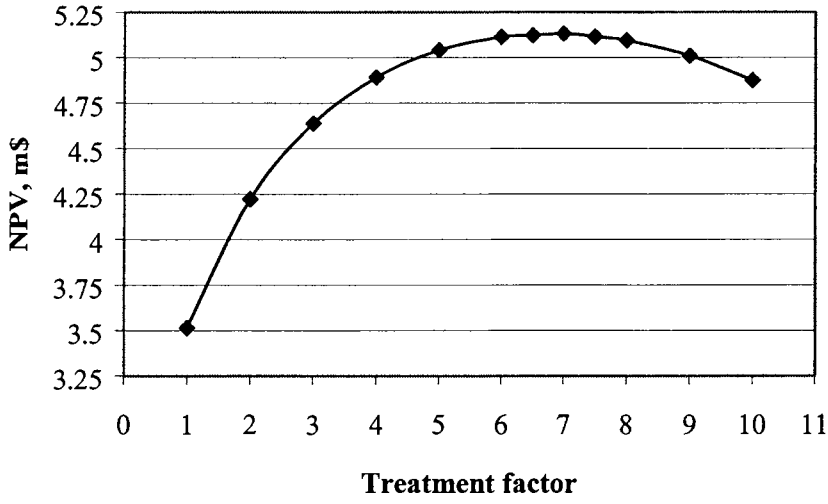

Figure 6.12. NPV at different treatment (optimisation) factors while optimising with FRACPRO.

Table 6.8. Optimum output results from fracture optimisation mode with FRACPRO

Fracture half-length, ft	2275
Fracture width, inch	1.048
Fracture conductivity, md-ft	887.4
Total injection, bbls	8727
Total proppant, klbs	1042
Fixed cost, $	250,000
Variable cost, $ (7.0 x $194,430)	1,361,010
Total treatment cost, $	1,611,010
Cumulative hydrocarbon production in ten years, bscf	9.418
Net present value, m$	5.130

Table 6.9. Optimum treatment schedule from fracture optimisation mode with FRACPRO

Stage #	Time Elapsed (min)	Pumping Rate (bpm)	Clean Volume (kgal)	Prop. Conc. (ppg)	Pumping (Fluid or Slurry)
1	33.92	70.0	99.730	0.0	Fluid
2	36.57	70.0	5.958	7.0	Slurry
3	44.08	70.0	13.640	14.0	Slurry
4	60.45	70.0	24.962	21.0	Slurry
5	89.58	70.0	38.273	28.0	Slurry
6	135.56	70.0	53.075	35.0	Slurry
7	202.62	70.0	69.029	42.0	Slurry
8	218.18	70.0	14.449	49.0	Slurry

6.5.3. Assessment of FRACPRO optimised treatment

From Tables 6.8 and 6.9, the optimum treatment parameters are: injection rate of 70 bbl/min, injection time of 218.2 minutes, EOJ proppant concentration of 49 ppg and the fracturing fluid viscosity of 369.7 cp and fracture half-length is 2275 ft. Using various formulations developed in chapters 3 & 5 with these treatment parameters, fracture parameters and extremely reverse faulting stress regime (see section 6.2), the net fracture pressure was found to be 1650, the frictional loss to be 20378 psi, the surface pressure to be 27261 psi, bottomhole treatment pressure to be 11750 psi and the required pump capacity to be 46752 hp. These immediately reveal that the proposed operational facilities, such as pump, tubing and surface equipment (see Table 6.3) are severely inadequate to execute this treatment and thus FRACPRO design violates constraints 1, 2 & 3 (see constraints in section 5.2.3). Further, bottomhole treatment pressure exceeds the formation critical pressure (11500 psi, available from industry), implicating the uncontrolled fracture growth (violating the constraint 8, see section 5.2.3). In case of moderate reverse faulting stress regime, net fracture pressure and frictional pressure loss were found same, but the surface pressure was found to be 26271 psi, bottomhole treatment pressure to be 10760 psi and the required pump capacity to be 45055 hp, violating constraints 1, 2 & 3. Further, 70% of the net fracture pressure (1155 psi) exceeds significantly the difference between the maximum and the minimum horizontal stresses (700 psi) in the pay zone (violating constraint 10, see section 5.2.3),

implicating the initiation of secondary fractures and large fluid loss. Also, the fluid efficiency of this treatment is about 7.1%, which is obviously very low (violating constraint 7, sec section 5.2.3) found in both cases. In brief, if the designed treatment were executed in the field, it would require high capacity pump and other surface equipment. Given such operational facilities, the treatment would cause formation damage by uncontrolled fracture growth, initiation of multiple fractures and low efficiency; exactly the type of complexities experienced and reported in many occasions of hydraulic treatment in the field.

The optimum EOJ proppant concentration of 49 ppg based on maximum NPV is almost impossible to achieve in practice, because this can not be pumped. For sand with specific gravity of 2.65, approximately 40 ppg is a 40% porosity sandstone, i.e., the sand grains are in contact and this can not be pumped (Smith, 2001). The typical maximum proppant concentraiton is 10-12 ppg, though higher concentrations (up to 20 ppg) may be pumped with very special planning (Smith, 2001). Injection rate of 70 bbl/min is also very high as experienced by Chipperfield (2000). This high injection rate with high EOJ proppant concentration causes high frictional loss, requiring high capacity pump. In such a case, the designer using the FRACPRO might run the optimisation module with a lower treatment factor (lower optimisation parameter), for which the EOJ proppant concentration would be pumpable. This can only be done by trial and error and with the aid of an external scheme to check various design requirements discussed. Thus, it is appropriate to emphasize here that if the designer designs the fracturing treatment using an unconstrained software such as FRACPRO (where there is no room for specific constraints to avoid complexities, as considered by the proposed model), the treatment itself may be a source of complexities in the field.

Five optimum parameters obtained by FRACPRO, when entered in a program with 2D PKN-C fracture model and the coupled analytical production model (as described in chapters 3 and 4 respectively), create the conductivity of 500.2 mD-ft, based on the model described in chapter 3. FRACPRO calculated conductivity is 887.4 mD-ft, using the same conductivity damage factor and proppant data. The coupled analytical model finds the cumulative production for ten years as 8.20502 bscf. This suggests that the

conductivity calculated by the proposed model as well as the reservoir fluid flow model integrated in the proposed optimisation scheme are more conservative than those in the FRACPRO.

It was further studied to adjust the FRACRO design using the proposed model to avoid treatment complexities. FRACPRO optimisation was run with various values of maximum optimisation treatment factor lower than 7.0. It was found that for a lower treatment factor of 2.0 the treatment has an injection rate of 20 bbl/min, injection time of 139.9 minutes, EOJ proppant concentration of 14 ppg. The corresponding fracture length is 1163 ft and the fracturing fluid is always 369.7 cp. This design meets all the constraints except the requirement of 40% fluid efficiency, which has been only 13.4% (based on proposed model) in case of extremely reverse faulting stress regime (but the design violates constraint 10 marginally in case of moderate reverse faulting stress regime). Although this treatment does not cause any of the treatment complexities, it would yield a lower production (6.974 bscf with NPV of $4.22m from FRACPRO and 5.888 bscf with NPV of $3.3835m from the proposed model).

6.6. Optimum treatment design by the proposed model

The proposed optimisation model was run to conduct hydraulic fracture treatment optimisation for this reservoir with extremely reverse faulting stress regime only. All design constraints including fracture growth control requirements, as described in chapter 5, were also considered. Two optimum designs were obtained: one with five free design variables as was done in chapter 5, and the other with four free design variables fixing the viscosity value to 369.7 cp, obtained from FRACPRO design. In the second case, it is assumed that the fracturing fluid will not be adjusted by treatment to use its optimum viscosity value, rather, the standard fluid HL_HYB_H50_2 will be used. Fracture height is allowed to grow into the bounding layers by not more than 50% of the pay zone height, which is kept consistent with the findings (optimum fracture height of 90 ft) from FRACPRO optimisation (section 6.5.2). The results from both runs are presented and discussed in the following section.

6.6.1. Presentation of results from the proposed optimisation model

Table 6.10 shows the results from optimisation with five variables and four variables. Both designs are optimised based on NPV maximisation. The optimum parameters like injection rate and injection time are reasonably comparable between the two designs. The design with 5 variables shows higher EOJ proppant concentration, higher fluid viscosity but a shorter fracture half-length. These give a higher fracture conductivity and, in turn, a higher cumulative production. Both designs could not reach the upper bound of fracture height (1.5 times the pay zone height, i.e. 90 ft), which is perhaps because of extremely reverse faulting stress regime, however, the design with five variables achieved 82.8 ft and the other design achieved 75 ft. It is obvious that the second design's fracture height (75 ft) is lower because of fixed fluid viscosity (369.7 cp). The fracturing fluid efficiency is found to be at the lower bound (40%) for both designs, perhaps because the leak-off coefficient is higher in this reservoir. Thus, this constraint is always active at the lower bound and has no direct effect on the amount of proppant/in-situ proppant concentration, rather the EOJ proppant concentration has effect on it. It has been observed that constraints relating to the burst strength of the tubing (constraint 2) and uncontrolled fracture growth (constraint 8) are severely active in both cases. These indicate both the optimum designs have been constrained to avoid excessive fracture growth (which is uneconomic and may damage the formation) and to keep the surface pressure within the capacity of proposed facilities. EOJ proppant concentration is lower for the fixed viscosity design then the viscosity variable design as can be seen in the Table 6.10, which gives lower conductivity and ultimtaley lower production return.

Table 6.10. Optimum treatment parameters and other values from the proposed optimisation model

Design parameters/other optimum values	**Proposed model (5 variables)**	**Proposed model (4 variables and fixed viscosity)**
Injection rate, bbl/min	25.8	27.5
Injection time, minute	38.6	31.4
EOJ proppant conc., ppg	13.3	10.3
Fracturing fluid viscosity, cp	523.7	369.7
Fracture half-length, ft	1168.5	1245.4
Fracture height, ft	82.8	75.0
Average fracture width, inch	0.1766	0.1592
Fracture conductivity, md-ft	427.4	312.0
Fracture efficiency, %	40.0	40.0
Total injections, cu.ft (bbl)	5591.2 (995.8)	4839.4 (861.9)
Total proppant injected, klb	102.755	72.059
Treatment cost, m$	0.3973254	0.3564476
Cumulative gas production, bscf	6.50370	6.42586
NPV, m$	3.811125	3.80065

The optimum viscosity from optimisation with five variables is 523.7 cp. It has been observed from chapter 5 (section 5.3.6), where effect of fracturing fluid viscosity on NPV was conducted, that any viscosity value other than its optimum value deteriorates the production/NPV. Thus, the fixed value of viscosity of 369.7 cp, while optimising the remaining four variables, has sensibly generated a lower production/NPV. In principle, the fluid viscosity can be modeled as a variable so that the optimisation model finds the optimum value of viscosity with an assumption that this viscosity will be achieved by a necessary treatment of fracturing fluid. In practice, however, the operator may use a standard fluid with certain viscosity. In this situation, it is better to optimise the other four free variables fixing the viscosity and this will improve the design and objective function of cumulative production/NPV. But such a design will not be as optimum as obtained by the optimisation with five variables. Thus, the noble idea of variability of fluid viscosity in the optimisation model will further improve the treatment design with the best combination of all treatment parameters for maximum possible cumulative production/NPV. In both cases, the model satisfies all constraints to alleviate fracturing

complexities, which may arise due to unconstrained optimisation by commercial software.

6.7. Water-frac as an alternative stimulation technique

The conventional hydraulic fracturing technique considered so far is assumed to create two wings of a massive planar fracture at the wellbore. This technique has been attempted in many occasions to stimulate naturally fractured reservoirs but ended up without much success. When a conventionally induced hydraulic fracture intersects natural fractures on both sides of the wellbore, the fracture is initially arrested, but with continued pumping, it either crosses the natural fractures or open them, diverting fluid into the natural fractures (Blanton, 1986). This results in high treatment pressure, accelerated fluid leak-off, extremely complex fracture geometry and inefficient proppant transport (Warpinski and Teufel, 1987). The productivity improvement by conventional hydraulic fracture treatments of these reservoirs is also found very low (Branagan *et al.*, 1987). Recently, Warpinski (1991) revisited the issue and indicated that the conventional fracturing in naturally fractured reservoirs may also result in early screenouts and significantly reduced fracture lengths. Warpinski (1991) thus rightly recommended the investigation of the use of alternative stimulation strategies. Most of these symptoms were observed in the field in question and various logs indicated the presence of natural fractures. Therefore, an alternative stimulation strategy was pursued for this field.

In recent years, there has been a growing interest in proppant free stimulation, recognized as water-frac stimulation applied mainly to Hot Dry Rock (HDR) geothermal reservoirs. This has been an essential technology for HDR reservoir development with a recent trend to apply to tight gas and petroleum reservoirs. The hydraulic stimulation designed by this technology was carried out in the Austin Chalk formation of the Gidding Field (Meehan, 1992). Since 1986 water fracs have been carried out in this field on both vertical and horizontal oil and gas wells. The successful water fracs have also been realised in the High Island 384 field and the East Texas Cotton Valley sand

(Claiborne Jr. *et al.* 1996; Mayerhofer *et al.* 1997), though theoretical basis for water fracs, compared to conventional hydraulic fracturing, is still not well understood in the petroleum industry.

The concept of this emerging technology is based on the theory of shear dilation involving predominantly mode II (sliding or shear fracturing) of fracture mechanics, which is mainly active in naturally fractured tight reservoirs. The natural fractures are stimulated to slip by shear and then to dilate under appropriate fluid pressure. The surfaces of fractures then resist each other to regain it original matted alignment and thus leave a flow conduit for hydrocarbon. The fractures slip when the shear stress acting parallel to the fracture plane exceeds its frictional resistance which is a function of the effective normal stress across the same plane. The injected fluid reduces the effective normal stress, in turn the resistance, and thus induce the slip and dilation process. High shear stress due to in-situ stresses in hard rock containing rough natural fractures is favourable for this process.

A preliminary three-dimensional model was developed by Willis-Richards *et al.* (1996) to simulate stochastically natural fractures in the reservoir and then to analyse permeability enhancement due to shear dilation as a function of injected fluid pressure. In the stochastic approach of natural fracture simulation, fracture centres are randomly distributed and fracture radii follow fractal distribution (Willis-Richards *et al.*, 1996). Similarly, other attributes of fractures such as attitude (dip and dip-azimuth) and density, are also described by probability functions. The Mohr-Coulomb criterion was used to assess the fracture slippage assuming that none of the fractures would propagate under the applied fluid pressure. Hossain (2001) found that some of the fractures are likely to propagate before, or simultaneously with, shear slippage. The fracture propagation was thus incorporated according to a computationally efficient approximate method (Rahman *et al.*, 2000). The modified model (Hossain, 2001, Hossain *et al.*, 2002) is briefly presented in Appendix E. In simulating naturally fractured reservoirs by this program, up to 20 stimulation wells can be used and grid resolution in excess of 100x100x100 elements is possible to obtain on a suitable specified personal computer. More details of this model can be found in the thesis by Hossain (2001).

6.7.1. Application of the modified shear-dilation stimulation model

As mentioned earlier, it is believed that there could be co-existence of three in-situ stress regimes in the field. In this study, the extreme reverse faulting regime, with high deviatoric stress, was considered to be favourable for waterfrac stimulation. The mean orientation of the minimum horizontal in-situ stress was estimated to be 04° (maximum horizontal stress direction being 96°) in the field. A statistically representative sample of natural fractures was obtained from the FMS logs, and fracture dip, azimuth and the fractal dimension were analysed. Using these data, a geometric model was constructed to represent a cubic reservoir of 3281 ft x 3281 ft x 3281 ft. A stimulation well was placed at the centre of the reservoir. Statistical data of natural fractures characterised in the region are listed in Table 6.11. Rock mechanical properties are given in Table 6.2. The model is applied to investigate the pressure-permeability response of the reservoir.

Table 6.11. Statistical data of natural fractures used for simulation

Fracture Sets	Dip	Azimuth
Set No.1	18	345
Set No.2	28	136
Set No.3	45	158
Fracture density, ft^2/ft^3	0.1524 (0.5 m^2/m^3)	
Fractal dimension	2.1	
Basic friction angle (deg)	40	
Shear dilation angle (deg)	4	

Figure 6.13 illustrates the effect of stimulation fluid pressure on permeability enhancement of the stimulated reservoir. It can be seen that for the given stress condition, there exists a threshold pressure (5220 psi / 36 MPa) which must be reached in order to initiate shear dilation and permeability enhancement. Above the threshold pressure (5220 psi / 36 MPa), the permeability increases sharply up to about 300 times the initial value (0.06 mD).

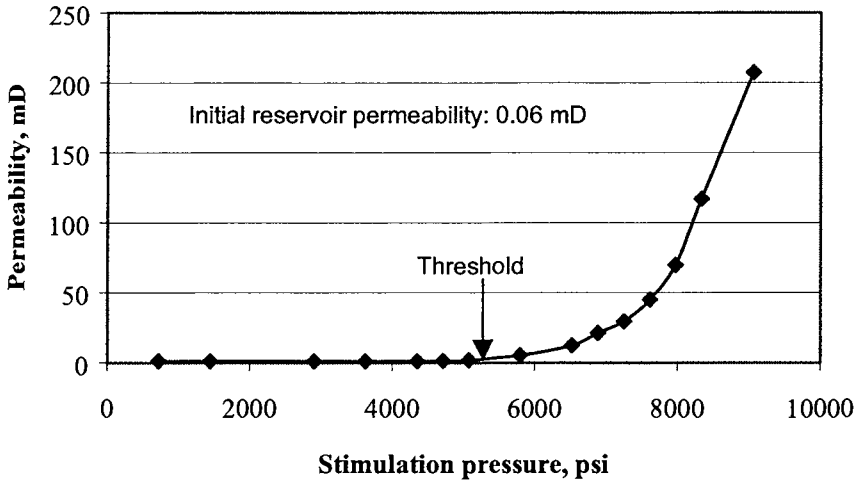

Figure 6.13. Effect of injection fluid pressure on the permeability of a reservoir subject to an extreme reverse faulting in-situ stress regime.

It is evident from Figure 6.3 that the observed bottom hole treating pressure (OBHTP) of hydraulic fracturing tests in the field was about 12750 psi (88 MPa). By the application of water-frac model, it is found that the bottom hole pressure required to initiate shear dilation is about 9220 psi (63.6 MPa) (4000 psi hydrostatic fluid pressure plus 5220 psi threshold pressure). To raise the permeability to 18 mD, 300 times the initial value (0.06 mD), the bottomhole pressure required is 10760 psi (74 MPa) (4000 psi plus 6760 psi), which is considerably smaller than the observed bottom hole treating pressure (12750 psi) during conventional hydraulic fracturing. This suggests that the water-frac stimulation technology could be a viable solution to alleviate the complexity with conventional hydraulic fracturing technology, while applied to naturally tight gas reservoirs in the field. It is, therefore, suggested to carry out further research to lead this technology to a matured state for successful applications in the region.

6.8. Discussion and conclusions

In order to explain anomalous treatment pressures observed during fracturing tests in a number of wells in onshore Australia, various forms of complexities associated with hydraulic fracturing have been recognized in this study. Potential scenarios of such complexities studied are: (1) highly confined vertical fracture due to high stress contrast in bounding layers; (2) multiple vertical fractures; (3) multiple horizontal fractures and (4) convoluted fractures which start vertically at the wellbore wall and then turn to be horizontal at the far-field. In order to analyze these scenarios, the in-situ stress conditions were characterized in the region. Based on analysis of minifrac shut-in pressure declines, two possible in-situ stress regimes were established in the region: moderate reverse fault stress regime and extreme reverse fault stress regime.

Two-dimensional hindsight treatment pressure analyses were performed on minifrac for the first three scenarios. These show that stress gradients of 1.0 psi/ft and 1.3 psi/ft are required for the fractured zone and bounding shales to justify the presence of a highly confined vertical fracture (Scenario 1). However, the relatively flat pattern of observed pressure contradicts the presence of such a highly confined vertical fracture. The contradiction is also supported by previous experience in the region, log interpretation of lithologies and the nature of observed near-wellbore frictional pressure drops. Thus, this scenario has been dismissed in this study as an unrealistic complexity.

The treatment pressure analysis supported convincingly the presence of multiple fractures and explains the high net treating pressures and near-wellbore friction observed during fracturing tests. Four closely-spaced and identically shaped multiple vertical fractures were simulated (Scenario 2) only to demonstrate the possibility of multiple vertical fractures. By similar simulation, it was also established that the possibility of multiple horizontal fractures can not be discounted, at least at the far field (Scenario 3).

More sophisticated three-dimensional numerical analysis was undertaken to establish the effects of fractures which initiate vertically at the wellbore wall and then become

horizontal at the far field through complex turning and twisting (Scenario 4). The numerical study demonstrated that under a moderate reverse fault stress regime, hydraulic fractures propagate vertically away from the wellbore, whereas under the extreme reverse fault stress regime, hydraulic fractures re-orient during propagation to turn horizontally away from the wellbore wall. Such re-orientation causes a convolute fracture shape resulting in costly high treating pressure and reduced fracture volume. Thus, the pressure behaviour obtained from the numerical study and observed during fracturing tests indicates the possibility that such convolute fractures are formed under an extreme reverse fault stress regime.

It has been recognised so far that hydraulic fracturing complexities are experienced during execution in the field. These complexities are developed due to high deviatoric stress, multiple fractures, natural fractures, orientation of perforation, wellbore trajectory and also inappropriate treatment design. It has been observed that if the treatment design procedure is not constrained to alleviate complexities like high treating pressure, initiation of multiple fractures and excessive fluid loss, uncontrolled fracture growth in the bounding layers and to be compatible with the available equipment, then this inappropriate design will develop complexities. Some of these complexities have been experienced by the design with commercial software FRACPRO, which is of unconstrained nature (see section 6.5.3) and this design may not be executable in the field successfully because of inadequate capacity of equipment. The proposed treatment design model with various realistic constraints (as discussed above) and operational requirements is highly likely to be implemented safely in the field without any operational hindrance and complexity (see section 6.6.1). Thus, the productivity predicted by the proposed treatment model is more realistic and conservative than that by FRACPRO.

Despite alternative possibilities analyzed in this study, it is not possible to determine definitely the exact nature of complexity associated with hydraulic fracturing in the region. Moreover, the simulated hydraulic fractures are very idealized. Multiple fracture networks in the field will certainly not possess such idealised geometries. Therefore, definitive recommendations to alleviate complexities are difficult to derive and require

further extensive studies. However, based on the study in this chapter, the following conclusions and recommendations are made:

1. Complexities like high treating pressures, multiple auxiliary/secondary fractures and excessive fluid loss, and uncontrolled fracture growth (also discussed in chapter 5) are critical issues in hydraulic fracturing. These complexities may arise due to a treatment designed using commercial software, such as experienced with FRACPRO (section 6.5.3), because of their unconstrained nature of design procedure. Thus, while designing with such software care must be taken to verify the final design by another computational scheme, and if necessary, the optimisation design obtained from the in-built procedure of software must be adjusted to avoid such design-induced fracture complexities.

2. The proposed optimisation model can find the optimum design, adjusted automatically through satisfying a number of design constraints formulated with an intention to avoid such complexities. Thus, it is highly likely that the above complexities will be alleviated if this optimum design is executed in the field. Moreover, two important ideas are incorporated in this model: the noble idea of optimising fracturing fluid viscosity and formulation of realistic fracture conductivity or estimation of production. Because of variability of viscosity, the model finds the maximum possible value of objective function with an optimum value of viscosity and this objective function value is better than when the viscosity is fixed. The use of optimum fluid viscosity, however, will require the treatment of any standard fracturing fluid to adjust its viscosity. The model incorporates a systematic formulation of in-situ fracture conductivity, which is found conservative compared to that in FRACPRO. Thus, optimum production predicted by the proposed model is less than that predicted by FRACPRO for similar fracture geometry.

3. Reduction in the number of perforations is one of the techniques for mitigation of multiple fracture initiation. Successful multiple fracture mitigation efforts by Stadulis (1995) included the use of large (0.6 inch diameter) zero-phase perforations

shot at 1 shot per foot. Moreover, efforts should be made to perforate on the preferred direction only, i.e. on the direction of the maximum stress orthogonal to the wellbore axis, in order to minimize fracture initiation pressure and to avoid fracture turning (Hossain *et al.*, 2000).

4. The excellent pressure-permeability response by 'water-frac' stimulation of the reservoir suggests that the 'water-frac' technology is another high emerging possibility to mitigate the multiple fracturing complexity avoiding perforations completely. However, it is recognised that further research is required before definitive conclusion about the successful applicability of the technology at its current state.

5. Other than adjusting perforation practices, the use of proppant slug techniques may be another practical solution to problems associated with multiple fracturing. The proper use of proppant slugs are adequately described by Cleary *et al.*, (1993) and Stadulis (1995). Ratios of σ_H/σ_v and σ_H/σ_h for the extremely reverse fault stress regime indicate that aligning the wellbore horizontal along the σ_h direction will also reduce the fracture initiation pressure, to some extent, and eliminate fracture reorientation (Hossain *et al.*, 2000). Therefore, the drilling of horizontal wells in the region should also not be ruled out.

CHAPTER SEVEN

CONCLUSIONS AND RECOMMENDATIONS

7.1. Summary and conclusions

This thesis has mainly concentrated to:

- develop a general-purpose multivariate, multiobjective optimisation model for improved hydraulic fracturing treatment design,
- demonstrate the capabilities and benefits of the proposed optimisation model, and
- demonstrate the potentiality of minimising fracture complexities in the field by designing treatments using the proposed model, whereas treatments designed by some of the commercial software may be one of the possible causes to induce undesirable complexities.

During the development of this optimisation model, the following elements have been investigated systematically and incorporated in the model:

- in-situ reservoir properties,
- fracture geometry models,
- treatment and fracture parameters to be optimised and their practical ranges,
- design constraints to satisfy operational, formation compatibility and mass balance requirements,
- production from fractured reservoir and
- fracture treatment cost.

All these elements with data information are defined systematically and integrated with an optimisation tool which can maximise/minimise a stated design objective function(s) of hydraulic fracturing. Of these elements, design constraints to consider the critical issues of fracture growth control requirements and operational limitations, which are not well defined with commercial software, are mathematically formulated to avoid undesirable complexities in the field during execution. Any treatment designed without these constraints may cause the following complexities while executed in the field:

- uncontrolled fracture growth in bounding layers,
- initiation of multiple secondary fractures and excessive fluid loss,
- high treating pressure, and
- mechanical failure of perforation tunnel and sand production in later production stage.

At least one or more of these complexities affect the effective development of fracture geometry in the pay zone and the over all treatment. Considering all the above mentioned issues within the scope of this study, the thesis has included three major parts:

1 Hydraulic fracture model
2 Analytical production model
3 Proposed optimisation model

Based on the numerical/analytical results from the fracture and production models and the results from the multiobjective optimisation model, while applied to field cases, the major findings are concluded in the following sections.

7.1.1. Hydraulic fracture model

A review of 2D and 3D fracture models has been undertaken in chapter 3 for the selection of appropriate model to be incorporated with the proposed optimisation model. The 2D PKN-C model is selected for this work because of its assumption for height constrained long fractures. The pseudo-3D (P-3D) fracture model is also considered for its simplification of height growth at the wellbore in multi-layered formations. P-3D model is then improved by incorporating the Carter Equation II and is denoted as P-3D-C fracture model. For both selected models, closed-form mathematical equations are solved numerically to conduct parametric study by applying to a typical tight-gas formation. The predictive differences of these two models are compared, and can be summarized as follows:

1. For the same treatment parameters (injection rate, injection time, EOJ proppant concentration and fracturing fluid viscosity) and a given fracture height at the wellbore, the fracture half-length, fracture width, net fracture pressure and fracturing fluid efficiency obtained from P-3D-C model are slightly higher than that from PKN-C model. The propped fracture width, in-situ proppant concentration and fracture conductivity are slightly higher according to PKN-C model up to a certain injection period beyond which the reverse is true.

2. The non-dimensional fracture conductivity, which is directly proportional to the well productivity, is found slightly lower by P-3D-C model, and is significantly reduced with increasing conductivity damage factor. Thus, deciding the value of appropriate damage factor with respect to formation and treatment condition is crucial in hydraulic fracturing design so that the predicted productivity is realistic.

3. In terms of variation in various fracture parameters, very little difference is found between PKN-C and P-3D-C models. Therefore, the 2D PKN-C model is sufficient to design fracture treatments, certainly for three-layer problems and may be for multi-layer problems as well (Rahim and Holditch, 1995). Both models can be

integrated with the proposed model for treatment optimisation, resulting in very little difference in optimum treatment parameters.

7.1.2. Production model

A production model, relating to reservoir fluid flow from a hydraulically fractured reservoir, has been required for production estimation in the proposed optimisation model. Analytical production models (transient and pseudo-steady state flow conditions) for depletion-type fractured reservoir under constant bottomhole flowing pressure have been investigated. Then a hybrid production model has been developed in chapter 4, combining transient and pseudo-steady state flow conditions to simulate flow behaviour in a tight gas formation. The results are compared with those from *IMEX Blackoil Simulator* while the same fracture geometry is simulated. The following conclusions can be drawn from this study:

1. For very low-permeability gas reservoirs, the transient flow period is significantly long. Thus, this flow regime has been considered for the proposed optimisation model. In order to consider this flow regime, a hybridized transient-pseudo-steady state (TPSS) production model is proposed in which the transient and pseudo-steady state flow regimes are coupled based on productivity matching. The production profile predicted by this proposed model is found very close to that simulated by a numerical simulator for reservoir permeability less than 0.5mD.

2. For reservoir permeability equal to and above 0.5mD, the pseudo-steady state (PSS) production model has predicted production profiles, which are close to simulation results.

3. In spite of different behaviours in time-dependent production profiles with varying reservoir permeability, the cumulative production from both TPSS and PSS models over 10 years are found very close, both being slightly higher than simulation results. It indicates that if the interest simply lies in the total production from a reservoir, the PSS model is sufficient to predict with acceptable accuracy.

4. Reservoir pressure declines as a result of production are consistently proportional to cumulative productions from TPSS and PSS models.

7.1.3. Proposed optimisation model

The proposed optimisation model for hydraulic fracture treatment design presented in chapter 5 has accounted for complex interactions among all elements mentioned in section 7.1. It also interacts with multiple design objectives simultaneously and is integrated with 2D PKN-C and P-3D-C fracture models separately. The capabilities and benefits of the proposed model are demonstrated by applying it to some field cases. The following are the conclusions:

1. The model is capable of finding a true optimum design starting with any initial design, which may or may not satisfy all the design constraints, and the optimum design is significantly better than any arbitrary design.

2. An optimum design depends on the specified design objective. A maximum NPV design is almost identical to a maximum production design and both designs involve high treatment costs. By using the multi-objective optimisation technique, it is possible to resolve the conflict between production/NPV maximisation and treatment cost minimisation. It is also possible to obtain an optimum hydraulic fracturing design in order to achieve a production target as long as the target is below the maximum possible production.

3. The model can perform trade-off analyses between production/NPV and associated treatment cost for a wide range of target productions. A balanced solution in terms of production/NPV and treatment cost can be obtained from such analysis. For the set of reservoir, economic and other data used for such analysis of the problem, it is found that 44-52% of treatment cost saving is possible with only 12-13% reduction in production/NPV over 10 years. This capability of the proposed model can enable an operator to achieve a treatment that would save a considerable amount of

immediate treatment cost by sacrificing a marginal amount of production/NPV over an uncertain period of time.

4. The model gives the proppant scheduling for the optimum fracture design. Proppant loading is delayed in maximum production/NPV design and the proppant scheduling is continued longer. The model shows higher EOJ proppant concentration with higher production targets. The model also shows that a shorter fracture with higher fracturing fluid viscosity is optimum in a relatively high permeability reservoir.

5. Using the capability of this optimisation model, sensitivities of various treatment parameters have been studied in NPV maximisation. Results demonstrate that fixing a parameter to a value other than its free optimum value always deterorates a design. The percentage of reduction in NPV can be estimated using the sensitivity results if a treatment parameter is necessary to fix to a non-optimum value for any practical convenience.

6. The fracture migration by an appropriate extent into non-paying bounding layers increases reservoir production and NPV due to increased fracture width inthe pay zone. Excessive fracture migration, however, diminishes the NPV increase due to increased treatment cost. The optimum fracture height migration may be reservoir dependent. Using the optimisation model, the optimum fracture height migration can be automatically determined for a specified design objective. The fracture height migration into bounding layers by about 80% of the pay zone height s found to yield an absolute maximum NPV design for the reservoir studied herein with both PKN-C and P-3D-C fracture models.

7. Most optimum fracture parameters and cumulative productions over 10 years obtained from the optimisation scheme using both PKN-C and P-3D-C fracture models are close. Therefore, the PKN-C fracture model can be successfullyused to design a hydraulic fracture treatment for three-layered formations, unless there are

multi-layered formations with high stress regions in between them for which P-3D-C model is perhaps more appropriate.

8. Hydraulic-fracturing-induced formation damage due to uncontrolled fracture growth and multiple fracture initiation is very likely during fracturing tight formations. The proposed model with constrained treatment optimisation scheme is highly capable to offer a treatment that would avoid/minimise such formation damage and can be executed with specified operational facilities and would ensure efficient treatments.

9. The critical drawdown pressure (*CDP*) for sand production decreases with production time as a function of depleting reservoir pressure among other factors. Thus, sand production at the latter production stage is highly likely in weak formation. The proposed model would optimise treatment parameters to adjust fracture geometry so that the *CDP* does not fall below a target producing drawdown pressure, and hence sand production is avoided. However, the operator can adjust the producing drawdown pressure to avoid sand production for an unconstrained treatment design if *CDP* is plotted against the resulting fracture geometry as a function of producing time.

10. The proposed model is also applied to a field case of onshore Australia, where high-treating pressures related fracture complexities were observed during hydraulic fracturing treatment. The nature of complexity associated with hydraulic fracturing in the region has been investigated by commercial software FRACPRO. Optimum treatment designs by FRACPRO and the proposed model, while applying to this field case, are evaluated and following conclusions are drawn.

    (a) Hydraulic fracturing complexities like high treating pressures, auxiliary/secondary fractures and excessive fluid loss, uncontrolled fracture growth and low in-palce proppant concentration are experienced during execution and are critical issues in hydraulic fracturing. These complexities may arise due to initiation of multiple fractures, presence of natural fractures,

inappropriate orientation of perforation and wellbore trajectory, and treatment designed by commercial software of unconstrained nature (such as experienced with FRACPRO). The proposed optimisation model can find the optimum design, adjusted automatically through satisfying a number of design constraints formulated with an intention to avoid such complexities. Thus, it is highly likely that the above complexities will be alleviated if this optimum design is executed in the field. However, the treatment designed by any program of unconstrained nature may not avoid such complexities, rather may create one or more such complexities during execution. Thus, while designing with any software care should be taken to verify the final design by another computational scheme, and if necessary, the optimum design obtained from the in-built procedure of software must be adjusted to avoid such design-induced fracture complexities.

(b) The novel idea of optimising fracturing fluid viscosity and its benefit are evaluated. Because of variability of viscosity, the model finds the maximum possible value of objective function with an optimum value of viscosity and this objective function value is better than when the viscosity is fixed at other than the optimum. The model incorporates a systematic formulation of in-situ fracture conductivity, which is found conservative compared to that in FRACPRO. Thus, optimum production predicted by the proposed model is less than that predicted by FRACPRO for similar fracture geometry and same conductivity damage factor.

11. Proppant-free hydraulic fracturing 'water-frac' has also been considered for application to the same field case of onshore Australia, assuming the formation containing many natural fractures. The simulation results show an excellent pressure-permeability response by 'water-frac' technology and this analysis suggests that the 'water-frac' technology is another high emerging possibility to mitigate the fracturing complexities avoiding perforations completely. However, it

is recognised that further research is required before definitive conclusion about the successful applicability of the technology at its current state.

7.2. Recommendation of further studies

The following areas are recommended for further studies:

1. In this proposed optimisation model (either with 2D PKN-C or P-3D-C), proppant settling has not been modeled during fracture propagation, though high fracture conductivity damage factor has been considered. Further efforts should be made to incorporate the proppant settling to improve the reliability of this optimisation model. The optimisation of fracturing fluid viscosity in this study as a continuous parameter may be criticised and sometimes inconvenient from practical points of view. Using the capability of the optimisation algorithm this parameter can be modeled as a discrete variable so that an optimum viscosity is selected from the database of available standard fracturing fluids. Prevention of proppant back production should also be considered in further studies.

2. Fluid flow from a fractured reservoir is an important module in the treatment optimisation model. In the current model, only depletion-type dry gas reservoir is considered. Other reservoirs should also be considered, for example, dry-gas reservoir with water influx and volumetric wet-gas and gas-condensate reservoirs. These will have certainly different production behaviours, but may or may not affect fracture propagation and treatment optimisation. This should be investigated further.

3. Efforts should be made to model single or multiple transverse fracturing of horizontal wells. Rahman *et al.* (2002) have studied transverse fracture propagation from horizontal well experimentally and numerically and their findings could be considered while developing a radial fracture model to transversely fracture these wells. Appropriate production model for this transverse fracture should also be incorporated for better estimation of production. Guo and Evans (1993) have already

developed a production-forecasting model for horizontal well with multiple transverse fractures in low permeability gas reservoirs. The radial fracture model and this production model could be used for treatment optimisation for these wells.

4. Although a few approximate formulations have been considered to minimise/avoid uncontrolled fracture growth, multiple fracture initiation and formation failure related complexities while conducting hydraulic fracturing and during production, further research should be continued to incorporate improved analytical/numerical formulations/constraints in the optimisation scheme, and also other constraints to avoid other potential complexities.

5. Longitudinal fracturing of horizontal wells may be preferable for reservoirs containing very thin layer of producing formation. Depending on the stress condition, the hydraulic fracture may be on the top and bottom sides of the well. In such a case, the fracture height (along the length of the well) is significantly greater than the fracture length (lateral to the well). Due to their inherent assumption, the PKN-C and P-3D models will not be reliable for this fracture configuration, however, the KGD model will probably be useful. Optimisation of treatments using this fracture model for such well and fracture configurations may be conducted in a future study. Also depending on the stress condition (probably reverse faulting) in such a reservoir, the fracture may extends horizontally lateral to the well direction. In such a case, fracture height and length will not be well constrained by stress contrast. Adjusting fracture model, devising strategy for fracture confinement and optimising treatments for this type of configuration would be an interesting for further study.

6. Hydraulic fracturing is optimised in this study assuming a single well in the reservoir and adjusting production rate with time by depleting nature of the reservoir at a constant flowing pressure. In practice, the reservoir may contain several wells and production rates over time are adjusted and different for different wells. Further

research of hydraulic fracturing optimisation for such complex production requirements might be more useful.

REFERENCES

Agarwal, R.G., Carter, R.D. and Pollock, C.B., (1979), Evaluation and performance prediction of low permeability gas wells stimulated by massive hydraulic fracturing, *J. of Pet. Tech.*, 362-372.

Aggour, T.M., and Economides, M.J., (1998), Optimization of the performance of high-permeability fractured wells, SPE 39474, *Int. Symp. on Formation Damage Control*, Lafayette, Louisiana, Feb. 18-19.

Aggour, T., (2001), Optimization strategies for hydraulic fractures in high permeability reservoirs. SPE 68131, *Middle East Oil Show and Conf.*, Bahrain, March, 17-20.

Ahmed, U., Newberry, B.M. and Cannon, D.E., (1985), Hydraulic fracture treatment design of wells with multiple zones, SPE 13857, *SPE/DOE Joint Symp. on Low Permeability Reservoirs*, Denver, Colorado, May 19-22.

Al-Hussainy, R., and Ramey, H.J., Jr., (1966), Application of real gas theory to well testing and deliverability forecasting, *J. of Pet. Tech.*, May, 637-642.

Aly, A.M., El-Banbi, A.H., Holditch, S.A., Wahdan, M., Salah, N., Aly, N.M., and Boerrigter, P., (2001), Optimization of gas condensate reservoir development by coupling reservoir modelling and hydraulic fracturing design, SPE 68175, *Middle East Show and Conf.*, Bahrain, March 17-20.

Aronofsky, J.S. and Lee, A.S., (1958), Linear programming model for scheduling crude oil production, *Trans.*, AIME, **213**, 51-54.

Aronofsky, J.S. and Williams, A.C., (1962), The use of linear programming and mathematical models in underground oil production, *Management Science*, **8**, 394-407.

Attra, H.D., Wise, H.B. and Black, W.M., (1961), Application of optimizing techniques for studying field producing operaitions, *J. of Pet. Tech.*, Jan., 82-86; *Trans.*, AIME, **222**.

Aud, W.W., Wright, T.B., Cipolla, C.L., Harkrider, J.D. and Hansen, J.T., (1994), The effect of viscosity on near-wellbore tortuosity and premature screen-outs, SPE 28492, *Annual Tech. Conf. and Exh.*, New Orleans, LA, September 25-28.

Aziz, K., Mathar, L., Ko, S., Brar, G.S., (1976), Use of pressure, pressure-squared or pseudo-pressure in the analysis of transient pressure drawdown data from gas wells. *J. of Canadian Pet. Tech.*, April-June, 58-65.

Balachandran, M. and Gero, J.S., (1984), A comparison of three methods for generating the Pareto optimal set, *Eng. Optim.*, 7(4), 319-336.

Banerjee, P.K., (1994), *The Boundary Element Methods in Engineeing*, Mc-Graw-Hills Book Company, second edition, New York, USA.

Barton, N., Bandis, S. and Bakhtar, K., (1985), Strength, deformation and conductivity coupling of rock joints, *Int. J. Rock Mech. Min. Sci. & Geomech. Abstr.*, **22**(3), 121-140.

Barton, C.C. and Hsieh, P.A., (1989), Physical and hydrologic-flow properties of fractures, *Field Trip Guidebook T385*, American Geophysical Union, Vol. 36, Washington D.C.

Beale, E.M.L., (1959), On quadratic programming, *Naval Research Logistics Quaterly*, **6**, 227-243.

Berke, L. and Venkayya, V.B., (1974), Review of optimality criteria approaches to structural optimization, *ASME, AMD*, **7**, 23-24.

Blanton, T.L., (1986), Propagation of hydraulically and dynamically induced fractures in naturally fractured reservoirs, SPE 15261, *Unconventional Gas Tech. Symp.*, Louisville, KY, May 18-21.

Bohannon, J.M., (1970), A linear programming model for optimum development of multi-reservoir pipeline systems, *J. of Pet. Tech.*, Nov., 1429-1436; *Trans.*, AIME, **249**.

Bouteca, M.J., (1988), Hydraulic fracturing model based on a three-dimensional closed form: Tests and analysis of fracture geometry and containment, *SPE Prod. Eng.*, November, 445-454.

Branagan, P.T., Cipolla, C.L. and Lee, S.J., (1987), Designing and evaluating hydraulic fracture treatments in naturally fractured reservoirs, SPE 16439, *SPE/DOE Symp. on Low Permeability Reservoirs*, Denver, CO, May 18-19.

Brown, J.E. and Economides, M.J., (1992), Practical considerations in fracture treatment design, in Economides, M.J.: *Practical Companion to Reservoir Stimulation*, Elsevier, Amsterdam.

Bunch, J.W. and Kaufman, L., (1977), Indefinite quadratic programming, *Computing Science Technical Report*, **61**, Bell. Labs., Murray Hill, New Jersey.

Bunday, B.D., (1984), *Basic Optimization Methods*, Edward Arnold Ltd., London.

Caldwell, J.B., (1972), Modern ship structural design philosopy, *Koninklijk Instituut Van Ingenieurs Sectie Voor Scheeps Techniek*, 27-38.

Carroll, J.A. and Horne, R.N., (1992), Multivariate optimization of production systems, *J. of Pet. Tech.*, July, 782-789.

Casares, M.A. and Talavera, J.F., (2001), Hydraulic fracturing as a sand control method: Experimental work on the VBR-24 well, Vibora Field, Bolivia, SPE 69584, *Latin American and Caribbean Pet. Eng. Conf.*, Buenos Aires, Argentina, March 25-28.

Charnes, A. and Cooper, W.W., (1961), *Management Models and Industrial Applications of Linear Programming*, Vols. 1 and 2, Wiley, New York.

Chen, J.L. and Tsao, Y.C., (1993), Optimal design of machine elements using genetic algorithms, *J. of the Chinese Soc. of Mech. Engrs.*, **14**(2), 193-199.

Cheng, F.Y. and Li, X.S., (1999), Generalized center method for multiobjective engineering optimization, *Eng., Optim.*, **31**, 641-661.

Chipperfield, S., (2000), Personal communication with Mr. Simon Chipperfield, Petroleum Engineer of Santos Ltd., Adelaide, Australia.

Cinco-Ley, H., Samaniego-V, F. and Dominguez, N., (1978), Transient pressure behavior for a well with a finite conductivity vertical fracture, *Soc. of Pet. Engrs. J.*, August, 253-264.

Cinco-Ley, H. and Samaniego, V.J., (1981), Transient pressure analysis for fractured wells, *J. of Pet. Tech.*, 1749-1766.

Claiborne JR., E.B., Saucier, R. and Wilkinson, T.W., (1996), Water Frac applications in High Island 384 Field, SPE 36459, *Annual Tech. Conf. and Exh.*, Denver, CO, October 6-9.

Cleary, M.P, Wright, C.A. and Wright, T.B., (1991), Experimental and modeling evidence for major changes in hydraulic fracturing design and field procedures, SPE 21494, *Gas Tech. Symp.*, Houston, TX, January 23-25.

Cleary, M.P., Johnson, D.E., Kogsboll, H.H., Owens, K.A., Perry, K.F., de Pater, C.J., Stachel, A., Schmidt, H. and Tambini, M., (1993), Field implementation of proppant slugs to avoid premature screen-out of hydraulic fractures with adequate proppant concentration, SPE 25892, *Rocky Mountain Regional/Low Permeability Reservoirs Symp.*, Denver, CO, April 12-14.

Coello, C.A.C. and Christiansen, A.D., (1999), Moses: a multiobjective optimization tool for engineering design, *Eng. Optim.*, 31, 337-368.

Cohon, J.L. and Marks, D.H., (1975), A review and evaluation of multiobjective programming techniques, *Water Resources Reseacrh*, **11**(2), 208-228.

Cottle, R.W. and Dantzig, G.B., (1968), Complementary pivot theory of mathematical programming, in: G.B. Dantzig and A.F. Veinott, eds., *Lectures in Applied Mathematics II, Mathematics of the Decision Sciences*, Part I (American Mathematical Society, Providence, RI), 115-136.

Dake, L.P., (1978), *Fundamental of Reservoir Engineering*, Elsevier Scientific Publishing, Vol. 249, Amsterdam.

Das, I. and Dennis, J.E. JR., (1998), Normal-boundary intersection: a new method for generating the pareto surface in nonlinear multicriteria optimization problems. *SIAM J. Optim.*, **8**, 631-657.

Das, N.C., Mazumder, S.K. and Kajal, D.E., (1999), Constrained non-linear programming: a minimum cross-entropy algorithm, *Eng. Optim.*, **31**, 479-487.

Dantzig, G.B., (1963), *Linear Programming and Extensions*, Princeton University Press, Princeton, New Jersey.

Davidson, B.M., Saunders, B.F., Robinson, B.M., Holditch, S.A., (1993), Analysis of abnormally high fracture treating pressures caused by complex fracture growth, SPE 26154, *Gas Tech. Symp.*, Calgary, Alberta, Canada, June 28-30.

Dembo, R.S., (1976), A set of geometric programming test problems and their solutions, *Math. Program.*, **10**, 192-213.

Dempsey, B.J., Taki, H., and Druyff, J.C., (2001), Case history of hydraulic fracture optimization in tight case wells with water production in the Wind River Basin, Wyoming, SPE 67300, *Production and Operations Symp.*, Oklahoma City, OK, March 24-25.

de Kluyver, C.A., (1979), An exploration of various goal programming formulations with application to advertising media scheduling, *J. of the Operational Research Society*, **30**, 167-171.

Desroches, J. and Carter, B.J., (1996), Three dimensional modelling of a hydraulic fracture. In *Rock Mechanics*, Aubertin, Hassani & Mitri (eds.), Balkema, Rotterdam.

Dieterich, J.H., (1992), Earthquake nucleation on faults with rate-dependent and state dependent strength, *Technophysics*, **211**, 115-134.

Dodge, D.W. and Metzner, A.B., (1959), Turbulent flow of non-Newtonian systems, *A.I.Ch.E.J.*, **5** (2), June, 189-204.

Duckstein, L., (1984), Multiobjective optimization in structural design: the model choice problem, in: *New Direction in Optimum Structural Design*, (eds. E. Atrek et al.), John Wiley & Sons, New York.

Earlougher, R.C. Jr., (1977), *Advances in Well Test Analysis*, Monograph, Vol. 5, SPE, Richardson, TX.

Economides, M.J. and Nolte, K.G., (1989), *Reservoir Stimulation*, Schlumberger Educational Services, Second Edition, Houston, TX.

Economides, M.J., Hill, A.D., and Ehlig-Economides, C., (1994), *Petroleum Production Systems*, Prentice Hall PTR, New Jersey.

Elbel, J.L., (1985), Considerations for optimum fracture geometry design, SPE/DOE 13866, *SPE/DOE Low Permeability Gas Reservoirs Symp.*, Denver, CO, May 19-22.

Erdogan, F. and Sih, G.C., (1963), On the crack extension in plate under plane loading and transverse shear, *J. of Basic Eng.*, Dec., 519-527.

Eshelby, J.D., (1957), The determination of the elastic field of an ellipsoidal inclusion and related problem, *Proc. of Rock Soc. London*, **241**, 376-396.

Evans, G.W., (1984), An overview of techniques for solving multiobjective mathematical programs, *Management Science*, **30**(11), 1268-1282.

Fletcher, R., (1971), A general quadratic programming algorithm, *J. of the Institute of Mathematics and Its Applications*, **7**(1), 76-91.

Fletcher, P.A., Montgomery, C.T., Ramos, G.G., Miller, M.E., Rich, D.A., Guillory, R.J. and Francis, M.J., (1996), Using fracturing as a technique for controlling formation failure, *SPE Production & Facilities*, May, 117-121.

Fligelman, H., Cinco-Ley, H., Ramley Jr., H.J., Braester, C., Couri, F., (1989), Pressure-drawdown test analysis of a gas well application of new correlations, SPE 17551, *SPE Facilities Engineering*, September, 406-412.

Fox, R.L., (1971), *Optimization Methods for Engineering Design*, Affison-Wesley, Massachusetts.

FRACPRO (1996), Real-Time Hydraulic Fracture Treatment Design and Analysis Software, Version 8, Resources Engineering systems, Inc., Houston, TX.

Fu, J., Fenton, R.G. and Cleghorn, W., (1991), A mixed integer-discrete-continuous programming method and its application to engineering design optimization, *Eng. Optim.*, **17**, 263-280.

Fujii, H. and Horne, R., (1995), Multivariate optimization of networked production systems, *SPE Production & Facilities*, August, 165-171.

Gabay, D. and Luenberger, D.G., (1976), Efficiently converging minimization methods based on the reduced gradient, *SIAM J. Contr. & Optim.*, **14**(1), 42-61.

Geertsma, J. and de Klerk, F., (1969), A rapid method of predicting width and extent of hydraulically induced fractures, *J. of Pet. Tech.*, December, 1571-1581.

Ghani, S.N., (1989), A versatile procedure for optimization of a nonlinear nondifferentiable constrained objective function, AERE R13714, United Kingdom Atomic Energy Authority, Nuclear Physics and Instrumentation Division, Harwell Laboratory, Oxfordshire, UK, December.

Gill, P.E. and Murray, W., (1978), Numerically stable methods for quadratic programming, *Math. Program.*, **14**, 349-372.

Goicoechea, A., Hansen, D. and Duckstein, L., (1982), *Introduction to Multi-Objective Analysis with Engineering and Business Applications*, John Wiley, New York.

Goldfarb, D., (1972), Extension of Newton's method and simplex methods for solving quadratic programs, in: F.A. Lootsma, ed., *Numerical Methods for Nonlinear Optimization*, Academic Press, London, 239-254.

Goldfarb, D. and Idnani, A., (1983), A numerically stable dual method for solving strictly convex quadratic programs, *Math. Program.*, **27**, 1-33.

Goldberg, D.E., (1989), *Genetic Algorithms in Search, Optimization, and Machine Learning*, Addison-Wesley Publishing Co., New York.

Goldstein, A.A. and Price, J.F., (1971), On descent from local minima, *Mathematics of Computation,* **25** (115), 569-574.

Goncalves, A.S., (1972),A primal-dual method for quadratic programming with bounded variables, in: F.A. Lootsma, ed., *Numerical Methods for Nonlinear Optimization*, Academic Press, London, 255-263.

Goodman, R.E., (1976), *Methods of Geological Engineering in Discontinuous Rocks*, West, New York.

Goodman, R.E., (1989), *Introduction to Rock Mechanics*, 2nd edition, Wiley, New York.

Grigoriadis, M.D. and Ritter, K., (1969), A parametric method for semidefinite quadratic programs, *SIAM J. Control*, **7**, 559-577.

Gringarten, A.C. and Ramey, A.J. Jr., (1974), Unsteady state pressure distributions created by a well with a single-infinite conductivity vertical fracture, *Soc. of Pet. Engrs. J.*, August, 347-360.

Guo, G. and Evans, R.D. (1993), Inflow performance and production forecasting of horizontal wells with multiple hydraulic fractures in low-permeability gas reservoirs, SPE 26169, *Gas Technology Symp.*, Calgary, Alberta, Canada, June 28-30.

Gurwitz, C. and Overton, M., (1989), Sequential quadratic programming methods based on approximating a projected Hessian matrix, *SIAM J. Sci. Comput.*, **10**, 631-653.

Haftka, R.T. and Starnes Jr., J.H., (1975), Applications of a quadratic extended interior penalty function for structural optimization, AIAA paper No. 75-764, *16th Conference.*

Haims, Y.Y., Hall, W. and Freedman, H., (1975), *Multi-objective Optimization in Water Resources Systems; the Surrogate Worth Trade-off Method*, Elsevier, Amsterdam.

Hareland, G., Pampersad, P. Dharaphop, J. and Sasnanand, S., (1993), Hydraulic fracturing design optimization, SPE 26950, *Eastern Regional Conf. & Exh.*, Pittsburgh, PA, November 2-4.

Hareland, G. and Pampersad, P.R., (1994), Hydraulic fracturing design optimization in low-permeability gas reservoirs, SPE 27033, *Latin American/Caribbean Petroleum Engineering Conf.*, Buenos Aires, Argentina, April 27-29.

Heinz, J. and Spellucci, J., (1994), A successful implementation of the Pantoja-Mayne SQP method, *Optim. Meth. Software*, **4**, 1-28.

Hicks, T.W., Pine, R.J., Willis-Richards, J., Xu, S., Jupe, A.J. and Rodgrigues, N.E.V., (1996), A hydro-thermo-mechanical numerical model for HDR geothermal reservoir evaluation, *Int. J. of Rock Mech. Min. Sci. & Geomech. Abstr.*, **33**(5), 499-511.

Hossain, M.M., (2001), Reservoir stimulation by hydraulic fracturing: complexities and remedies with reference to initiation and propagation of induced and natural fractures, Ph.D. Thesis, *The University of New South Wales*, Sydney, Australia.

Hossain, M.M., Rahman, M.K. and Rahman, S.S., (2002), A shear dilation stimulation model for production enhancement from naturally fractured reservoirs, SPE 63173, *Soc. of Pet. Engrs. J.* (accepted).

Hossain, M.M., Rahman, M.K. and Rahman, S.S., (2001), Modelling of hydraulic fracture propagation by boundary element method as coupled fluid flow-deformation problems, *Proc. of the First Asian-Pacific Congress on Computational Mechanics*, Sydney, Australia, November 20-23.

Hossain, M.M., Rahman, M.K. and Rahman, S.S., (2000), Hydraulic fracture initiation and propagation: roles of wellbore trajectory, perforation and stress regimes, *J. of Pet. Sci. & Eng.*, **27**, 129-149.

Howard, G.C. and Fast, C.R., (1957), Optimum fluid characteristics for fracture extension, *Drilling and Production Practices*, API, (Appendix by E.D. Carter: Derivation of the general equation for estimating the extent of the fractured area), 261-270.

Hussain, M.A., Pu, S.L. and Underwood, J., (1974), Strain energy release rate for a crack under combined Mode I and Mode II, *Fracture Analysis*, ASTM, STP 560, 2-28.

Ignizio, J.P., (1982), *Linear Programming in Single and Multiple-objective Systems*, Prentice-Hall, Inc., Englewood Cliffs, New Jersey.

IMEX 95.00, 1995. *Balckoil Simulator*, User's Guide, Computer Monitoring Group, Calgary, Alberta, Canada.

Ingraffea, A. and Manu, C., (1980), Stress-intensity factor computation in three dimensions with quarter-point element, *Int. J. for Num. Meth. in Eng.*, **15**, 1427-1445.

Jacoby, S.L.S., Kowalik, J.S. and Pizzo, J.T., (1972), *Iterative Methods for Nonlinear Optimization Problems*, Prentice-Hall, Inc., Englewood Cliffs, New Jersey.

Jaeger, J.C. and Cook, N.G.W., (1969), *Fundamentals of Rock Mechanics*, Methuen & Co. Ltd., London.

Jaynes, E.T., (1957), Information theory and statistical mechanics, *The Physical Review*, **106**, 620-630.

Jones, S.C., (1987), Using the inertial coefficient, b, to characterize heterogeneity in reservoir rock, SPE 16949, *Annual Tech. Conf. and Exh.*, Dallas, September 27-30.

Kapur, J.N., (1989), *Maximum Entropy Models in Science and Engineering*, Wiley Eastern, New Delhi.

Keeny, R.L. and Raiffa, H., (1976), *Decisions with Multiple Objectives: Preferences and Value Trade offs*, John Wiley & Sons, Inc., New York.

Khot, N.S., Venkayya, V.B. and Berke, L., (1976), Optimum structural design with stability constraints, *Int. J. for Num. Methods in Eng.*, **10**, 1097-1114.

Khristianovitch, S.A. and Zheltov, Y.P., (1955), Formation of vertical fractures by means of highly viscous fluids, *Proc. of the 4th World Petroleum Congress*, Rome, **2**, 579-586.

Klingman, W.R. and Himmelblau, D.M., (1964), Nonlinear programming with the aid of a multi-gradient summation technique, *J. of the Assoc. for Comp. Machinery*, **11**(4), 400-415.

Koopmans, T.C., (1951), *Activity Analysis of Production and Allocation*, (ed.), Wiley, New York.

Koski, J., (1984), Multicriterion optimization in structural design, in: *New Directions in Optimum Structural Design*, (eds. E. Atrek et al.), John Wiley & Sons.

Kuhn, H.W. and Tucker, A.W., (1951), Nonlinear Programming, *Proc. Second Berkeley Symp. on Math. Statistics and Probability*, University of California, 481-491.

Langedijk, R.A., Al-Naabi, S., Al-Lawati, H., Pongratz, R., Elia, M.P. and Abdulrab, T., (2000), Optimization of hydraulic fracturing in a deep, multilayered, gas-condensate reservoir, SPE 63109, *Annual Tech. Conf. and Exh.*, Dallas, TX, Oct. 1-4.

Lasdon, L.S., Waren, A.D., Jain, A. and Ratner, M., (1978), Design and testing of a generalized reduced gradient code for nonlinear programming, *ACM Transactions on Mathematical Software*, **4**(1), 34-50.

Lee, J., and Wattenbarger, R.A., (1996), *Gas Reservoir Engineering*, SPE Textbook Series, Vol. 5, Richardson, TX.

Lee, S.M., (1972), *Goal Programming for Decision Analysis*, Auerbach, Philadelphia.

Lemke, C.E., (1962), A method of solution for quadratic programs, *Management Science*, **8**, 442-453.

Lewis, K. and Mistree, F., (1998), The other side of multidisciplinary design optimization: accommodating a multi-objective, uncertain and non-deterministic world, *Eng. Optim.*, **31**, 161-189.

Mahrer, K.D., (1999), A review and perspective on far-field hydraulic fracture geometry studies, *J. Pet. Sci. & Eng.*, **24**, 13-28.

Marcelin, J.L., (1999), Evolutionary optimization of mechanical structures, *Eng. Optim.*, **31**, 571-588.

Mathews, C.S. and Russell, D.G. (1967), *Pressure Buildup and Flow Tests in Wells*, Monograph, Vol.1, SPE, Richardson, TX.

Mayerhofer, M.J., Richardson, M.F., Walker, R.N., Meehan, D.N., Oehler, M.W. and Browning, R.R., (1997), Proppants? We don't need no proppants, SPE 38611, *Annual Tech. Conf. and Exh.*, San Antonio, TX, October 5-8.

McFarland, J.W., Lasdon, L., and Loose, V., (1984), Development planning and management of petroleum reservoirs using tank models and nonlinear programming. *Operations Research*, **32**(2), 270-289.

McLennon, J.D., Roegiers, J-C. and Economides, M.J., (1989), Extended reach and horizontal wells, in: *Reservoir Simulation* by Economides, M.J. and Nolte, K.G., Second Edition, Prentice Hall, New Jersey, 19-01 – 19-28.

Meehan, D.N., (1992), Stimulation results in the Giddings (Austin Chalk) Field, SPE 24783, *Annual Tech. Conf. and Exh.*, Washington DC, October 4-7.

Meng, H.-Z. and Brown, K.E. (1987), Coupling of production forecasting, fracture geometry requirements and treatment scheduling in the optimum hydraulic fracture design, SPE 16435, *SPE/DOE Low Permeability Reservoirs Symp.*, Denver, CO, May 18-19.

Mistree, F., Hughes, O.F. and Phouc, H.B., (1981), An optimization method for the design of large, highly constrained complex systems, *Eng. Optim.*, **5**, 179-197.

Mistree, F., Ittimakin, P. and Kuppuraju, N., (1985), An algorithm for solving multiple objective decision support problems in engineering design, *CAD/CAM Robotics and Automation Conference*, Tuesson, Ariz, Feb. 11-15.

Mohaghegh, S., Balan, B. and Ameri, S., (1996), A hybrid, neuro-genetic approach to hydraulic fracture treatment design and optimization, SPE 36602, *Annual Tech. Conf. and Exh.*, Denver, CO, October 6-9.

Mohaghegh, S., Balan, B., Platon, V. and Ameri, S., (1999), Hydraulic fracture design and optimization of gas storage wells, *J. Pet. Sci. & Eng.*, **23**, 161-171.

Montgomery, K.T., Holditch, S.A. and Berthelot, J.M., (1990), Effects of fracture fluid invasion on cleanup behavior and pressure buildup analysis, SPE 20643, *Annual Tech. Conf. and Exh.*, New Orleans, LA, September 23-26.

Morales, R.H. and Abu-Sayed, A.S., (1989), Microcomputer analysis of hydraulic fracture behavior with a pseudo-three-dimensional model, *SPE Prod. Eng.*, February, 198-205.

Morris, A.J., (1972), Approximation and complementary geometric programming, *SIAM J. Appl. Math.*, **23**(4), 527-531.

Muskat, M., (1937), *The Flow of Homogeneous Fluids Through Porous Media*, Edwards, Ann Arbor, Mich.

Murray, W. and Prieto, J.P., (1995), A sequential quadratic programming algorithm using an incomplete solution of the subproblem, *SIAM J. Optim.*, **5**, 590-640.

Ndiritu, J.G. and Daniell, T.M., (1999), An improved genetic algorithm for continuous and mixed discrete-continuous optimization, *Eng. Optim.*, **31**, 589-614.

Nelder, J.A. and Mead, R., (1965), A simplex method for function minimization, *Computer Journal*, 7(4), 308-313.

Nordgren, R.P. (1972), Propagation of a vertical hydraulic fracture, *Soc. of Pet. Eng. J.*, August, 306-314.

Nolte, K.G., (1979), Determination of fracture parameters from fracturing pressure decline. SPE 8341, *Annual Fall Tech. Conf. and Exh.*, Las Vegas, Nevada, September 23-26.

Nolte, K.G. and Smith, M.B., (1981), Interpretation of fracturing pressures, *J. of Pet. Tech.*, September, 1767-1775.

Nolte, K.G., (1982), Fracture design considerations based on pressure analysis, SPE 10911, *Cotton Valley Symp.*, Tylor, TX, May 20.

Nolte, K.G., (1986), Determination of proppant and fluid schedules from fracturing pressure decline, SPE 13278, *SPE Prod. Eng.*, July, 255-265.

Nolte, K.G., (1988), Principles of fracture design based on pressure analysis, *SPE Prod. Eng.*, February, 22-30.

Nolte, K.G., (1989), Fracturing-pressure analysis, in Gidley, J.L. *et al.*: *Recent Advances in Hydraulic Fracturing*, Monograph Vol. 12, SPE, Richardson, TX.

O'Dell, P.M., Steubing, N.W. and Gray, J.W., (1973), Optimization of gas field operation, *J. of Pet. Tech.*, April, 419-425.

Patton, F.D., (1966), Multiple modes of shear failure in rock, *Proc. of 1st Cong. ISRM*, Lisbon, **1**, 509-513.

Pearson, C.M., (2001), Dimensionless fracture conductivity: Better input values make better wells, SPE 60184, *J. of Pet. Tech.*, January, 59-63.

Perkins, T.K. and Kern, L.R. (1961), Widths of hydraulic fractures, *J. of Pet. Tech.*, September, 937-949.

Peterson, E.L., (1976), Geometric Programming, *SIAM Review*, **18** (1), 1-51.

Pierre, D.A., (1969), *Optimization Theory with Applications*, John Wiley & Sons, New York.

Pierre, D.A. and Lowe, M.J., (1975), *Mathematical Programming via Augmented Lagrangian: An Introduction with Computer Programs*, Addison-Wesley Publishing Co., Inc., Reading, Massachusetts.

Polyak, B.T., (1987), *Introduction to Optimization*, Optimization Software Inc., New York.

Powell, M.J.D., (1978), Algorithms for nonlinear constraints that use Lagrangian Functions, *Math. Program.*, **14**(2), 224-248.

Prats, M. (1961), Effect of vertical fractures on reservoir behavior – incompressible fluid case, *Soc. of Pet. Engrs. J.*, June, 105-108.

Rahim, Z. and Holditch, S.A., (1995), Using a three-dimensional concept in a two-dimensional model to predict accurate hydraulic fracture dimensions, *J. of Pet. Sci. & Eng.*, **13**, 15-27.

Rahman, M.K., (1991), Production-oriented Structural Design of Ships; with particular application to inland waterway vessels, Ph.D. Thesis, *The University of Newcastle upon Tyne*, England, UK.

Rahman, M.K., (1996), Optimization of panel forms for improvement in ship structures, *Structural Optimization*, **11**, 195-212.

Rahman, M.K., (1998), Automated optimization of transverse frame layouts for ships by elastic-plastic finite element analysis, *Structural Optimization*, **15**, 187-200.

Rahman, M.K. and Caldwell, J.B., (1992), Rule-based optimization of midship structures, *Marine Structure*, **5**, 467-490.

Rahman, M.K., Hossain, M.M. and Rahman, S.S., (2000), An analytical method for mixed-mode propagation of pressurized fractures in remotely compressed rocks, *Int. J. of Fracture*, **103**(3), 243-258.

Rahman, M.M., Hossain, M.M., Crosby, D.G., Rahman, M.K. and Rahman, S.S. (2002), Analytical, numerical and experimental investigations of transverse fracture propagation from horizontal wells, *J. of Pet. Sci. & Eng.* (accepted).

Ramey, H.J.,Jr., Wattenbarger, R.A., (1968), Gas well testing with turbulence, damage and wellbore storage, *J. of Pet. Tech.*, August, 877-887.

Rangel-German, E. and Samaniego V, F., (2000), On the determination of the skin factor and the turbulence term coefficient through a single constant gas pressure test, *J. of Pet. Sci. & Eng.*, **26**, 121-131.

Rao, S.S., (1984), *Optimization: Theory and Applications*, second ed., Halsted Press, New York.

Rasmussen, J. and Lund, E., (1997), The issue of generality in design optimization systems, *Eng. Optim.*, **29**, 23-37.

Rice, J.R., (1968), Mathematical analysis in the mechanics of fracture, *Fracture* by H. Liebowitz (ed.), Vol. 2, Academic Press, New York City.

Richardson, M., (2000), A new and practical method for fracture design and optimization, SPE 59736, *SPE/CERI Gas Tech. Symposium*, Calgary, Alberta, Canada, April 3-5.

Rietman, N.D., (1998), An integrated method for optimizing hydraulic fracture design for tight gas wells, SPE 39930, *Rocky Mountain Regional/Low Permeability Reservoirs Symp. and Exh.*, Denver, CO, April 5-8.

Rimmer, B., MacFarlane, C., Mitchell, C., Wolfs, H., and Samuel, M., (2000), Fracture geometry optimization: designs utilizing new polymer-free fracturing fluid and log-derived stress profile/rock properties, SPE 58761, *Int. Symp. on Formation Damage Control*, Lafayette, Louisiana , February 23-24.

Rosenwald, G.W. and Green, D.W., (1974), A method for determining the optimal location of wells in a reservoir using mixed-integer programming, *Soc. of Pet. Engrs. J.*, Feb., 44-54; *Trans.*, AIME, **257**.

Rowan, G. and Warren, J.E., (1967), A systems approach to reservoir engineering, optimum development planning, *J. Cdn. Pet. Tech.*, July, 84-94.

Russell, D.G., Goodrich, J.H., Perry, G.E., Bruskotter, J.F., (1966), Methods of predicting gas well performance, *J. of Pet. Tech.*, January, 99-108.

Sandgren, E., (1990), Nonlinear integer and discrete programming in mechanical design optimization, Trans. of the ASME, *J. of Mech. Design*, **112** (2), 223-229.

Schechter, R.S., (1992), *Oil Well Stimulation*, Prentice Hall, Englewood Cliffs, New Jersey.

SCR Geomechanics Group, (1993), On the modeling of near tip processes in hydraulic fractures, *Int. J. of Rock Mech. Min. Sci. & Geomech. Abstr.*, **30**(3), 1127-1134.

Settari, A. and Cleary, M.P., (1986), Development and testing of a pseudo-three – dimensional model of hydraulic fracture geometry, *SPE Prod. Eng.*, November, 449-466.

Sen, P. and Bari, A., (1985), Inland waterway fleet replacement: evaluation with multiple objectives, *Trans. of Royal Inst. of Naval Arch.*, **127**, 205-220.

Sherman, J.B. and Holditch, S.A., (1991), Effect of injected fracture fluids and operating procedures on ultimtae gas recovery, SPE 21496, *Gas Tech. Symp.*, Houston, TX, January 23-25.

Shi, W.B., (1988), Optimization of Marine Structural Forms: A Multi-level Multiple Objective Design Approach, Ph.D. Thesis, *University of Newcastle Upon Tyne*, England, UK.

Siddall, J.N., (1982), Optimal Engineering Design: Principles and Applications, Marcel Dekker, New York.

Sih, G.C., (1974), Strain energy density factor applied to mixed mode crack problems, *Int. J. of Fracture*, **10**(3), 305-321.

Simonson, E.R., Abou-Sayed, A.S. and Clifton, R.J., (1978), Containment of massive hydraulic fractures, *Soc. of Pet. Engrs. J.*, February, 27-32.

Smith, M.B. (1992), *Hydraulic Fracturing*, 2nd Edition, NSI Technologies, Inc., Tulsa Oklahoma.

Smith, M.B., (2001), Personal communication by e-mail with Dr. Mike B Smith of NSI Technologies, Tulsa, OK, in October.

Soliman, M.Y. and Hunt, J.L., (1985), Effect of fracturing fluid and its cleanup on well performance, SPE 14514, *Eastern Regional Meeting*, Morgantown, West Virginia, November 6-8.

Sousa, S.J., Carter, B.J. and Ingraffea, A.R., (1993), Numerical simulation of 3D hydraulic fracture using newtonian and power-law fluid. Int. J. of Rock Mechanics Mining Science & Geomechanics Abstracts, **30**, 1265-1271.

Spellucci, P., (1998), An SQP method for general nonlinear programs using only equality constrained subprograms, *Math. Program.*, **82**, 413-448.

Stadulis, J.M., (1995), Development of a completion design to control screen-outs caused by multiple near-wellbore fractures, SPE 29549, *Rocky Mountain Regional/Low-Permeability Reservoirs Symp.*, Denver, CO, March 20-22.

Templeman, A.B., (1993), Entropy-based optimization methods for engineering design, In: *Advanced Techniques in the Optimum Design of Structures* (Ed. Hernandez, S.), Computational Mechanics, Southampton, 109-139.

Theil, H. and Van De Panne, C., (1960), Quadratic programming as an extension of conventional quadratic maximization, *Management Science*, **7**, 1-20.

Turcotte, D.L., (1992), *Fractals and Chaos in Geology and Geophysics,* Cambridge University Press, Cambridge.

Umnuayponwiwat, S., Ozkan, E., Pearson, C.M. and Vincent, M., (2000), Effect of non-Darcy flow on the interpretation of transient pressure responses of hydraulically fractured wells, SPE 63176, *Annual Tech. Conf. and Exh.*, Dallas, TX, October1-4.

Valko, P. and Economides, M.J. (1995), *Hydraulic Fracture Mechanics*, John Wiley & Sons, Chichester, England.

Valko, P., Oligney, R.E. and Economides, M.J., (1997), High permeability fracturing of gas wells, *Gas TIPS (Fall)*, **3**(3), 31-40.

Valko, P., (2000), Personal communication with A/Prof. Peter Valko, Texas A&M University, by e-mail regarding production model for a hydraulically fractured gas reservoir, August.

Van Everdingen, A.F., (1953), The skin effect and its influence on the productivity capacity of a well, *Trans., AIME*, **198**, 171-76.

Van De Panne, C. and Whinston, A., (1964), The simplex and the dual method for quadratic programming, *Operations Research Quarterly*, **15**, 355-389.

Warpinski, N.R., (1991), Hydraulic fracturing in tight, fissured media, *J. of Pet. Tech.*, Feb., 146-209.

Warpinski, N.R. and Smith, M.B., (1989), Rock mechanics and fracture geometry, in Gidley, J.L. *et al*: *Recent Advances in Hydraulic Fracturing*, Monograph Vol. 12, SPE, Richardson, TX.

Warpinski, N.R. and Teufel, L.W., (1987), Influence of geologic discontinuities on hydraulic fracture propagation, SPE 13224, *J. of Pet. Tech.*, February, 209-220.

Watanabe, K. and Takahashi, H., (1995), Fractal geometry characterization of geothermal reservoir fracture netwroks, *J. of Geophysical Research*, **100**(B1), 521-528.

Weingarten, J.S. and Perkins, T.K., (1995), Prediction of sand production in gas wells: Methods and Gulf of Mexico case studies, *J. of Pet. Tech.*, July, 596-600.

Wilson, A.G., Coelho, J.D., Macgill, S.M. and Williams, H.C.W.L., (1981), Optimization in Locational and Transport Analysis, John Wiley & Sons, Chichester, UK.

Willis-Richards, J., Watanabe, K. and Takahashi, H., (1996), Progress toward a stochastic rock mechanics model of engineered geothermal systems, *J. of Geophysical Research*, **101**(B8), 17481-17496.

Wilson, A.G., Coelho, J.D., Macgill, S.M. and Williams, H.C.W.L., (1981), *Optimization in Locational and Transport Analysis*, John Wiley & Sons, Chichester, UK.

Wismer, D.A., (1971), *Optimization Methods for Large-scale Systems*, McGraw-Hill, New York.

Wu, S. and Chow, P, (1995), Genetic algorithms for nonlinear mixed discrete-integer optimization problems via meta-genetic parameter optimization, *Eng. Optim.*, **24**, 137-159.

Yang, Z., Crosby, D.G. and Khurana, A.K., (1996), Multivariate optimization of hydraulic fracture design, *J. of Aust. Pet. Prod. and Expl. Assoc.*, 516-527.

APPENDIX A

PROPPANT WEIGHT IN THE SLURRY

Volume of proppant-laden fluid (slurry) is given by

$$V_{pl} = V_{fl} + V_{pr} \tag{A1}$$

where

V_{pl} = volume of proppant laden fluid, ft^3

V_{fl} = volume of fracturing fluid, ft^3

V_{pr} = volume of proppant, ft^3

The volume of fracturing fluid, V_{fl}, is:

$$V_{fl} = \frac{W_{pr}}{\overline{P}_c \times 7.48052} \tag{A2}$$

where

W_{pr} = weight of proppant in the slurry, lb

$\overline{P}_c$ = Average proppant concentration, ppg

(Note: 1 ft^3 = 7.48052 gallon)

The volume of proppant, V_{pr}, is:

$$V_{pr} = \frac{W_{pr}}{\rho_p \times 7.48052} \tag{A3}$$

where

ρ_p = density of proppant, ppg.

Now, Eqs. A2 & A3 are substituted into Eq. A1 and the expression for V_{pl} is given by

$$V_{pl} = \frac{W_{pr}}{\overline{P}_c \times 7.48052} + \frac{W_{pr}}{\rho_p \times 7.48052} \tag{A4}$$

After simplification, proppant weight, W_{pr} is given by

$$W_{pr} = \frac{V_{pl} \times 7.48052}{\left(\frac{1}{\overline{P}_c} + \frac{1}{\rho_p}\right)} \tag{A5}$$

The above equations are in oilfield units. In SI units the expression for proppant weight is given by

$$W_{pr} = \frac{V_{pl}}{\left(\frac{1}{\overline{P}_c} + \frac{1}{\rho_p}\right)} \tag{A6}$$

where

W_{pr} = proppant weight, kg

V_{pl} = volume of proppant in the slurry, m^3

$\overline{P}_c$ = average proppant concentration, kg/m^3

ρ_p = density of proppant, kg/m^3

V_{fl} = volume of fracturing fluid, m^3

V_{pr} = volume of proppant, m^3.

APPENDIX B

REQUIRED PUMP CAPACITY AND DEVELOPED SURFACE PRESSURE

To develop the fracture geometry using the treatment parameters as decided by the optimisation algorithm, the pump has to deliver the required net fracture pressure, p_{net}. The pump capacity required to deliver p_{net} can be estimated by considering static head and dynamic friction loss with respect to the surface level. The pressure developed at the surface to deliver p_{net} in the fracture can also be computed. Only then can the constraints be formulated to adjust design such that the required pump capacity does not exceed the available pump capacity and the resulting surface pressure does not exceed the tubing strength and the pressure rating of other equipment. The calculation procedure is presented as follows:

Hydrostatic head

Hydrostatic head (psi) in the tubing while pumping fracturing fluid/slurry is estimated by:

$$p_{head} = 0.052 H \rho_f \rho_r \tag{B1}$$

where H is length of the tubing (ft) from surface to the fracture centre, ρ_f is average density of fracturing fluid (ppg), ρ_r is relative density (dimensionless). The relative density can be calculated by (Smith, 1992):

$$\rho_r = \frac{\left(8.33 + \frac{\overline{P}_c}{S_{gf}}\right)}{\left(8.33 + \frac{\overline{P}_c}{S_{gp}}\right)} \tag{B2}$$

where S_{gf} is specific gravity of fluid (dimensionless), S_{gp} is specific gravity of proppant (dimensionless) and $\overline{P}_c$ is average proppant concentration (ppg), which can be obtained from Eq. 3.34.

Frictional pressure loss in the tubing

The frictional pressure loss in the tubing is estimated by

$$\Delta P_{fric.loss} = f(\rho_f)\overline{v}^2 \frac{H}{25.8(d)} CF \tag{B3}$$

where $\Delta P_{fric.loss}$ is frictional pressure drop (psi), f is friction factor (dimensionless), $\overline{v}$ is average velocity in the tubing (ft/sec), d is internal diameter of the tubing (inch), and CF is the factor to incorporate increase in frictional pressure loss due to proppant addition.

The average velocity, $\overline{v}$, in the tubing is given by

$$\overline{v} = \frac{q_i}{377.3898 * \pi\left(\frac{d}{2}\right)^2} \times 35.3144 \times 144.0 \tag{B4}$$

where q_i is the injection rate (bbl/min).

For turbulent flow, which is usually the case during injection of fracturing fluid, the frictional factor, f can be obtained by solving numerically the following equation (Dodge and Metzner, 1959):

$$\sqrt{\frac{1}{f}} = \frac{4}{(n)^{0.75}} \log\left[N_r(f)^{\left(1-\frac{n}{2}\right)}\right] - \frac{0.395}{(n)^{1.2}} \tag{B5}$$

where N_r is Reynold's number (dimensionless) which can be calculated by

$$N_r = 928(\rho_f)(\bar{v})\frac{d}{\mu_e} \tag{B6}$$

The effective viscosity μ_e (Pa.s) in the above equation can be calculated as:

$$\mu_e = K(d)^{1-n}\frac{\left(3+n^{-1}\right)^n}{96(\bar{v})^{1-n}(0.0416)^n} \tag{B7}$$

where n and K (mPa-sec^n) are power law parameters (Eqs. 3.19 and 3.20 respectively).

The factor, CF to incorporate increase in frictional pressure loss due to proppant addition (Smith, 1992) is:

$$CF = \mu_r^{0.2} \times \rho_r^{0.8} \tag{B8}$$

where

$$\mu_r = 1 + 2.5\varphi + 10.05\varphi^2 + 0.00273e^{16.6\varphi} \tag{B9}$$

in which

$$\varphi = \frac{\bar{P}_c}{\left(8.33S_{gp} + \bar{P}_c\right)} \tag{B10}$$

Required pump capacity and surface pressure

The treatment pressure (psi) required to deliver p_{net} is:

$$p_{treat} = p_{net} + \sigma_h \tag{B11}$$

where σ_h is the minimum in-situ stress in the zone to be fractured. The pressure required (psi) at the surface, p_{surf} to develop the above treatment pressure is calculated as follows:

$$p_{surf} = p_{treat} + \Delta p_{fric.loss} + \Delta p_{surf.eq.loss} - p_{head} \tag{B12}$$

where $\Delta p_{surf.eq.loss}$ is the pressure loss in the surface equipment.

The pump capacity (horsepower) required to develop the above surface pressure is:

$$HP_{reqd} = p_{surf} \frac{q_i}{377.3898 * 550} \times 35.3144 \times 144.0 = p_{surf} \frac{q_i}{40.8168} \tag{B13}$$

APPENDIX C

CRITICAL DRAWDOWN PRESSURE

Crtical drawdown pressure, *CDP* is the pressure (psi) when the perforation formation near the wellbore fails mechanically. It is defined by the following expression (Fletcher *et al.*, 1996):

$$CDP = dp_{wc} + dp_{nw}(x_f) \tag{C1}$$

where

$$dp_{wc} = p_{nwc} - p_{wf} \tag{C2}$$

Here, perforation drawdown, dp_{wc} is the critical drwadown as a function of p_{nwc}, the critical near-perforation reservoir pressure and wellbore pressure, p_{wf} (bottomhole flowing pressure).

$$dp_{nw}(x_f) = p_{\inf} - p_{nw}(x_f) \tag{C3}$$

The pressure difference $dp_{nw}(x_f)$ quantifies the effect of the fracture on pore pressure near the perforation. This is the additional allowable drawdown contributed by the hydraulic fracture and is a function of the far-field reservoir pressure (at infinity), p_{inf} and the pore pressure near the wellbore, $p_{nw}(x_f)$.

The critical near-perforation reservoir pressure, p_{nwc} can be estimated as a function of rock strength and non-ideal gas properties assuming Mohr-Coulomb failure of plastic rock as follows (Weingarten and Perkins, 1995):

$$p_{nw} = \frac{C}{\tan(\alpha)}(p'_{nw})^{\frac{1}{m+1}} \tag{C4}$$

where C is the cohesive strength (psi) and α is the angle of internal friction (radian). The exponent, m, is given by the following equation.

$$\rho = \gamma_g p^m \tag{C5}$$

where ρ is the density (lb/ft^3) of gas at pressure p (psi) and γ_g is the gas gravity of a non-ideal gas.

The term p'_{nw} can be calculated numerically from the following equation.

$$\frac{4\sin(\alpha)}{1-\sin(\alpha)} - \left(\frac{p'_{nw} - p'_w}{m+1}\right)(p'_{nw})^{-m/(m+1)} = 0 \tag{C6}$$

where

$$p'_w = \left(\frac{p_{wf}\tan(\alpha)}{C}\right)^{m+1} \tag{C7}$$

The far field reservoir pressure (pressure at the boundary), p_{inf} and the near wellbore reservoir pressure, $p_{nw(x_f)}$ at any time during production life can be obtained by the following expression (Dake, 1978; Economides *et al.*, 1994):

$$p^2 = p_{wf}^2 + \frac{1424 q_g \mu_g Z_g T\left(\ln\left(\frac{r}{r_w}\right) + s_f - \frac{r^2}{2r_e^2}\right)}{kh} \tag{C8}$$

where r is the distance from the wellbore (ft). Pressure, p (psi) is p_{inf} when r is r_e and is $p_{nw(x_f)}$ when r is any near wellbore distance. The pseudo-skin, s_f created by the fracture is defined by Eq. 4.14.

APPENDIX D

BOUNDARY ELEMENT FORMULATION OF HYDRAULIC FRACTURING

The basic boundary integral equation that provides the relationship between the displacement, U and the traction, T (stress normal to a surface, $T = \sigma . n$, where n is unit outward normal) at a surface Γ of an elastic homogeneous isotropic media (linear elastic), or a sub-domain into which the body has been divided can be written, after disregarding the body force term, as (Banerjee, 1994):

$$C_{ij}(A_1)U_j(A_1) + \int_{\Gamma} F_{ij}(A_1, A_2)U_j(A_2)d\Gamma = \int_{\Gamma} G_{ij}(A_1, A_2)T_j(A_2)d\Gamma \qquad \text{(D1)}$$

where A_1 and A_2 are the points on the boundary sub surface and the boundary surface respectively. $F_{ij}(A_1, A_2)$, $G_{ij}(A_1, A_2)$ are the functions representing displacements and tractions respectively in the j directions at point A_2 corresponding to a unit point load acting in the i direction applied at A_1 and C_{ij} is coefficient function (Banerjee, 1994).

For hydraulic fracturing problems, the traction, T contains the pressure term arising due to fluid flow through the fractures and the displacement, U contains resultant displacement obtained from the solution of the problem of coupled fluid flow and structural elastic response. The total fracture aperture can thus be expressed as:

$$w = w_o + w_p \qquad \text{(D2)}$$

where w_o is the aperture contribution from the external stress and w_p from the fluid pressure as $w_p = \lambda p$, in which λ is the influence coefficient. Applying the principle of fluid flow through parallel plates (i.e. $q = -\frac{w^3}{12\mu} grad\ p$) and mass conservation, the final

form of the boundary integral equation for the coupled problem of hydraulic fracturing can be expressed by the manipulation of Eq. D1 as (Hossain, 2001):

$$\int_{\Omega} \delta p \frac{\partial w}{\partial t} d\Omega + \int_{\Omega} \frac{w^3}{12\mu} (grad\ p.grad\ \delta p) d\Omega + \int_{\Gamma} \delta p\ \beta V^{4/3} d\Gamma = Q(t)\delta p(O) \qquad \text{(D3)}$$

in which Ω is a sub-domain bounded by Γ in a 3D space containing the fracture surface; p is the pressure inside the fracture; w is the total fracture aperture; q is flow rate through the fracture; t is the flow time and Q is the source or sink strength of any point O inside a fracture region. According to Linear Elastic Hydraulic Fracturing (LEHF) theory (SCR geomechanics group, 1993), the solution of crack tip fields is represented by fracture width, $w(\rho)$ and expressed for the Newtonian fluid and impermeable formation as, $w(\rho) = \beta V^{1/3}$ where $\beta = 2(3^{7/6})\left(\frac{\mu}{E'}\right)^{1/3} \rho^{2/3}$, in which E' is the plane strain modulus which is related to Young's modulus E and Poisson's ratio ν as $E' = E/(1-\nu^2)$; ρ is the curvilinear distance measured on the fracture surface between any point and fracture front; μ is the fracturing fluid viscosity and V is fracture propagation speed. For boundary element solution, nodal discretisation of Eq. D3 can be expressed as:

$$\int_{\Omega_i} N_i \left(\sum_{j=1}^{j=n} N_j \frac{\hat{w}_j(t_{n+1}) - \hat{w}_j(t_n)}{t_{n+1} - t_n} \right) d\Omega + \frac{1}{12\mu} \int_{\Omega_i} \left(\sum_{k=1}^{k=n} N_k \hat{w}_k \right)^3 grad N_i grad \left(\sum_{j=1}^{j=n} N_j \hat{p}_j \right) d\Omega + \int_{\Gamma_i} N_i \beta V^{4/3} d\Gamma = Q(t) N_i(O)$$

(D4)

where the fracture pressure, p is approximately related with nodal pressures, $\hat{p}$ (in the finite element sense) as: $p = \sum_{i=1}^{n} N_i \hat{p}_i$ and the incremental pressure, δp as: $\delta p = \sum_{i=1}^{n} N_i \delta \hat{p}_i$; in which n is the total nodes in the overall domain (structure) and N is the shape function of the domain.

Considering the fracture boundary surface and the structure boundary surface in two separate domains, Eq. D4 can be rearranged as (Hossain, 2001):

$$\sum_{j=1}^{j=n}\frac{\hat{w}_j}{\Delta t}\int_{\Omega_i}N_iN_j d\Omega+\sum_{j=1}^{j=n}\hat{p}_j\int_{\Omega_i}\frac{1}{12\mu}\left(\sum_{k=1}^{k=n}N_k\hat{w}_k\right)^3 grad\,N_i\;grad\,N_j d\Omega$$
$$=\sum_{j=1}^{j=n}\frac{\hat{w}_j(t_n)}{\Delta t}\int_{\Omega_i}N_iN_j d\Omega-\int_{\Gamma_i}N_i\left(\sum_{k=1}^{k=l}M_k\hat{\beta}_k\hat{V}_k^{4/3}\right)d\Gamma+Q(t)N_i(O) \qquad \text{(D5)}$$
$$+\int_{\Omega_i}\frac{1}{12\mu}\left(\sum_{k=1}^{k=n}N_k\hat{w}_k\right)^3 grad\,N_i\;grad\left(\sum_{j=m+1}^{n}N_j\hat{B}_j\hat{V}_j^{1/3}\right)d\Omega$$

where $\hat{B}_j=E'^{2/3}\left(\frac{\mu}{3\hat{p}_j}\right)^{1/3}$ that accounts for the effects of crack tip nodal speed on the pressure at the node; m is the number of nodes on the structure boundary; l is the number of nodes on the fracture boundary ($n = m+l$); M is the shape function of the domain excluding the fracture. It is important to note that integral in Eqs. D4 and D5 applies to all nodes, i.e. $i = 1, ..., n$. Eq. D5, therefore, results in a set of n fluid flow equations, n structural equations with n unknown nodal widths, $\hat{w}$ and fluid pressures, $\hat{p}$ and hence, the solution process is quite complex as it is a non-linear time depended equation involving a moving boundary (the fracture boundary moves during propagation).

Numerical solution of hydraulic fracture propagation

Because of discretisation in both time and space, the solution of Eq. D5 corresponds to a series of "snapshots" that correspond to unique instances in time and crack shape. Either of two approaches can be followed to obtain the solution efficiently: (i) the time step can be fixed and corresponding geometry can be searched, or, (ii) the geometry can be fixed and corresponding time can be searched. The first approach is intuitive but the latter approach minimises the amount of computation. To implement the latter approach in this study, an initial starter crack is assumed as the starting point for all subsequent analyses as the hydraulic fracture propagates stepwise.

For each step of crack propagation, an *ad-hoc* propagation length, $\Delta L(x)$ is specified (see Figure. D1), 10% of the current fracture length. The time step, Δt, the crack propagation speed, $v(x)$ and the propagation step length, $\Delta L(x)$ can be related as $\Delta L(x) = v(x).\Delta t$. In each step, the time step is adjusted iteratively until the injected fluid volume converges with the fracture volume. The direction of mixed mode fracture propagation, $\theta(x)$ in each propagation step is determined according to the maximum tensile stress criterion (Erdogan and Sih, 1963). The stress intensity factors K_I and K_{II} required to formulate mixed mode propagation are computed using the displacement correlation technique (Ingraffea and Manu, 1980).

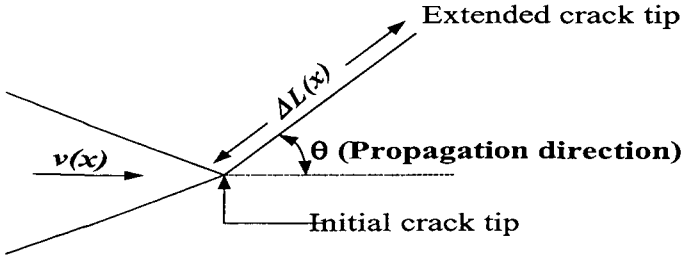

Figure D1. Schematic of fracture propagation process.

The above theories were implemented in a code, HYdraulic FRacture ANalysis Code (HYFRANC3D), by the Cornell Fracture Group, Cornell University, Ithaca, NY, USA (www.cfg.cornell.edu). HYFRANC-3D is a Unix-based modeling system that analyses the response of linear-elastic materials, containing three-dimensional fractures of arbitrary geometries, to applied stresses (Desroches and Carter, 1996). The software can simulate fracture propagation using any of the criteria: (1) Maximum Tangential Stress (Erdogan and Sih, 1963), (2) Maximum Energy Release Rate (Hussain *et al.*, 1974), (3) Minimum Strain Energy Density (Sih, 1974) and (4) Planar Propagation (fracture extension co-planar with initial fracture). The software incorporates functionality to discretise or mesh the structure, attach boundary conditions at the geometry level allowing the mesh to inherit these values and modify the geometry during crack growth by only local re-meshing around the crack. It has also the capability to generate element

automatically with different mesh schemes, such as bi-linear mesh (quarter point element) and arbitrary automatic mesh scheme (either triangular element or quarter point element).

APPENDIX E

WATERFRAC TECHNOLOGY: A SHEAR DILATION MECHANISM

The physical process of shear slippage and dilation is illustrated in Figure E1. During fluid injection, the pressure is elevated inside a natural fracture, and thus the stress distribution around the fracture changes. Beyond a threshold pressure, rock material around the fracture fails by 'sliding' (Mode-II), instead of 'opening' (Mode-I) considered in conventional hydraulic fracturing. The sliding of two rough fracture surfaces (shear slippage) dilates an aperture normal to the fracture surface. After pumping stops, asperities of the rough fracture surfaces resist their sliding back to the original position, and thus the permeability of a shear dilated fracture is retained. The overall reservoir permeability is the combined effect of numerous dilated fractures. Estimation of stimulated reservoir permeability includes the following steps.

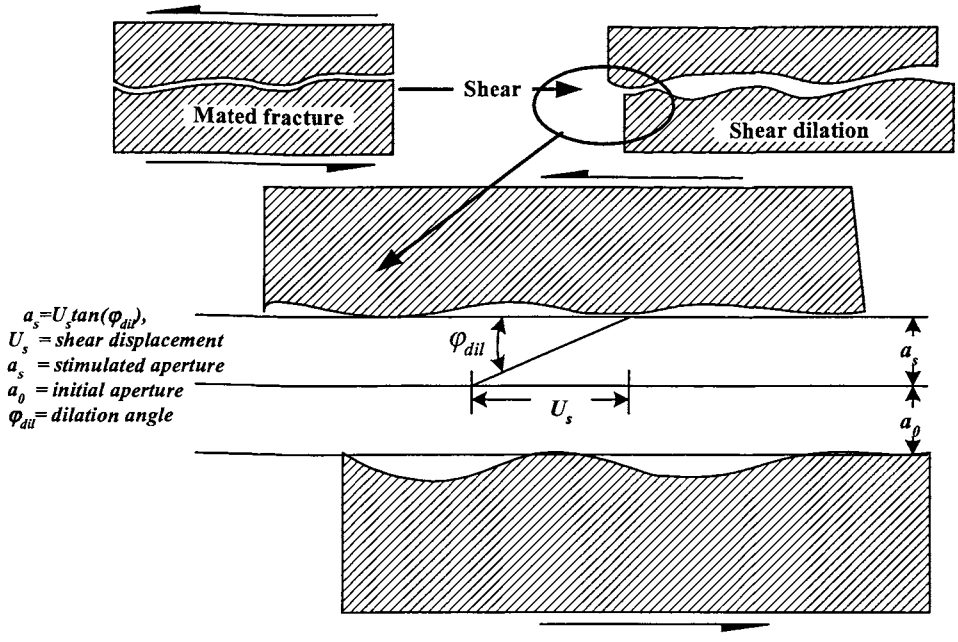

Figure E1. Fracture aperture caused by shear displacement

Modeling Fractured Reservoir

To develop a model that can simulate the natural fracture network and compatible fluid flow system it is first required to derive a range of fracture parameters through natural fracture characterization at a number of well locations. Then natural fractures in the whole reservoir are simulated using these parameters as input to the model.

Natural fracture data, such as the fracture orientation, size and other fracture parameters are characterized from fracture outcrops, field observations, measurements on core, borehole images from bottom hole television [BHTV], logging operations, etc. By laboratory experiments and other analyses, fracture properties (e.g. mechanical properties such as basic friction angle, shear dilation angle, fractal dimension etc.) are determined. The fracture density is determined as the fracture area per unit volume of rock mass. The fracture orientations are specified by ranges of azimuth and dip angles for a number of fracture sets obtained from field observation and/or core analysis. A relationship between a fracture size and the number of fractures of that size present in the reservoir is developed based on fractal distribution (Watanabe and Takahashi, 1995). The box-counting method (Barton and Hsieh, 1989) is used to determine the fractal dimension of fracture traces on a map. Usual range of the fractal dimension (D) for natural fracture systems is $1.0<D<2.0$ in two-dimensions (Watanabe and Takahashi, 1995) and $2.0<D<3.0$ in three-dimensions (Turcotte, 1992).

Using characterized fracture parameters and fractal dimension based on sample data at well locations, natural fractures with fractal distribution are simulated in the reservoir. A cubic block of rock with edge length L is considered as shown in Figure E2a, within which fractures are generated. All fracture shapes are assumed as penny-shape (circular). In order to simplify and generalize the discussion, normalized dimensions are considered in Figure E2b. To start the fracture simulation process, n fracture identifications are created: i = 1,2,3..., n; where i represents a fracture without any attribute whatsoever so far. Using the normalized probability method in conjunction with the weighting factors of different fracture sets as characterized from samples, these fractures are divided into groups each of which represents a fracture set. All the

fractures in a fracture set immediately inherits the orientation parameters, dip and azimuth that were assigned for that set by characterization. The number of characteristic fractures, n_r whose radii are equal to or greater than r can be expressed as:

$$n_r = Cr^{-D} \tag{E1}$$

Manipulating Eq. E1, the maximum fracture radius, r_α in a fraction, α representing the total number of fractures between r_α and the minimum fracture radius, r_{min} can be related as:

$$r_\alpha = \left[(1-\alpha)r_{\min}^{-D} + \alpha r_{\max}^{-D}\right]^{-1/D} \tag{E2}$$

where r_{max} is the maximum fracture radius in all.

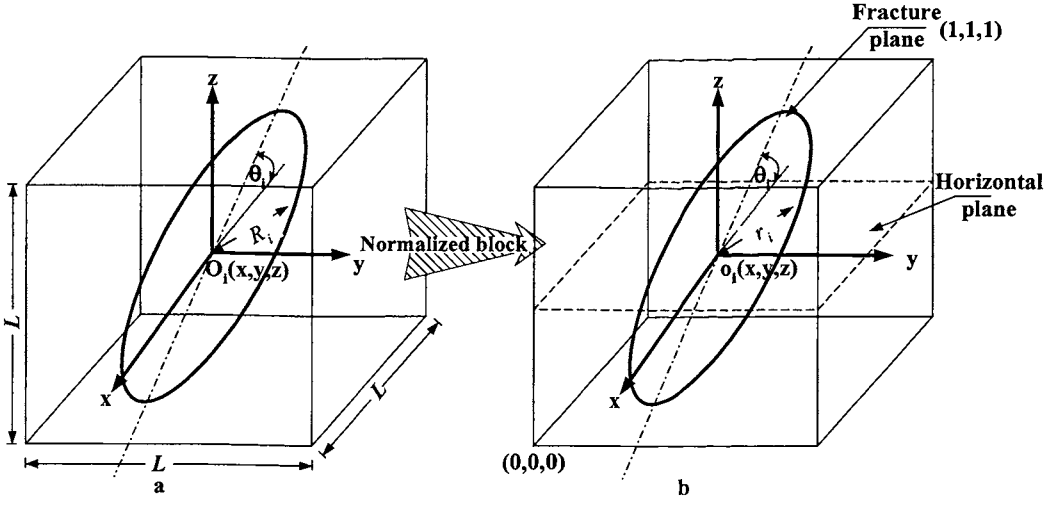

Figure E2. Three-dimensional fracture network modeling: (a) a cubic block of side length L, (b) normalized block of unit length in (x,y,z) coordinate system.

For each fracture (i.e. for each i), a random value of α is generated between 0 and 1, and the value is accepted if the same number was not already generated in the current fracture set.

Having the fracture radii defined, a basic fracture database is created. Each record (row) in the database contains attributes: identification, orientation parameters and radius for a fracture. Every fracture is unique in terms of fracture attributes from rest of the fractures in this database. To place these fractures in the reservoir, a fracture is picked up randomly from the database and then its center, O is generated by random values of x, y and z co-ordinates between 0 and 1, i.e. in terms of the normalized reservoir dimensions. If a fracture crosses the reservoir boundary during this process, that fracture is deleted. The process of random placement continues until the characterized fracture density is achieved.

The final step in the fracture simulation process is to specify the initial apertures of the fractures placed in the reservoir. The initial fracture aperture, a_0 at zero effective stress is assumed to be proportional to the fracture radius and thus is expressed as:

$$a_0 = \beta r_i \tag{E3}$$

At zero effective stress in the undisturbed rock mass, the value of β for total of n fractures can be estimated in terms of an average virgin permeability, k_0 as (Willis-Richards *et al.*, 1996):

$$\beta = \left(\frac{12\,\overline{S} k_0 \sum_{all\ n} r_n}{\sum_{all\ n} \frac{r_n^4}{\left(1 + 9\,\sigma_{eff\ n}/\sigma_{nref}\right)^3}} \right)^{\frac{1}{3}} \tag{E4}$$

The material property, σ_{nref} is normal stress to a fracture to cause 90% reduction in the compliant aperture and can be obtained from laboratory tests. The estimation of

effective normal stress, σ_{eff} will be explained later. The mean virgin permeability, k_0 for the fractured medium can be determined by laboratory tests, and the mean fracture spacing, $\bar{S}$ is reciprocal of the fracture density.

Fracture Responses to Stimulation

Due to an applied stimulation pressure under a certain in-situ stress condition, a natural fracture may propagate and undergo shear and normal displacements. An approximate method of logarithmic distribution due to radial flow (Muskat, 1937) is used to estimate the fluid pressures inside fractures:

$$p_f = p_w - \frac{p_w - p_b}{\ln\frac{r_b}{r_w}} \ln\frac{r_f}{r_w}, \qquad r_f \geq r_w > 0 \tag{E5}$$

where p_f is the pressure at the fracture center, p_w is the wellbore pressure, p_b is the pressure at the reservoir boundary, r_b is the maximum reservoir radius, r_f is the radial distance between fracture center and wellbore center and r_w is the wellbore radius.

The total wellbore stimulation pressure, p_w at the level of fracture center is calculated as (Figure E3):

$$p_w = p_s + p_F + p_{hf} \tag{E6}$$

where p_s is the stimulation pressure at the surface, p_F is the hydrostatic pressure at the bottomhole and p_{hf} is the hydrostatic pressure at a height hf from the wellbore bottom.

p_w and p_{hf} are calculated as:

$$p_F = d_r \rho_f g \tag{E7}$$

$$p_{hf} = h_f \rho_f g \tag{E8}$$

where d_r is the reservoir depth, g is the gravitational acceleration and ρ_f is the fluid density.

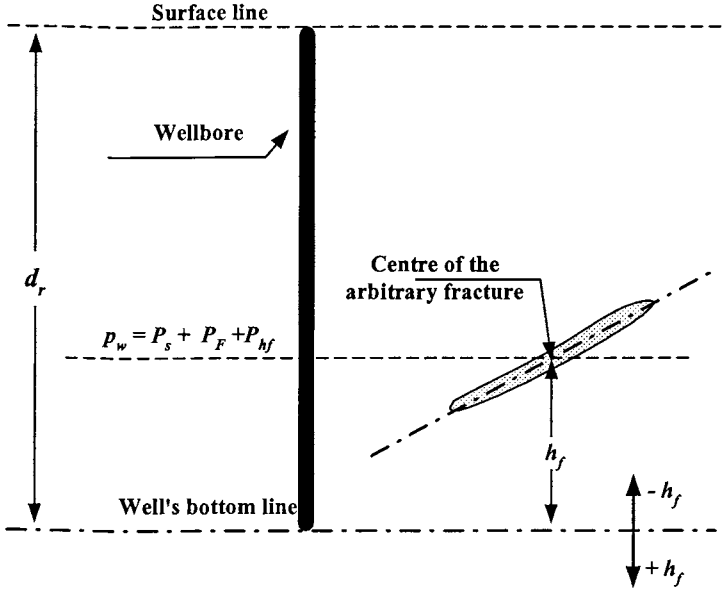

Figure E3. Hydrostatic pressure at the fracture center w.r.t. well's bottom

The pressure drop at the reservoir boundary far away from the injected well is assumed to be 20% of the pressure at the well, giving $p_b = 0.8p_w$.

With reference to Figure E4, the compressive and shear stresses on the fracture surface due to principal stresses, σ_1, σ_2 and σ_3 can be defined as (Jaeger and Cook, 1969):

$$\sigma_n = l^2\sigma_1 + m^2\sigma_2 + n^2\sigma_3 \tag{E9}$$

$$\tau_n = \left\{ \begin{matrix} (\sigma_1 - \sigma_2)^2 l^2 m^2 + (\sigma_2 - \sigma_3)^2 m^2 n^2 \\ + (\sigma_3 - \sigma_1)^2 n^2 l^2 \end{matrix} \right\}^{1/2} \tag{E10}$$

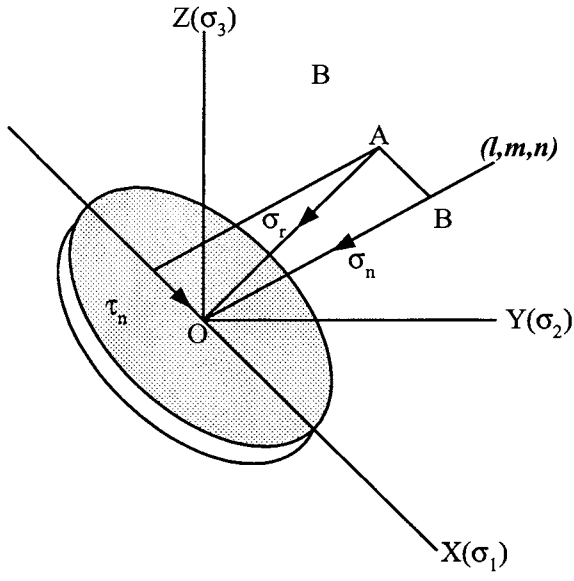

Figure E4. Schematic for calculation of normal and shear stresses in the fracture

The direction cosines (l, m, and n) normal to the fracture plane can be calculated as (Goodman, 1989):

$$l = \cos\delta\cos\gamma; m = \cos\delta\sin\gamma; n = \sin\delta \tag{E11}$$

The angles γ and δ can be related with fracture dip and azimuth angles as: $\delta = 90^{o}$ - *dip* and $\gamma = 90^{o}$ - *azimuth*. Therefore, the direction cosines of the fracture in terms of fracture dip and azimuth are:

$$\left.\begin{aligned} l &= \sin(\,dip\,)\sin(\,azimuth\,) \\ m &= \sin(\,dip\,)\cos(\,azimuth\,) \\ n &= \cos(\,dip\,) \end{aligned}\right\} \tag{E12}$$

Assuming compressive stress positive and considering back stress effect (Willis-Richards *et al.*, 1996), the effective normal stress, σ_{eff} is estimated by linear superposition as:

$$\sigma_{eff} = \sigma_n - p_f + \sigma_b \tag{E13}$$

where σ_n is the normal stress and σ_b is the back stress.

The fracture net pressure is defined as just the reverse of the effective normal stress:

$$P_{net} = -\sigma_{eff} = p_f - \sigma_n - \sigma_b \tag{E14}$$

Shear Slippage and Fracture Deformation. The condition at which the shear slippage occurs is derived based on Mohr-Coulomb's linear theory of shear failure. Applying the Mohr-Coulomb criterion to the Patton's saw-tooth fracture model (Patton, 1966) (Figure E1), the peak shear stress can be calculated as:

$$\tau_p = \sigma_{eff} \tan(\varphi_{basic} + \varphi_{dil}^{eff}) \tag{E15}$$

The basic friction angle, φ_{basic} which is a material property of the fracture surface, usually varies between 30° - 40°. The effective shear dilation angle, φ_{dil}^{eff} reflects the roughness of fractures, and is equivalent to joint roughness coefficient (Barton *et al.*, 1985). The effective shear dilation angle can be estimated based on a laboratory measured dilation angle, φ_{dil} as (Willis-Richards *et al.*, 1996):

$$\varphi_{dil}^{eff} = \frac{\varphi_{dil}}{1 + 9\sigma_{eff}/\sigma_{nref}} \tag{E16}$$

The shear slippage occurs when the shear stress acting parallel to the fracture plane exceeds the peak shear stress:

$$\tau_n \geq \sigma_{eff} \tan(\varphi_{basic} + \varphi_{dil}^{eff}) \quad \text{(E17)}$$

Shear displacement as a result of shear slippage causes permeability enhancement of natural fractures. According to linear elastic theory, the shear displacement (U_s in Figure E1) is proportional to the excess shear stress (Hicks *et al.*, 1996), and can be expressed as:

$$U_s = \frac{\Delta\tau}{K_s} \quad \text{(E18)}$$

where $\Delta\tau$ is the excess shear stress and K_s is the shear stiffness.

The access shear stress, $\Delta\tau$ is calculated as:

$$\Delta\tau = \tau_n - \sigma_{eff} \tan(\varphi_{basic} + \varphi_{dil}^{eff}) \quad \text{(E19)}$$

The shear stiffness, K_s of idealized fractures has been extensively studied for a variety of simple fracture shapes; the general form is as follows (Dieterich, 1992):

$$K_s = C_g \frac{G}{r} \quad \text{(E20)}$$

where C_g is the geometric parameter for shear stiffness and G is the shear modulus.

For a penny-shaped circular crack, C_g is approximated as (Eshelby, 1957):

$$C_g = \frac{7\pi}{24} \tag{E21}$$

In order to calculate the shear stiffness of a fracture that has propagated due to the applied stimulation pressure, the radius of the stabilized fracture is estimated by an approximate analytical method (Rahman *et al.*, 2000b) and used in Eq. E20.

From Eq. E13, it can be seen that the effective normal stress may become negative when the fracture pressure is high for a given in-situ stress condition. With such a condition, the fracture will be fully open and surfaces will no longer remain in contact: a condition that is called 'shear jacking'. The shear stress developed is then fully available for shear displacement and hence, the shear displacement, U_s is calculated as:

$$U_s = \frac{\tau_n}{K_s} \tag{E22}$$

Dilated Aperture. The shear displacement of a fracture causes dilation in the direction normal to the fracture surfaces (a_s in Figure E1) due to their roughness. Fracture apertures are affected by the effective normal stress and are proportional to shear displacements (Dieterich, 1992; Goodman, 1976). The change in aperture due to shear dilation can be expressed as (Barton *et al.*, 1985; Willis-Richards *et al.*, 1996):

$$a_s = U_s \tan(\varphi_{dil}^{eff}) \tag{E23}$$

The total stimulated aperture can be determined from the following expression (Willis-Richards *et al.*, 1996; Hicks *et al.*, 1996):

$$a = \frac{a_0}{1+9\sigma_{eff}/\sigma_{nref}} + a_s + a_{res} \tag{E24}$$

where a_0 is the initial fracture aperture, a_s is the fracture aperture due to shear displacement and a_{res} is the residual aperture.

The residual aperture, a_{res} usually exists at high effective stress and is considered to be zero for this study. The total stimulated aperture, a can finally be expressed by mathematical manipulation as:

$$a = \frac{a_0 + U_s \tan(\varphi_{dil})}{1 + 9\sigma_{eff}/\sigma_{nref}} \tag{E25}$$

Numerical Flow Simulation

After fracture dilation and aperture opening, the fluid flows through the network of fractures and extends the shape of the reservoir towards its final growth. Analysis of permeability enhancement requires numerical simulation of fluid flow within the stimulated fractured reservoir.

A single-phase steady state Darcian fluid flow condition is assumed. The superficial velocity of the flow field is defined as the volumetric flow rate per unit area normal to the flow. In the Cartesian co-ordinate system, the final form of Darcy's law, with porosity, $\phi = 0$ for fractured cells, can be written as:

$$k_x \frac{\partial^2 p}{\partial x^2} + k_y \frac{\partial^2 p}{\partial y^2} + k_z \frac{\partial^2 p}{\partial z^2} = 0 \tag{E26}$$

where k_x, k_y and k_z are directional permeabilities, p is the pressure and d is the distance between two adjacent blocks.

Eq. E26 states that the sum of rate of flows in the three orthogonal directions is zero. This condition has to be satisfied in the model with respect to the permeability and pressure variation in each direction.

To solve Eq. E26, the whole reservoir is divided into small cuboids (Figure E5) with say n_b divisions along each of x, y and z directions, thus giving a total of $n_b^3 = N_B$ small cubic blocks in the reservoir. Fracture lengths intersected on each directional block interface are calculated. The local directional permeability from a block to its adjacent block is then calculated by the manipulation of the cubic law as:

$$k_i = \sum_{j=1}^{n_{fi}} \frac{a_{ij}^3 l_{ij}}{12 d^2}, \; i = x, y, z \qquad \text{(E27)}$$

Once the local directional permeabilities (k_i, $i = x, y, z$) of all the N_B blocks are estimated, the steady state flow equation (Eq. E26) is solved numerically using finite difference approach to update the pressure distribution in the reservoir. The stimulated fracture apertures are then updated using the updated local pressures. This updating procedure may require a few iterations.

The overall reservoir permeability is calculated as the root mean square (r.m.s) value of the resultant dirtectional permeabilities, k_{Rx}, k_{Ry} and k_{Rz}. These resultant directional permeabilities are calculated by summing up the contributions of all the interblock flow boundaries along x, y and z directions, respectively, as:

$$k_{Ri} = \sum_{m=1}^{n_{bi}} \sum_{j=1}^{n_{fi}} \frac{a_{ij}^3 l_{ij}}{12 d^2}, \; i = x,y,z \qquad \text{(E28)}$$

The total interblock flow boundaries in each direction can be calculated as: $n_{bi} = n_b^2(n_b - 1)$. The mean reservoir permeability is then calculated as:

$$k_{rms} = \frac{1}{3N_B}\left(k_{Rx}^2 + k_{Ry}^2 + k_{Rz}^2\right)^{\frac{1}{2}} \tag{E29}$$

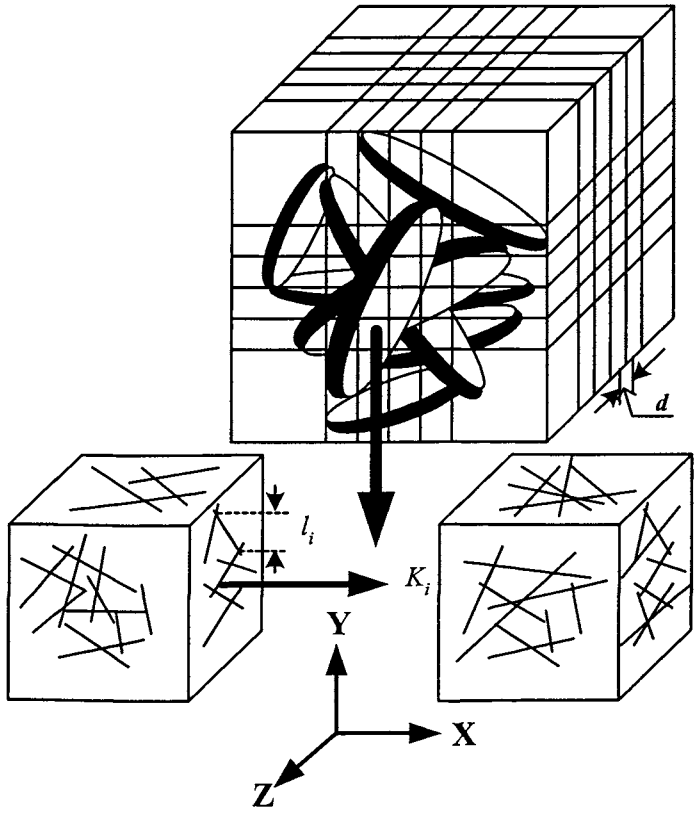

Figure E5. Local permeabilities (K_x, K_y, K_z) at the element interface